DEVELOPMENT OF CATIONIC NANOSYSTEMS BASED ON POLY (STYRENE-ALT-MALEIC ANHYDRIDE) FOR COMBINATORIAL DELIVERY OF DRUG AND NUCLEIC ACID IN CANCER THERAPY

AJI ALEX M.R.

CENTRE FOR BIOMEDICAL ENGINEERING

INDIAN INSTITUTE OF TECHNOLOGY DELHI

OCTOBER 2017

DEVELOPMENT OF CATIONIC NANOSYSTEMS

BASED ON POLY (STYRENE-ALT-MALEIC ANHYDRIDE)

FOR COMBINATORIAL DELIVERY OF DRUG AND

NUCLEIC ACID IN CANCER THERAPY

By

AJI ALEX M.R.

Submitted

in fulfilment of the requirements of the degree of Doctor of Philosophy

to the

CENTRE FOR BIOMEDICAL ENGINEERING

INDIAN INSTITUTE OF TECHNOLOGY DELHI

OCTOBER 2017

DEDICATED TO

MY BELOVED FAMILY

CERTIFICATE

This is to certify that the thesis entitled **'Development of cationic nanosystems based on poly (styrene-alt-maleic anhydride) for combinatorial delivery of drug and nucleic acid in cancer therapy'** being submitted by **Mr. Aji Alex M.R.** to the Indian Institute of Technology Delhi for the award of degree of **Doctor of Philosophy** is a record of bonafide research work carried out by him. **Mr. Aji Alex M.R.** has worked under our guidance and supervision and has fulfilled the requirements for the submission of this thesis, which to our knowledge has reached the requisite standard.

The results contained in this thesis are original and have not been submitted, in part or full, to any other University or Institute for the award of any other degree or diploma.

Prof. Veena Koul

Centre for Biomedical Engineering,

Indian Institute of Technology Delhi,

Hauz Khas, New Delhi-110016

India

Dr. Ritu Kulshreshtha

Department of Biochemical

Engineering and Biotechnology

Indian Institute of Technology Delhi,

Hauz Khas, New Delhi-110016

India

ACKNOWLEDGEMENTS

सार

कैंसर चिकित्सा में सक्रिय एजेंटों को वितरित करने के लिए पॉलिमेरिक नैनोसिस्टम्स की बड़े पैमाने पर जांच की गई है। कैंसर के उपचार में पारंपरिक सक्रिय घटकों की नैदानिक प्रभावोत्पादकता नोआरेरिअर्स का उपयोग करके काफी बढ़ाया जा सकता है। नैनोकायरियर्स कैंसर कोशिकाओं को बढ़ाए हुए पारगम्यता और प्रतिधारण (ईपीआर) प्रभाव से लोड किए गए सक्रिय घटकों के संचलन समय को बढ़ा सकते हैं, स्वस्थ कोशिकाओं को विषैले प्रभावों को कम कर सकते हैं और बहुऔषधि प्रतिरोध को दूर कर सकते हैं। इसके अलावा, नैनोकारियर्स द्वारा सक्रिय घटकों की जैवउपलब्धता और निरंतर स्नाव को प्राप्त किया जा सकता है।

औषधि और न्यूक्लिक अम्ल जैसे कि प्लाज्मिड जैसे की प्लाज्मिड डीएनए (pDNA) ,द्विलड़ीय RNAs (dsRNAs), लघु हेयरपिन RNAs (shRNAs) , सूक्ष्म रना (miRNAs) लघु हश्तक्षेपपूर्ण RNAs (siRNAs) इत्यादि के संयुक्त वितरण द्वारा रसायनोपचार की विभिन्न त्रुटियों को दूर किया जा सकता है।ज्यादातर आनुवंशिक पदार्थ कर्क कोशिकाओं के प्रसार को RNA हश्तक्षेप क्रिया द्वारा विशिष्ट जीनों की अभिव्यक्ति को निष्क्रिय करके रोकते हैं। मिश्रित परिदान द्वारा रासायनिक औषधियों की मात्रा को प्रभावशाली रूप से कम किया जा सकता है जिसके फलस्वरूप रासायनिक औषधियों के दुष्प्रभावों को न्यूनतम स्तर तक लाया जा सके।सीरम नुक्लिएस आनुवंशिक पदार्थों का पतन कर देते

हैं अतः उन्हें जैविक संचरण में उपयोग में नहीं लिया जा सकता। इसके अतिरिक्त अनुवांशिक पदार्थों के पाली अनिओनिक स्वाभाव , उच्च आणविक भर और निहित अस्थिरता के कारणवश इनकी कौशिकीय प्रविस्टि अत्यंत प्रतिबंधित होती है। संचारिक कौशिकीय अवरोधों को निष्क्रिय करने हेतु उपयुक्त नुस्खे को विकसित करने की अत्यधिक आवशयकता है जो की औषधि एवम नुक्लेइक अम्ल को प्रवृत करने में सक्षम हो । वर्तमान शोध कार्य का प्रमुख उद्देश्य कतिओनिक बहुलक नैनो सिस्टम्स द्वारा औषधि एवम नुक्लेइक अम्ल का अंत: कौशिकी वितरण करना है । इस शोध द्वारा कतिओनिक एम्फीफिलिक निम्न आणविक भार के PSMA सह-बहुलकों का संश्लेषण एवम विशेषीकरण करना तथा उनकी उनकी अंत: कौशिकी जीन वितरण की प्रभावकारिता का मूल्याङ्कन करना है ।

उपरोप सह-बहुलकों के संश्लेषण के लिए विभिन्न कतिओनिक कार्यात्मक समूहों का चयन विभिन्न रासयनिक वर्गों से किया गया है जैसी की इसोनिकोटिनिक अम्ल, 2-अमीनोपीप्राजिन, ग्लीसीडील त्रिमेथ्य्ल अम्मोनियमक्लोरिड, l - अर्गिनीने एवम स्पेर्मिन । इस शोध द्वारा संश्लेषित कतिओनिक उपरोपित सह- बहुलक नैनो वाहकों का संश्लेषण , विशेषीकरण एवम उनका अवलोकन जैव- अनुकूलता , रक्तानुकूलता , एण्डोसोमाल विच्छेद गुण और अभिकर्मक दक्षता का अवलोकन किया गया है ।

 विभिन्न उपरोपि सह-बहुलकों ने एण्डोसोमाल विच्छेद गुण का प्रदर्शन निम्न क्रम में दिया है: क्वाटरनिसद इसोनिकोटिनिक अम्ल > स्पेर्मिन > l -आर्जिनिन । वहीँ स्पेर्मिन एवम l -आर्जिनिन

उपरोपित PSMA यौगिकों ने अन्य उपरोपित बहुलकों की तुलना में बेहतर अभिकर्मक दक्षता का प्रदर्शन किया है ।

PSMA के कतिओनिक नैनो वाहको की कोर शैल संरचना के कारण उनमें जल विरोधी कर्क रोग औषधियों को भारित किया जा सकता है । चूँकि कर्क रोग के उपचार हेतु कर्क रोग औषधि एवम si - RNA का मिश्रित प्रतिपादन एक आशावादी कार्य निति है । अतः PSMA को औषधि एवम si -RNA के सह-प्रतिपादन हेतु उपयुक्त रूप से संशोधित किया गया है । अतः इस अध्ययन में डोक्सोरुबिसिन एवम PLK -1 si - RNA का चयन मॉडल औषधि एवम si - RNA के लिए किया गया है । PSMA आधार पर इसोनिकोटिनिक अम्ल एवम आर्जिनिन -असतील लायसिन के संयुग्मन द्वारा कतिओनिक नैनो - वाहकों का संश्लेषण किया गया है जिसमे 4 , 7 ,10 -ट्रीऑक्सा-1 , 13 -डेकैन डाई अमिन को श्रृंखलख अणु के रूप में उपयोग में लिया है । कतिओनिक बहुलक निर्बाध वृत्ताकार मीसल्स में स्वयं एकत्रित हो जाते हैं , जिनकी CMC ~ 3 µg/mL और कण माप 14-30 nm की श्रृंखला में था । इन मीसल्स में डोक्सोरुबिसिन की अनुकूल भार क्षमता ~ 9 % w/w थी. si -RNA के प्रभावशाली संयुग्मन हेतु बहुलक/ si -RNA का भार अनुपात 10 के ऊपर प्राप्त हुआ था । MCF-7 कोशिकाओं के कोशिका द्रव्य के अंदर डोक्सोरुबिसिन और फ्लोरोसेंट वर्गीकृत si -RNA धारक मिसलीस ने उत्कृष्ट सह- स्थानीकरण का प्रदर्शन किया है । MTT कोशिका ऐसे द्वारा यह निष्कर्ष निकला की सह-वितरित सक्रिय घटकों (औषधि एवम siRNA) ने कोशिका विषाक्तता हेतु सह-क्रियाशीलता क्रियाविधि को

प्रदर्शित किया है । एहरलिच जलोदरता अर्बुद धारक स्विस एल्बिनो चूहों में कतिओनिक मीसल्स द्वारा औषधि एवम si-RNA के सह-वितरण द्वारा अर्बुद रोधी प्रभाव में सार्थक वृद्धि की है ।

PSMA आधारित उत्प्रेरित संवेदनशील बहुलक नैनो तंत्र को बहुलक आधार पर विभिन्न डाइसल्फ़ाइड की सहलग्नता द्वारा विकसित किया गया जो की भारित सक्रिय घटक के अर्बुद विशिष्ट परिदान को बढ़ा देते हैं । मूल बहुलक की एनहाइड्राइड इकाई को मेथोक्सी पाली ईथीलीन ग्लाइकोल द्वारा विवृत किया गया है । कोशिका भेदन व् एण्डोसोमाल बफरिंग गुणों से युक्त आर्जिनिन व् हिस्टीडीन को डाइसल्फ़ाइड कड़ियों के द्वारा बहुलक पर उपरोपित किया गया है । बहुलक व्युत्पन्न ने जल में स्वयंसकलित होकर निर्विघ्न वृताकार मिसेलर संरचना प्रदान की , जिनका CMC ˜ 7 µg/mL पाया गया है । डोक्सोरुबिसन को मीसल्स में नैनो- अवक्षेपण विधि से अधिकतम -8.6 % w/w की भार क्षमता में भारित किया गया था । पॉलीमर/ siRNA ने 40 के भार अनुपात पर siRNA में प्रभावशाली बाध्यकारी क्षमता संघनन क्षमता प्रदर्शित की है एवम पॉलीप्लेक्सेस को BSA के आवरण द्वारा स्थिर बनाया गया है । कृत्रिम एवम प्राकर्तिक परिवेशीय प्रयोगों में औषधि भारित मिसेलप्लेक्सेस ने कौशिका प्रसार को प्रतिबंधित करने में अत्यधिक क्षमता का प्रदर्शन किया है ।

यह शोध प्रबंध पांच अध्यायों मे विभाजित किया गया है । प्रथम अध्याय में कर्क रोग में नैनो प्रौद्योगिकी के महत्व को शामिल किया गया है, जिसमे विशेषतः औषधि और नुक्लेइक अम्ल के संयुग्मित वितरण को संदर्भित किया गया है । द्वितीय अध्याय में पाली (स्टाइरीन-ऑल्ट-मलेइक एनहाइड्राइड) ,

(PSMA) को कतिओनिक संशोधित उपरोपित बहुलकों के संश्लेषण एवं कृत्रिम परिवेश में अंत:कौशिकीय जीन वितरण के मूल्यांकन का विवरण प्रस्तुत किया गया है । तृत्य अध्याय में PSMA के उभय स्नेही उपरोपित सह-बहुलक मीसल्स का औषधि एवं siRNA के संयुग्मित प्रतिपादन हेतु विकास किया गया है एवं उसकी कृत्रिम और प्राकृतिक परिवेश में प्रभावकारिता का अवलोकन किया गया है.चतुर्थ अध्याय में उत्प्रेरित संवेदनशील PSMA आधारित नैनोवाहकों के विकास एवं अवलोकन पर विशेष ध्यान केंद्रित किया गया है और इसके साथ ही उनकी कृत्रिम एवं प्राकृतिक परिवेश में औषधि और siRNA की सह-प्रतिपादन क्षमता का अवलोकन किया गया है । पंचम अध्याय में सारांश, निष्कर्ष एवं किया गए शोध के फलस्वरूप उत्पन्न परिणामों हेतु भविष्य के दिशानिर्देशों पर प्रकाश डाला गया है ।

ABSTRACT

Polymeric nanosystems have been extensively investigated for delivering active agents in cancer therapy. Clinical efficacy of conventional active ingredients in cancer treatment can be significantly enhanced using nanocarriers. Nanocarriers can passively target the cancer cells by enhanced permeation and retention (EPR) effect, prolong circulation time of the loaded active agents, minimize toxic effects to healthy cells and overcome multidrug resistance. In addition, enhanced bioavailability and sustained release of the incorporated active ingredients can be achieved by nanocarriers mediated delivery.

Co-delivery of drugs and nucleic acids like plasmid DNA (pDNA) vectors, double stranded RNAs (dsRNAs), short hairpin RNAs (shRNAs), micro RNAs (miRNAs), small interfering RNAs (siRNAs) etc. has been shown to overcome various drawbacks of chemotherapeutics. Most of the genetic materials utilize RNA interference mechanism to knock down the expression of specific genes responsible for cancer cell proliferation. Dose of toxic chemotherapeutic drugs needed for clinical efficiency can be substantially reduced using the combinatorial approach, thereby minimizing the side effects of chemotherapeutics. The genetic materials cannot be administered as such in to systemic circulation for the serum nucleases will facilitate their degradation. Further, cellular entry of these nucleic acids is extremely restricted due to their poly anionic nature, high molecular weight and inherent instability. Hence it is essential to develop a suitable formulation which can dispose the loaded cargos viz. drugs and nucleic acids, by overcoming the systemic and cellular barriers. The main objective of present research work was to develop cationic polymeric nanosystems for intracellular delivery of drugs and nucleic acids. The study involves synthesis and characterization of cationic amphiphilic graft co-polymers of low molecular weight PSMA, and evaluation of their intracellular gene delivery efficacy. Various cationic moieties were selected

from different chemical families to synthesize graft co-polymers. These cationic structures included isonicotinic acid, 2-aminoethyl piperazine, glycidyl trimethyl ammonium chloride, L-arginine and spermine. Nanocarriers of the synthesized cationic graft co-polymers were formulated, characterized and evaluated for their biocompatibility, haemocompatibility, endosomal rupturing property and transfection efficiency. Highest endosomal rupturing potential was depicted by quaternized isonicotinic acid grafted polymer followed by spermine and L-arginine grafts. Spermine and L-arginine grafted PSMA derivatives exhibited better transfection efficiency in comparison to the other polymeric grafts.

The cationic nanocarriers of PSMA depicted core shell type morphology, which indicated the feasibility to load hydrophobic anti cancer drugs in them. Since combinatorial delivery of anti cancer drugs and siRNAs is a promising strategy to combat cancer, PSMA was suitably modified to co-deliver both drug and siRNA. Doxorubicin and PLK-1 siRNA were selected as model drug and siRNA, respectively, for the study. A cationic nanosystem was developed by grafting isonicotinic acid and arginine-acetyl lysine conjugate to the PSMA backbone using 4, 7, 10-trioxa-1,13-decanediamine as linker molecule. The cationic polymer could self-assemble in to smooth, spherical micelles with a CMC of ~3 µg∕mL and particle size ranging from ~14 - 30 nm. Doxorubicin was loaded in the micelles with an optimum loading content of ~ 9% w∕w. Efficient complexation of siRNA occured above polymer∕siRNA weight ratio of 10. Doxorubicin and fluorescent labeled siRNA bearing micelles depicted excellent co localization within the cytoplasm of MCF-7 cells. MTT cell viability assay showed synergistic cytotoxic effect of the co delivered active agents. Co-delivery of drug and siRNA in Ehrlich ascites tumor (EAT) bearing Swiss albino mice, using the cationic micelles, significantly enhanced the antitumor efficacy.

A stimuli sensitive polymeric nanosystem based on PSMA, which could enhance tumor specific delivery of the loaded active agents, was developed by grafting multiple disulfide linkages to the polymeric backbone. Anhydride units of the parent polymer were ring opened with methoxy polyethyleneglycol. Arginine and histidine molecules, possessing respective cell penetrating and endosomal buffering properties, were grafted to the polymer through disulfide linkages. The polymeric derivative could easily self-assemble in water to form smooth, spherical micellar structures, with a CMC of ~7 μg∕ mL. Doxorubicin was loaded in the micelles using nanoprecipitation method, with an optimum loading content of ~ 8.6 % w∕w. Efficient binding and condensation of siRNA occurred above polymer∕siRNA weight ratio of 40, and stability of the polyplexes was achieved by coating them with bovine serum albumin (BSA). *In vitro* cell culture studies and *in vivo* tumor regression study have shown synergistic effect of the drug loaded micelleplexes, in arresting cancer cell proliferation.

The thesis is divided into five chapters. First chapter include literature review on the significance of nanotechnology in cancer with specific reference to combinatorial delivery of drugs and nucleic acids. Second chapter details synthesis of cationically modified amphiphilic graft co polymers of poly (styrene-alt-maleic anhydride) (PSMA) and evaluation of their intracellular gene delivery efficacy, *in vitro*. Third chapter discusses development of amphiphilic graft co polymeric micelles of poly (styrene-alt-maleic anhydride), for combinatorial delivery of drug and siRNA, and evaluation of the nanosystem, *in vitro* and *in vivo*. Fourth chapter focuses on the development and optimization of stimuli sensitive nanocarriers based on poly (styrene-alt-maleic anhydride) and evaluation of their efficacy in co delivering drug and siRNA, *in vitro* and *in vivo*. Fifth chapter highlights summary, conclusion and future directions of the outcome of research works performed.

TABLE OF CONTENTS

Chapter II: Synthesis and Evaluation of Cationically Modified Poly (styrene-alt-maleic anhydride) Grafts for Intracellular Gene Delivery

Chapter III: Development of click modified amphiphilic graft co-polymeric micelles of PSMA for combinatorial delivery of doxorubicin and PLK-1 siRNA

Chapter IV: Development of stimuli sensitive polymeric micelles based on poly (styrene-alt-maleic anhydride) for combinatorial delivery of doxorubicin and PLK-1 siRNA

LIST OF FIGURES

Chapter III

NEt$_3$,RT,12 h (dry CH$_2$Cl$_2$) (v) DIPEA, CuI, RT,N$_2$, 24 h (vi) DMF: Piperidine (1:1v/v), RT, 3 h (vii) HBTU,DIPEA, 0 ℃ - RT, 12 h (viii) (CH$_3$CO)$_2$O, NEt$_3$,RT,12 h (dry DMF) (ix) TFA: triisopropylsilane: water (95 :2.5 : 2.5 v/v/v), RT, 3 h

LIST OF TABLES

Chapter V

ABBREVIATIONS

ABC	ATP binding cassette
ADME	Absorption, distribution, metabolism and elimination
AFM	Atomic force microscopy
ATR-FTIR	Attenuated total reflectance- Fourier transform infrared spectroscopy
BSA	Bovine serum albumin
CCC	Central composite circumscribed
CCD	Central circumscribed design
CCF	Central composite faced
CCI	Central composite inscribed
CK-MB	Creatine kinase-MB
CLSM	Confocal laser scanning microscopy
CMC	Critical micelle concentration
CRISPR	Clustered regularly interspaced short palindromic repeats
CuI	Copper Iodide
Da	Dalton
DCC	N,N' dicyclohexylcarbodiimide
DCM	Dichloromethane
DLS	Dynamic light scattering
DMAEMA	2-(dimethylamino)ethyl methacrylate
DMEM	Dulbecco's modified Eagle's medium
DMF	Dimethylformamide
DMSO	Dimethyl sulfoxide
DNA	Deoxyribonucleic acid
DNase I	Deoxyribonuclease I
DOE	Design of experiments
Dox	Doxorubicin
dsDNA	Double stranded deoxyribonucleic acid
dsRNA	Double stranded ribonucleic acid
EAT	Ehrlich ascites tumor

EDC	1-Ethyl-3-(3-dimethylaminopropyl)carbodiimide
EDTA	Ethylenediaminetetraacetic acid
EGFR2	Epidermal growth factor receptor 2
EphA2	Ephrin type-A receptor 2
EPR	Enhanced permeation and retention effect
FACS	Fluorescence-activated cell sorting
FBS	Fetal bovine serum
FESEM	Field emission scanning electron microscopy
GFP	Green fluorescent protein
GPC	Gel permeation chromatography
GSH	Glutathione
GSSG	Glutathione disulfide
h	hours
H&E	Haematoxylin and Eosin
HPV	Human papillomavirus
HR-TEM	High-resolution transmission electron microscopy
HSP47	Heat shock protein 47
hTERT	Human telomerase reverse transcriptase
Ig	Immunoglobulin
kDa	Kilo Dalton
LCST	Lower critical solution temperature
MGMT	Methylguanine-DNA methyltransferase
miRNA	Micro RNA
Mol.wt	Molecular weight
MMPs	Matrix metalloproteinase
MRI	Magnetic resonance imaging
mRNA	Messenger RNA
MRP1	Multidrug resistant protein 1
MSNPs	Mesoporous silica nanoparticles
MTT	3-(4,5-dimethylthiazol-2-yl)-2,5-diphenyltetrazolium bromide
M_w	Weight average molecular weight

N$_2$	Nitrogen gas
NEt$_3$	Triethyl amine
NHS	N-hydroxysuccinimide
NMR	Nuclear magnetic resonance
NPs	Nanoparticles
PAsp (AED)	Poly (N-(2,2'-dithiobis (ethylamine) aspartamide)
PBS	Phosphate buffer saline
PCL	Poly (caprolactone)
PDI	Polydispersity index
PDMAEMA	Polydimethylaminoethyl methacrylate
pDNA	Plasmid DNA
PDPA	Poly (2-(diisopropyl amino) ethyl methacrylate)
PEG	Poly (ethylene glycol)
PEI	Polyethylenimine
P-gp	P-glycoprotein
PI	Propidium iodide
PLK-1	Polo like kinase 1
PNIPAM	Poly(N-isopropylacrylamide)
PSMA	Poly (styrene-alt-maleic anhydride)
RBC	Red blood cell
RES	Reticuloendothelial system
RFP	Red fluorescent protein
RISC	RNA induced silencing complex
RISUG	Reversible inhibition of sperm under guidance
RNA	Ribonucleic acid
RNAi	RNA interference
RNase	Ribonuclease
ROS	Reactive oxygen species
RTPCR	Real time polymerase chain reaction
SCID	Severe combined immunodeficiency
Scr	Scrambled

sec	Seconds
SEM	Scanning electron microscopy
shRNA	Short hairpin RNA
siRNA	Small interfering RNA
TALENs	Transcription activator like effector nucleases
TEM	Transmission electron microscopy
TFA	Trifluoroacetic acid
TNBS	2,4,6-Trinitrobenzenesulfonic acid
TNF-α	Tumor necrosis factor alpha
TSLs	Thermosensitive liposomes
UV	Ultra-violet
VEGF	Vascular endothelial growth factor
W	Watt
w.r.t.	With respect to

CHAPTER I

Introduction & Literature Review

CHAPTER I

Introduction & Literature Review

1.1. Cancer

Multiple mutations in a single cell cause the cells to proliferate out of control leading to cancer. Cancer cells differ from the healthy cells by specific phenotypic variations such as rapid cell division, invasion of adjacent tissues, enhanced metabolic rate and altered morphology [1]. Transformation from a normal cell to a tumor cell is a multistage process involving acquisition of various characteristics such as sustained proliferative signaling, evading growth suppressors, and deregulation of cellular energetics, overcoming immune destruction, enabling replicative immortality, tumor promoting inflammation, angiogenesis, metastasis, genome instability and resistance to cell death. Tumor lesion is constituted by a heterogenous mixture of fibroblasts, stem cells, cancer cells, immune inflammatory cells, progenitor cells, endothelial cells etc. as depicted in figure 1.1 [2].
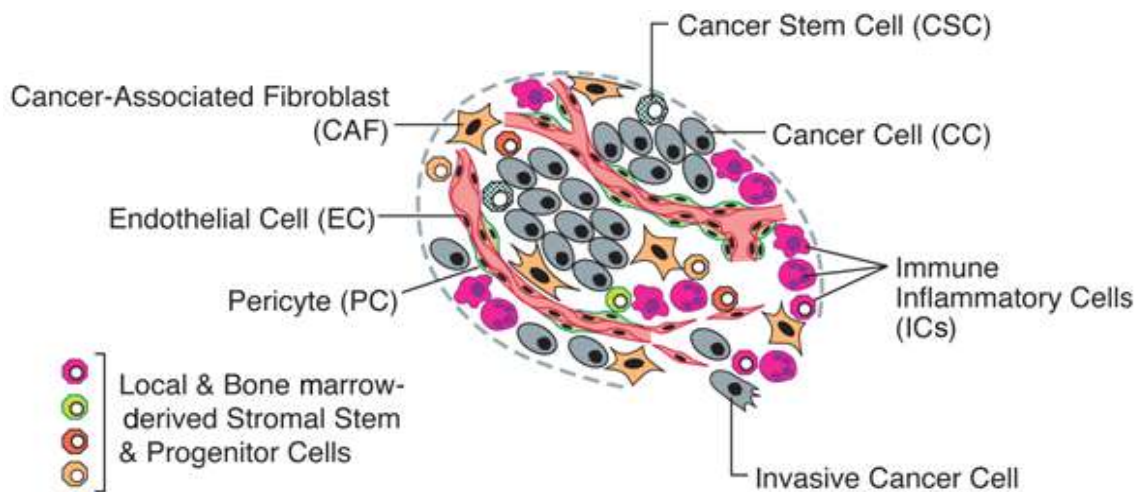
Figure 1.1. Biology of tumor (adapted from Hanahan et al. [2])

Factors responsible for cancer development can be broadly categorized as genetic, physical (radiations with ionizing property), chemical (known carcinogens such as tobacco smoke,

asbestos, arsenic etc.) or biological (infections caused by viruses, bacteria etc). Stress, polluted environment, reduced physical activity, unhealthy diet, and aging are also considered as cancer risk factors. Efficiency of cellular repair mechanisms get impaired with age resulting in the increased vulnerability of genome of an individual to the attack of carcinogens. Chronic infectious conditions like hepatitis B, human papillomavirus (HPV) and human immune deficiency virus (HIV) infections are also reported to enhance the risk of cancer [3, 4].

Morbidity and mortality occurring due to cancer is more than that due to various diseases like HIV, malaria and tuberculosis, combined. In developed countries, cancer is the second leading cause of mortality (first is cardiovascular disease) and in developing countries, it is the third leading disease resulting in death (first and second being cardiovascular and infectious diseases, respectively) [3] . Based on the estimates of International Agency for Research on Cancer (IARC), 14.1 million new cancer cases were reported worldwide, in 2012. Approximately 8 million of these cases were from economically developing countries. These estimates exclude non-melanoma skin cancers as they are not recorded in cancer registries. Cancers of prostate, lung and colorectal were diagonised predominantly among males, in developed countries, whereas breast, colorectal and lung cancers were more prevalent among women. In developing countries, male population were mostly diagonised with lung, liver and stomach cancers, and women with breast, cervix uteri and lung cancers. The global burden of cancer is expected to rise to 21.7 million new cases and 13 million deaths, by 2030, due to aging of the population. However, change in lifestyles such as smoking, physical inactivity, poor diet and fewer pregnancies can probably cause rise in the estimated cancer burden [3,4].

1.2. Cancer treatment strategies

Surgery, radiation, and chemotherapy are the commonly employed methods to treat cancers [5]. Surgery can be employed to diagnose, treat, or even prevent cancer in certain cases. It is a potential treatment mode for cure, especially if the cancer has not spread to other areas of the body. Radiation therapy uses high-energy radiation to shrink the tumors and kill cancer cells. X-rays, gamma rays, and charged particles are the commonly used radiations for cancer treatment. The radiation can be externally applied by a machine which is called external-beam radiation therapy, or it may be delivered using radioactive material kept near to the tumor region termed as internal radiation therapy, also called brachytherapy. Approximately half of all cancer patients receive some type of radiation therapy during the course of treatment. However, surgery and radiation are ineffective when the tumor is malignant, where the cancer cells could have migrated to other parts of the body [6]. Administration of antineoplastic drugs alone or in combination, following a standardized treatment regimen, to treat cancer is called chemotherapy [7]. Due to its effectiveness in killing cancer cells, chemotherapy has emerged as a significant and integrated part of cancer treatment. Drugs belonging to various chemical categories like antimetabolites, hormone inhibitors, topoisomerase inhibitors, corticosteroids, alkylating agents, antitumor antibiotics etc. are often employed for chemotherapy. Combination of different chemotherapeutic drugs can be used to enhance the clinical efficacy of treatment. Factors deciding the optimized chemotherapy regimen include type and stage of the cancer, age and health of patient, types of cancer treatments given in the past etc. [8-10].

1.3. Limitations of chemotherapy

Despite significant anticancer efficacy chemotherapeutic drugs have various limitations such as-

3

1. Non specificity: The chemotherapeutic drugs usually cause potential damage to actively dividing normal cells like hair follicle cells, cells of blood and bone marrow, those lining reproductive and digestive tracts etc. This non specific cell damage leads to serious side effects in patients [11].

2. Poor solubility

Most of the clinically employed chemotherapeutics are hydrophobic in nature which makes them less soluble in aqueous conditions. This result in low bioavailability, patient to patient variability and difficulty in formulating them to appropriate dosage form. The solubility of these drugs in pharmaceutical dosage forms is usually improved with the help of surfactants like Cremophor® EL and Cremophor® RH 40. These surfactants can cause severe adverse effects such as hypersensitivity, peripheral neuropathy etc. [12].

3. Multidrug resistance

Efflux pumps such as P-glycoprotein (P-gp) in the cancer cell membrane can facilitate the transport of drug molecules out of cancer cells. This will drastically reduce the efficacy of therapy and enhance cancer cell resistance to the chemotherapeutic drugs [13].

Application of nanosystems for delivering chemotherapeutics has been established as an effective strategy to overcome the limitations of conventional chemotherapy.

1.4. Significance of nanotechnology in cancer

The prime objective of designing a chemotherapeutic regimen is to attain desired therapeutic drug concentration in tumor cells while minimizing side effects to healthy cells. Application of nanotechnology in cancer therapeutics involves a multidisciplinary research comprising medicine, biology, chemistry and engineering aspects. Incorporating the chemotherapeutics in to nanocarriers has been successfully employed as a potential strategy to achieve tumor specific

delivery and better therapeutic efficacy, with minimal side effects. These nanocarriers possess unique features, as compared to conventional drugs, which make them suitable for accomplishing more efficient clinical efficacy in cancer therapy. Significant advantageous features of the nanocarriers used in chemotherapy are given below [14] -

- Nanocarriers can selectively target cancer cells by enhanced permeation and retention (EPR) effect.

- Nanocarriers can incorporate large amount of therapeutic payload.

- Multiple active ingredients (drugs, genetic materials, imaging agents etc.) can be encapsulated in same nanocarriers facilitating their combinatorial delivery to cancer cells.

- Nanocarriers can overcome multidrug resistance of cancer cells.

- Nanocarriers offer protection to labile therapeutic agents during *in vivo* transit events.

- Systemic circulation time and tissue distribution of the active ingredients can be significantly improved using nanocarriers.

- Surface functionalization of nanocarriers can be performed for imparting them with additional advantageous features like active targeting, stealth nature etc.

1.4.1. Overcoming multidrug resistance of cancer cells using nanocarriers

During the course of chemotherapy, cancer cells develop resistance to various anti cancer drugs by host related, genetic or epigenetic mechanisms. This phenomenon is termed as multi drug resistance. MDR mechanisms have been extensively studied although not all have been elucidated. Over expression of adenosine triphosphate (ATP) binding cassette (ABC) transporters is one of the important mechanisms causing MDR in cancer cells. These proteins can efflux a wide spectrum of chemotherapeutic drugs using ATP driven energy. P-glycoprotein, a membrane transporter protein of ABC super family, is one of the prominent efflux pumps over

expressed in cancer cells. Entry of drugs to the cancer cells is facilitated by passive diffusion following which a major portion of the uptaken drugs will be recognized and effluxed out by efflux pumps. This put forth the necessity of administering high doses of conventional chemotherapeutics, for accomplishing clinical efficacy in patients. Since all the conventional anticancer drugs have deleterious side effects to normal cells, administration of their high doses reduces the benefit/risk ratio. Nanocarriers enter the cells via endocytosis and release the therapeutic load within cytosol. Endocytosis mediated cellular uptake can bypass efflux pumps and enhance efficiency of treatment. Overcoming multidrug resistance using nanocarriers has been experimentally demonstrated by various research groups [15-17].

1.4.2. Nanocarriers mediated specificity of chemotherapy

Nanocarriers can selectively dispose the loaded drugs in cancer cells by passive and active targeting. Using these targeting strategies high therapeutic payload can be achieved in cancer cells thereby minimizing systemic toxicity.

1.4.2.1. Passive targeting of nanocarriers

High metabolic process is a characteristic feature of solid tumors, which arises due to their actively dividing pattern. More blood supply is needed to meet the high metabolic requirements of cancer cells, which in turn leads to the formation of new blood vessels through a process called neoangiogenesis. The so formed blood vessels and capillaries have structural irregularities such as high permeability, large gaps between the vascular endothelial cells etc. Unlike the endothelial cells of normal blood vessels with tight endothelial junctions, tumor vasculature endothelial cells have wide fenestrations with effective cut-off pore size ranging from 300-700nm [17]. In addition, tumor microenvironment is characterized by impaired lymphatic drainage system. Nanocarriers can easily penetrate the tumor tissues utilizing their leaky

vasculature, and shall be retained there due to ineffective lymphatic drainage. This process is termed as enhanced permeation and retention (EPR) effect as shown in figure 1.2. Various other pathophysiological factors promoting the extravasation of nanocarriers to solid tumors such as tumor necrosis factor, bradykinin, nitric oxide, prostaglandins etc. contribute to the enhancement of EPR effect. This leads to passive targeting of nanocarriers and improves bioavailability of loaded chemotherapeutic drugs, to the tumor tissues.
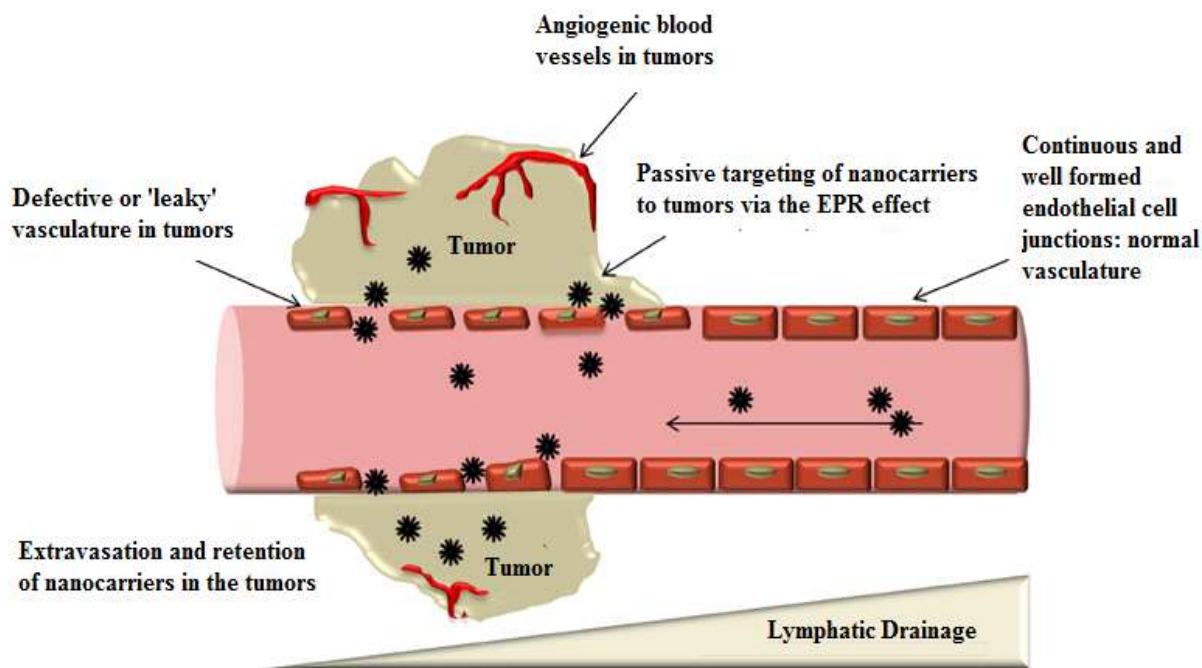
Figure 1.2. Enhanced permeation and retention (EPR) effect of nanocarriers in solid tumors (adapted from Jhaveri et al. [18])

1.4.2.2. Active targeting of nanocarriers

Active targeting of nanocarriers to tumor cells is considered as an efficient complementary strategy to passive targeting, which will further improve therapeutic efficacy of the nanomedicine. In comparison to healthy cells, tumor cells significantly overexpress various receptors/proteins on their surface, due to their typical pathophysiological characteristics. Active

targeting is a ligand mediated targeting process, in which targeting ligands coupled to the surface of nanocarriers selectively bind to their complementary receptors, and delivers the loaded active agents, in specific sites of the body. For active targeting of cancer cells, targeting ligands are chosen based on their affinity and selectivity to the receptors overexpressed on cancer cells (Figure 1.3.). Cellular uptake of active targeted nanocarriers is facilitated by receptor mediated endocytosis, bypassing the efflux mechanisms of cancer cells. Multivalent characteristic of nanocarriers enhances the interaction of coupled targeting ligands with their complementary receptors on cancer cells. This increases the binding ability of nanocarriers to cancer cells and their intracellular distribution, leading to high concentration of active agents within cancer cells. Folic acid, aptamers, monoclonal antibodies, peptides etc. are some of the commonly employed ligands for tumor cell targeting [19-21].
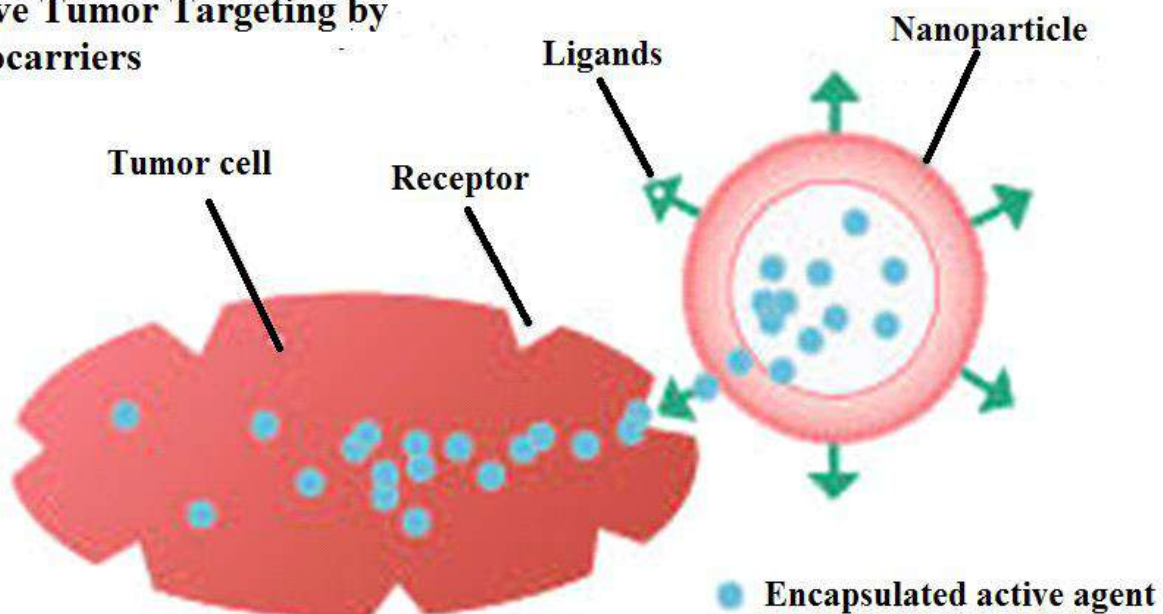
Figure 1.3. Active targeting of tumor cell [22]

1.4.3. Nanocarriers for cancer chemotherapy

A wide range of nanocarriers have been designed and investigated for their application in cancer therapy owing to their versatility in composition and surface functionalities. Nanocarriers can be obtained in a variety of sizes, shapes and chemical compositions for achieving therapeutic efficacy. Absorption, distribution, metabolism and elimination (ADME) of active ingredients shall be modified by the physicochemical properties of nanocarriers such as size, surface charge, hydrophilic-hydrophobic ratio etc. Modification of these parameters has been shown to have profound impact on *in vivo* behavior of nanocarriers and their efficacy as drug delivery vehicle [23]. The most commonly employed nanoplatforms for cancer chemotherapy include polymer based nanocarriers (micelles, polymersomes, nanospheres, nanocapsules), lipid based nanocarriers (liposomes, solid lipid nanoparticles, nanostructured lipid carriers, nanoemulsions), metallic nanocarriers, dendrimers etc [24]. Nanocarriers can effectively reduce the toxic side effects of chemotherapeutic drugs. Stimuli responsive nanocarriers can be designed in such a way as to secure the loaded active ingredients in the absence of stimuli and facilitate their release in response to the stimuli. Simuli which are inherent and intrinsic to the tumor tissues such as acidic pH, higher temperature, redox environment or activity of some enzymes can be used for enhancing the disposition of loaded drugs, specifically in cancer cells. Externally applied stimuli such as magnetic field, temperature, ultrasonic waves etc. have also been explored for the tumor specific drug disposition [25, 26].

1.4.3.1. Thermoresponsive systems

Thermoresponsive nanocarriers can promote the delivery of loaded drug molecules to tumor cells which are locally heated (~40-42 °C), simultaneously minimizing the release at normal body temperature (~37 °C). Lipid or polymer based materials which depict lower critical solution

temperature (LCST) can constitute thermoresponsive nanocarriers. Localized heating is normally achieved using radiofrequency waves, temperature-controlled water sacks or miniature annular-phased microwave arrays [27]. Thermoresponsive liposomes (TSLs) have been extensively investigated for tumor therapy. Phase transition of the constituent lipids and the resulting conformational changes of lipid bilayers induce thermoresponsive nature to liposomes. ThermoDox® from Celsion Corporation is an example of thermoresponsive liposome which is in clinical trials (phase II) for the treatment of breast and colorectal cancers [26]. Al-Ahmady et al. formulated temperature sensitive leucine zipper peptide–liposome hybrids, combining features of traditional TSLs with the dissociative, unfolding characteristics of a thermosensitive peptide [28]. Poly(N-isopropyl acrylamide) (PNIPAM) and poly(γ-2-(2-(2-methoxyethoxy)-ethoxy)ethoxy-ε-caprolactone) –b– poly(γ-octyloxy-ε-capro-lactone) are examples of polymer based thermoresponsive materials which have been widely employed for thermoresponsive drug delivery in cancer [29].

1.4.3.2. Magnetically responsive nanosystems

Magnetically responsive systems are either guided under the influence of a permanent magnetic field or act by elevating temperature in the presence of alternating magnetic field. Drug accumulation at the tumor site can be achieved using magnetic responsive nanocarriers, under the magnetic guidance. Polymer coated magnetite (Fe_3O_4) or maghemite (Fe_2O_3) nanoparticles have been widely explored as magnetically responsive nanosystems. Encapsulation of these metallic nanoparticles in to liposomes to form magnetic liposomes has also been attempted for cancer therapy [27, 30]. These nanocarriers can also be employed for the selective heating of tumors (hyperthermia). Magnetic nanoparticles can be coated with thermosensitive polymers and

liposomes to modulate drug release by magnetically induced heating.. Satarkar et al. depicted controlled drug release by incorporating Fe_3O_4 NPs in crosslinked PNIPAM hydrogels [31].

1.4.3.3. Ultrasound responsive nanocarriers

Ultrasound waves can induce drug release from nanocarriers due to the thermal and mechanical effects of cavitation. Cavitation can lead to destabilization of nanocarriers thereby enhancing their permeability to the loaded drug. Advantageous features of ultrasound triggered drug delivery are non-invasiveness, absence of ionizing radiations and feasibility to regulate depth of tissue penetration [32]. Echogenic liposomes or bubble liposomes bearing air pockets or nanoemulsions of liquid PFC44 and xenon loaded bubble liposomes etc. are some of the reported example of ultrasound responsive nanocarriers [33, 34].

1.4.3.4. Light responsive nanocarriers

Light responsive nanocarriers are stimulated after application of irradiations such as ultraviolet (UV) or infrared (IR) [35]. The major limitation of light responsive nanosystems is the inability of UV-Visible light to penetrate deep in to the tissues. Hence, light-responsive drug delivery can only be used for directly illuminated parts of the body such as the eye, skin etc. [27]. Near infrared (NIR) lasers (700-1,000 nm range) can penetrate deeply to tissues due to lower scattering by the tissues. Ability of NIR-absorbing plasmonic materials to transform adsorbed photon energy to heat energy has been used to promote drug release from NIR responsive nanocarriers [36]. You et al. demonstrated enhanced release of doxorubicin from hollow gold nanospheres, on NIR irradiation, and the strategy was shown to minimize systemic toxicity of doxorubicin [37].

1.4.3.5. Enzyme responsive nanosystems

Enzyme responsive nanocarriers trigger drug release in response to the activity of certain enzymes which are up regulated in cancer cells. Proteases, matrix metalloproteinases, phospholipases, glycosidases etc. are some of the examples of these enzymes. Zhu et al. employed short peptide sequences, for coupling TAT functionalized liposomes and PEG chains, which were cleavable by matrix metalloproteinases (MMPs). Once the peptides were cleaved by MMPs, surface bioactive ligands were exposed and resulted in enhanced intracellular penetration and gene-silencing activity of the nanocarriers NPs in tumour-bearing mice [38]. Singh et al. designed drug loaded silica nanoparticles coated with protease enzyme sensitive polymer coatings as a drug release enhancing constituent [39].

1.4.3.6. Redox responsive nanosystems

There is significant difference in redox potential between tumor cells and healthy normals cells. Glutathione (GSH) and glutathione disulfide (GSSG) constitutes a potent redox couple in cells, which mediates intracellular redox homeostasis. GSH is a tripeptide having antioxidant property and possess the ability to cleave disulfide linkages. It protects mammalian cells against oxidative stress. Another biological function of GSH is to facilitate phase II detoxification mechanism of the cells, with the help of glutathione transferases [40]. Expression of GSH in tumor cells is ~ 3-4 folds higher than that in normal healthy cells. This over expression of GSH in cancer cells is their defensive mechanism to detoxify the free radicals formed during cellular metabolism and to eliminate drugs. Endo-lysosomal compartment is also redox-active due to the presence of reducing agents (eg: cysteine) and reducing enzymes like gamma interferon inducible lysosomal thiol reductase (GILT). GSH concentration of extracellular matrix and physiological fluids (2-20 µM) is 100-1000 times lesser than that of intracellular compartment (2-10 mM). This redox

active nature of cancer cells has been utilized for designing redox responsive nanosystems, which can degrade specifically within the cancer cells. The redox responsive nanosystems can remain intact during their transit through physiological fluids and extracellular matrices with low GSH concentration, thereby minimizing burst release of the loaded drug molecules. Nanocarriers with redox responsive nature can be designed by incorporation of disulfide linkages, which can be cleaved in reductive environment. Some of the reported examples of redox responsive nanocarriers include dendrimer-drug conjugates linked through thiol-cleavable bonds, liposomes formulated from a quinone-lipid conjugate, nanogels formed by crosslinking with disulfide linkers etc. The disulfide linkage has been incorporated in the hydrophobic backbone of amphiphilic copolymers for rendering them redox sensitivity. Commonly reported methods for incorporation of disulfide linkages to drug delivery systems are oxidation of thiol groups, using disulfide containing moieties as cross linkers and by exchange reaction of disulfide and thiols [41].

Anticancer efficacy of drugs has been significantly enhanced by delivering them using redox responsive nanocarriers. Ryu et al. formulated micelles constituted from undecanethiol and trimethylene glycol and used for doxorubicin delivery. Micelles have shown GSH dependent doxorubicin release in MCF-7 cells [42]. Han et al. synthesized block copolymer with hyaluronic acid-polycaprolactone, coupled through disulfide linkages, as repeating units of polymer backbone. Nanocarriers of the synthesized polymer depicted enhanced anticancer property of doxorubicin, *in vitro* in SCC7 cells and *in vivo* in SCC7 tumor-bearing mice [43].

1.4.3.7. pH responsive nanosystems

Irregular angiogenesis is a characteristic feature of tumor tissues, which results in rapid deficit of nutrients and oxygen. Energy production in cancer cells is through rapid glycolysis within the

cytoplasm, which is termed as Warbug effect. These salient features of the tumor microenvironment cause accumulation of lactic acid around the tumor tissues, in high concentration. The lactic acid accumulation will lower pH of tumor extracellular environment [44, 45]. Similarly, endolysosomal vesicles exhibit acidic pH (endosomes pH 5-6, lysosomes pH 4-5). Acidic nature of tumor microenvironment and endolysosomal vesicles can be utilized for designing pH responsive nanocarriers in cancer therapy. Two strategies which have been widely employed for designing pH responsive nanocarriers include – synthesizing polymers (polyacids or polybases) carrying ionizable groups that can undergo conformational and/or solubility changes when subjected to environmental pH variation; and incorporating acid-sensitive linkages to the polymer backbone, which will enhance the release of conjugated drug molecules in the tumor microenvironment [27].

pH responsive nanocarriers have been shown to achieve efficient delivery of chemotherapeutic drugs to tumors. Deng et al. reported enhanced release of tumor necrosis factor alpha (TNFα) to tumor cells, when delivered using chitosan NPs. Amino groups of chitosan (pKa ~ 6.3) can get protonated in the acidic pH of tumor microenvironment and lead to swelling of the polymer and enhanced release of loaded active ingredient [46]. Min et al. developed pH responsive micelles of PEG-poly(β-amino ester) for efficient delivery of camptothecin in acidic conditions [47]. Various acid-sensitive linkages have been utilized for conjugating drugs to the nanocarriers, which can selectively release drug in cancer cells and prevent any unwanted release during circulation. Examples of these acid sensitive linkages include acetal, ketal, hydrazone, β-propionate, cis-aconityl etc. [27]. Lane et al. designed a series of linear copolymers of N,N-dimethylacrylamide and 2-hydroxyethylacrylamide to which doxorubicin was conjugated through hydrazone linkage. The polymer-drug conjugate depicted enhanced drug release (~90 %)

in acidic pH, after 24 h of release study [48]. Sun et al. and Wang et al. conjugated doxorubicin to gold nanoparticles via hydrazone linkage and achieved enhanced drug release in MCF 7 cells and antitumor efficacy in female SCID mice [49, 50].

1.5. Gene therapy in cancer

Gene therapy is an approach primarily focused on modifying, deleting or replacing defective genes of target cells such as malignant, primary, circulating tumor cells, metastatic nodules etc. Mutation, aberration, dysfunction or deletion of active genes due to hereditary factors, environmental factors, infections etc. can lead to cancer [51]. Clinical presentations of cancers normally show a branched evolution from primary to metastases. For example, whole − exome sequencing of breast cancer samples indicated that mutations of estrogen receptor genes in breast cancer were in proportion with metastases and not with primary tumors. Top 17 mutated genes were found in metastases samples in comparison to five mutated genes of primary tumors [52]. This branched evolution makes the success rate of gene therapy alone, in treating tumors with heterogenicity and genomic instability, limited. Current approach to combat cancer using gene therapy is being focused on monogenic therapy, where one or more critical gene defects will be targeted. Suitable mode of gene therapy is selected based on the patients' immune status and evaluation of molecular nature of the disease [51].

1.6. Modes for implementation of gene therapy

Gene therapy can be implemented in different ways such as modification or repair of target cell genes, down regulation and induction of silencing. According to the intensity of gene expression, gene therapy can facilitate either cell death (suicide gene therapy) or impaired cell growth (silencing gene). Gene modification can be used to enhance the clinical efficacy of other treatment modalities like chemotherapy, radiation, surgery etc. Prevention of recurrent

malignancies or tumor related complications such as thrombosis can be prevented by repairing the target genes [51].

1.6.1. Suicide gene therapy

Suicide genes are transgenes which can make up apoptosis inducing agents within the cancer cells. These gene products are normally transcribed by promoters thereby accomplishing necrosis. A typical example of the said promoters is *H19* RNA gene. This promoter is highly expressed within the fetal organs and is rapidly cleared after the birth. *H19* RNA gene has been
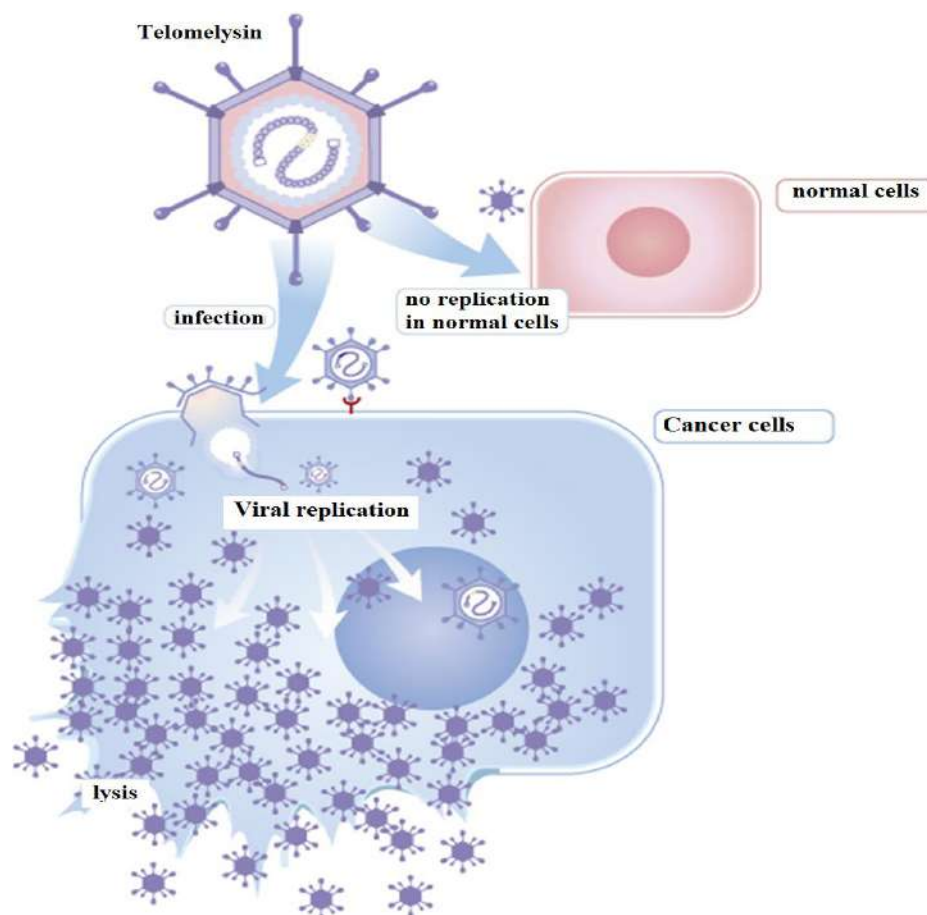
Figure 1.4. Genetically modified adenovirus, telomelysin, acting as a suicide gene to cancer cells (adapted from Oncolys Biopharma Company, Tokyo, Japan [56])

found to have significant role in proliferation of cancer cells, angiogenesis, metastases, drug resistance and survival of cell by overcoming hypoxia. Hence suppression of *H19* RNA gene can result in cancer cell death and necrosis [53, 54]. Human telomerase reverse transcriptase (hTERT) is another prominent promoter acting as a crucial factor in tumorigenesis and immortalization of cells [55]. Suppression of hTERT via agents like telomelysin (OBP-301) shall result in tumor regression and necrosis (Figure 1.4) [56].

1.6.2. Modification of gene

Gene modification is useful in improving the effect of cancer therapeutic strategies. For example, radiation therapy can be efficiently employed with accompanying gene modification. Sensitivity of the tumors to radiation can be enhanced by radiosensitive gene therapy, which facilitates transgene expression in cancer cells [57, 58]. Radioprotective gene therapy is another version of gene modification in which transgenes and their products are distributed to normal cells in order to limit radiation related toxicities to them [59]. Approaches to combine both these contrasting effects are currently being investigated in various preclinical studies.

1.6.3. Gene repair

Gene repair can be accomplished using zinc finger nuclease tagged to lentiviral vector. The viral vector can bind with specific sequence of double stranded DNA (dsDNA) within the nucleus and break it at specific site leading to the formation of a newly edited dsDNA, through endogenous repair mechanisms [60]. Transcription activator like effector nucleases (TALENs), clustered regularly interspaced short palindromic repeats (CRISPR) etc. are other investigated technologies for gene repair [61, 62].

1.6.4. Gene therapy for organelles

Cytosolic organelles can also act as targets of gene therapy. Mitochondria, the organelle mediating metabolic functions of cell, are a potential target. Approximately 300 metabolic disease causing mutations have been found to be secondary to mitochondrial genome defects. Hence gene transfer to mitochondria is being investigated as a mode of gene therapy [63].

1.6.5. Gene silencing

Gene silencing has been achieved utilizing RNA interference (RNAi) mechanism. Gene therapy using RNAi machinery has a significant potential for treatment in cancer and it is also used as a tool in biomedical research [64]. RNAi is a natural cellular mechanism by which a specific mRNA is targeted followed by its degradation with the purpose of decreasing the synthesis of the encoded protein [65,66]. RNAi relies on an intracellular multistep process as shown in figure 1.5.
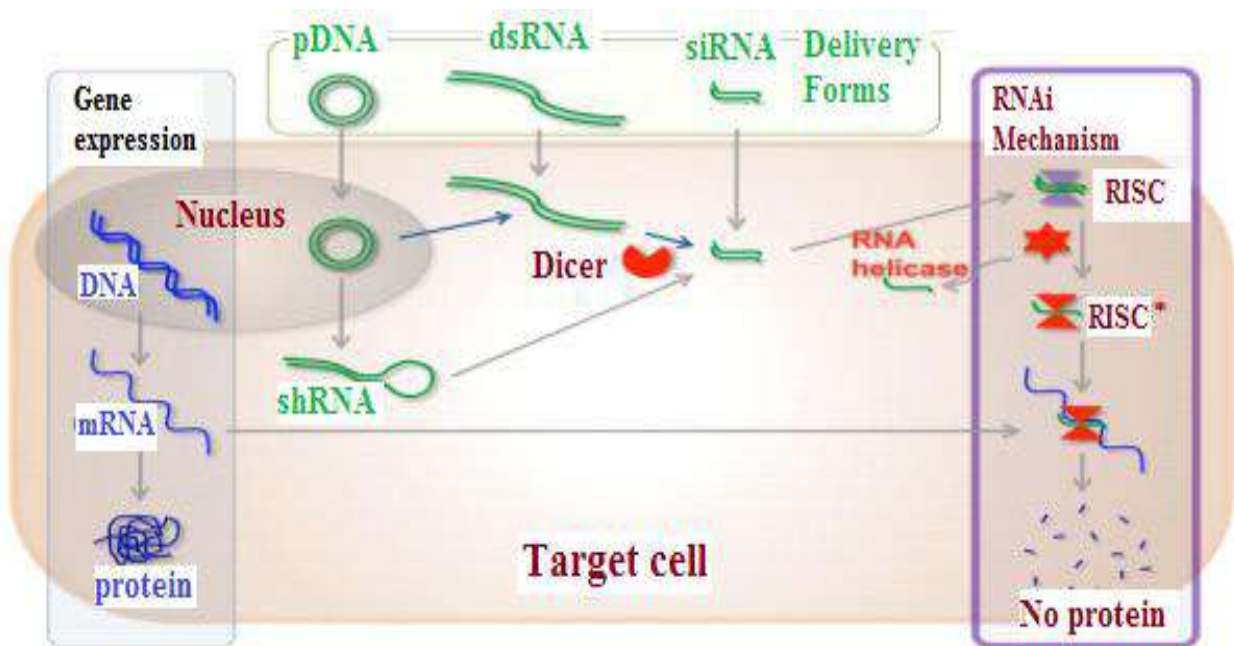
Figure 1.5. RNAi mechanism (adapted from Hannon et al [64])

RNA can be introduced into cells in various forms such as by itself, dsRNA, short-hairpin RNA (shRNA) or plasmid DNA (pDNA). When introduced as pDNA or shRNA, it is transcribed and processed into dsRNA. The dsRNA thus formed is cut by an endoribonuclease called Dicer into smaller siRNAs. In the next step, siRNAs enter the multi-protein cluster, RNA induced silencing complex (RISC). By recognizing the least stable 5' end of the double strand, RNA helicase in the RISC unwinds double-stranded siRNA into two single strands viz. passenger strand and guide strand. The passenger strand is cleaved and discarded. Guide strand is retained and directs a sequence–specific hybridization to the target mRNA which has the complementary sequence to the guide strand. This process leads to the specificity of the RNAi silencing mechanism. The target mRNA is cleaved by RISC and degraded. The degradation is accelerated by the unprotected ends of mRNA. The RISC is recycled for subsequent rounds leading this process to the selective silencing in the target mRNA, which in turn results in decreased expression of the target gene.

1.6.5.1. Advantages of siRNA based gene therapy

- siRNA does not interact with chromosomal DNA, during its course of action, and will not cause any genetic alterations or mutations to target cells [67].

- siRNAs are highly specific to target genes [67, 68].

- Unlike long double stranded RNA (dsRNA) or shRNA, siRNA can exert its action in the native form [68].

- No systemic toxic effects have been reported due to siRNAs [69].

- siRNA does not induce multidrug resistance [67, 68].

1.6.5.2. Limitations of siRNA based gene therapy

For efficient delivery of siRNA *in vivo*, various obstacles have to be overcome. siRNA backbone contains an extra hydroxyl group, unlike DNA, which makes RNA more vulnerable to hydrolysis by serum nucleases [70]. This process results in a shorter half-life of the nucleic acids. Furthermore, siRNA cannot passively diffuse through the cellular membrane by itself due to its

Table 1.1. Lipid and polymer based formulations in clinical trials for RNAi delivery [73]

Name	RNAi target	Carrier type	Therapeutic target	Delivery method (dose)	Study phase
ALN-VSP02	VEGF	Stable nucleic acid lipid nanoparticle	Liver solid tumors	Intravenous (every 2 weeks)	Phase I
EphA2 siRNA-DOPC	EphA2	Neutral DOPC liposome	Advanced solid tumors	Intravenous (twice weekly)	Phase I
ND-L02-s0201	HSP47	Vitamin A-coupled lipid nanoparticle	Healthy normal subjects	Intravenous (single dose)	Phase I
siG12D LODER (Local Drug Elute R)	KRASG12D	Biodegradable polymeric matrix	Pancreatic ductal adenocarcinoma	Placed in the subjects tumor using an endoscopic ultrasound biopsy needle (single dose)	Phase II
CALAA-01	M2 subunit of ribonucleotide reductase (R2)	Cyclodextrin-polymer based nanoparticle	Solid tumors refractory to standard-of-care therapies	Intravenous (30 minutes intravenous infusions, four times within a period of 21 days. Two similar cycles will be done)	Phase I
Atu027	PNK3	Cationic lipid based lipoplex	Advanced solid tumors	Intravenous (single and repeated doses)	Phase I
TKM-080301	PLK-1	Stable nucleic acid lipid nanoparticle	Colorectal, pancreatic, gastric, breast, and ovarian cancers with hepatic metastases	Intravenous	Phase I

inherent instability, high molecular weight (about 13kDa) and polyanionic nature. Because of these limitations, native siRNA has low delivery efficiencies. Chemical modification of siRNA has been shown to reduce the enzymatic degradation [71]. But the formation of entirely new metabolites from these modified siRNA and their possible adverse effects restricts its application. To overcome this challenge, both viral and non-viral carriers have been developed to facilitate siRNA delivery. Non viral carriers are preferable because of their less vulnerability to evoke immune response [72]. Lipid and polymer based nanocarriers have emerged as the most promising vehicles for gene delivery. Various lipid and polymer based formulations, which are presently in clinical trials, for RNAi delivery are provided in table 1.1 [73].

1.7. Significance of gene therapy in combination with chemotherapy

The ability of cancer cells to develop robust drug resistance acts as an insurmountable obstacle for achieving clinical efficacy through chemotherapy. Among the two major mechanisms of drug resistance viz. pump related and non pump related, pump related drug efflux mechanism could be overcome by nanocarriers mediated drug delivery [74, 75]. Various lipid and polymer based nanocarriers have been effectively employed for this cause, and depicted their efficiency in evading the drug efflux pumps like P-gp and multi drug resistance associated protein [76-79]. Unfortunately, the clinical application potential of nanocarriers mediated drug delivery is still hampered by the up regulation of anti-apoptotic proteins in cancer cells. These anti-apoptotic proteins can sensitize the cancer cells to resist chemotherapy by inducing non pump related drug resistance. Hence, for achieving optimal therapeutic effect, simultaneous suppression of these anti-apoptotic gene expressions along with the nanocarriers mediated drug delivery is needed [80, 81]. Combination of gene therapy with chemotherapy can be useful for patients in these stages due to its ability to suppress the genes responsible for anti-apoptotic defense.

1.8. Combinatorial delivery of siRNA and drug in cancer therapy

siRNA is 21-27 base-pair double-stranded RNA which plays a crucial role in initiating the RNAi mechanism. Each strand of siRNA has a 5' phosphate group and a 3' hydroxyl (-OH) group. This structural feature of siRNA can be attributed to the processing by dicer, an enzyme which cleaves either long dsRNAs or short hairpin RNAs into siRNAs [82]. siRNA can be utilized in cancer therapy by down regulating the expression of proteins which are responsible for the antiapoptopic property of cancer cells. Some examples of these target proteins include survivin, P-glycoprotein, polo like kinases etc. Survivin is an apoptosis inhibitor protein which shows differential expression in various human cancers but not in most normal cells. The expression of survivin can be silenced by cleavage and degradation of mRNA specific to the protein using survivin specific siRNA [83]. siRNA can also down regulate P-glycoprotein expression which is responsible for multi drug resistance (MDR) effect. By reducing the MDR effect, efficacy of chemotherapeutic drugs can be enhanced [84]. Polo like kinases are a family of proteins which actively participate in the mitosis of cancer cells. Suppression of these protein expressions can help in preventing the active proliferation of cancer cells. Recent literatures suggest that the most promising approach in utilizing RNAi for effective cancer therapy is to incorporate small interfering RNA (siRNA) and chemotherapeutics in to the same nanocarriers [85, 86]. siRNAs can suppress the expression of targeted anti apoptotic genes, which may accomplish enhanced chemosensitivity of the tumor cells. This strategy may be used to overcome both pump and non pump mediated drug resistance, simultaneously. The fascinating aspect of delivering siRNA and drug using same nanocarrier is that both the active agents will synchronize their *in vivo* transit events and act on same cells, thereby minimizing off target effects. Synergistic effect of both drug and siRNA can be achieved by co-delivering them using same nanocarriers.

1.9. Nanocarriers for combinatorial delivery of siRNA and drug

Non-viral carriers are preferred for nucleic acid delivery because they are easy to handle and generate reduced specific immune responses, compared to viral carriers. The potential for large scale production is another advantage of non-viral carriers [87, 88]. Nanocarriers for co-delivery of siRNA and drugs require additional structural features in comparison to that used for drug delivery. All nucleic acids, including siRNAs, possess abundant phosphate groups in their structure. These phosphate groups can acquire negative charge in aqueous media. Cationic carrier molecules bind and condense the nucleic acids in a reversible, non-damaging manner mainly through electrostatic interactions between the cationic groups of carrier molecules and negatively charged phosphate groups of nucleic acids [89]. Cellular uptake of the nucleic acid – carrier complex mainly occurs via endocytosis. Cationic lipid and polymer based nanosystems are the most commonly used non-viral vectors, which can bind and condense the negatively charged genetic materials into particles of virus like dimensions and prevent their degradation by nuclease enzymes [90]. A suitable nanocarrier which can be employed for co-delivery of drug and siRNA should possess the following characteristics -

- Particle size of the nanocarriers should be in the range of 10-200 nm.

- They should be safe and biocompatible.

- Nanocarriers should have appropriate balance between hydrophobic and hydrophilic parts to facilitate their stable dispersion in physiological fluid and efficient drug loading

- The nanocarriers should stably bind and condense siRNAs through their cationic sites in order to protect them from the attack of serum nucleases.

- Stealth nature is a prerequisite for the nanocarriers to achieve prolonged systemic circulation time.

- Release patter of the therapeutic payload from the nanocarriers should be favorable for *in vivo* applications.

- The nanocarriers should be able to overcome endolysosomal barrier for efficient intracellular delivery of the loaded cargos.

- Nanocarriers should have the feasibility to be scaled up.

- They should possess stability during storage and administration.
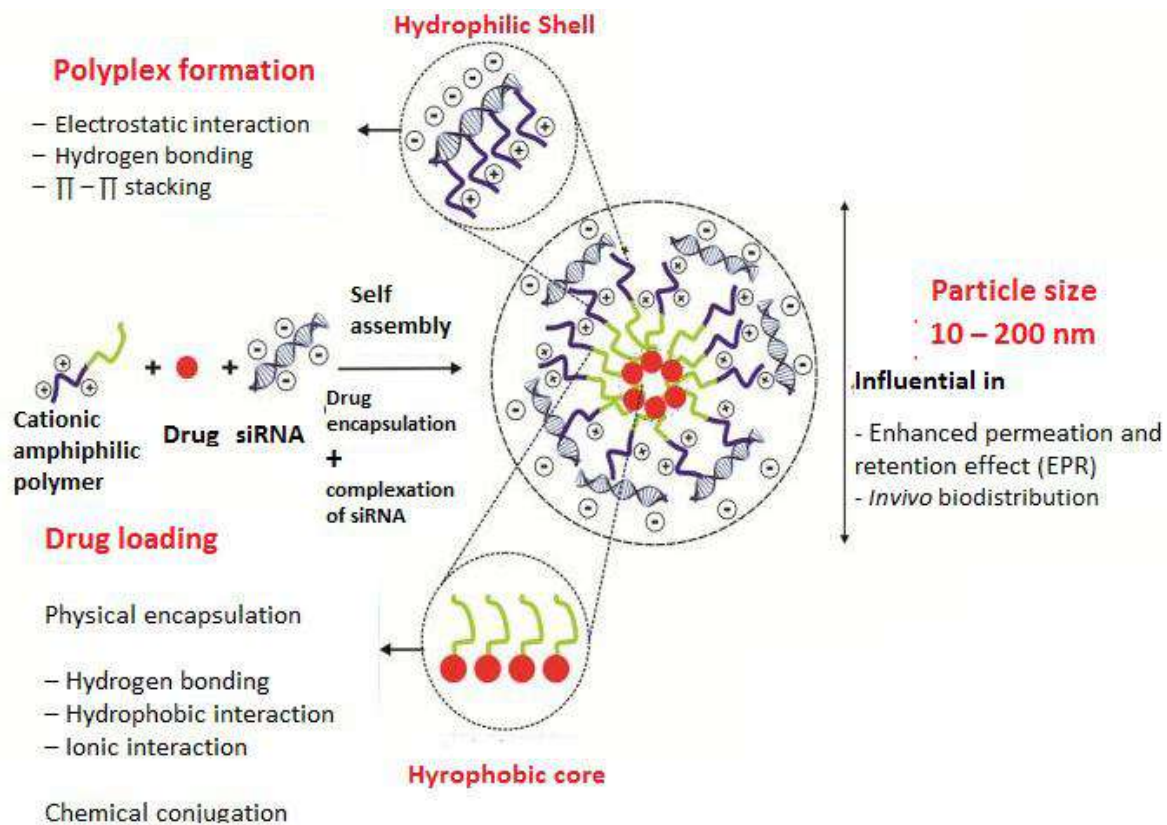
Figure 1.6. Schematic representation of the criteria for designing a suitable carrier for co-delivery of siRNAs and chemotherapeutics

1.9.1. Lipoplexes

Lipoplexes are non-covalent complexes of cationic lipids with negatively charged nucleic acids. Cationic lipid based vectors can spontaneously aggregate in aqueous media with hydrophobic

units (long alkyl chains) forming the hydrophobic cores and positively charged polar head groups providing a polycationic surface [91]. After cellular uptake, lipoplexes can intercalate with the endocytotic membrane and lyse the endocytic vesicles. Subsequently lipoplexes get break down and efficiently release the complexed nucleic acids into cytoplasm. The major disadvantage of cationic lipid based vectors is their relative instability in physiological (i.e. serum containing) conditions, which hinders their use for extensive *in vivo* applications. Suitable
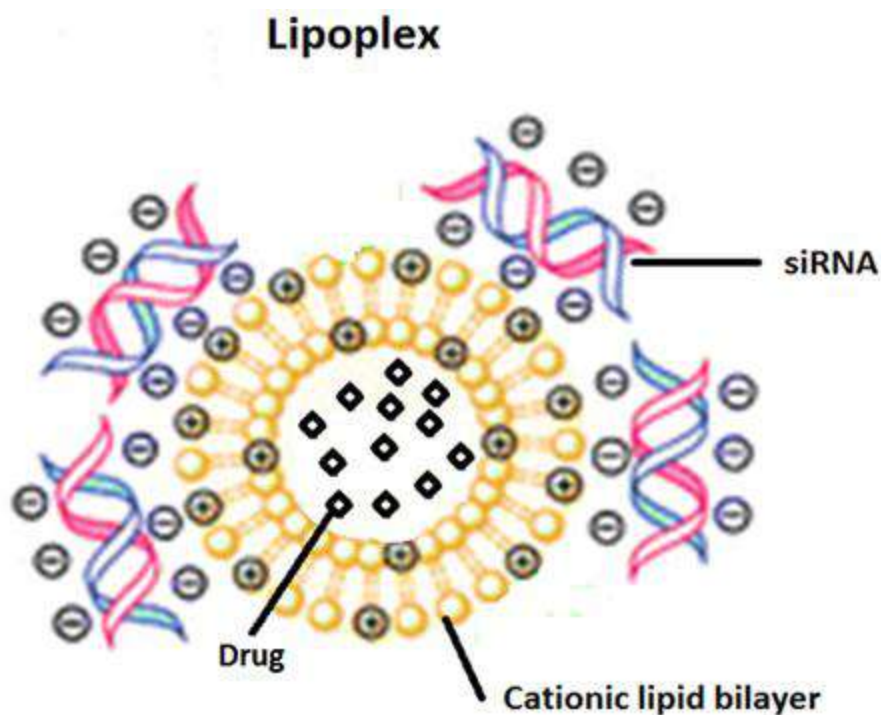
Lipoplex

Figure 1.7. Schematic illustration of a lipoplex co-delivery system

stability enhancers (eg: polyethylene glycol, cholesterol etc.) have to be attached to the lipid based carriers or modification of the carrier itself has to be done for successful in *vivo* application [92, 93]. Lipoplexes can efficiently load hydrophobic drugs to their core and bind nucleic acids to hydrophilic cationic sites.

Kato et al used combinatorial delivery of siRNA targeting the DNA repair protein, O^6-methylguanine-DNA methyltransferase (MGMT), and temozolomide, for improving the clinical efficacy of drug [94]. A novel liposome named LipoTrust was used for transfection and significant improvement in the sensitivity of transduced glioma initiating cells to temozolomide treatment was achieved, *in vitro* and *in vivo*. Saad et al designed cationic liposome based on 1,2-dioleoyl-3-trimethylammonium-propane for co delivery of MRP1 and BCL-2 siRNAs along with doxorubicin and achieved synergistic cytotoxic effects in H69AR, MCF-7/AD and HCT15 cell lines [95]. Liu et al designed a prodrug of doxorubicin by conjugating the drug with stearoyl chloride through N-methyldiethanol as linker [96]. Self assembly of the prodrug in aqueous media was facilitated using 1,2-distearoyl-sn-glycero-3-phosphoethanolamine-N-methoxy-poly (ethylene glycol 2000). Tertiary amines of the prodrug were able to successfully complex and deliver PLK-1 siRNA to tumor cells, *in vitro* and *in vivo*.

1.9.2. Micelleplex nanocarriers

Most commonly reported co-delivery vehicles for siRNA and chemotherapeutic drug payload are based on polymeric materials such as amphiphilic block co-polymers and cyclodextrin based polymers [97]. They are collectively termed as micelleplex nanocarriers due to their ability to self assemble as micelles in aqueous environments. Above critical micellar concentration (CMC), these micelles self-assemble with their hydrophobic regions constituting the core and hydrophilic parts forming the shell [98]. Hydrophobic core of the micelles can incorporate poorly soluble hydrophobic drugs with efficient drug loading and release pattern, thus improving the pharmacokinetics of the loaded drugs. Hydrophilic shells of the micelles are usually cationic in nature which can bind and condense nucleic acids (pDNA, siRNA etc.) [99]. In most of the reported micelleplex delivery systems, polyethylene glycols (PEG) constitute a significant

proportion of the hydrophilic shell. PEG can enhance stability of the micelleplex dispersions in physiological fluids and provide stealth nature to the nanocarriers Commonly reported hydrophobic cores of the micelleplex formulations are based on caprolactones, lactides etc [100-103]. Examples of commonly employed cationic groups include polyethyleneimines, spermine, cationic amino acids, quaternary ammonium compounds etc. Amphiphilic block co-polymeric nanocarriers have been reported to have the ability to prevent drug resistance by themselves. Targeting ligands such as folate and transferrin have also been conjugated in some micelleplex systems and investigated for their site specific delivery. Eventhough targeting ligands have been found to enhance the internalization of micelleplexes to cells *in vitro* overall tumor tissue accumulation of the nanocarriers *in vivo* has not been increased significantly, compared to non targeted micelleplexes [73].

Polymeric materials have become highly preferred candidates for designing co delivery vehicles of drugs and nucleic acids, due to the relative ease in tailoring their physical and chemical properties [104]. Polymer based nanocarriers also offers the feasibility to scale up. Major drawback of polymeric nanocarriers, in comparison to lipid based vehicles, is that they are subjected to endolysosomal degradation. So the polymeric carriers have to be suitably modified with moieties (eg: amine containing compounds) facilitating endosomal disruption and release of the loaded active ingredients [73, 105]. Zhu et al developed cationic block co polymer based on polycaprolactone (PCL) and polydimethylaminoethyl methacrylate (PDMAEMA) for co delivery of VEGF siRNA and paclitaxel [103]. Synergistic effect of the co delivered drug and siRNA in arresting cancer cell proliferation was observed in PC-3 cell line. Chen et al designed reduction and pH sensitive ternary block co polymer, PEG-PAsp (AED) -PDPA, for combinatorial delivery of doxorubicin and BCL-2 siRNA [107]. The ternary block co polymer was constituted with pH

sensitive poly (2-(diisopropyl amino) ethyl methacrylate) (PDPA) and redox responsive poly (N-(2,2'-dithiobis (ethylamine) aspartamide), PAsp (AED). Polyethyleneglycol (PEG) was employed as third constituent of the co polymer for enabling self assembly of the nanocarriers.
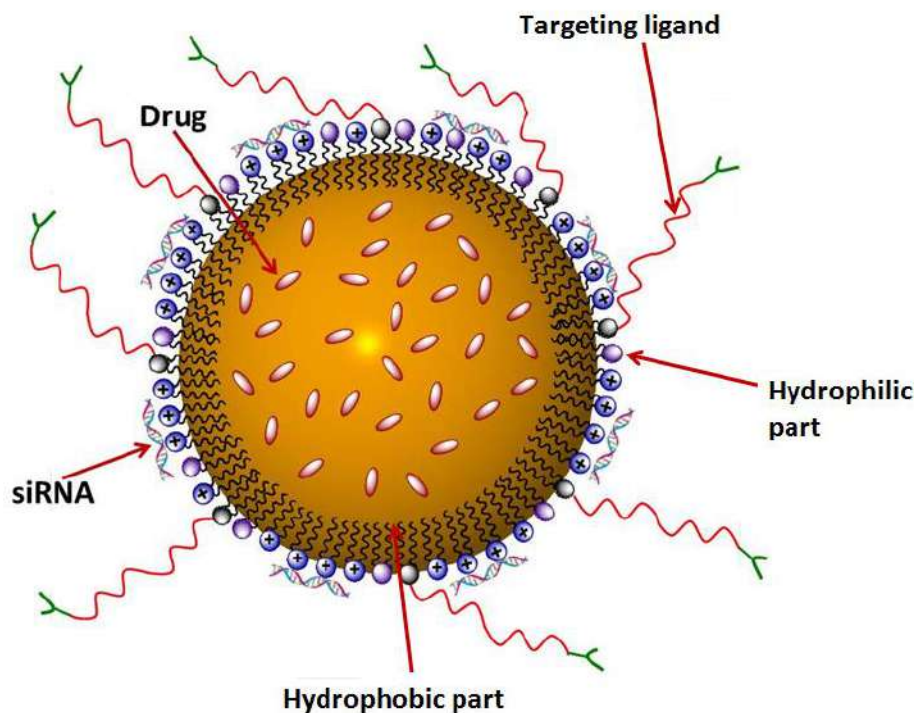
Figure 1.8. Schematic illustration of a micelleplex co-delivery system (adapted from Oregon State University [106])

pH and reduction sensitive release pattern of the loaded drug and siRNA was observed with the nanoplexes. Co delivery of BCL-2 siRNA along with doxorubicin resulted in the down regulation of doxorubicin induced BCL-2 production in human ovarian cancer (SKOV-3) cells. Apoptosis of the cancer cells was enhanced synergistically after the co delivery of active agents. Sun et al synthesized triblock co polymer of poly (ethylene glycol)-b-poly (ε-caprolactone)-b-poly (2-aminoethyl ethylene phosphate) for co delivery of paclitaxel and PLK-1 siRNA [108]. Systemic administration of the micelleplexes in xenograft murine model depicted synergistic tumor suppression.

1.9.3. Miscellaneous nanocarriers for co-delivery of drugs and siRNAs

Mesoporous silica nanoparticles (MSNPs) have been shown to effectively co-deliver hydrophobic anticancer drug such as doxorubicin and siRNAs [109]. Advantage of MSNPs is that they can get localized in the perinuclear region, after cellular uptake, and hence don't need to overcome pump mediated resistance. Quantum dots have also depicted their efficacy in co-delivery of drugs and siRNAs. CdSe/ZnSe quantum dots which were modified with β-cyclodextran and L-arginine/L-histidine were able to successively co-deliver doxorubicin and MDR1 silencing siRNA [110]. Quantum dots possess intrinsic fluorescence which can facilitate their intracellular tracking. Gold nanorods, carbonate-apatite nanoparticles etc. are some other examples of co-delivery vehicles [73].

1.10. Poly (styrene-alt-maleic anhydride)

Poly (styrene-alt-maleic anhydride) (PSMA) is a synthetic co-polymer constituted by styrene and maleic anhydride monomers (Figure 1.8). The polymer is normally synthesized using radical polymerization, employing organic peroxide as initiator. Glass transition temperature of PSMA ranges from 130-160 ℃. Characteristic features of PSMA include heat resistance, dimensional
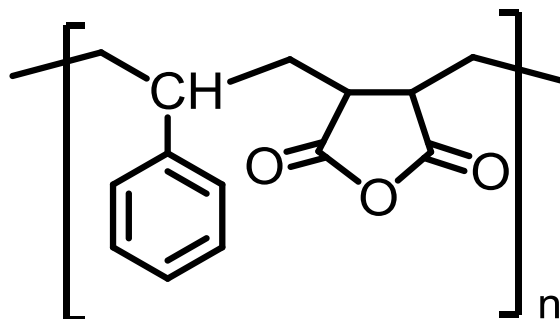
Figure 1.9. Chemical structure of PSMA

stability, transparency and specific reactivity of anhydride groups. Reactivity of the anhydride groups promotes solubility of PSMA in alkaline conditions. PSMA can be obtained in a wide range of molecular weights and maleic anhydride contents [111].

1.10.1. Biomedical applications of poly (styrene-alt-maleic anhydride)

PSMA is a co-polymer which provides ample opportunities for functionalization due to the presence of maleic anhydride groups [112]. Ring opening of maleic anhydride units impart amphiphilic nature to PSMA, thus promoting its self assembly in aqueous media [113]. Protonation of the carboxylate ions of this amphiphilic polymer, at endosomal pH, triggers the conversion of a hydrophilic and biologically inert state to hydrophobic state [114]. In this protonated state, PSMA can destabilize the endosomal membrane facilitating the delivery of incorporated bioactive molecules to cytosol. This pH responsive behaviour of PSMA makes it an excellent carrier for intracellular delivery.

Clinical applications of PSMA have been well studied and reported. Various polymeric prodrugs have been prepared using PSMA with enhanced physicochemical, pharmacokinetic and pharmacodynamic properties. Combination of PSMA with dimethylsulfoxide is being investigated for an application called reversible inhibition of sperm under guidance (RISUG). RISUG is a non surgical, efficient, cost effective and reversible method for male sterilization, which is under phase III clinical trials in India [115]. Low molecular weight (< 6 kDa) PSMA has been successfully employed to deliver neocarzinostatin, an antitumor protein [116]. The protein–polymer conjugate exhibited enhanced lipid solubility and achieved 10 fold increase in the plasma half life of neocarzinostatin. This protein conjugate has been launched in market as an effective treatment for hepatocellular carcinoma, under the commercial name *zinostatin,* which has shown 70-90 % success rate in treated patients [117]. Various other anticancer drugs have

also been successfully conjugated to PSMA and studied. Antitumor activities of drugs like doxorubicin, pirarubicin, YIGSR (a sequence present in laminin) etc. have shown to be significantly improved after incorporating in to PSMA [118-120]. PSMA conjugates were shown to promote immunopotentiation in host cells by activating macrophages, T cells, interferons etc. They also form a non covalent binding with albumin during circulation, which in turn decreases their systemic clearance [121]. Alkylamine derivatives of PSMA have shown enormous potential for intracellular drug delivery due to their pH responsive behavior [122]. Duan et al synthesized conjugate of PSMA with low molecular weight polyethyleneimine (800 Da) for transfection of green fluorescent protein (GFP) expressing plasmid DNA (pDNA). The designed polyplexes exhibited better transfection efficiency than branched polyethyleneimine (average molecular weight of 25 kDa), in MCF-7 and MCF-7∕ADR cell lines [123].

1.11. Doxorubicin

Doxorubicin is an anthracycline antitumor antibiotic, which is also known as Adriamycin or hydroxydaunorubicin, used in chemotherapy. It is employed for the treatment of various cancers such as cancers of breast, endometrium, ovary, testicle, liver, lung, soft tissue, osteosarcoma, rhabdomyosarcoma etc. [124]. Chemical structure of doxorubicin is provided in Figure 1.10. Doxorubicin is commonly used in combination with other chemotherapeutic drugs for cancer treatment. Some examples of these treatment regimens include AC (Adriamycin, Cyclophosphamide), TAC (Taxotere, Adriamycin, Cyclophosphamide), ABVD (Adriamycin, Bleomycin, Vinblastine, Dacarbazine), FAC (5-Fluorouracil, Adriamycin, Cyclophosphamide) etc. [125]. Recommended dose of doxorubicin is 60-75 mg/m^2, per cycle, every three weeks. The drug is normally administered as a single dose per cycle or in divided doses (e.g. day 1 through 3, or days 1 and 8) [126]. Doxorubicin exerts its cytotoxic effect by intercalating with the DNA

base pairs. Intercalation of the planar rings of doxorubicin with nucleotide base pairs of DNA results in inhibition of DNA synthesis and DNA dependent RNA synthesis. Doxorubicin also inhibits topoisomerase II, which is an enzyme needed for relaxing supercoils of DNA for transcription. Doxorubicin also causes free radical mediated cytotoxicity. Doxorubicin molecules can be reduced to semiquinone free radicals by NADPH-dependent cellular reductases. These semiquinone free radicals can react with molecular oxygen to form highly reactive superoxide radicals.
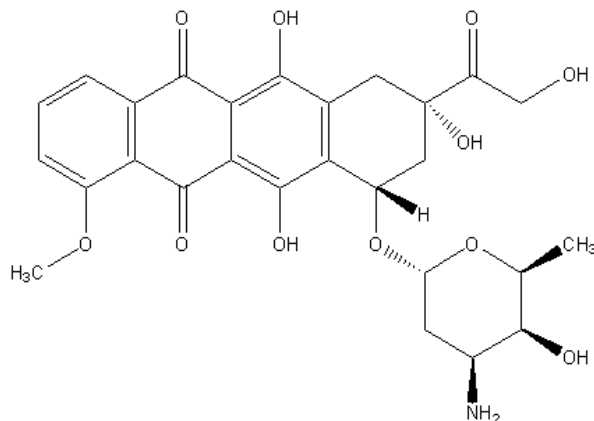
Figure 1.10. Chemical structure of doxorubicin

Primary adverse effect caused by doxorubicin is cardiomyopathy, which can result in congestive cardiac failure. Mechanisms of doxorubicin mediated cardiotoxicity are oxidative stress, down-regulation of genes involved for the synthesis of contractile proteins, blocking of sodium and calcium channels and p53 mediated apoptosis. Other commonly occurring side effects of doxorubicin treatment include hepatotoxicity, nephrotoxicity, myelosuppression and palmar-plantar erythrodysesthesia (PPE) or hand-foot syndrome [127]. Minimizing the side effects of doxorubicin can only be achieved by designing formulations which can selectively and efficiently deliver the drug to cancer cells while sparing normal healthy cells from its cytotoxic

effects. Passively targeting nano-formulations of doxorubicin have been designed and are available in the market under the names Doxil®, Myocet®, Lipodox® etc. Extensive research is being conducted to develop more efficient strategies, such as active targeting, to enhance the clinical efficacy of doxorubicin with minimal side effects. Combinatorial delivery of nucleic acids like siRNA along with doxorubicin is also a potential method to achieve better clinical efficacy with minimal dose of chemotherapeutic drug.   .

1.12. PLK-1 siRNA

Polo like kinase 1 (PLK-1) is a serine-threonine kinase which has significant role in different aspects of mitosis like maturation and regulation of centrosome, separation of sister chromatin, cytokinesis and exit from M phase. Cellular level of PLK-1 remains maximum during the G_2-M phase of mitosis and is rapidly diminished after mitosis. During this phase, phosphorylation of PLK-1 occurs and its kinase function gets stimulated. Nuclear localization and nucleocytoplasmic translocation of the protein is facilitated by the presence of nuclear localization sequence (NLS) in its domain [128]. Mitotic activity of the rapidly proliferating tumor cells is predominantly dependent on polo like kinases. Knock down of polo like kinase proteins, using PLK-1 siRNA, can lead to mitotic arrest and reduced proliferation of cancer cells. Further, inhibitory effect of PLK-1 siRNAs on the cell proliferation of normal cells is weak compared to that of tumor cells [129, 130]. This makes PLK-1 siRNA an attractive candidate for cancer therapy. In short, combination therapy of PLK-1 siRNA with anti cancer drugs can be employed to achieve better pharmacological activity with lower drug dose, thereby reducing the unwanted side effects of chemotherapeutic drugs.

1.13. Experimental designs

Design of experiments (DOE) is a systematic and formal approach to investigate a system or process. It includes designing planned changes to the independent variables of a system or process, by conducting a series of structured tests. The effects of these changes on a pre-defined output can be evaluated. Fascinating aspect of DOE is the feasibility to gain maximum information about a system or process while minimizing resources needed for the same. It also offers significant advantage over 'one change at a time' experimental methods, because it can judge the influence of independent variables acting alone or in combination with other variables to the output [131, 132]. Response surface designs are normally employed for evaluating the differences between formulations.

1.13.1. Response surface designs

Simple linear interaction models are not always adequate for optimization. A mathematical model which can represent curvature with a local optimum is needed, especially when the optimal points remain in the interior of the region where the experiment is to be performed [133]. A simplest such model usually exhibit the quadratic form

$$Y = \beta_0 + \beta_1 X_1 + \beta_2 X_2 + \beta_{12} X_1 X_2 + \beta_{11} X_1^2 + \beta_{22} X_2^2$$

which include linear and squared terms of all factors and products of pairs of the factors.

Designs which can fit such types of models are termed as response surface designs [134]. Central circumscribed design (CCD) and Box- Behnken designs are the two commonly used response surface designs [135]. Inputs of response surface designs have 3-5 distinct values (levels), but all combinations of these levels don't appear in the design.

CCD is a second-order design which provides response surfaces depicting the ranking of each variable according to its influence on the responses studied. This approach can minimize the time and experimental effort to predict the formulation composition which can provide a desired response [136, 137]. CCD can be a factorial or fractional factorial design, in which a center point is augmented with a number of `star points' allowing determination of curvature. Considering the distance between the center of design space and factorial point as ±1 for each factor, the distance between the center of the design space and a star point can be taken as ± α, where |α| > 1. Exact value of α is decided by some properties desired for the design and number of factors included. The number of center point runs to be performed by the design also depends on some properties desired for the design. Number of star points in CCD is always twice as that of the factors involved. Star points indicate extreme levels (low and high) for each factor present in the design [138]. A central composite design can be further classified in to three types such as circumscribed, inscribed and face centered designs. The classification is mainly based on the distribution of star points with respect to the center of the design. Table 1.2 summarizes the properties of the three varieties of central composite designs. Relationships among the different types of central composite designs are illustrated in Figure 1.11.
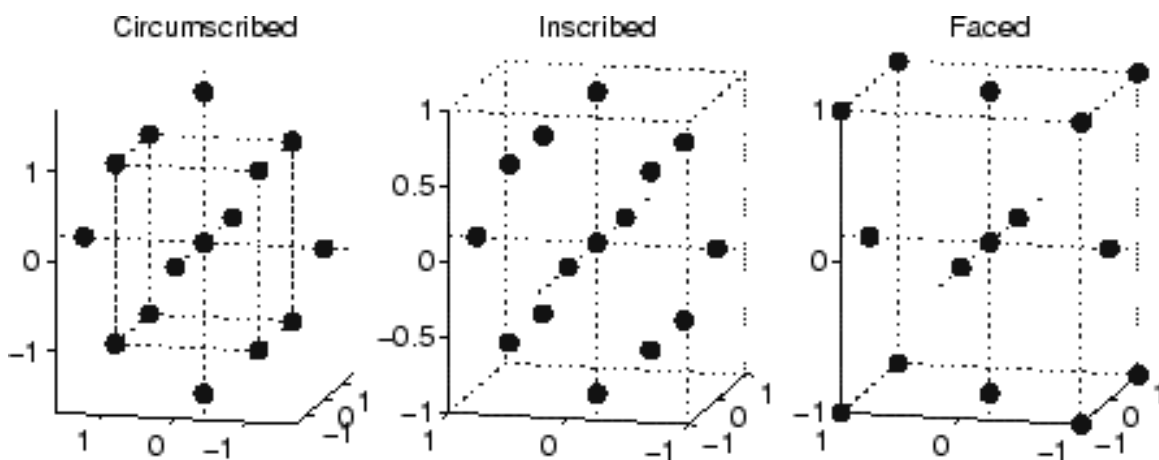
Figure 1.11. Illustration of different types of central composite designs

Table 1.2. Comparative features of three types of central composite designs [139]

Central Composite Designs		
Central Composite Design Type	**Terminology**	**Comments**
Circumscribed	CCC	CCC design distributes the star points at certain distance α, from the center, depending upon the properties of design and factors involved. Star points show new extremes for low and high values of all the factors. CCC designs depict circular, spherical or hyperspherical symmetry and need five levels for each factor involved.
Inscribed	CCI	CCI design can be considered as a scaled down form of CCC design where level of each factor involved in CCC design is divided by α. CCI design also needs 5 levels for each factor.
Face Centered	CCF	CCF design is a form of central composite design where star points are seen at the center of each face of the factorial space so that the distance $\alpha = \pm 1$. This design needs only 3 levels for each factor.

1.13.2. Box-Behnken designs

Box-Behnken designs are response surface designs which require only 3 levels of each factor and fit to a full quadratic model [140]. This design is more applicable when the factors involved are quantitative. Central composite faced (CCF) designs also require only 3 factor levels like Box-Behnken designs. But CCF designs are not rotatable like Box-Behnken designs. Drawback of

Box-Behnken designs is their weak prediction ability in the corners of the cube enclosing the design. This is due to the lack of points at the corners of the cube [141]. Figure 1.12 illustrates a Box-Behnken design involving three factors.
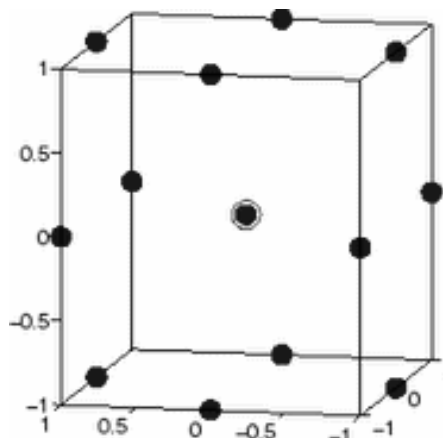
Figure 1.12. Box-Behnken design

1.14. Scope of the present work

Achieving clinical efficacy with minimal adverse effects to normal healthy tissues is the prime objective of ongoing research in cancer therapy. Combinatorial delivery of siRNA, which can knock down antiapoptotic proteins, and chemotherapeutic drug to cancer cells can be used as a potential strategy to achieve this goal. Designing an efficient, cost-effective and scalable delivery vehicle for co-delivery of siRNA and drug is a major challenge persisting in the implementation of drug-nucleic acid co-delivery. Present work explores the application potential of poly (styrene-alt-maleic anhydride) based cationic nanosystems for nucleic acid delivery and combinatorial delivery of drugs and nucleic acids. Cationic nanocarriers of PSMA were developed and evaluated for their co delivery efficacy in cancer cells, *in vitro*, as well as in Ehrlich ascites tumor bearing Swiss albino mice model, *in vivo*, employing doxorubicin as a model anticancer drug and PLK-1 siRNA as a model nucleic acid.

1.15. Objective of the work

The main objective of the thesis research work was to develop cationic polymeric nanosystems, based on low molecular weight PSMA, for nucleic acid delivery and co-delivery of nucleic acid and drug. To achieve this, a systematic design and evaluation procedure was employed as follows-

1. Synthesis and evaluation of cationically modified poly (styrene-alt-maleic anhydride) derivatives for intracellular gene delivery

   • Synthesis and characterization of poly (styrene-alt-maleic anhydride) derivatives grafted with various cationic structures

   • Formulation and characterization of nanoparticles of the synthesized polymeric grafts

   • Evaluation of the cationic nanosystems for biocompatibility and nucleic acid complexation

   • Comparative evaluation of the transfection efficiencies of the formulated polymeric nanosystems

2. Development of click modified amphiphilic graft co polymeric micelles of poly (styrene-alt-maleic anhydride) for combinatorial delivery of doxorubicin and PLK-1 siRNA

   • Synthesis and characterization of arginine-lysine grafted cationic derivative of PSMA

   • Formulation and characterization of the nanocarriers of synthesized polymeric derivative

   • Formulation and evaluation of drug loaded micelleplexes

   • *In vitro* studies - Cellular uptake and cytocompatibility

   • *In vivo* studies – Biocompatibility and anti tumor efficacy of the developed formulation

3. Development of stimuli sensitive nanocarriers of poly (styrene-alt-maleic anhydride) for combinatorial delivery of doxorubicin and PLK-1 siRNA.

- Synthesis and characterization of arginine-histidine grafted PSMA

- Formulation and characterization of the nanocarriers of synthesized polymeric derivative

- Formulation and evaluation of drug loaded micelleplexes

- In vitro studies - Cellular uptake and cytocompatibility

- *In vivo* studies – biocompatibility and anti tumor efficacy of the developed formulation

1.16. Format of the thesis

The thesis has been compiled in the following chapters-

Chapter I   Introduction and literature review

Chapter II   Synthesis and evaluation of cationically modified poly (styrene-alt-maleic anhydride) grafts for intracellular gene delivery

Chapter III   Development of click modified amphiphilic graft co polymeric micelles of poly (styrene-alt-maleic anhydride) for combinatorial delivery of doxorubicin and PLK-1 siRNA

Chapter IV   Development of stimuli sensitive nanocarriers of poly (styrene-alt-maleic anhydride) for   combinatorial delivery of doxorubicin and PLK-1 siRNA.

Chapter V   Summary, conclusions and future directions

References

1.   Ruddon, R.W., *Cancer Biology*. Oxford University Press: **2007**; 4-16.

2.   Hanahan, D.; Weinberg, R., Hallmarks of cancer: The next generation. *Cell* **2011,** 144, (5), 646-674.

3.   Siegel, R.; Ma, J.; Zou, Z.; Jemal, A., Cancer statistics, 2014. *CA-Cancer J. Clin.* **2014,** 64, (1), 9-29.

4.   World   Health   Organization.   http://www.who.int/mediacentre/factsheets/fs297/en/ (accessed May 21, **2015**).

5.   World   Health   Organization.   Cancer   **2012**   [cited   15.4.2012];   Available   from: http://www.who.int/cancer/en/index.html.

6.   Baba, A.; Catoi, C., Principles of anticancer therapy. In *Comparative Oncology*, The Publishing House of the Romanian Academy, Bucharest: **2007**; Available from: http://www.ncbi.nlm.nih.gov/books/NBK9546/.

7.   National Cancer Institute. Types of treatment [cited 15.4.**2012**]; Available from: http://www.cancer.gov/cancertopics/treatment/types-of-treatment.

8.   Liu, Y.; Li, K.; Liu, B.; Feng, S.S., A strategy for precision engineering of nanoparticles of biodegradable copolymers for quantitative control of targeted drug delivery. *Biomaterials* **2010,** 31, (35), 9145-9155.

9.   Wu, J.; Song, C.; Jiang, C.; Shen, X.; Qiao, Q.; Hu, Y., Nucleolin Targeting AS1411 Modified Protein Nanoparticle for Antitumor Drugs Delivery. *Mol Pharm* **2013,** 10, 3555–3563.

10. Kalia, J.; Raines, R.T., Hydrolytic Stability of Hydrazones and Oximes. *Angew Chemie Int Ed* **2008,** 47, 7523–7526.

11. Cross, D.; Burmester, J.K., Gene Therapy for Cancer Treatment: Past, Present and Future. *Clin Med Res* **2006,** 4, 218–227.

12. Chidambaram, M.; Manavalan, R.; Kathiresan, K., Nanotherapeutics to overcome conventional cancer chemotherapy limitations. *J. Pharm. Pharm. Sci.* **2011,** 14, (1), 67-77.

13. Callaghan, R.; Luk, F.; Bebawy, M., Inhibition of the Multidrug Resistance P-Glycoprotein: Time for a Change of Strategy? *Drug Metab Dispos* **2014,** 42, 623–631.

14. Misra, R.; Acharya, S.; Sahoo, S. K., Cancer nanotechnology: Application of nanotechnology in cancer therapy. *Drug Discovery Today* **2010,** 15, 842-850.

15. Heidel, J. D.; Davis, M. E., Clinical developments in nanotechnology for cancer therapy. *Pharm. Res.* **2011,** 28, (2), 187-199.

16. Zhong, Y.; Meng, F.; Deng, C.; Zhong, Z., Ligand-directed active tumor-targeting polymeric nanoparticles for cancer chemotherapy. *Biomacromolecules* **2014,** 15, (6), 1955-1969.

17. Bertrand, N.; Wu, J.; Xu, X.; Kamaly, N.; Farokhzad, O. C., Cancer nanotechnology: the impact of passive and active targeting in the era of modern cancer biology. *Adv. Drug Delivery Rev.* **2014,** 66, 2-25.

18. Jhaveri, A.M.; Torchilin, V.P., Multifunctional polymeric micelles for delivery of drugs and siRNA. *Front Pharmacol* **2014,** 5, 1-26.

19. Gao, H.; Xiong, Y.; Zhang, S.; Yang, Z.; Cao, S.; Jiang, X., RGD and interleukin-13 peptide functionalized nanoparticles for enhanced glioblastoma cells and neovasculature dual targeting delivery and elevated tumor penetration. *Mol. Pharmaceutics* **2014,** 11, (3), 1042-1052.

20. Chen, H.; Chen, Y.; Yang, H.; Xu, W.; Zhang, M.; Ma, Y., et al., A dual-targeting nanocarrier based on modified chitosan micelles for tumor imaging and therapy. *Polym. Chem.* **2014,** 5, (16), 4734-4746.

21. Veeranarayanan, S.; Poulose, A. C.; Mohamed, M. S.; Varghese, S. H.; Nagaoka, Y.; Yoshida, Y., et al., Synergistic targeting of cancer and associated angiogenesis using triple-targeted dual-drug silica nanoformulations for theragnostics. *Small* **2012,** 8, (22), 3476-3489.

22. National Cancer Institute. Tumor seeking nanoparticles [cited 15.9.2006]; Available from: http://nano.cancer.gov/action/news/featurestories/monthly_feature_2006_sep.asp

23. Jabr-Milane, L. S.; van Vlerken, L. E.; Yadav, S.; Amiji, M. M., Multi-functional nanocarriers to overcome tumor drug resistance. *Cancer Treat. Rev.* **2008,** 34, (7), 592-602.

24. Peer, D.; Karp, J. M.; Hong, S.; Farokhzad, O. C.; Margalit, R.; Langer, R., Nanocarriers as an emerging platform for cancer therapy. *Nat. Nanotechnol.* **2007,** 2, (12), 751-760.

25. Cheng, W.; Gu, L.; Ren, W.; Liu, Y., Stimuli-responsive polymers for anti-cancer drug delivery. *Mater. Sci. Eng., C* **2014,** 45, 600-608.

26. Mura, S.; Nicolas, J.; Couvreur, P., Stimuli-responsive nanocarriers for drug delivery. *Nat. Mater.* **2013,** 12, (11), 991-1003.

27. Shao, P.; Wang, B.; Wang, Y.; Li, J.; Zhang, Y., The application of thermosensitive nanocarriers in controlled drug delivery. *J. Nanomater.* **2011,** 2011,1-12.

28. Al-Ahmady, Z. S.; Al-Jamal, W. T.; Bossche, J. V.; Bui, T. T.; Drake, A. F.; Mason, A. J., et al., Lipid-peptide vesicle nanoscale hybrids for triggered drug release by mild hyperthermia in vitro and in vivo. *ACS Nano* **2012,** 6, (10), 9335-9346.

29. Cheng, Y.; Hao, J.; Lee, L. A.; Biewer, M. C.; Wang, Q.; Stefan, M. C., Thermally controlled release of anticancer drug from self-assembled gamma-substituted amphiphilic poly(ε-caprolactone) micellar nanoparticles. *Biomacromolecules* **2012,** 13, (7), 2163-2173.

30. Mahajan, S.; Koul, V.; Choudhary, V.; Shishodia, G.; Bharti, A. C., Preparation and in vitro evaluation of folate-receptor-targeted SPION-polymer micelle hybrids for MRI contrast enhancement in cancer imaging. *Nanotechnology* **2013,** 24, (1), 015603.

31. Satarkar, N. S.; Zach Hilt, J., Hydrogel nanocomposites as remote-controlled biomaterials. *Acta Biomater.* **2008,** 4, (1), 11-16.

32. Sirsi, S. R.; Borden, M. A., State-of-the-art materials for ultrasound-triggered drug delivery. *Adv. Drug Delivery Rev.* **2014,** 72, 3-14.

33. Javadi, M.; Pitt, W. G.; Belnap, D. M.; Tsosie, N. H.; Hartley, J. M., Encapsulating nanoemulsions inside eLiposomes for ultrasonic drug delivery. *Langmuir* **2012,** 28, (41), 14720-14729.

34. Britton, G. L.; Kim, H.; Kee, P. H.; Aronowski, J.; Holland, C. K.; McPherson, D. D et al., In vivo therapeutic gas delivery for neuroprotection with echogenic liposomes. *Circulation* **2010,** 122, (16), 1578-1587.

35. Lu, J.; Choi, E.; Tamanoi, F.; Zink, J. I., Light-activated nanoimpeller-controlled drug release in cancer cells. *Small* **2008,** 4, (4), 421-426.

36. Yang, Y.; Velmurugan, B.; Liu, X.; Xing, B., NIR photoresponsive crosslinked upconverting nanocarriers toward selective intracellular drug release. *Small* **2013,** 9, (17), 2937-2944.

37. You J; Zhang R; Xiong C; Zhong M; Melancon M; Gupta S, et al., Effective photothermal chemotherapy using doxorubicin-loaded gold nanospheres that target EphB4 receptors in tumors. *Cancer Res.* **2014,** 72, 4777-4786.

38. Zhu, L.; Kate, P.; Torchilin, V. P., Matrix metalloprotease 2-responsive multifunctional liposomal nanocarrier for enhanced tumor targeting. *ACS Nano* **2012,** 6, (4), 3491-3498.

39. Singh, N.; Karambelkar, A.; Gu, L.; Lin, K.; Miller, J. S.; Chen, C. S., et al., Bioresponsive mesoporous silica nanoparticles for triggered drug release. *J. Am. Chem. Soc.* **2011,** 133, (49), 19582-19585.

40. Balendiran, G. K.; Dabur, R.; Fraser, D., The role of glutathione in cancer. *Cell Biochem. Funct.* **2004,** 22, (6), 343-352.

41. Torchilin, V. P., Multifunctional, stimuli-sensitive nanoparticulate systems for drug delivery. *Nat. Rev. Drug Discovery* **2014,** 13, (11), 813-827.

42. Ryu, J. H.; Roy, R.; Ventura, J.; Thayumanavan, S., Redox-sensitive disassembly of amphiphilic copolymer based micelles. *Langmuir* **2010,** 26, (10), 7086-7092.

43. Han, H. S.; Thambi, T.; Choi, K. Y.; Son, S.; Ko, H.; Lee, M. C., et al., Bioreducible shell-cross-linked hyaluronic acid nanoparticles for tumor-targeted drug delivery. *Biomacromolecules* **2015,** 16, (2), 447-456.

44. Choi, S. Y. C.; Collins, C. C.; Gout, P. W.; Wang, Y., Cancer-generated lactic acid: A regulatory, immunosuppressive metabolite? *J. Pathol.* **2013,** 230, (4), 350-355.

45. Vander Heiden, M. G.; Cantley, L. C.; Thompson, C. B., Understanding the Warburg effect: The metabolic requirements of cell proliferation. *Science* **2009,** 324, (5930), 1029-1033.

46. Deng, Z.; Zhen, Z.; Hu, X.; Wu, S.; Xu, Z.; Chu, P. K., Hollow chitosan-silica nanospheres as pH-sensitive targeted delivery carriers in breast cancer therapy. *Biomaterials* **2011,** 32, (21), 4976-4986.

47. Min, K. H.; Kim, J. H.; Bae, S. M.; Shin, H.; Kim, M. S.; Park, S., et al., Tumoral acidic pH-responsive MPEG-poly(beta-amino ester) polymeric micelles for cancer targeting therapy. *J. Controlled Release* **2010,** 144, (2), 259-266.

48. Lane, D. D.; Chiu, D. Y.; Su, F. Y.; Srinivasan, S.; Kern, H. B.; Press, O. W., et al., Well-defined single polymer nanoparticles for the antibody-targeted delivery of chemotherapeutic agents. *Polym. Chem.* **2015,** 6, 1286-1299.

49. Sun, T. M.; Wang, Y. C.; Wang, F.; Du, J. Z.; Mao, C. Q.; Sun, C. Y., et al., Cancer stem cell therapy using doxorubicin conjugated to gold nanoparticles via hydrazone bonds. *Biomaterials* **2014,** 35, 836-845.

50. Wang, F.; Wang, Y. C.; Dou, S.; Xiong, M. H.; Sun, T. M.; Wang, J., Doxorubicin tethered responsive gold nanoparticles facilitate intracellular drug delivery for overcoming multidrug resistance in cancer cells. *ACS Nano* **2011,** 5, 3679-3692.

51. Amer, M.H., Gene therapy for cancer: present status and future perspective. *Mol Cell Ther* **2014,** 2, 27-45.

52. Koboldt, D.C.; Fulton, R.S.; Mclellan, M.D.; Schmidt, H.; Kalicki-Veizer, J.; McMichael, J.F.; Fulton, L.L., et al. Comprehensive molecular portraits of human breast tumours. *Nature* **2012,** 490, 61–70.

53. Matouk, I.; Raveh, E.; Ohana, P.; Lail, R.A.; Gershtain, E.; Gilon, M., et al. The increasing complexity of the oncofetal H19 gene locus: Functional dissection and therapeutic intervention. *Int J Mol Sci* **2013,** 14, 4298–4316.

54. Pachnis, V.; Brannan, C.I.; Tilghman, S.M., The structure and expression of a novel gene activated in early mouse embryogenesis. *EMBO J* **1988,** 7, 673–681.

55. Osaki, S.;Tazawa, H.; Hasei, J.; Yamakawa, Y.; Omori, T.; Sugiu, K., et al. Ablation of MCL1 expression by virally induced microRNA-29 reverses chemoresistance in human osteosarcomas. *Sci Rep* **2016,** 6, 28953-28964.

56. Oncolys BioPharma. Telomelysin (OBP-301); Available from: http://www.oncolys.com/en/pipeline/telomelysin.html.

57. Pan, J.; Zhang, S.; Chen, C.; Xiao, S.; Sun, Y.; Liu, C., et al. Effect of Recombinant Adenovirus-p53 Combined With Radiotherapy on Long-Term Prognosis of Advanced Nasopharyngeal Carcinoma. *J Clin Oncol* **2009,** 27, 799–804.

58. Lai, S.Y.; Koppikar, P.; Thomas, S.M.; Childs, E.E.; Egloff, A.M.; Seethala, R.R., et al. Intratumoral Epidermal Growth Factor Receptor Antisense DNA Therapy in Head and Neck Cancer: First Human Application and Potential Antitumor Mechanisms. *J Clin Oncol* **2009,** 27, 1235–1242.

59. Greenberger, J.S., Radioprotection. *In Vivo* **2009,** 23, 323–336.

60. Qasim, W.; Vink, C.A.; Thrasher, A.J., Hybrid Lentiviral Vectors. *Mol Ther* **2010,** 18, 1263–1267.

61. Sun, N.; Zhao, H., Transcription activator-like effector nucleases (TALENs): A highly efficient and versatile tool for genome editing. *Biotechnol Bioeng* **2013,** 110, 1811–1821.

62. Sander, J.D.; Joung ,J.K., CRISPR-Cas systems for editing, regulating and targeting genomes. *Nat Biotech* **2014,** 32, 347–355.

63. Sakhrani, N.M.; Padh, H., Organelle targeting: third level of drug targeting. *Drug Des Devel Ther* **2013,** 7, 585–599.

64. Hannon, G.J., RNA interference. *Nature.* **2002,** 418, 244-251.

65. Agrawal, N.; Dasaradhi, P.V.N.; Mohmmed, A.; Malhotra, P.; Bhatnagar, R.K.; Mukherjee, S.K., RNA Interference: Biology, Mechanism, and Applications. *Microbiol Mol Biol Rev* **2003,** 67, 657–685.

66. Kim, D.H.; Rossi, J.J., RNAi mechanisms and applications. *Biotechniques* **2008,** 44, 613–616.

67. Ryther, R.C.C.; Flynt, A.S.; Phillips, J.A.; Patton, J.G., siRNA therapeutics: big potential from small RNAs. *Gene Ther* **2004,** 12, 5–11.

68. Dorsett, Y.; Tuschl, T., *Drug Disc* **2004,** 3, 318–329.

69. Gavrilov, K.; Saltzman, W.M., Therapeutic siRNA: Principles, Challenges, and Strategies. *Yale J Biol Med* **2012,** 85, 187–200.

70. Merdan, T.; Kopeček, J.; Kissel, T., Prospects for cationic polymers in gene and oligonucleotide therapy against cancer. *Adv Drug Deliv Rev* **2002,** 54, 715–758.

71. Navarro, G.; Sawant, R.R.; Biswas, S.; Essex, S.; Tros de Ilarduya, C.; Torchilin, V.P., P-glycoprotein silencing with siRNA delivered by DOPE-modified PEI overcomes doxorubicin resistance in breast cancer cells. *Nanomedicine* **2011,** 7, 65–78.

72. Oh, Y.K.; Park, T.G., siRNA delivery systems for cancer treatment. *Adv Drug Deliv Rev* **2009,** 61, 850–862.

73. Tsouris, V.; Joo, M.K.; Kim, S.H.; Kwon, I.C.; Won, Y.Y., Nano carriers that enable co-delivery of chemotherapy and RNAi agents for treatment of drug-resistant cancers. *Biotechnol Adv* **2014,** 32, 1037–1050.

74. Estey, E.H., Cellular mechanisms of multidrug resistance of tumor cells. *Biochem* **2000,** 65, 95–106.

75. Sutradhar, K.B.; Amin, M.L., Nanotechnology in Cancer Drug Delivery and Selective Targeting. *ISRN Nanotechnology* **2014,** 2014, 1-12.

76. Mamasheva, E.; O'Donnell, C.; Bandekar, A.; Sofou, S., Heterogeneous liposome membranes with pH-triggered permeability enhance the in vitro antitumor activity of folate-receptor targeted liposomal doxorubicin. *Mol Pharm* **2011,** 8, 224–232.

77. Wu, J.; Lu, Y.; Lee, A.; Pan, X.; Yang, X.; Zhao, X., et al. Reversal of Multidrug Resistance by Liposomes Co-encapsulating Doxorubicin and Verapamil. *J Pharm Pharm Sci* **2007,** 10, 350–357.

78. Lale, S. V.; Kumar, A.; Prasad, S.; Bharti, A.C.; Koul, V., Folic acid and trastuzumab functionalized redox responsive polymersomes for intracellular doxorubicin delivery in breast cancer. *Biomacromolecules* **2015,** 16, 1736–1752.

79. Kapse-Mistry, S.; Govender, T.; Srivastava, R.; Yergeri, M., Nanodrug delivery in reversing multidrug resistance in cancer cells. *Front Pharmacol* **2014,** 5, 1-22.

80. Hu, C.M.J.; Zhang, L., Nanoparticle-based combination therapy toward overcoming drug resistance in cancer. *Biochem Pharmacol* **2012,** 83, 1104–1111.

81. Kang, L.; Gao, Z.; Huang, W.; Jin, M.; Wang, Q., Nanocarrier-mediated co-delivery of chemotherapeutic drugs and gene agents for cancer treatment. *Acta Pharm Sin B* **2015,** 5, 169–175.

82. Fröhlich, T.; Edinger, D.; Kläger, R.; Troiber, C.; Salcher, E.; Badgujar, N., et al. Structure–activity relationships of siRNA carriers based on sequence-defined oligo (ethane amino) amides. *J Control Release* **2012,** 160, 532–541.

83. Becker, A.L.; Orlotti, N.I.; Folini, M.; Cavalieri, F.; Zelikin, A.N.; Johnston, A.P.R., et al. Redox-Active Polymer Microcapsules for the Delivery of a Survivin-Specific siRNA in Prostate Cancer Cells. *ACS Nano* **2011,** 5, 1335–1444.

84. Li, J.M.; Wang, Y.Y.; Zhao, M.X.; Tan, C.P.; Li, Y.Q.; Le, X.Y., et al. Multifunctional QD-based co-delivery of siRNA and doxorubicin to HeLa cells for reversal of multidrug resistance and real-time tracking. *Biomaterials* **2012,** 33, 2780–2790.

85. Creixell, M.; Peppas, N.A., Co-delivery of siRNA and therapeutic agents using nanocarriers to overcome cancer resistance. *Nano Today* **2012,** 7, 367–379.

86. Liu, H.; Qiao, C.; Yang, J.; Weng, J.; Zhang, X., Self-assembling doxorubicin-prodrug nanoparticles as siRNA drug delivery system for cancer treatment: in vitro and in vivo. *J Mater Chem B Mater Biol Med* **2014,** 2, 5910–5924.

87. Ramamoorth, M.; Narvekar, A., Non Viral Vectors in Gene Therapy- An Overview. *J Clin Diagn Res* **2015,** 9, 1–6.

88. Jin, L.; Zeng, X.; Liu, M.; Deng, Y.; He, N., Current progress in gene delivery technology based on chemical methods and nano-carriers. *Theranostics* **2014,** 4, 240–255.

89. Gebala, M.; Giambasu, G.M.; Lipfert, J.; Bisaria, N.; Bonilla, S.; Li. G., et al. Cation–Anion Interactions within the Nucleic Acid Ion Atmosphere Revealed by Ion Counting. *J Am Chem Soc* **2015,** 137, 14705–14715.

90. Germershaus, O.; Nultsch, K., Localized, non-viral delivery of nucleic acids: Opportunities, challenges and current strategies. *Asian J Pharm Sci* **2015,** 10, 159–175.

91. Moghaddam, B.; McNeil, S.E.; Zheng, Q.; Mohammed, A.R.; Perrie, Y., Exploring the correlation between lipid packaging in lipoplexes and their transfection efficacy. *Pharmaceutics* **2011,** 3, 848–864.

92. Jones, C.H.; Chen, C.K.; Ravikrishnan, A.; Rane, S.; Pfeifer, B.A., Overcoming Nonviral Gene Delivery Barriers: Perspective and Future. *Mol Pharm* **2013,** 10, 4082–4098.

93. Al-Dosari, M.S.; Gao, X., Nonviral Gene Delivery: Principle, Limitations, and Recent Progress. *AAPS J* **2009,** 11, 671-681.

94. Kato, T.; Natsume, A.; Toda, H.; Iwamizu, H.; Sugita, T.; Hachisu, R., et al. Efficient delivery of liposome-mediated MGMT-siRNA reinforces the cytotoxity of temozolomide in GBM-initiating cells. *Gene Ther* **2010,** 17, 1363–1371.

95. Saad, M.; Garbuzenko, O.B.; Minko, T., Co-delivery of siRNA and an anticancer drug for treatment of multidrug-resistant cancer. *Nanomedicine* **2008,** 3, 761–776.

96. Liu, H.; Qiao, C.; Yang, J.; Weng, J.; Zhang, X., Self-assembling doxorubicin-prodrug nanoparticles as siRNA drug delivery system for cancer treatment: in vitro and in vivo. *J Mater Chem B Mater Biol Med* **2014,** 2, 5910–5924.

97. Zhang, Y.; Buhrman, J.S.; Liu, Y.; Rayahin, J.E.; Gemeinhart, R.A., Reducible Micelleplexes are Stable Systems for Anti-miRNA Delivery in Cerebrospinal Fluid. *Mol Pharm* **2016,** 13, 1791–1799.

98. Sarisozen, C.; Pan, J.; Dutta, I.; Torchilin, V.P., Polymers in the co-delivery of siRNA and anticancer drugs to treat multidrug-resistant tumors. *J Pharm Investig* **2017,** 47, 37–49.

99. Oerlemans, C.; Bult, W.; Bos, M.; Storm, G.; Nijsen, J.F.W.; Hennink, W.E., Polymeric Micelles in Anticancer Therapy: Targeting, Imaging and Triggered Release. *Pharm Res* **2010,** 27, 2569–2589.

100. Wang, Y.; Ke, C.Y.; Beh, C.W.; Liu, S.Q.; Goh, S.H.; Yang, Y.Y., The self-assembly of biodegradable cationic polymer micelles as vectors for gene transfection. *Biomaterials* **2007,** 28, 5358–5368.

101. Knudsen, K.B.; Northeved, H.; EK, P.K.; Permin, A.; Gjetting, T.; Andresen, T.L., et al. In vivo toxicity of cationic micelles and liposomes. *Nanomedicine Nanotechnology, Biol Med* **2015,** 11, 467–477.

102. Mao, C.Q.; Du, J.Z.; Sun, T.M.; Yao, Y.D.; Zhang, P.Z.; Song, E.W., et al. A biodegradable amphiphilic and cationic triblock copolymer for the delivery of siRNA targeting the acid ceramidase gene for cancer therapy. *Biomaterials* **2011,** 32, 3124–3133.

103. Zhu, C.; Jung, S.; Luo, S.; Meng, F.; Zhu, X.; Park, T.G., et al. Co-delivery of siRNA and paclitaxel into cancer cells by biodegradable cationic micelles based on PDMAEMA–PCL–PDMAEMA triblock copolymers. *Biomaterials* **2010,** 31, 2408–2416.

104. Wang, H.; Wu, Y.; Zhao, R.; Nie, G., Engineering the Assemblies of Biomaterial Nanocarriers for Delivery of Multiple Theranostic Agents with Enhanced Antitumor Efficacy. *Adv Mater* **2013,** 25, 1616–1622.

105. Magadala, P.; Vlerken, L.E.; Van Shahiwala, A.; Amiji, M.M., Multifunctional polymeric nanosystems for Tumor-Targeted Delivery. *Multifunctional Pharmaceutical Nanocarriers* **2008,** 4, 33–67.

106. Oregon State University. News and Research Communications; Available from: http://oregonstate.edu/ua/ncs/archives/2013/may/research-offers-promising-new-approach-treatment-lung-cancer.

107. Chen, W.; Yuan, Y.; Cheng, D.; Chen, J.; Wang, L.; Shuai, X., Co-Delivery of Doxorubicin and siRNA with Reduction and pH Dually Sensitive Nanocarrier for Synergistic Cancer Therapy. *Small* **2014,** 10, 2678–2687.

108. Sun, T.M.; Du, J.Z.; Yao, Y.D.; Mao, C.Q.; Dou, S.; Huang, S.Y., et al. Simultaneous Delivery of siRNA and Paclitaxel via a "Two-in-One" Micelleplex Promotes Synergistic Tumor Suppression. *ACS Nano* **2011,** 5, 1483–1494.

109. Chen, A.M.; Zhang, M.; Wei, D.; Stueber, D.; Taratula, O.; Minko, T., et al. Co-delivery of Doxorubicin and Bcl-2 siRNA by Mesoporous Silica Nanoparticles Enhances the Efficacy of Chemotherapy in Multidrug-Resistant Cancer Cells. *Small* **2009,** 5, 2673–2677.

110. Li, J.M.; Wang, Y.Y.; Zha, M.X.; Tan, C.P.; Li, Y.Q.; Le, X.Y., et al. Multifunctional QD-based co-delivery of siRNA and doxorubicin to HeLa cells for reversal of multidrug resistance and real-time tracking. *Biomaterials* **2012,** 33, 2780–2790.

111. Moore, E.R., Properties of styrene-maleic anhydride copolymers. *Ind Eng Chem Prod Res Dev* **1986,** 25, 315–321.

112. Malins, E.L.; Waterson, C.; Becer, C.R., Alternating copolymers of functionalized [small alpha]-methyl styrene monomers and maleic anhydride. *Polym Chem* **2015,** 6, 6543–6552.

113. Han, J.; Silcock, P.; McQuillan, A.J.; Bremer, P., Preparation and characterization of poly(styrene-alt-maleic acid)-b-polystyrene block copolymer self-assembled nanoparticles. *Colloid Polym Sci* **2008,** 286, 1605–1612.

114. Lackey, C.A.; Press, O.W.; Hoffman, A.S.; Stayton, P.S., A Biomimetic pH-Responsive Polymer Directs Endosomal Release and Intracellular Delivery of an Endocytosed Antibody Complex. *Bioconjug Chem* **2002,** 13, 996–1001.

115. Ansari, A.S.; Badar, A.; Balasubramanian, K.; Lohiya, N.K., Contraception with RISUG and functional reversal through DMSO and $NaHCO_3$ in male rabbits. *Asian J Androl* **2017,** pp 1–9.

116. Maeda, H.; Ueda, M.; Morinaga, T.; Matsumoto, T., Conjugation of poly(styrene-co-maleic acid) derivatives to the antitumor protein neocarzinostatin: pronounced improvements in pharmacological properties. *J Med Chem* **1985,** 28, 455–461.

117. Konno, T., Targeting chemotherapy for hepatoma: Arterial administration of anticancer drugs dissolved in lipiodol. *Eur J Cancer* **1992,** 28, 403–409.

118. Greish, K.; Sawa, T.; Fang, J.; Akaike, T.; Maeda, H., SMA–doxorubicin, a new polymeric micellar drug for effective targeting to solid tumours. J Control Release **2004,** 97, 219–230.

119. Greish, K.; Nagamitsu, A.; Fang, J.; Maeda, H., Copoly(styrene-maleic acid)−Pirarubicin Micelles: High Tumor-Targeting Efficiency with Little Toxicity1. *Bioconjug Chem* **2005,** 16, 230–236.

120. Mu, Y.; Kamada, H.; Kaneda, Y.; Yamamoto, Y.; Kodaira, H.; Tsunoda, S., et al. Bioconjugation of Laminin Peptide YIGSR with Poly(Styrene Co-maleic Acid) Increases Its Antimetastatic Effect on Lung Metastasis of B16-BL6 Melanoma Cells. *Biochem Biophys Res Commun* **1999,** 255, 75–79.

121. Maeda, H., SMANCS and polymer-conjugated macromolecular drugs: advantages in cancer chemotherapy. *Adv Drug Deliv Rev* **2001,** 46, 169–185.

122. Henry, S.M.; El-Sayed, M.E.H.; Pirie, C.M.; Hoffman, A.S.; Stayton, P.S., pH-Responsive Poly(styrene-alt-maleic anhydride) Alkylamide Copolymers for Intracellular Drug Delivery. *Biomacromolecules* **2006,** 7, 2407−2414.

123. Duan, X.; Xiao, J.; Yin, Q.; Zhang, Z.; Ma, S.; Li, Y., Amphiphilic graft copolymer based on poly(styrene-co-maleic anhydride) with low molecular weight polyethylenimine for efficient gene delivery. *Int J Nanomedicine* **2012,** 7, 4961–4972.

124. Katzung, B. G., *Basic & Clinical Pharmacology*. 10th ed.; McGraw-Hill: New York, 2006.

125. Mycek, M. J.; Harvey, R. A.; Champe, P. C., Pharmacology. In *Lippincott's Illustrated Reviews*, 2nd ed.; Harvey, R. A.; Champe, P. C., Eds. Lippicott Williams Wilkins: 2000 pp 373-400.

126. Doxorubicin dosage. http://www.drugs.com/dosage/doxorubicin.html (accessed May 21, 2015).

127. Thorn, C. F.; Oshiro, C.; Marsh, S.; Hernandez-Boussard, T.; McLeod, H.; Klein, T. E., et al., Doxorubicin pathways: Pharmacodynamics and adverse effects. *Pharmacogenet. Genomics* **2011,** 21, 440-446.

128. Taniguchi, E.; Toyoshima-morimoto, F.; Nishida, E., Nuclear Translocation of PLK-1 Mediated by Its Bipartite Nuclear Localization Signal. *J Biol Chem* **2002,** 277, 48884–48888.

129. Dou, S.; Yang, X.Z.; Xiong, M.H.; Sun, C.Y.; Yao, Y.D.; Zhu, Y.H., et al. ScFv-decorated PEG-PLA-based nanoparticles for enhanced siRNA delivery to Her2+ breast cancer. *Adv Healthc Mater* **2014,** 3, 1792–1803.

130. Spänkuch-Schmitt, B.; Bereiter-Hahn, J.; Kaufmann, M.; Strebhardt, K., Effect of RNA silencing of polo-like kinase-1 (PLK1) on apoptosis and spindle formation in human cancer cells. *J Natl Cancer Inst* **2002,** 94,1863–1877.

131. Hwang, R.; Noack, R.M., Application of design of experiments to pharmaceutical formulation development. *Int J Exp Des Process Optim* **2011,** 2, 58–65.

132. Ranga, S.; Jaimini, M.; Sharma, S.K.; Chauhan, B.S.; Kumar, A., Review Article A Review on Design OF Experiments (DOE). *Int J Pharm Chem Sci* **2014,** 3, 216–224.

133. Gilmour, S.G., Response Surface Designs for Experiments in Bioprocessing. *Biometrics* **2006,** 62, 323–331.

134. Rakić, T.; Kasagić-Vujanović, I.; Jovanović, M.; Jančić-Stojanović, B.; Ivanović, D., Comparison of Full Factorial Design, Central Composite Design, and Box-Behnken Design in Chromatographic Method Development for the Determination of Fluconazole and Its Impurities. *Anal Lett* **2014,** 47, 1334–1447.

135. Ferreira, S.L.C.; Bruns, R.E.; da Silva, E.G.P.; dos Santos, W.N.L.; Quintella, C.M.; David, J.M., et al. Statistical designs and response surface techniques for the optimization of chromatographic systems. *J Chromatogr A* **2007,** 1158, 2–14.

136. Bei, Y.Y.; Zhou, X.F.; You, B.G.; Yuan, Z.Q.; Chen, W.L.; Xia, P., et al. Application of the central composite design to optimize the preparation of novel micelles of harmine. *Int J Nanomedicine* **2013,** 8, 1795–1808.

137. Pabari, R.M.; Ramtoola, Z., Application of face centred central composite design to optimise compression force and tablet diameter for the formulation of mechanically strong and fast disintegrating orodispersible tablets. *Int J pharm* **2012,** 430, 18-25.

138. Oyejola, B.A.; Nwanya, J.C., Selecting the Right Central Composite Design. *IntJStatistics Appl* **2015,** 5, 21–30.

139. Chodankar, R.S.; Dev, A., Optimisaton techniques : a futuristic approach for formulating and processing of pharmaceuticals. *IJPBR* **2016,** 4, 32–40.

140. Aslan, N.; Cebeci, Y., Application of Box–Behnken design and response surface methodology for modeling of some Turkish coals. *Fuel* **2007,** 86, 90–97.

141. Ferreira, S.L.C.; Bruns, R.E.; Ferreira, H.S.; Matos, G.D.; David, J.M.; Brandão, G.C., et al. Box-Behnken design: An alternative for the optimization of analytical methods. *Anal Chim Acta* **2007,** 597, 179–186.

CHAPTER II

Synthesis and Evaluation of Cationically Modified

Poly (styrene-alt-maleic anhydride)

Grafts for Intracellular Gene Delivery

CHAPTER II

Synthesis and Evaluation of Cationically Modified Poly (styrene-alt-maleic anhydride) Grafts for Intracellular Gene Delivery

2.1. Introduction

This chapter describes evaluation of the intracellular gene delivery efficacy of PSMA in combination with various cationic moieties. The cationic groups were selected from aromatic, aliphatic and cyclo aliphatic chemical families. Influence of quaternary ammonium containing cationic moieties and primary amine or secondary amine containing cationic structures in modifying the gene delivery efficacy of PSMA was systematically evaluated and compared. For this purpose, we have derivatized the polymer with quaternary ammonium cations via aromatic (isonicotinic acid), aliphatic (glycidyl trimethylammonium chloride) and cyclo aliphatic (1-(2-aminoethyl) piperazine) compounds. In addition, commonly employed and efficient transfecting molecules such as L-arginine and spermine were also conjugated to PSMA. The synthesized amphiphilic polymeric derivatives were characterized using ^{1}H-NMR and FT-IR. Nanocarriers of the polymeric grafts were formulated by nanoprecipitation method and evaluated for their cytotoxicity, haemocompatibility, endosomal rupturing property, polyplex formation, resistance against DNase I degradation and transfection efficiency.

2.2. Experimental

2.2.1. Materials

PSMA with a styrene to maleic anhydride molar ratio of 2:1 (M_w, 7500 Da) was obtained from Sartomer Company Inc (Quarry bay, Hong Kong). 3-amino-1-propanol, Di-tert-butyl dicarbonate, 1-(2-aminoethyl)piperazine, dicyclohexyl carbodiimide (DCC), N-hydroxy

succinimide, spermine, glycidyl trimethyl ammonium chloride, Boc-Arginine(Mts)-OH cyclohexylammonium salt, trifluoromethanesulfonicacid, thioanisole, bovine serum albumin (molecular weight 66 kDa), 3-(4,5-dimethylthiazol-2-yl)-2,5-diphenyltetrazolium bromide(MTT), branched polyethyleneimine (PEI) (average molecular weight 25,000 kDa), DNase I and ethidium bromide were purchased from Sigma-Aldrich (Bangalore, India). Trypsin-ethylenediamine tetra acetic acid, Dulbeccos modified eagles media (DMEM), penicillin/streptomycin antibiotic solution, fetal bovine serum and agarose were purchased from Himedia (India). 1-ethyl-3-(3-dimethylaminopropyl) carbodiimide hydrochloride (EDC. HCl), isonicotinic acid, trifluoroacetic acid, phenol and triethyl amine (NEt3) were obtained from Merck millipore (India). DsRed-Express-N1 plasmid vector (4.7 Kb) was obtained from Clontech laboratories, Inc (USA). All other solvents and reagents used were of analytical grade. Purified water obtained from Milli-Q system (Merck Millipore, Billerica, MA, USA) was used during synthesis procedures. Ultrapure^{TM} DNase / RNase free distilled water (Invitrogen) was used for experiments involving plasmid vector.

2.2.2. Synthesis of graft co-polymers of PSMA

2.2.2.1. Grafting of PSMA with quaternized isonicotinic acid

Isonicotinic acid was conjugated to 3-amino-1-propanol via EDC/NHS coupling. Breifly, 3-amino-1-propanol (1g, 13.3 mM) was reacted with di-tert-butyl dicarbonate (3.15 g, 14.43 mM) in the presence of triethyl amine (2.66g, 26.6 mM), using dichloromethane (30 mL) as solvent (Scheme I a, Figure 2.1). The reaction mixture was stirred at room temperature for 12 hours, followed by evaporating under vacuum using rotary flash evaporator (IKA 50, Germany). The residue was diluted with dichloromethane (DCM), and extracted with water, brine solution and 0.1 M H$_2$SO$_4$. The combined organic layer was concentrated to obtain 3-(Boc –amino)-1-

propanol. In the next step, isonicotinic acid (1g, 8.1 mM) was dissolved in dichloromethane (20 mL) followed by addition of N-hydroxy succinimide (1.12 g, 9.7 mM). After stirring the reaction mixture for 15 minutes at room temperature, 3-(Boc-amino)-1-propanol (1.7 g, 9.7 mM), EDC.HCl (1.866g, 9.7 mM) and triethylamine (2 g, 20 mM) were added, and the reaction was continued to proceed for overnight. The crude mixture was diluted with brine solution, and extracted with dichloromethane. Further, the combined organic layer was washed with saturated sodium bicarbonate solution. The obtained product viz.3-[(tert-butoxycarbonyl) amino] propyl isonicotinate was purified through silica gel column (60-120 mesh size), using chloroform: methanol (ratio ranging from 90:10 to 55:10) as mobile phase. The purified product was then dissolved in dichloromethane: trifluoroacetic acid mixture at 1: 1 ratio for 3 hours, to remove boc. The compound formed viz. 3-aminopropyl isonicotinate was dried under high vacuum and characterized using mass spectrometry (MALDI – TOF-ABI 4700).

3-aminopropyl isonicotinate was then grafted to PSMA (Scheme I, Figure 2.1). Briefly, 0.3 g PSMA (approx. 0.98 mM of monomer units) was added to dichloromethane (15 mL) containing 3-aminopropyl isonicotinate (0.55 g, 1.85 mM) and triethylamine (NEt$_3$) (0.2g, 2mM). The reaction was carried out for overnight at room temperature, and the solvent was then removed using rotary flash evaporator. The obtained polymeric derivative was purified by washing with acidic water (pH 5) followed by dichloromethane. The purified product was then quaternized by reacting with methyl iodide (2 mol equivalent), using dimethyl sulfoxide as solvent, for 24 hrs. The solvent was then removed under high vacuum (Hind Hivac, India), and the quaternized derivative was purified by washing successively with water and dichloromethane.

2.2.2.2. Synthesis of quaternized piperazine grafted PSMA

1-(2-aminoethyl) piperazine (1g, 7.7 mM) and PSMA (1.18 g, 3.85 mM) were reacted in DMF

(15 mL), for 12 h, at room temperature. After the completion of reaction, the precipitated product was filtered, and the crude product was washed with tetrahydrofuran followed by acetone. Quaternization of the polymeric derivative was done by reacting with methyl iodide (4 mol equivalent) in DMSO, for 24 h, at room temperature (Scheme II, Figure 2.1). The obtained product was precipitated by adding ethyl acetate to the reaction mixture, and purified by washing with methanol followed by evaporating under high vacuum.

2.2.2.3. Synthesis of glycidyl trimethylammonium chloride grafted PSMA

PSMA was grafted with 3-amino-1-propanol through esterification. Briefly, 3-(Boc-amino)-1-propanol (0.572 g, 3.26 mM) was conjugated to the polymer (0.5 g, 1.6 mM), in the presence of triethyl amine (0.326 g, 3.26 mM), using dichloromethane as solvent (scheme III, Figure 2.1). The reaction mixture was concentrated under high vacuum to remove solvent and triethylamine, and the resulting polymeric derivative was washed with water and dichloromethane, successively. Boc was then removed by treating with DCM: TFA (1:1 ratio), for 2 hours.   In the next step, glycidyl trimethyl ammonium chloride was coupled to the free amino groups of PSMA grafted with 3-amino-1-propanol. Briefly, PSMA conjugated with 3-amino-1-propanol (0.5 g, 1.3 mM) was dispersed in 15 mL of water (pH of water was adjusted to 8 using sodium bicarbonate) followed by the addition of glycidyl trimethylammonium chloride (0.4 g, 2.6 mM), and reaction was carried out at 80 °C for 24 hours (scheme III, Figure 2.1). The reaction mixture was then slightly acidified to precipitate the product. The polymeric graft was then repeatedly washed with milliQ water for purification.

2.2.2.4. Grafting of L-arginine to PSMA

Boc-Arginine (Mts)-OH cyclohexylammonium salt (0.6 g, 1.07 mM) was desalted (as per manufacturers protocol) and activated with N-hydroxy succinimide (0.108 g, 0.94 mM) and

DCC (0.194 g, 0.94 mM), in dimethyl formamide (10 mL), at room temperature for overnight. The precipitated by-product was removed by filtration and the filtrate was collected. The collected filtrate was slowly added to DMF (10 mL) containing PSMA grafted with 3-amino-1-propanol (0.25 g, 0.65 mM) and NEt$_3$ (0.13 g, 1.3 mM), and the reaction was carried out under continuous stirring for 12 hours (Scheme IV, Figure 2.1). After the completion of reaction, solvent was removed under high vacuum and the residue was washed with water followed by dichloromethane. Boc and mesitylene-2-sulfonyl groups in the obtained polymeric derivative were removed by treating with cleavage cocktail viz. tifluoroacetic acid: phenol: triisopropylsilane: water: thioanisole: ethylenedithiol (EDT), in the ratio 82.5: 5:5: 5: 1: 1.5, for 3 h, at room temperature. The resulting product was dried by evaporating the solvents under high vacuum, and purified by washing successively with n-hexane and acetone.

2.2.2.5. Synthesis of spermine grafted PSMA

Mono- N-Boc protected spermine was synthesized by reacting spermine with Boc anhydride. Briefly, spermine (2 g, 9.9 mM) was dissolved in methanol: DMF mixture at 1:1 ratio (35 mL), in the presence of triethyl amine (1.98 g, 19.8 mM). Then, Boc anhydride (0.54 g, 2.47 mM) was dissolved in dry DMF (5 mL) and added slowly to the reaction mixture over one hour, under continuous stirring. Reaction was carried out overnight, and the solvents were removed under high vacuum. The residue was then mixed with saturated sodium bicarbonate solution, and Boc-protected spermine was extracted with ethyl acetate and dichloromethane, in succession. Extract was then concentrated, dried under high vacuum and characterized using mass spectrometry (MALDI – TOF-ABI-4700). To the obtained viscous product, 1 N HCl was added, and further extracted with ethyl acetate. The pH of the aqueous layer was increased to 9.5 with 1 N NaOH, and again extracted with ethyl acetate followed by dichloromethane. Grafting of PSMA with
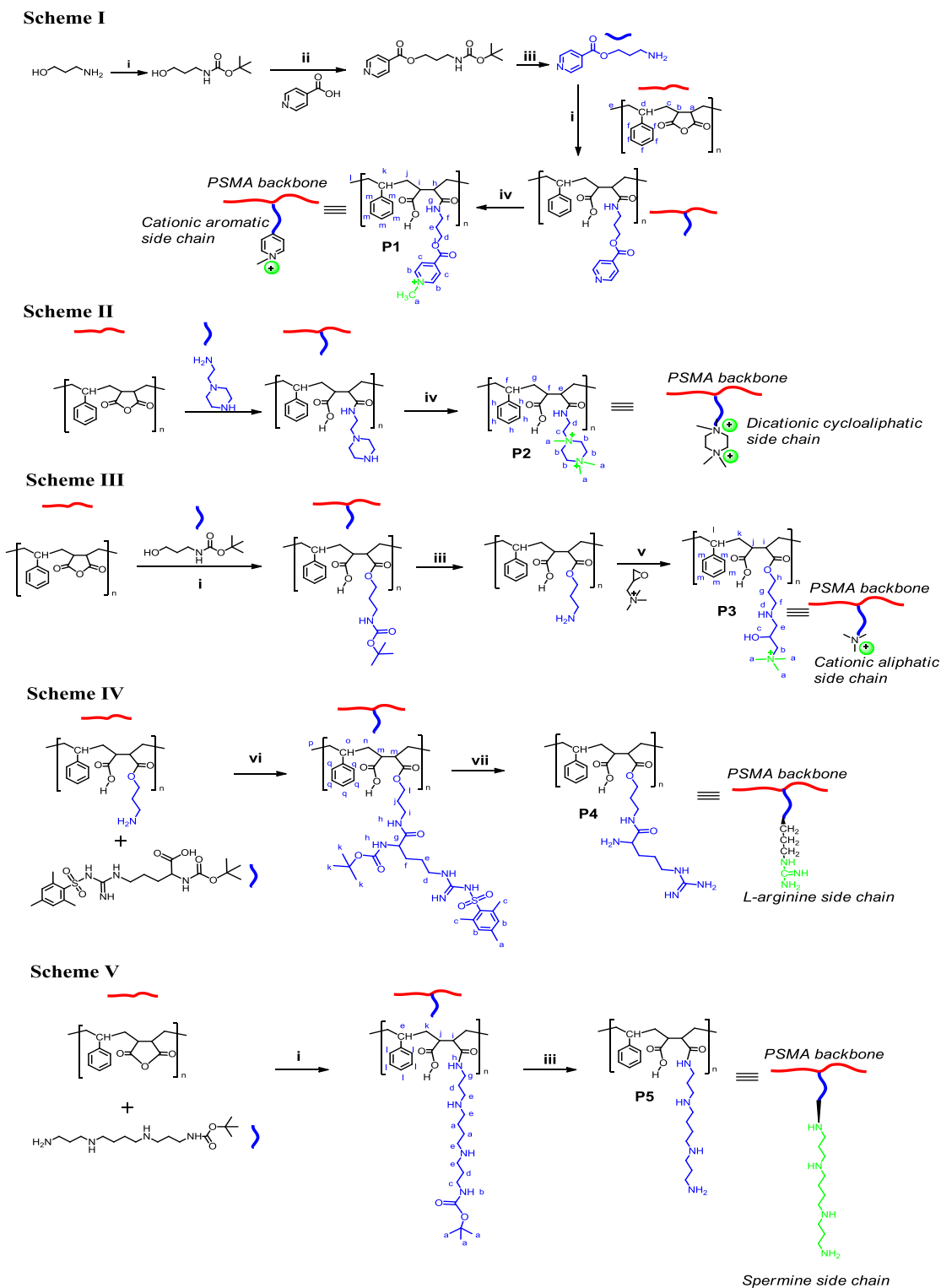
Figure 2.1. Schematic representation of the synthesis of various PSMA derivatives. (i) NEt$_3$, RT, 12 h (dry CH$_2$Cl$_2$) (ii) EDC/NHS, NEt$_3$, 0 ºC - RT, 12 h (iii) TFA- CH$_2$Cl$_2$, RT, 3 h (iv) CH$_3$I , (CH$_3$)$_2$ SO, RT, 24 h (v) 80 ºC, 24 h (vi) DCC/NHS, NEt$_3$, 0 ºC – RT, 12 h (vii) TFA: Phenol : H$_2$O: triisoprpylsilane: thioanisole : EDT (82.5:5:5:5:1:1.5), RT, 3 h

spermine was performed as follows. PSMA (0.125 g, 0.4 mM) was treated with mono N-Boc spermine (0.247 g, 0.8 mM), in the presence of NEt₃ (0.04 g, 0.4 mM), using dry DMF (10 mL) as solvent (Scheme V). In the final step, Boc was removed from the polymer by treating with TFA: DCM mixture (1:1) for 3 hours. The spermine grafted PSMA was then purified by washing repeatedly with water.

All the intermediate compounds in the synthesis and final products were suitably characterized using ^{1}H NMR (300 MHz, Brukers, USA) and ATR–FTIR (PerkinElmer, USA). For convenience, the co-polymeric grafts of PSMA with quaternized isonicotinic, quaternized piperazine, glycidyl trimethyl ammonium chloride, L-arginine and spermine are abbreviated as **P1**, **P2**, **P3**, **P4** and **P5** respectively.

2.2.3. Formulation of nanoparticles

Nanoparticles of PSMA derivatives were formulated using nanoprecipitation method developed by Fessi et al [1]. During formulation, weight of all the polymeric derivatives was fixed at 2 mg. Quaternized polymeric derivatives viz. **P1** and **P3** and L-arginine grafted PSMA (**P4**) were weighed and dissolved in 0.1 mL of DMSO. The DMSO solution was then mixed with milliQ water (4.9 mL) under stirring at 400 rpm. The polymeric particles were then subjected to probe sonication, at 100 W, for suitable time. Quaternized piperazine grafted PSMA (**P2**) nanoparticles were prepared by dispersing 2 mg of polymer in 5 mL of ethanol: water mixture (1: 15 ratio), followed by sonication at 100 W. In case of spermine grafted PSMA, nanoparticles were formed by dispersing the polymeric derivative (2 mg) in DMSO (0.4 mL): 0.01 N HCl (4.6 mL) mixture. The obtained polymeric dispersion was sonicated, at 100 W, till appropriate particle size was achieved. Nanoparticulate dispersions were filtered using Amicon Ultra–4 centrifugal filter device (Millipore) equipped with a 30 kDa membrane filter. The nanoparticles were then

redispersed in milliQ water, lyophilized (labconco, 4.5 L) and stored at 4 °C. Average particle size and zeta potential of all nanoparticle formulations were measured using DLS (Malvern, zetasizer). The morphology of nanoparticles was studied using transmission electron microscopy (TEM).

2.2.4. Cytotoxicity studies

MTT assay was performed on MCF 7 and L929 cell lines, as per published protocol [2, 3]. Cells were cultured on T-25 flasks in DMEM media, supplemented with 10% fetal bovine serum, at 37 °C and 5 % CO_2. Penicillin and streptomycin combination (1 %) was used as antimicrobial agent. When the cells attained 80 % confluency, they were trypsinized and seeded in to 96 well plate (10^4 cells/well). The cells were then incubated for 24 hours, at 37 °C and 5 % CO_2. Nanoparticles of various polymeric derivatives at different concentrations and polyplexes at various weight ratios of polymer/pDNA (5, 10, 15 and 20) were added to the wells, and incubated for 48 hours. Triton X 100 and phosphate buffer saline (pH 7.4) were used as positive and negative controls, respectively. After 48 hours of incubation, 10 μL of MTT solution (2.5 mg/mL) was added to each well, and further incubated for 4 hours. After removing the media, 100 μL of DMSO was added to each well, and readings were taken at 540 nm using microplate spectrophotometer (PowerWave XS2, Bio Tek Instruments, USA). The % cell viability was calculated according to following equation -

$$\% \text{ Cell viability} = \left\{ \frac{\text{Absorbance of sample} - \text{Absorbance of Positive control}}{\text{Absorbance of negative control} - \text{Absorbance of Positive control}} \right\} \times 100$$

2.2.5. Haemolysis and endosomal rupturing capacity of nanoparticles

Haemolysis experiments were performed at two pH values viz.7.4 and 5.5, according to previously reported procedures [4]. Human red blood cells were isolated from whole human blood (collected from healthy human volunteers at IIT Delhi hospital, New Delhi), by centrifuging at 1500 rpm for 5 minutes. 30 µL of human red blood cells were diluted to 10 mL with phosphate buffer salines (pH 7.4 and 5.5), and rinsed three times with the corresponding buffer salines. The RBCs were then resuspended in corresponding buffers. 100 µL of polymeric dispersions in different buffer salines were mixed with 100 µL of RBC suspensions in the same buffer, at nanoparticle concentrations ranging from 50 – 1000 µg/mL. Then the mixtures were incubated at 37 °C for 30 minutes. After the incubation, dispersions were centrifuged at 1500 rpm for 10 minutes, and the supernatants were transferred to 96 well plate. The absorbance of supernatants was measured at 540 nm using micro plate spectrophotometer (PowerWave XS2, Bio Tek Instruments, USA). 1 % triton X 100 solution was used as positive control and respective buffer salines (pH 7.4 and 5.5) were used as negative controls. % haemolysis was calculated according to the following equation -

$$\% \text{ Haemolysis} = \left\{ \frac{\text{Absorbance of sample} - \text{Absorbance of negative control}}{\text{Absorbance of Positive control} - \text{Absorbance of negative control}} \right\} \times 100$$

2.2.6. Preparation and characterization of pDNA- polymer complexes

Nanoparticles of various polymeric derivatives were dispersed in DNase free water and mixed with equal volumes of red fluorescent protein (RFP) expressing pDNA (DsRed-Express-N1) solutions (in DNase free water), at various weight ratios (5, 10,15 and 20). The mixtures were

vortexed for 30 seconds and incubated at room temperature for 30 minutes. DNA binding and condensation properties of polymeric nanoparticles were evaluated by performing agarose gel electrophoresis. The complexes were mixed with gel loading buffer (5:1 ratio by volume), and loaded on 1 % agarose gel containing ethidium bromide (0.5 µg/mL of gel) in Tris–acetate-ethylenediamine tetra acetic acid. Electrophoresis was carried out for 120 minutes, at 70 V. The bands of pDNA in the gel were observed using UV illuminator, and photographs were taken using molecular imager (Gel Doc XR, BIO RAD).

2.2.7. DNase I degradation assay of polyplexes

The efficiency of polymeric nanoparticles in protecting the complexed pDNA from enzymatic degradation was studied by treating the complexes with DNase I. Briefly, the pDNA-nanoparticle complexes were incubated with DNase I at a concentration of 1 U DNase/µg of pDNA, for 30 minutes, at 37 °C .Ethylenediamine tetra-acetic acid (EDTA) was then added to the enzyme-polyplex mixture, at a concentration of 2.5 mM, and the whole dispersion was heated for 10 minutes at 70 °C. The DNA molecules complexed to the polymeric nanoparticles were then released by treating with heparin at a concentration of 200 U/ µg of pDNA, for 30 minutes, at 37 °C. The released DNA molecules were analyzed using 1 % agarose gel electrophoresis.

2.2.8. *In vitro* transfection studies

Polyplexes of DsRed-Express-N1 were evaluated for their transfection efficiency on MCF 7 cells. Cells were seeded, at a density of 10^5 cells/well, into 24 well plates in the presence of 1 mL complete medium (DMEM). The seeded cells were incubated for 20 hours to obtain ~ 70 % confluency. The growth medium was then completely removed and replaced with fresh medium (without serum) containing polyplexes at different weight ratios. pDNA concentration used was

2 µg/well. After 4 hours of incubation, the medium was again replaced with complete growth medium and further incubated for 48 hours. The red fluorescent protein expressing cells were visualized using an inverted fluorescence microscope (Nikon Eclipse Ti, Japan) and the fluorescence measurements were performed using fluorescence activated cell sorter (BD Accuri-C6, BD Biosciences). Untransfected cells were taken as negative control, and cells treated with polyplexes of branched PEI, 25,000 Da (at an optimal N/P ratio of 10) were employed as positive control. For the measurement of fluorescence, 10,000 events were counted.

2.2.9. Statistical analysis

Data are presented as mean ± standard deviation. All the experiments were carried out in triplicate. Statistical analysis was performed using one-way analysis of variance (one-way ANOVA) using Sigma Stat (Version 3.5, Systat Software Inc., San Jose, CA, USA).

2.3. Results and Discussion

2.3.1. Synthesis and characterization of poly (styrene-alt-maleic anhydride) grafts

PSMA was characterized using ^{1}H NMR (Figure 2.2) and ATR-FTIR (Figure 2.3). ^{1}H NMR of PSMA is characterized by broad bimodal signals ranging from δ 1.8 - 3.6. These are attributed to methylene groups and tertiary carbons in the main chain of polymer. Styrene residues exhibit signals ranging from δ 7-7.6. Since low molecular weight PSMA is produced in cumene, using dicumyl peroxide as the initiator, polymeric chains are capped with terminal cumene residues. The proton signal at δ 1.25 was due to terminal methyl groups of cumene. ATR-FTIR of PSMA shows two characteristic absorption bands, due to the stretching vibrations of carbonyl groups of anhydride, at 1853 cm^{-1} and 1773 cm^{-1}.
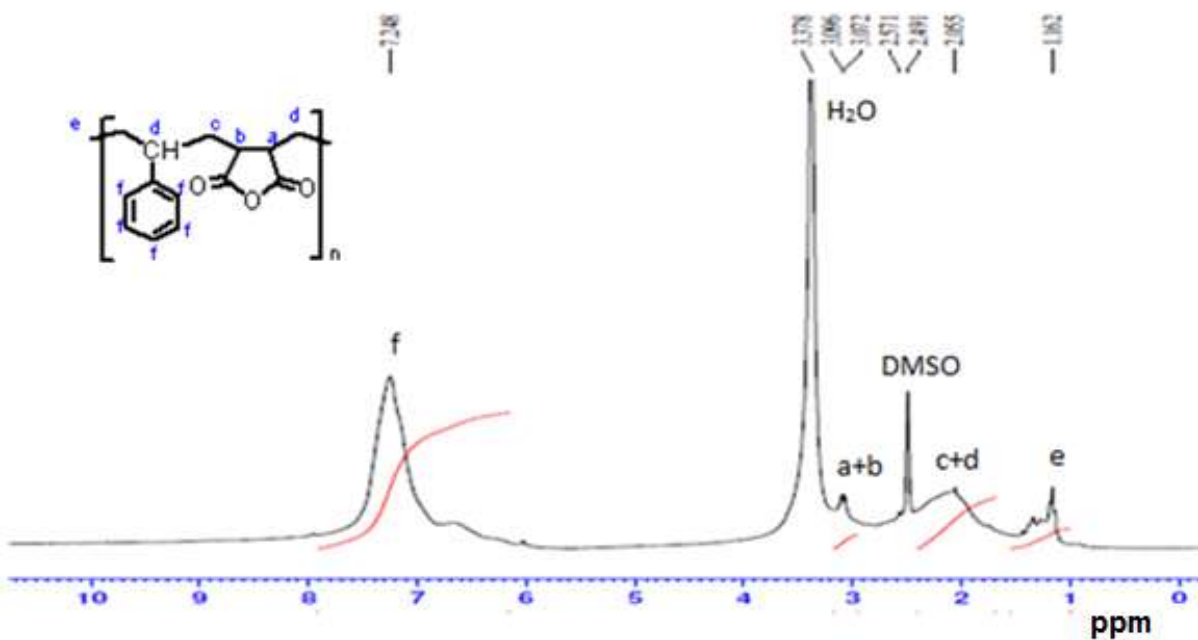
Figure 2.2. ^{1}H NMR spectrum (300 MHz, DMSO-d_6) of PSMA: δ 1.162 (br m, -C$\underline{H}_3$), 2.07 (br, aliphatic C$\underline{H}$+ C$\underline{H}_2$), 3.08 (m, C$\underline{H}$ anhydride), 7.25 (br m, Ar C$\underline{H}$)
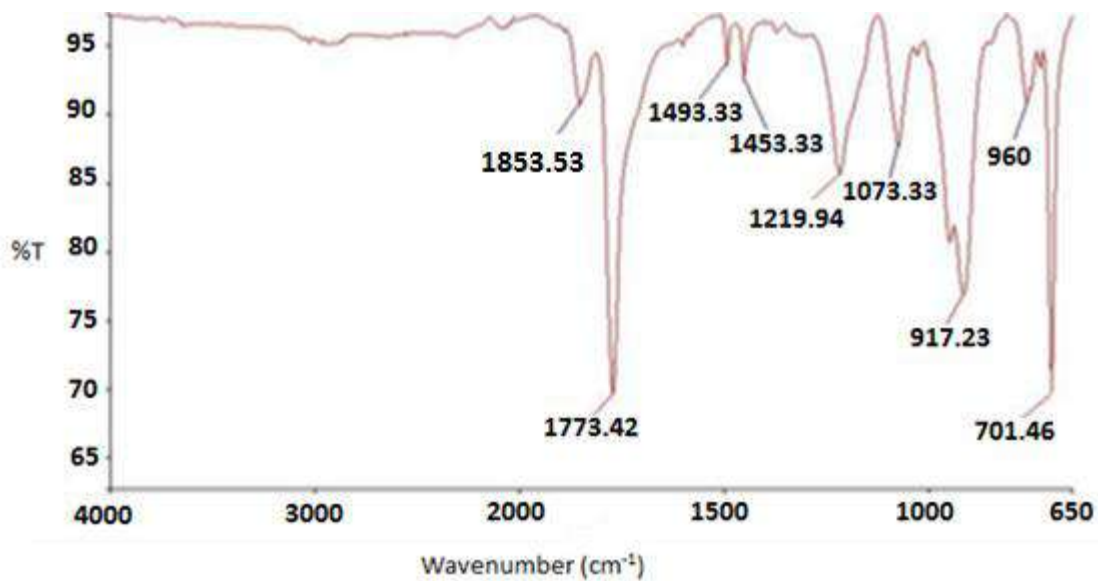
Figure 2.3. ATR-FTIR spectrum of poly (styrene-alt-maleic anhydride) (PSMA)

Different types of cationic structures were grafted to the polymer (PSMA) backbone to obtain their corresponding amphiphilic derivatives (Figure 2.1). To form quaternized polymeric grafts, derivatizing agents were selected from aromatic (isonicotinic acid), aliphatic (glycidyl trimethyl ammonium chloride) and cyclo aliphatic (1-(2-aminoethyl) piperazine) chemical families. L-arginine and spermine were employed as non quaternized derivatizing compounds. Rationale for synthesizing these different types of PSMA derivatives was to evaluate the impact of attached chemical structures in modulating the gene delivery efficacy of PSMA.

2.3.1.1. Synthesis of quaternized isonicotinic conjugated PSMA (P1)

Isonicotinic acid was grafted to PSMA using 3-amino-1-propanol. N-Boc protected 3-amino-1-propanol and 3-((tert-butoxy)-amino) propyl isonicotinate were synthesized (2.2.2.1) and characterized using ^{1}H NMR (Figure 2.4).   3-((tert-butoxy)-amino) propyl isonicotinate formation was further confirmed using mass spectrometry (MALDI TOF/TOF[TM], USA) (Figure 2.5). ^{1}H NMR of 3-((tert-butoxy)-amino) propyl isonicotinate depicted characteristic signals corresponding to methyl groups of Boc (δ 1.44) and aromatic protons (δ 7.8 and δ 8.7). Further, the product formation was confirmed by mass spectrum indicating peaks at 281 and 303, corresponding to M+H$^+$ and M + Na$^+$ respectively. Amino group of 3-((tert-butoxy)-amino) propyl isonicotinate was deprotected and the resulting product was grafted to PSMA backbone through alkaline hydrolysis of anhydride units. ^{1}H NMR of PSMA grafted with isonicotinic acid showed symmetric signals at δ 7.8 and δ 8.9 (Figure 2.6), which confirmed the presence of aromatic hydrogens of isonicotinic acid. For introducing cationic charge to the polymeric graft, the polymeric derivative was quaternized with methyl iodide (Scheme I, Figure 2.1).^{1}H NMR spectrum of the quaternized isonicotinic acid derivative (Figure 2.6) depicted a strong signal at δ 3.9, which was assigned to the methyl groups attached to the nitrogen atoms of pyridine unit.
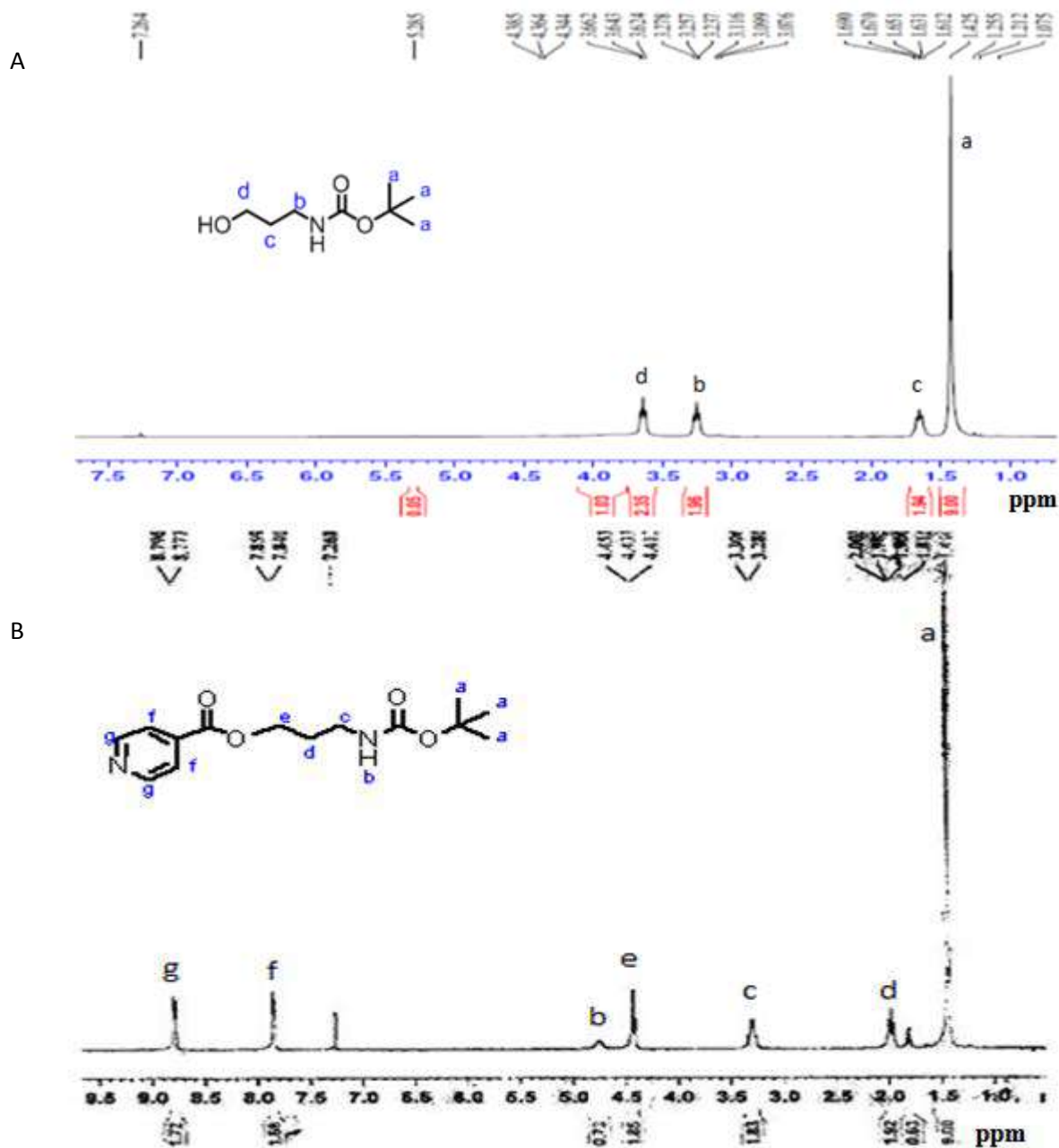
Figure 2.4. ¹H NMR spectra (300 MHz, CDCl₃) of (A) N-Boc -3-amino- 1-propanol; δ 1.43 (s, 9H, Boc C$\underline{H}_3$), 1.63 (m, 2H, HO-CH₂-C$\underline{H}_2$), 3.26 (t, J = 6 Hz, 2H, HO-C$\underline{H}_2$), 3.64 (t, J = 5.7 Hz, 2H, HN- CH₂) and (B) 3-(tert-butoxycarbonylamino)propyl isonicotinate; δ 1.44 (s, 9H, Boc C$\underline{H}_3$), 1.9 (m,2H, -O- CH₂- C$\underline{H}_2$), 3.3 (d, J = 6 Hz, 2H, HN-C$\underline{H}_2$), 4.4 (t, J = 6 Hz, 2H, -O-C$\underline{H}_2$), 4.75 (br s, 1H, Boc N$\underline{H}$), 7.85 (d, J = 5.8 Hz, 2H, Ar C$\underline{H}$), 8.8 (d, J = 6 Hz, 2H, Ar C$\underline{H}$)
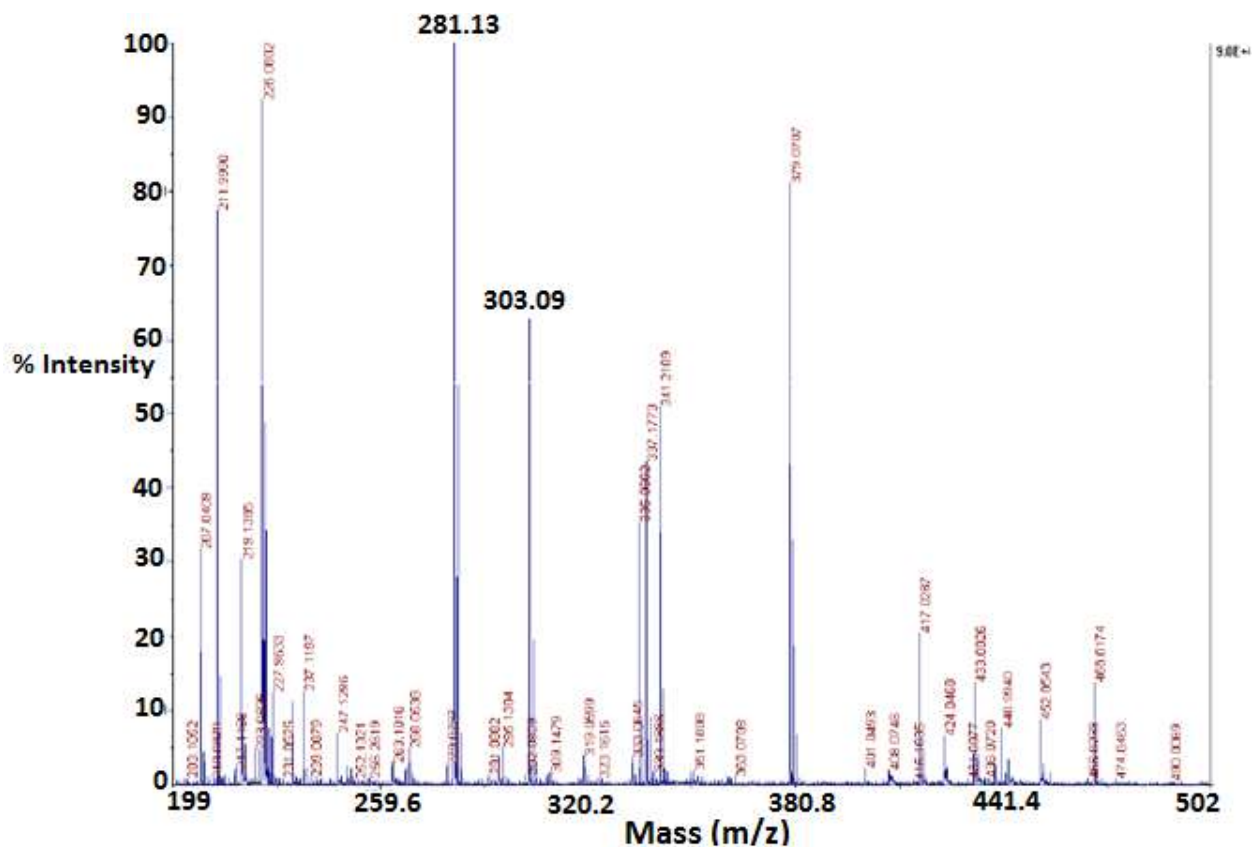
Figure 2.5. Mass spectrum of 3-(tert-butoxycarbonylamino) propyl isonicotinate. Mass spectrum calcd for $C_{14}H_{21}N_2O_4$ (H^+), m/z = 281.1501, obtained m/z = 281.1305

ATR-FTIR spectrum of **P1** showed disappearance of bands (1853 cm^{-1} and 1773 cm^{-1}) due to carbonyl stretching of anhydride groups (Figure 2.7. A), which indicates the hemi amide formation. – CH stretching frequency exhibited band around 2946 cm^{-1}. A slight shift in the value could be due to the presence of strained side chain. A very strong band of the carbonyl group of ester was present at 1727cm^{-1}.The weak band at 1670 cm^{-1} confirmed amide bond formation. This weak band could be due to the conjugation of the side chains. NH bending was shown by the presence of band at 1596 cm^{-1} in the spectrum, whereas CN stretching of the amide bond was indicated by the absorption band at 1450 cm^{-1}.
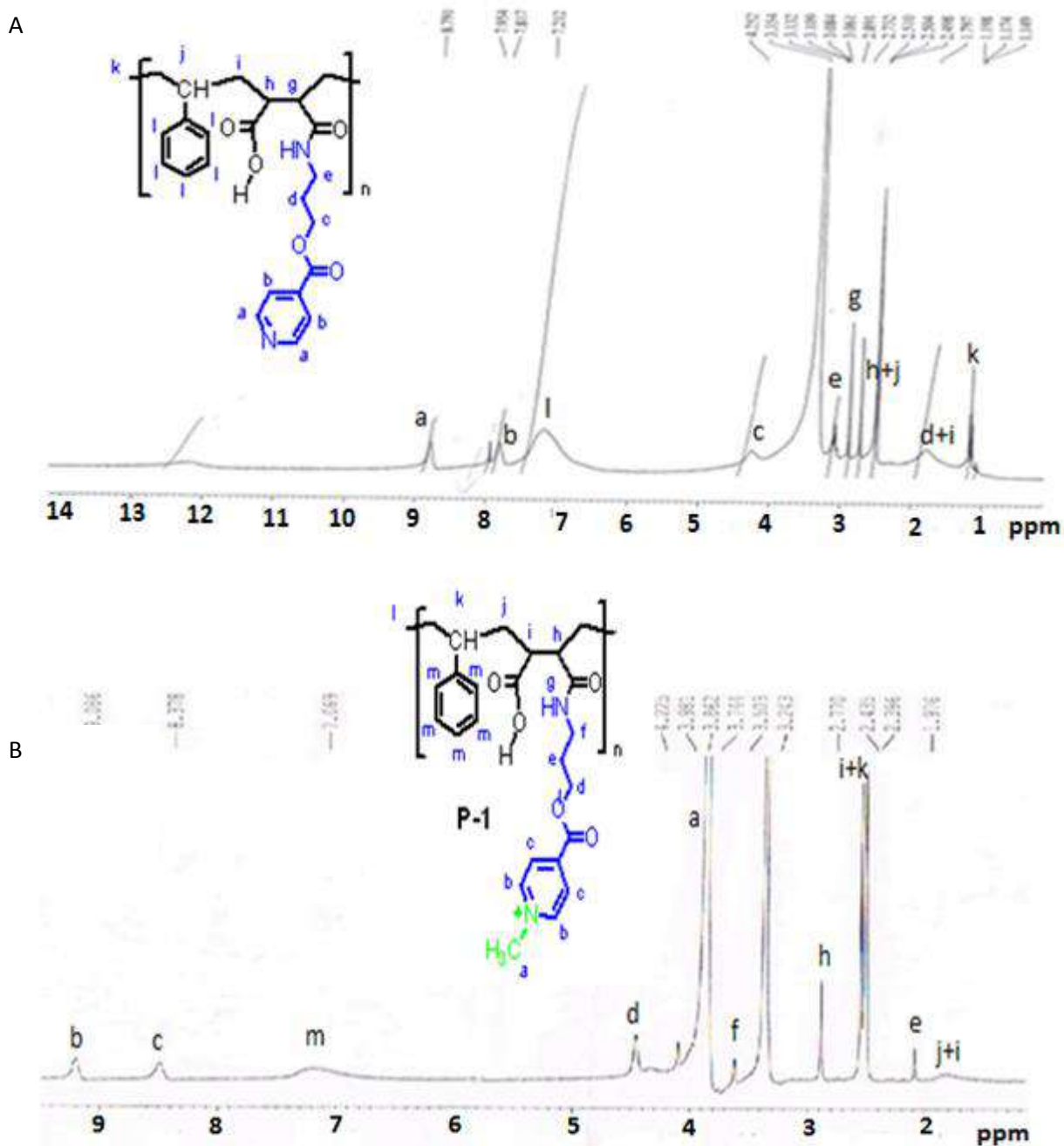
Figure 2.6. ^{1}H NMR spectra (300 MHz, DMSO-d_6) of (A) PSMA – isonicotinic acid conjugate; δ 1.18 (br m, -C$\underline{H}_3$), 1.8 (br, aliphatic C$\underline{H}_2$), 2.73 (m, aliphatic C$\underline{H}$), 2.8 (m, aliphatic C$\underline{H}$), 3.1 (m, aliphatic C$\underline{H}_2$), 4.2 (br m, aliphatic C$\underline{H}_2$), 7.2 (br m, Ar C$\underline{H}$), 7.8 (br d, Ar C$\underline{H}$), 7.9 (m, N$\underline{H}$), 8.8 (br d, Ar C$\underline{H}$) and (B) **P1**; δ 1.9 (br m, aliphatic C$\underline{H}_2$ + C$\underline{H}_3$), 2.1 (m, aliphatic C$\underline{H}_2$) , 2.6 (m, aliphatic C$\underline{H}$), 2.9 (m, aliphatic C$\underline{H}$), 3.7 (m, aliphatic C$\underline{H}_2$). 3.8 (br s, Ar N- C$\underline{H}_3$), 4.8 (br m, aliphatic C$\underline{H}_2$), 7.2 (br m, Ar C$\underline{H}$), 8.4 (br d, Ar C$\underline{H}$), 9.1 (br d, Ar C$\underline{H}$)
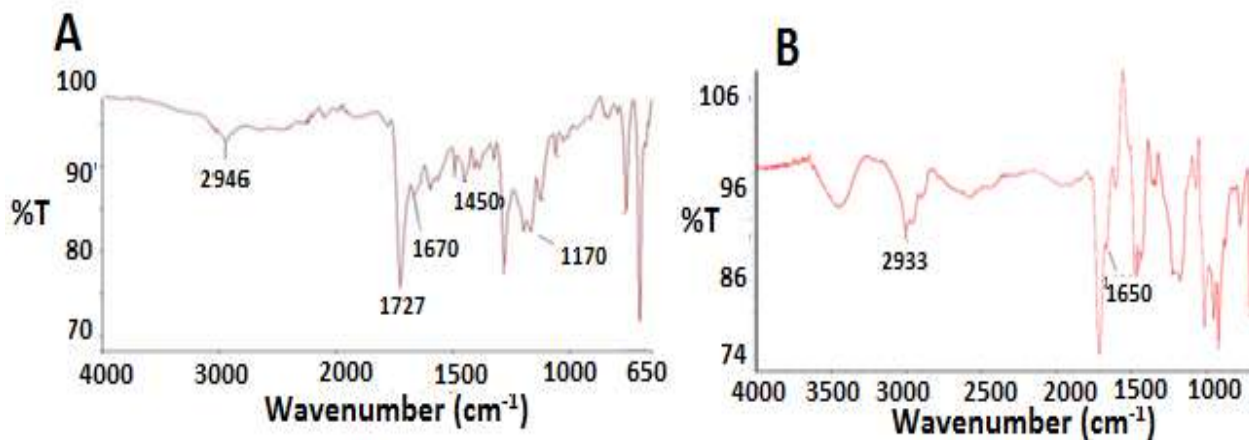
Figure 2.7. ATR-FTIR spectra of (A) quaternized isonicotinic conjugated PSMA (**P1**) and (B) quaternized piperazine grafted PSMA (**P2**)

2.3.1.2. Quaternized piperazine - PSMA conjugate (P2) formation

In the first step, 1-(2-aminoethyl) piperazine was conjugated to PSMA backbone via amide bond using dimethylformamide (DMF) as solvent. The product precipitated readily in the reaction medium and it has shown low solubility in various solvents tested, including water and DMSO. Intra- and/or inter- molecular hydrogen bonding, between the secondary nitrogens of attached piperazinyl groups and carbonyl groups of polymeric side chains, could be the probable reason for this reduced solubility [5]. To impart cationic charge in the obtained polymeric graft, it was reacted with methyl iodide in DMSO (Scheme II, Figure 2.1). The solubility of polymeric derivative was enhanced as the reaction progressed. After 24 hours, the product was completely soluble in DMSO, probably due to the elimination of hydrogen bonding. ^{1}H NMR of 1-(2-aminoethyl) piperazine grafted PSMA (Figure 2.8) in methanol–D4 (CD$_3$OD) containing one drop of trifluoroacetic acid (deuterated) showed the presence of methylene goups of piperazine at δ 2.7 – 2.9. ^{1}H NMR of quaternized piperazine grafted PSMA in DMSO-d_6 (Figure 2.9) exhibited signals due to methylene and methyl groups, in the vicinity of quaternary nitrogen
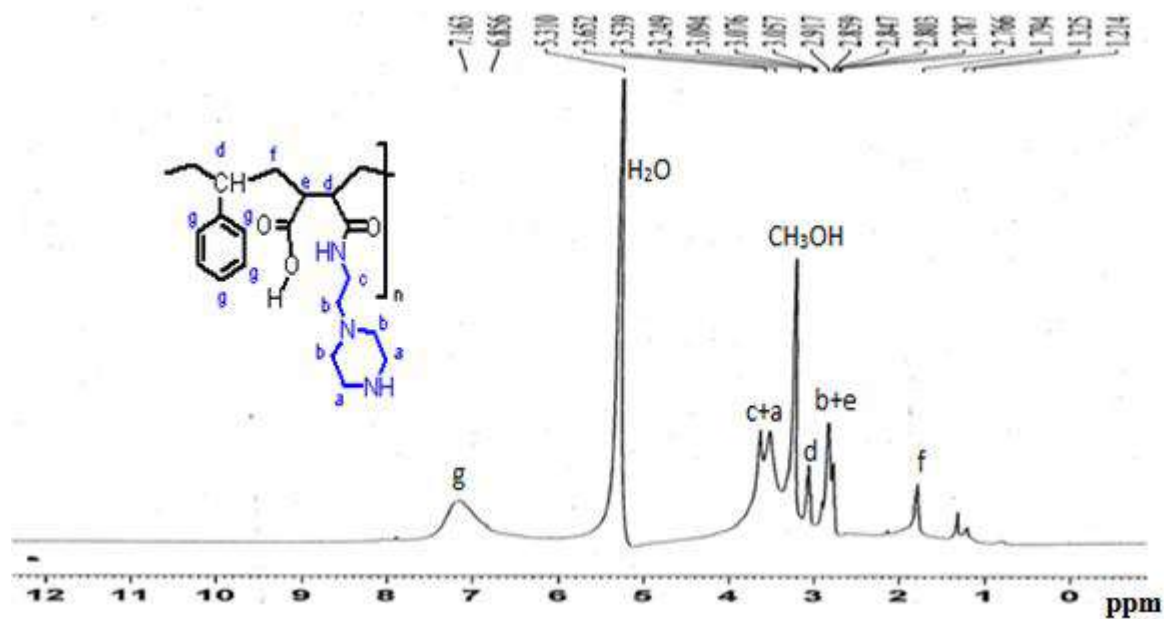
Figure 2.8. ¹H NMR spectrum (300 MHz, CD₃OD) of PSMA grafted with 1-(2-aminoethyl) piperazine. δ 1.2 (br m, -C$\underline{H}_3$), 1.8 (br m, aliphatic C$\underline{H}_2$), 2.85 (br m, aliphatic C$\underline{H}$+ C$\underline{H}_2$), 3.1 (br m, aliphatic C$\underline{H}$), 3.5 (br m, aliphatic C$\underline{H}_2$), 7.2 (br m, Ar C$\underline{H}$)
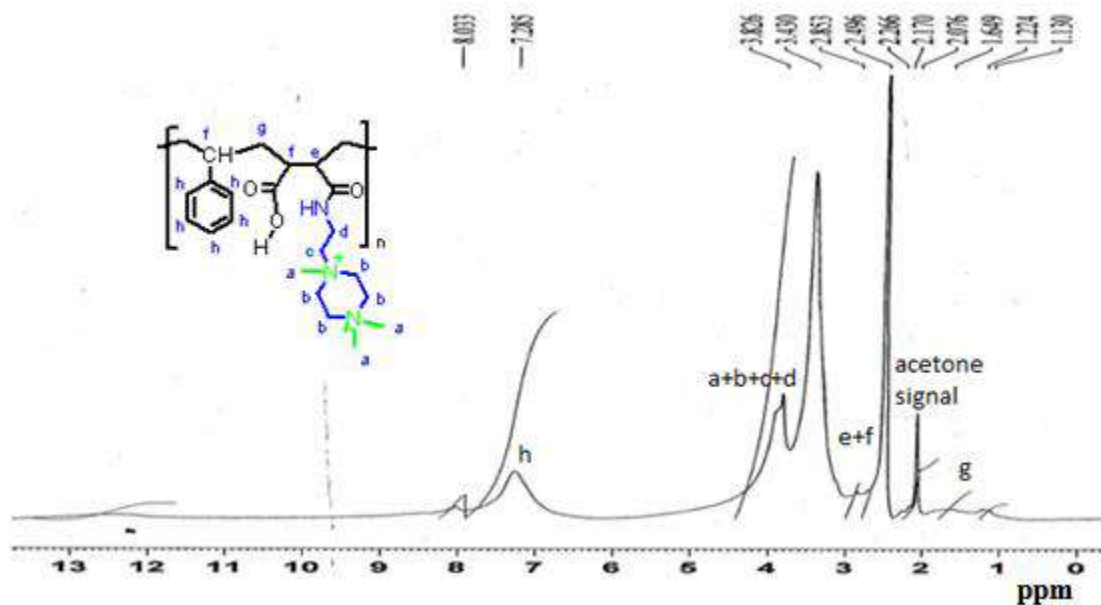
Figure 2.9. ¹H NMR spectrum (300 MHz, DMSO-d_6) of **P2**. δ 1.13 (br m, -C$\underline{H}_3$),1.65 (br, aliphatic C$\underline{H}_2$) , 2.85 (m, aliphatic C$\underline{H}$), 3.83 (br m, aliphatic C$\underline{H}_2$ + C$\underline{H}_3$), 7.29 (br m, Ar C$\underline{H}$)

atoms of the polymeric derivative **(P2)**, at δ 3.6 - 3.8. FT-IR spectrum of **P2** (Figure 2.7. B) displayed strong band at 1713 cm^{-1}, indicative of stretching vibrations of carbonyl groups of carboxylic acid. Amide bonds in the polymeric derivative showed bands at 1650 and 1560 cm^{-1}.

2.3.1.3. Synthesis of glycidyl trimethyl ammonium chloride grafted PSMA (P3)

Glycidyl trimethyl ammonium chloride was grafted to PSMA using 3-amino-1-propanol. N- Boc protected 3-amino-1- propanol was grafted to PSMA through esterification (Scheme III, Figure 2.1), followed by deprotection of Boc. Both the polymeric derivatives were characterized using ^{1}H NMR and ATR-FTIR. ^{1}H NMR of N-Boc- 3-amino-1-propanol grafted PSMA (Figure 2.10 A) in DMSO-d_6 exhibited a strong signal at δ 1.36, indicative of methyl groups of Boc whereas in the spectra of deprotected polymeric derivative (Figure 2.10. B), the signal due to Boc was completely disappeared. This confirmed the formation of 3-amino-1-propanol grafted PSMA. In the second step, epoxy groups of glycidyl trimethyl ammonium chloride were conjugated to the free amino groups of 3-amino-1-propanol grafted PSMA under basic conditions. ^{1}H NMR of **P3** (Figure 2.11.A), in DMSO-d_6, depicted a strong signal at δ 3.16 due to methyl groups of quaternary nitrogens. ATR-FTIR spectrum of **P3** (Figure 2.11.B) showed characteristic carbonyl stretching frequency of ester at 1725 cm^{-1}, and NH stretching at 3433 cm^{-1}, which confirmed that the grafting has occured.

2.3.1.4. Grafting of L-arginine to PSMA

L-arginine was also grafted to PSMA backbone using 3-amino-1-propanol. Primary amines of 3-amino-1-propanol grafted PSMA was conjugated to carboxylic acid groups of mesitylene- 2-sulfonyl and Boc protected arginine (Boc-Arg-Mts-OH) via DCC/NHS coupling. Boc-Arg-Mts-OH was chosen for the reaction in order to avoid intermolecular reaction between the aminoacid

molecules, and because of easy cleavage and removal of mesitylene groups compared to other protecting groups like tosyl. ¹H NMR of Boc-Arg-Mts-OH grafted PSMA (Figure 2.12 A).
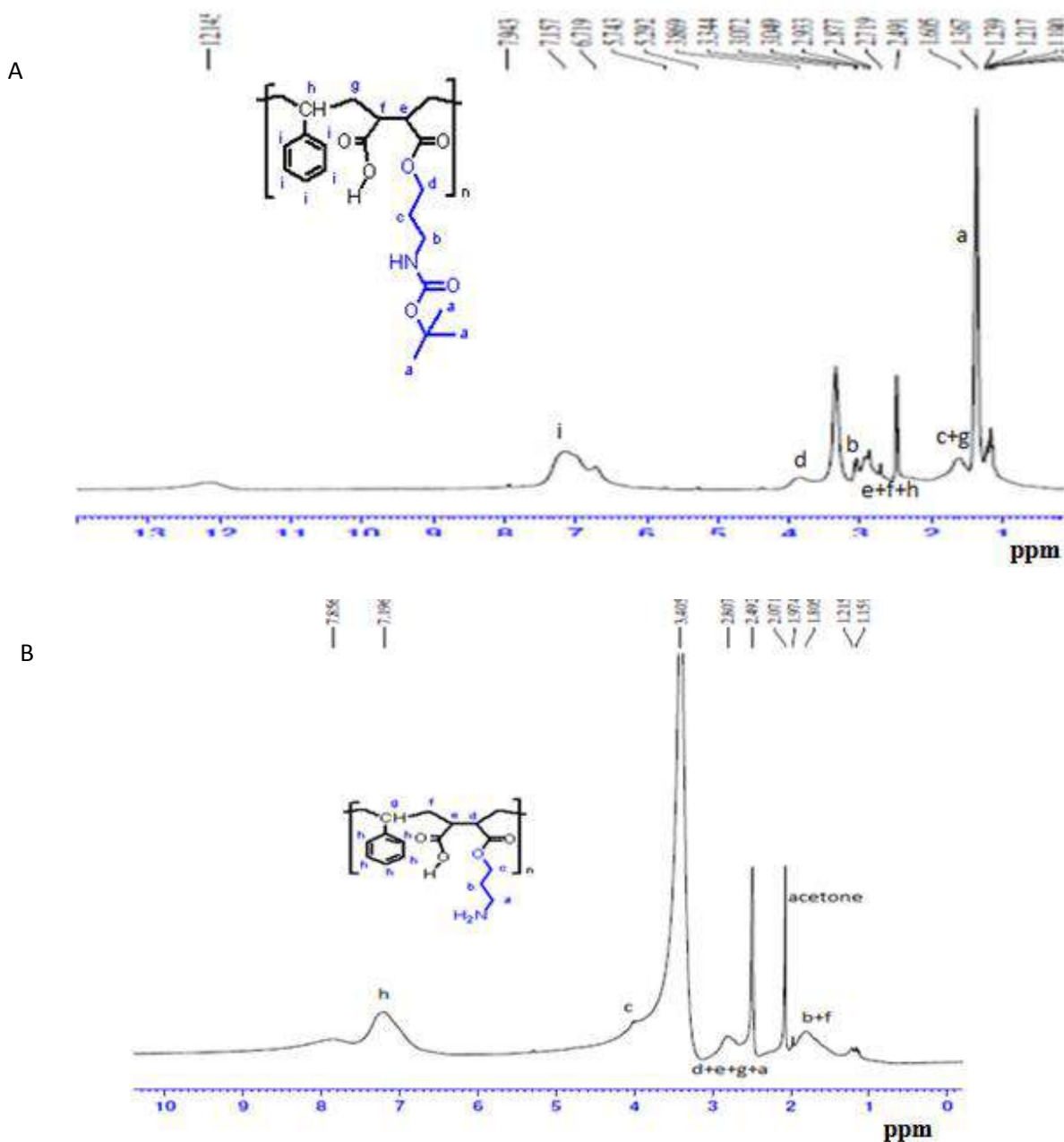
Figure 2.10. ¹H NMR spectra (300 MHz, DMSO-d_6) of (A) N-boc -3-amino-1-propanol grafted PSMA; δ 1.1(br m, -C$\underline{H}_3$), 1.36 (br s, Boc CH$_3$), 1.6 (br m, aliphatic C$\underline{H}$+ C$\underline{H}_2$), 2.9 (br m, aliphatic C$\underline{H}$+ C$\underline{H}_2$), 3.8 (br m, aliphatic C$\underline{H}_2$), 7.2 (br m, Ar C$\underline{H}$) and (B) 3-amino-1-propanol grafted PSMA; δ 1.16 (br m, -C$\underline{H}_3$), 1.8 (br m, aliphatic C$\underline{H}_2$), 2.8 (br m, aliphatic C$\underline{H}$+ C$\underline{H}_2$), 4 (br m, aliphatic C$\underline{H}_2$), 7.2 (br m, Ar C$\underline{H}$)
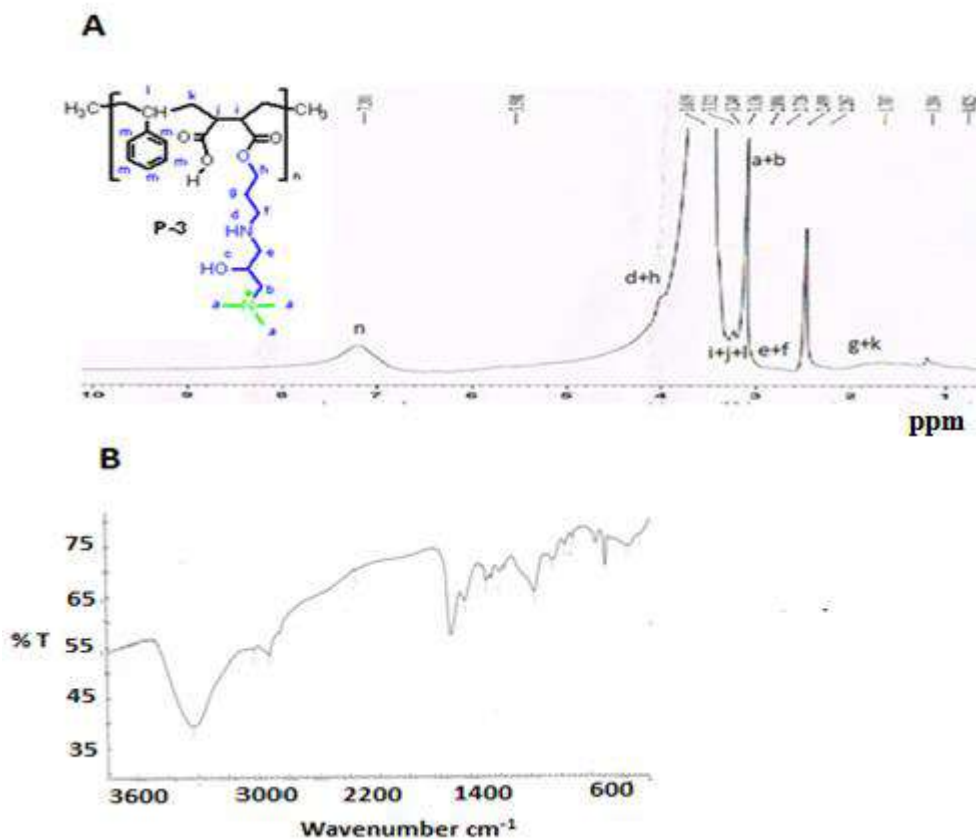
Figure 2.11. ^{1}H NMR spectrum (300 MHz, DMSO-d_6) (A) and ATR-FTIR spectrum (B) of glycidyl trimethyl ammonium chloride grafted PSMA **(P3)**

showed sharp signals of methyl groups attached to mesitylene at δ 2.2 and δ 2.6, and tertiary butyl groups of Boc at δ 1.360. An additional sharp peak merged with the peaks of styrene residues of polymer, at δ 7.0 ppm, could be due to aromatic protons of the mesitylene. The mesitylene-2-sulfonyl and Boc groups were removed by treating with a cleavage cocktail (Scheme IV, Figure 2.1), according to previously reported procedure [6]. L-arginine grafted PSMA (**P4**) formed a transparent gel, in DMSO-$d6$. This gel formation could be due to the hydrogen bonding between amines and carboxylic groups of polymer side chains. ^{1}H NMR spectra of **P4** (Figure 2.12 B) indicated absence of mesitylene and Boc signals, which could confirm the product formation. ATR-FTIR spectra of **P4** (Figure 2.13) displayed carbonyl stretching frequency at 1726 cm^{-1}, and amide bands at 1666 and 1450 cm^{-1}.

76
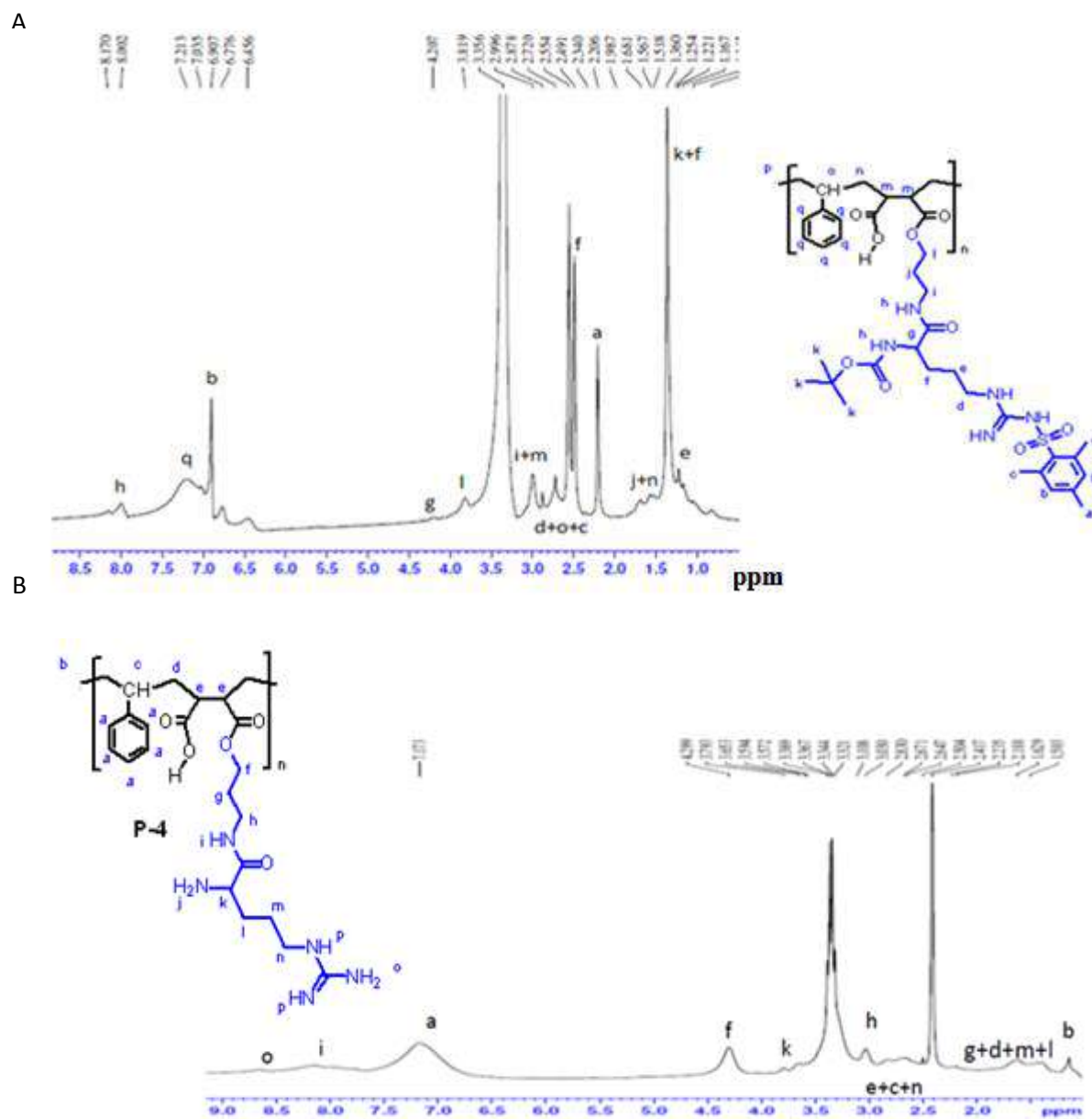
Figure 2.12. ^{1}H NMR spectra (300 MHz, DMSO-d_6) of (A) Boc-Arginine (Mts)-OH grafted PSMA; δ 1.17(br m, aliphatic C$\underline{H}_2$ + C$\underline{H}_3$), 1.36 (br s, Boc C$\underline{H}_3$), 1.68 (br m, aliphatic C$\underline{H}_2$), 2.2 (br d, Ar C$\underline{H}_3$), 2.55 (br d, Ar C$\underline{H}_3$), 2.72 (br m, aliphatic C$\underline{H}$+ C$\underline{H}_2$), 3 (br m, aliphatic C$\underline{H}$+ C$\underline{H}_2$), 3.82 (br m, aliphatic C$\underline{H}_2$), 4.2 (m, aliphatic C$\underline{H}$), 6.9 (br s, Ar C$\underline{H}$), 7.2 (br m, Ar C$\underline{H}$), 8 (br m, N$\underline{H}$) and (B) **P4**; δ 1.17 (br m, aliphatic C$\underline{H}_3$), 1.7 (br, aliphatic C$\underline{H}_2$), 2.7 (br, aliphatic C$\underline{H}$ + C$\underline{H}_2$), 3.1 (br m, aliphatic C$\underline{H}_2$), 3.7 (br m, aliphatic C$\underline{H}$), 4.3 (br m, aliphatic C$\underline{H}_2$), 7.2 (br m, Ar C$\underline{H}$)

77
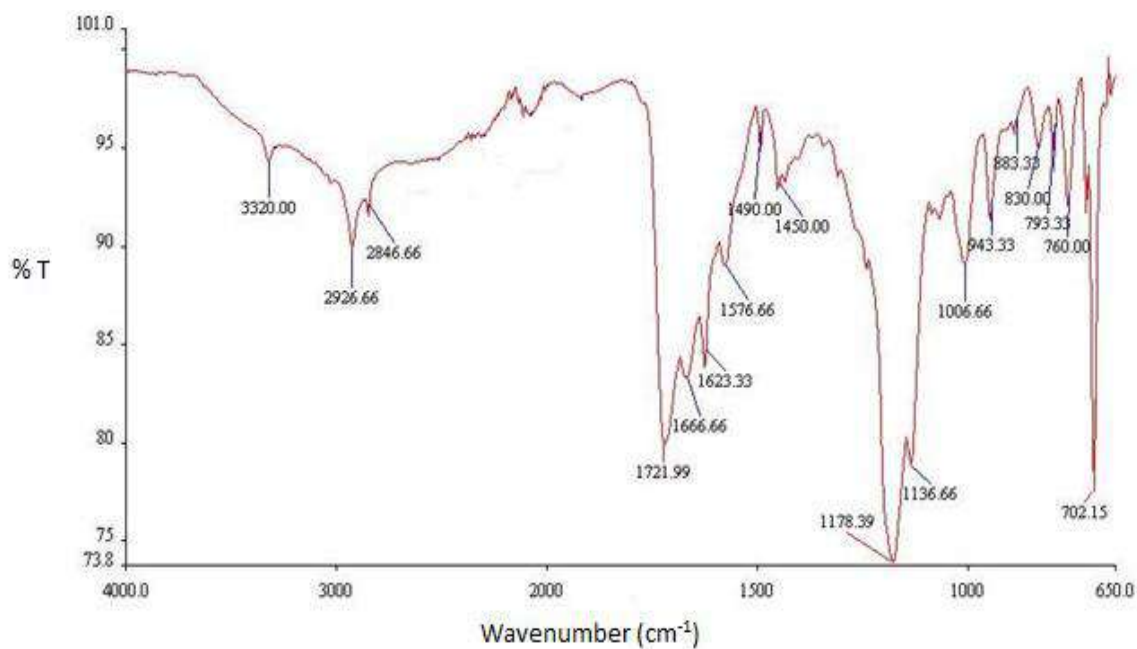
Figure 2.13. ATR-FTIR spectrum of L-arginine grafted PSMA (**P4**)

2.3.1.5. Conjugation of spermine to PSMA

Spermine grafted PSMA (**P5**) was prepared by reacting mono N- Boc-protected spermine with anhydride groups of the polymer. Spermine was selectively protected with Boc group for avoiding possible cross linking of PSMA chains. 1 equivalent of Boc anhydride was reacted with 4 equivalents of spermine, to yield mono N-Boc protected spermine (~ 90 % peak intensity) as indicated by mass spectra (Figure 2.14) . ^{1}H NMR spectra of mono N-Boc protected spermine (Figure 2.15) in CDCl$_3$ showed characteristic signals of Boc at δ 1.44, and methylene groups at δ 1.53, δ 1.68, δ 2.66 and δ 3.18. Spermine grafted PSMA (**P5**) was obtained by conjugating mono-N-Boc protected spermine to anhydride molecules, followed by the cleavage of Boc. ^{1}H NMR of Boc-spermine grafted PSMA (Figure 2.16 A) in CD$_3$OD showed a sharp signal at δ 1.36, indicative of methyl groups of Boc. When dispersed in DMSO, **P5** exhibited a turbid gel like consistency probably due to strong hydrogen bonding contributed by multiple amine groups

78
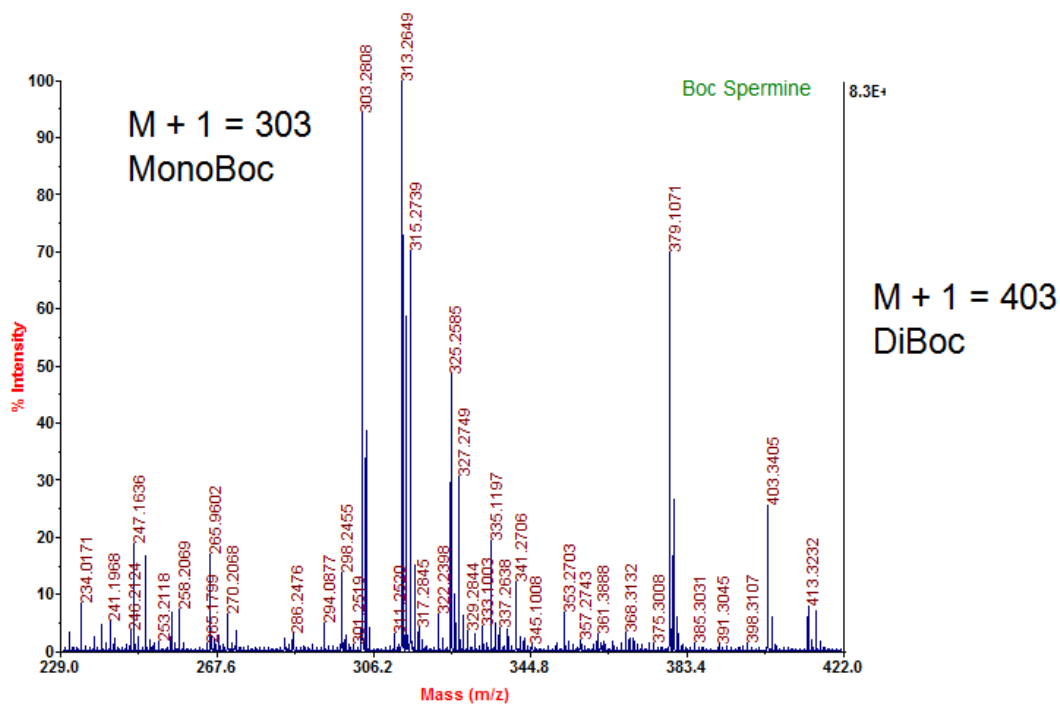
Figure 2.14. Mass spectrum of Boc- protected spermine
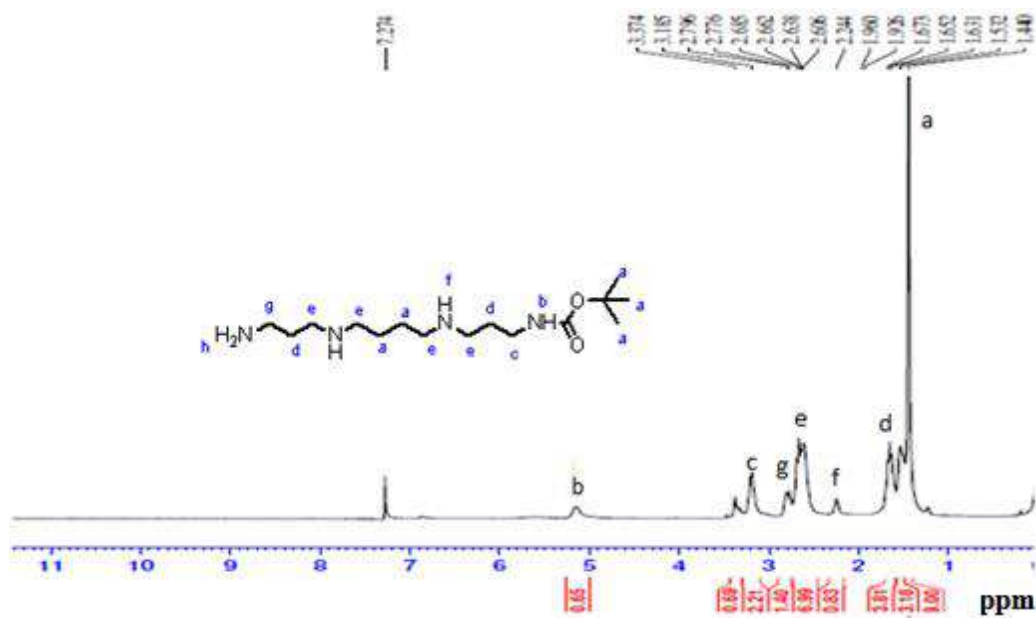
Figure 2.15. ^{1}H NMR spectrum (300 MHz, CDCl$_3$) of mono-N-Boc protected spermine. δ 1.44 (s, 9H, Boc C*H*$_3$), 1.53 (m, 4H, C*H*$_2$)1.67 (m, 4H, C*H*$_2$), 2.24 (br s, 1H, CH$_2$-N*H*-CH$_2$), 2.64 (m, 8H, HN-C*H*$_2$-CH$_2$-), 2.8 (m, 2H, C*H*$_2$) , 3.2 (m, 2H, HN-C*H*$_2$), 3.38 (br s, 1H, N*H*), 5.1 (br s, 1H, Boc NH)
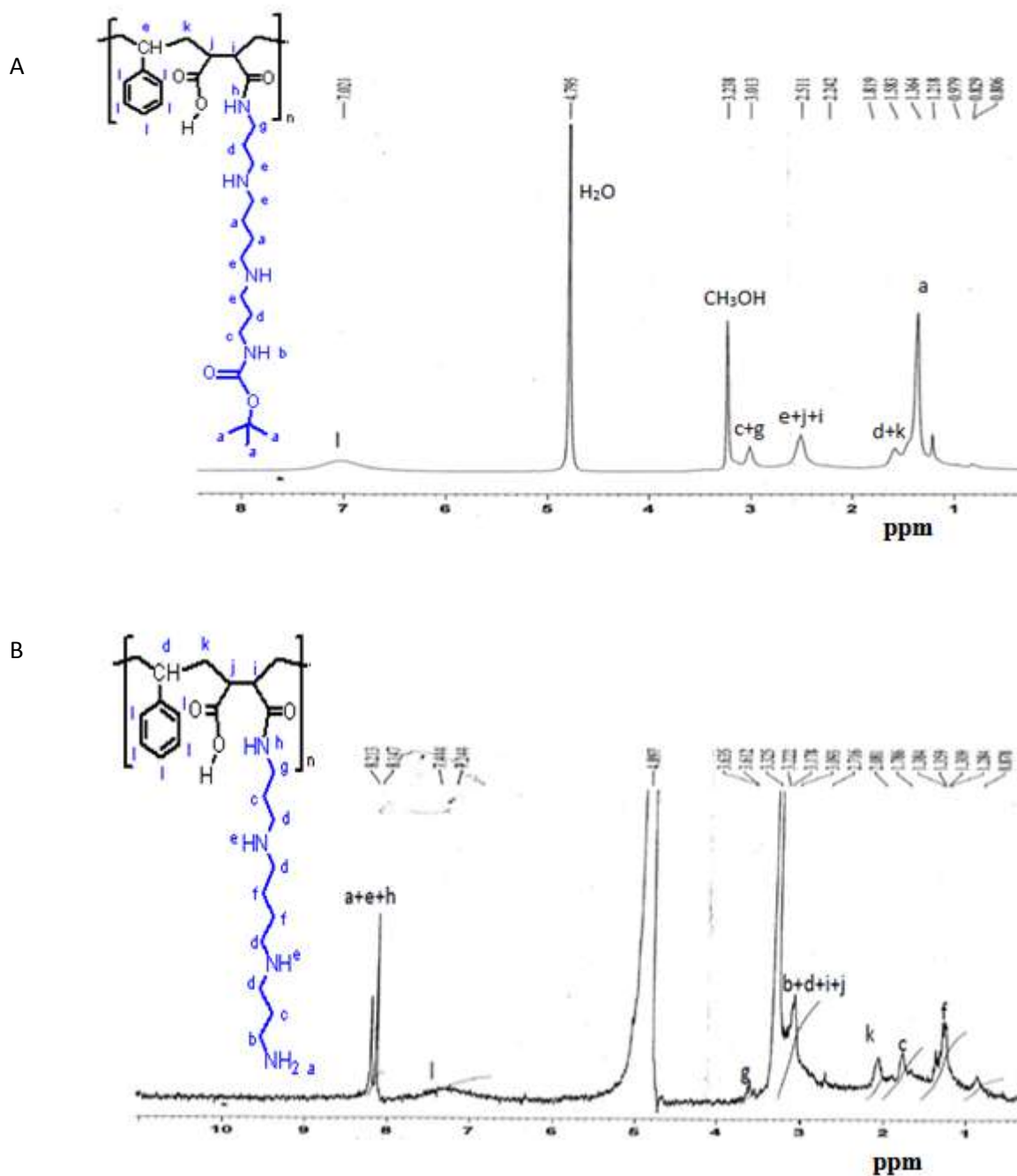
Figure 2.16. ^{1}H NMR spectra (300 MHz, CD$_3$OD) of (A) mono-N-Boc-protected spermine grafted PSMA; δ 1.2 (br m, aliphatic C$\underline{H}_3$), 1.36 (br s, Boc C$\underline{H}_3$), 1.6 (br m, aliphatic C$\underline{H}_2$), 2.5 (br m, aliphatic C$\underline{H}$ + C$\underline{H}_2$), 3 (br m, aliphatic C$\underline{H}_2$), 7 (br m, Ar C$\underline{H}$) and (B) of **P5** (300 MHz, DMSO-d_6); δ 1.2 (br m, aliphatic C$\underline{H}_2$ + C$\underline{H}_3$), 1.8 (br m, aliphatic C$\underline{H}_2$), 2.1 (br m, aliphatic C$\underline{H}_2$), 3.1 (br, aliphatic C$\underline{H}$ + C$\underline{H}_2$), 3.7 (br m, aliphatic C$\underline{H}_2$), 7.4 (br m, Ar C$\underline{H}$)

.

in spermine. But the solubility was improved upon addition of water. ^{1}H NMR of **P5** (Figure 2.16 B) was recorded using CD$_3$OD: D$_2$O mixture, at 1:1 ratio, to which a drop of TFA (deuterated) was added. The absence of sharp signal at δ 1.36 indicated complete deprotection, and the presence of methylene groups of spermine in the polymeric graft was confirmed by peaks at δ 1.3, δ 1.7 and δ 3.1. ATR-FTIR of **P5** (Figure 2.17) displayed characteristic frequency of carboxylic acid at 1726 cm^{-1}, and amide bands at 1669 cm^{-1} and 1543 cm^{-1}.
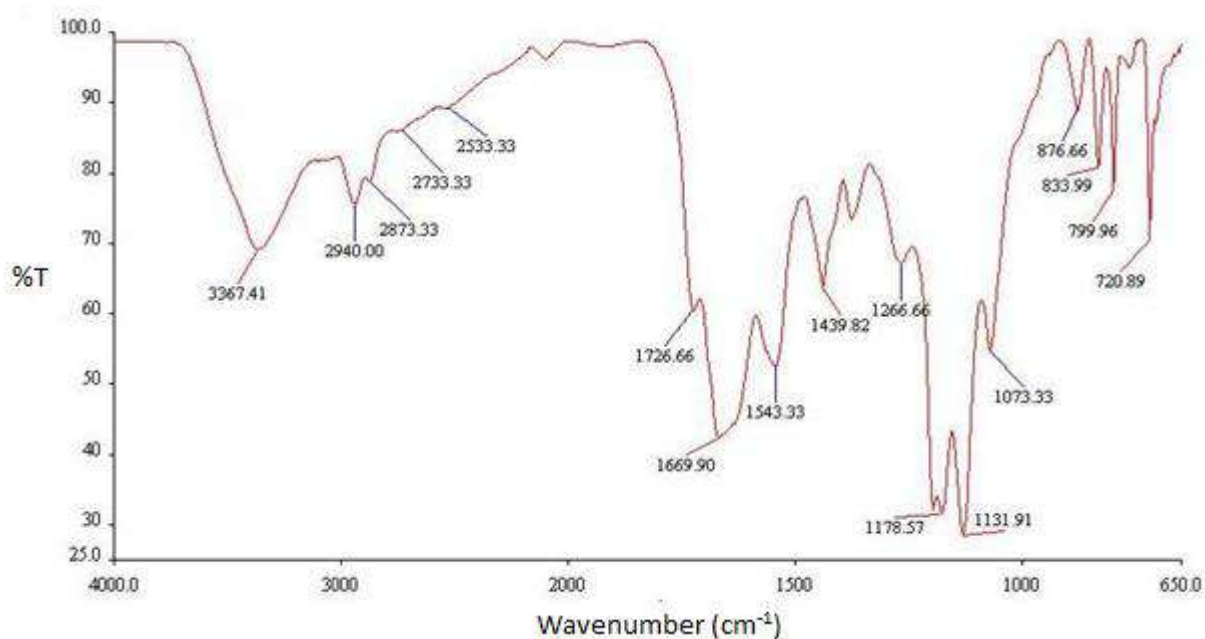
Figure 2.17. ATR-FTIR spectrum of spermine grafted PSMA (**P5**)

2.3.2. Formulation and characterization of polymeric nanoparticles

Due to their amphiphilic nature, all the PSMA derivatives self assembled in aqueous media to form stable nanoparticles. During the preparation of nanoparticles, formulation parameters viz. weight of the polymer, solvent: non solvent ratios and sonication amplitude were kept constant.

The sonication time was increased for each formulation till no further decrease in particle size was observed, and chosen as the optimum sonication time. Zeta potential of various nanoparticle formulations were measured after dispersing in milliQ water and phosphate buffer saline (pH 7.4). Details of particle size, zeta potential and optimum sonication time for each polymeric derivative are given in table 2.1. Nanoparticles of quaternized derivatives viz. **P1**and **P3** were formulated using DMSO: water mixture as solvent: non solvent, respectively. They were completely soluble in the solvent phase viz. DMSO, and formed nanoparticles of optimized size range and lower polydispersity indices (PDI). Optimized nanoparticles of **P1** have shown a polydispersity index of 0.108 ± 0.01, and that of **P3** exhibited PDI of 0.122 ± 0.01. PDI of the nanoparticles of **P2** viz. 0.226 ± 0.035 indicates their comparatively heterogeneous particle size distribution w.r.t nanoparticles of **P1** and **P3**.

Table 2.1. Optimized parameters of nanoparticulate formulations of PSMA grafts

Polymeric derivative	Optimum sonication time (min)	Average particle size (nm)	Polydispersity index (PDI)	Zetapotential (mV) in water	Zeta potential (mV) in PBS (pH 7.4)
P1	0.5	94 ± 3	0.108 ± 0.01	42.61 ± 1.17	-15.02 ± 2.33
P2	1.5	112 ± 5.22	0.226 ± 0.035	46.15 ± 1.64	12.28 ± 0.53
P3	1	107 ± 2.16	0.122 ± 0.01	30.18 ± 1.06	-17.18 ± 2.66
P4	2.5	134 ± 4.67	0.292 ± 0.023	32.01 ± 1.68	4.12 ± 0.71
P5	3	162 ± 6.82	0.34 ± 0.04	34.34 ± 3.4	12.16 ± 1.39

Mean $\pm$ SD, $n = 3$

P4 and **P5** formed a gel like consistency, when dispersed in DMSO. Formation of strong intra/inter molecular hydrogen bonding between the amines present in **P4** and **P5** might have contributed to this gel formation. On addition of aqueous phase and subsequent sonication, they formed stable nanoparticles with comparatively higer PDI than the quaternized ones. **P5**

nanoparticles exhibited maximum PDI followed by **P4** nanoparticles (0.34 ± 0.04 and 0.292 ± 0.023 respectively). The replacement of hydrogen bonding between the solutes by the same between solvent and solute molecules, on addition of aqueous phase, was the probable mechanism for nanoparticle formation of **P4** and **P5**.

All the formulations exhibited positive zeta potential, when dispersed in milliQ water. But, they have shown reduced zeta potential in phosphate buffered saline (PBS, pH 7.4). In case of **P1**, zeta potential decreased from $+ 42.61 \pm 1.17$ to -15.02 ± 2.33, when dispersed in PBS pH 7.4. This decrease in zeta potential to negative side was due to the ionization of free carboxylic acid groups present in the polymer. These carboxylic anions could neutralize the positive charge contributed by quaternary nitrogen of isonicotinic acid, and hence contributed to reduction in zeta potential. **P2** also exhibited reduction in zeta potential from $+ 46.15 \pm 1.64$ to $+ 12.28 \pm 0.53$, with increase in pH. But zeta potential of P2 nanoparticles didn't reduce to negative side, due to the presence of more quaternary nitrogen (contributed by piperazinyl side chains) in the polymeric side chains. The reduction in zetapotential of P3 nanoparticles from $+ 30.18 \pm 1.06$ to $- 17.18 \pm 2.66$, when dispersed in PBS, pH 7.4, could also be envisaged to the above mentioned reason.

L-arginine grafted PSMA nanoparticles have retained some positive charge viz. $+ 4.12 \pm 0.71$. This could be due to the property of the guanidino groups of L-arginine to remain protonated and positively charged, at physiological pH [7, 8]. Spermine grafted PSMA nanoparticles have also shown a reduction in zeta potential from $+ 34.34 \pm 3.4$ to $+ 12.16 \pm 1.39$. Spermine is a multivalent organic cation [9]. At physiological pH, the amines present in spermine get protonated [10]. Due to the protonation of primary and secondary amines, spermine grafted PSMA nanoparticles retained positive zeta potential in PBS, pH 7.4.

High resolution transmission electron microscopy (HR-TEM) images of the nanoparticles (Figure 2.18) showed core shell morphology, attributed to the amphiphilic nature of polymeric derivatives [11]. The particle size of nanoparticles obtained in HR-TEM was lesser than that of the DLS measurements. This could be explained on the basis of the formation of a hydrodynamic layer around the nanoparticles, when they were dispersed in water. DLS measures this hydrodynamic diameter, which in turn contribute to increased particle size [12]. The difference in particle size between DLS and HR-TEM measurements were more pronounced in case of quaternized derivatives, probably due to their minimal intermolecular hydrogen bonding and the resultant enhanced solubility in solvent phase. **P1** exhibited a particle size range of ~ 30-65 nm in HR-TEM, whereas the DLS measurements of the same resulted in an average paricle size (Z average) of 94 ± 3.06 nm. HR-TEM image of **P2** nanoparticles also shown narrow particle size range of ~ 40-70 nm in comparison to the average DLS particle size of 112 ± 5.22 nm. Average particle size of **P3** nanoparticles measured by DLS was 107 ± 2.16, in comparison to the lower particle size range of 42-56 nm obtained in HR-TEM. HR-TEM images of the nanostructures formed by **P4** and **P5** showed that the particles were of 30-70 nm and 60-120 nm size range, respectively. The wide range of particle size distributions observed in **P4 and P5** indicated their comparatively high polydispersed nature.
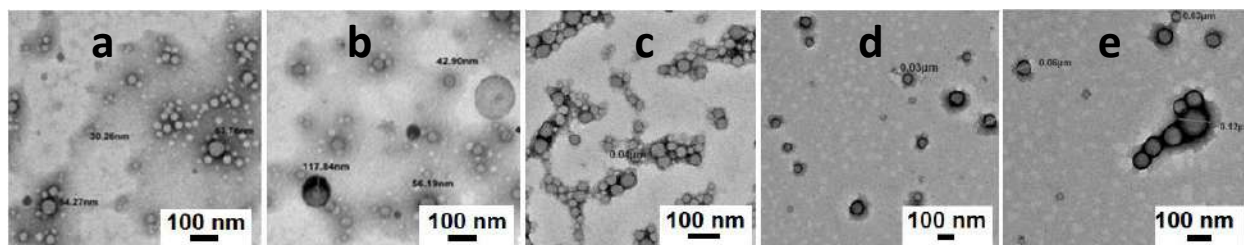
Figure 2.18. HR-TEM images of the nanoparticles of (a) **P1** (b) **P2** (c) **P3** (d) and **P4** (e) **P5**. All samples were prepared by drop-casting the aqueous dispersion of the respective polymer samples on copper grid and positively stained by phosphotungstic acid.

The core shell type morphology of nanoparticles depicts their ability for incorporating both drugs and genes. Combinatorial delivery of anticancer drugs and gene therapy agents, viz. siRNA, shRNA, miRNA etc. are gaining importance in the cancer therapy [13-15]. Another advantageous feature of these low molecular weight PSMA nanoparticles is their *in vivo* biodegradability. Since the derivatizing agents of PSMA are linked via ester or amide bonds to the polymer backbone they can be easily cleaved through enzymatic hydrolysis, within the biological system, facilitating their elimination from the body. After the hydrolytic cleavage of ester or amide bonds *in vivo,* the low molecular weight PSMA derivatives will get converted in to small units with reduced molecular weight and enhanced solubility [16]. These small polymeric fragments can be easily degraded and eliminated [17]. This is a major advantage of low molecular weight PSMA over high molecular weight ones, the biodegradability of later being an obstacle for *in vivo* application. In addition, due to the amphiphilic and self assembling properties of these polymeric grafts, large scale production of their nanoparticles is feasible [18]. Formulation of stable nanoparticles of various PSMA derivatives were easily accomplished, without the use of excipients like surfactants, co-surfactants etc. This cost effective production and high stability makes them an attractive vehicle for intracellular delivery. Hence, developing pharmaceutical formulations based on these polymers are less challenging.

2.3.3. Cytotoxicity studies

Cytotoxicity of all the nanoparticle formulations was evaluated in two cell lines viz. MCF 7 and L929. Concentrations of nanoparticles tested were in the range of 50-1000 µg/mL. The cells were treated with various nanoparticle formulations for 48 hours, and the % cell viability was assessed by MTT assay (Figure 2.19). At 1000 µg/mL, **P1** has shown 72 % and 56 % cell viability, respectively in MCF 7 and L929 cell lines. The viability of cells seemed to be increased

with lowering the nanoparticle concentrations. The % cell viability of **P1** nanoparticles were increased to 99 % and 88 %, respectively in MCF 7 and L929 cell lines, at the lowest concentration tested viz. 50 µg/mL. **P3** has also shown a similar pattern of increase in cell viability, at lower concentrations of nanoparticles tested. At 50 µg/mL concentration, **P3** nanoparticles achieved more than 94 % cell viability in L929 cells, and showed no toxicity in MCF 7 cells. Cytotoxic effects of **P2** nanoparticles were significantly higher than that of **P1** and
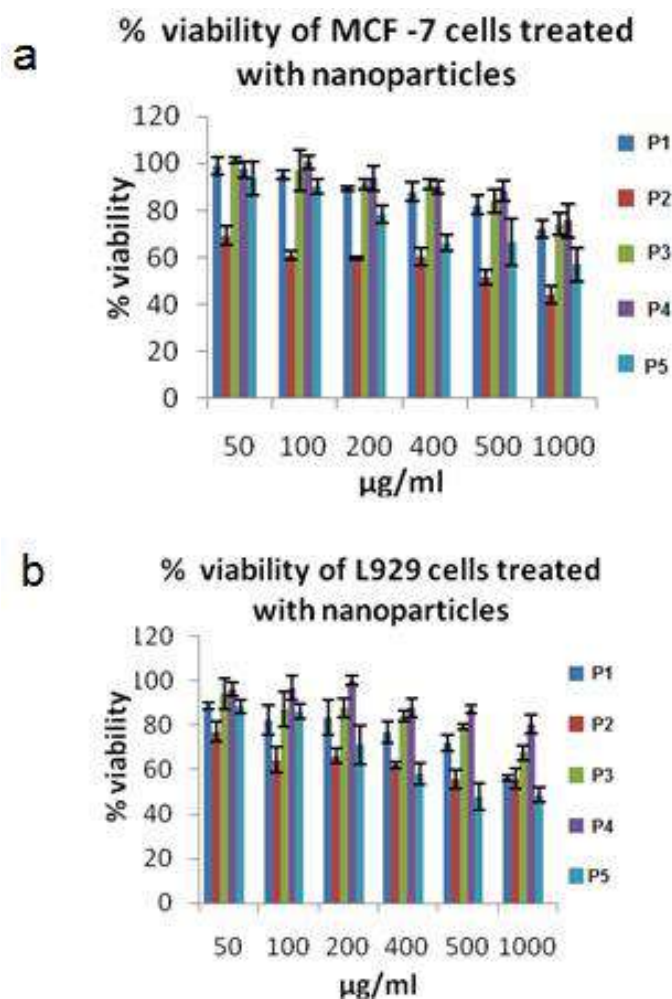
Figure 2.19. % cell viability of various nanoparticles in (a) MCF 7 cell lines and (b) L929 cells; (Mean ± SD, $n = 3$). Concentrations of nanoparticles (µg/mL) are represented in x-axis.

P3. Maximum cell viability observed for **P2** nanoparticles were 69 % and 77 %, respectively in MCF 7 and L929 cells, at 50 µg/mL. This pronounced cytotoxic effect could be due to the presence of quaternized piperazine side chains with more cationic charge densities and their interaction with the cell membranes. Lower cationic charge densities and extensive shielding by surface carboxylic acid side chains of polymer backbone could be the reasons for comparatively lower cytotoxicities of **P1** and **P3** [19]. For finding out safer concentration range of **P2** nanoparticles, we have performed cytotoxicity studies at concentrations below 50 µg/mL. **P2** nanoparticles exhibited more than 90 % viability at 20 µg/mL, in both the cell lines (data not shown).

L-arginine grafted PSMA (**P4**) nanoparticles also exhibited minimal cytotoxicity at various concentrations tested. They have shown cell viability values of 75 % and 80 % in MCF 7 and L929 cells, respectively, at the maximum concentration tested (1000 µg/mL). Below 200 µg/mL, no cytotoxicity was observed for **P4**. L-arginine moieties in **P4** have very basic side chains and their guanidine groups are positively charged at physiological pH. But the shielding by negatively charged carboxylic acid groups of polymer backbone could have minimized the interaction of gaunidinium groups with the cell membrane. This could be the probable reason for the minimal cytotoxicity of **P4** nanoparticles at various concentrations tested. Spermine grafted PSMA (**P5**) nanoparticles exhibited significant cytotoxicity at higher concentrations (200-1000 µg/mL), in both the cell lines. Cell viability of **P5** nanoparticles at 1000 µg/mL were 56 % and 48 %, respectively in MCF 7 and L929 cells. Below 100 µg/mL, **P5** nanoparticles depicted more than 85 % cell viability in both the cell lines. In case of **P5**, multiple protonating sites in the grafted spermine molecules induced more cationic charge, and thereby cytotoxicity. But the cytotoxic behaviour of spermine grafted PSMA nanoparticles were dose dependent, and they

were safer to cells at concentrations (100 µg/mL and below) suitable for *in vivo* gene delivery applications.

2.3.4. Blood compatability and endosomal release properties of nanoparticles

For evaluating blood compatability and endosomal release properties, haemolysis of nanoparticles was studied at two different pH values, viz. 7.4 and 5.5. Haemolytic behaviour of nanoparticles at pH 7.4 indicates their blood compatibility, whereas the same at 5.5 could provide information regarding their ability to overcome endosomal uptake. Membrane destabilizing polymers can cause haemolysis at the similar pH values of endosomes (5.5-5.8) [10]. Hence the haemolytic behaviour of these particles at pH 5.5 can be correlated with their endosomal release. The % haemolysis of various nanoparticle formulations is shown in figure 2.20. The results indicated that the haemolytic effects of all the formulations tested were directly proportional to the concentrations of nanoparticles.

Nanoparticles of quaternized polymeric derivatives viz.**P1**, **P2** and **P3** have shown almost similar pattern of haemolysis, at pH 7.4. Maximum % haemolysis shown by **P1**, **P2** and **P3** were, 4.83 ± 0.85, 6.13 ± 0.4 and 4.08 ± 1.33 respectively, at 1000 µg/mL. This significantly low haemolysis at physiological pH shows their excellent blood compatibility. Ionization of carboxylic acid groups of these quaternized polymeric derivatives at physiological pH and the resultant reduction in their surface positive charge (Table 2.1) might have contributed to the minimal haemolysis. At pH 5.5, **P1** has shown significantly higher % haemolysis compared to **P2** and **P3** (Figure 2.20. B). Maximum % haemolysis of 86.51 ± 3.2 and minimum % haemolysis of 17.17 ± 1.35 was obtained for **P1**, at the respective nanoparticle concentrations of 1000 µg/mL and 50 µg/mL. This high % haemolysis observed for **P1**, at pH 5.5, could be due to the membrane destabilizing effect of quaternized aromatic side chains of the polymer. Hydrophobic aromatic chains imparted

with positive charge can get easily incorporated in to the RBC membrane and cause their destabilization. The role of hydrophobic polymeric side chains in enhancing haemolysis at acidic pH has been experimentally reported by Henry et al [20].
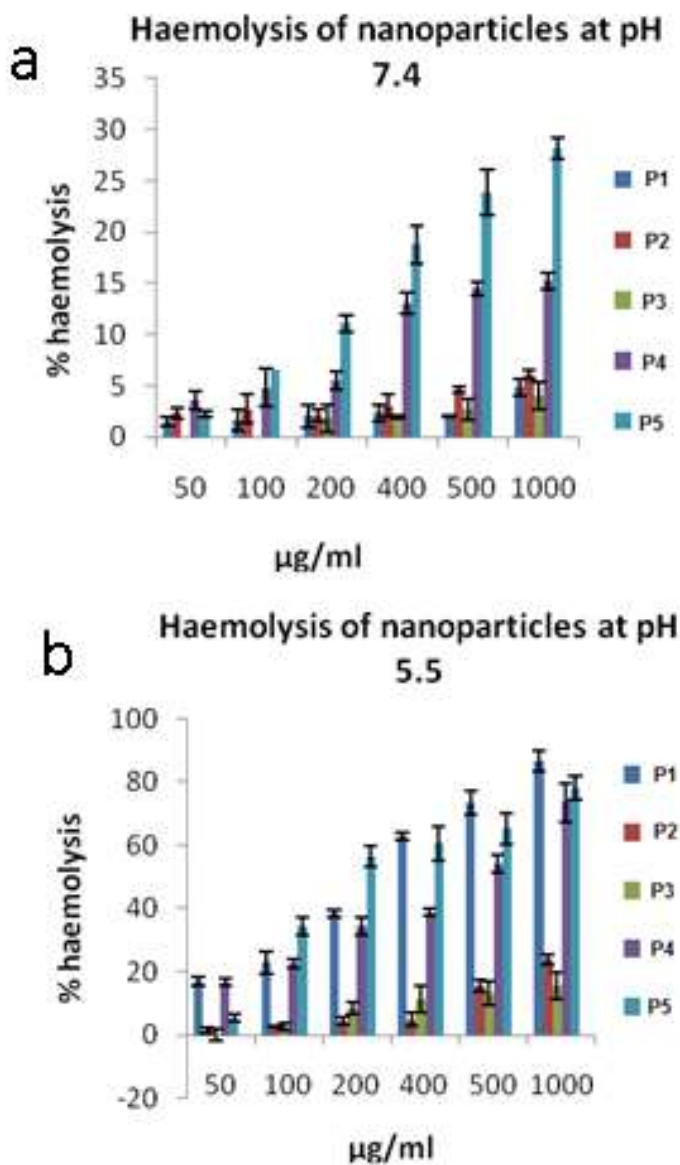
Figure 2.20. Haemolytic assay of various nanoparticulate formulations at (a) pH 7.4 and (b) pH 5.5 (Mean $\pm$ SD, $n = 3$). Concentrations of nanoparticles (µg/mL) are represented in x-axis.

Eventhough **P1**, **P2** and **P3** possess same features viz. unionized and protonated state of the carboxylic groups of polymeric side chains and the presence of quaternary nitrogens providing

cationic charge, % haemolysis of **P1** at 1000 µg/mL was 3.6 fold higher than **P2** and 5.5 fold higher than **P3**. **P2** and **P3** exhibited a moderate increase in % haemolysis at pH 5.5 (24.04 ± 1.64 and 15.68 ± 4.07 respectively, at 1000 µg/mL), compared to that at pH 7.4. This variation in haemoreactivity could be explained by the fact that, quaternized aromatic side chains of **P1** were able to disturb the inner parts of RBC membrane structure more effectively than the quaternized aliphatic groups of **P2** and **P3** [21]. From these results, it is clear that the presence of quaternary nitrogens in the polymeric side chains alone cannot induce haemolysis, because of their inability to bind protons and promote osmotic lysis of RBC membrane. Presence of hydrophobic groups in the polymer side chains plays a crucial role in RBC lysis at acidic pH (5.5), and hence the same can promote membrane rupture at endosomal pH conditions.

L-arginine grafted PSMA and spermine grafted PSMA nanoparticles have shown considerable haemolysis at pH 7.4. At 1000 µg/mL, **P4** showed 15.27 ± 0.79 % and **P5** induced 28.2 ± 1.08 % haemolysis. But haemoreactivity of the nanoparticles of **P4** and **P5** was found to reduce at lower concentrations (below 200 µg/mL) with a minimal % haemolysis of 3.61 ± 1.86 % and 2.28 ± 0.34 %, respectively, at 50 µg/mL. The haemolytic experiments were performed in saline buffer with washed RBC's, rather than in serum or whole blood. Reports are suggesting that, plasma proteins present in the blood can bind polycations and thus reduce their affinity towards RBC's [22]. This means that in actual physiological conditions of blood (pH 7.4), the haemolytic effect of these polymeric nanoparticles could be further lowered.

Both **P4** and **P5** have shown higher haemolysis at pH 5.5, due to the presence of primary and secondary nitrogens in their side chains which can bind protons at acidic pH and promote membrane lysis. Nanoparticles of **P4** and **P5** incubated with RBC's at pH 5.5 have shown maximum % haemolysis of 73.52 ± 6.2 and 78.05 ± 3.89, respectively, at 1000 µg/mL. They

have also shown higher % haemolysis at all concentrations in pH 5.5, compared to corresponding concentrations in pH 7.4. This could be due to the binding of protons to the primary and secondary amines in acidic pH. The protonation of primary and secondary amines will be accompanied by counter flow of anions and subsequent increase in osmotic pressure, which may be responsible for the rupturing of RBC membrane. Similar mechanism is also responsible for the endosomal membrane rupture and is termed as proton sponge effect [23]. From the haemolytic study of different polymeric derivatives, we have concluded that the major driving forces for promoting membrane rupture at endosomal pH are (i) membrane destabilization by the hydrophobic side chains and (ii) proton sponge effect produced by the protonation of primary or secondary amines present in the polymeric systems.

2.3.5. Formulation of polyplexes and their evaluation

Polyplex formation was achieved via electrostatic interactions between the phosphate groups of DNA base pairs and amine groups of polymeric nanoparticles. In addition, aromatic groups and amide linkages present in the polymeric derivatives can interact via hydrogen bonding to the DNA base pairs [24]. Gel retardation of pDNA in the polyplexes gives clear cut information regarding the DNA binding and condensation efficiency of the cationic polymeric nanoparticles. For the gel retardation study, we have kept the amount of pDNA constant at 1 µg, and varied the amount of polymeric nanoparticles. For comparative evaluation of different polyplexes, polymer/pDNA weight ratios of 20, 15, 10 and 5 were chosen. The selection of these weight ratios were based on the cytotoxic profile of polymeric nanoparticles. Maximum polymer/pDNA weight ratio selected was 20, equivalent to a concentration of 100 µg/mL of polyplex when dispersed in 96 wells containing 200 µL of media. Similarly, lower weight ratios viz. 5, 10 and 15 corresponded to polyplex concentrations of 25, 50 and 75 µg/mL, respectively. Since

nanoparticles of all the polymeric derivatives have shown reduced zeta potentials at physiological pH, their complex formation with pDNA was carried out in DNase free water (neutral pH). This was to prevent ionization of carboxylic acid groups in the polymer side chains, and there by facilitating efficient complex formation. Gel retardation of the pDNA by various PSMA derivatives, at different weight ratios, is shown in figure 2.21.
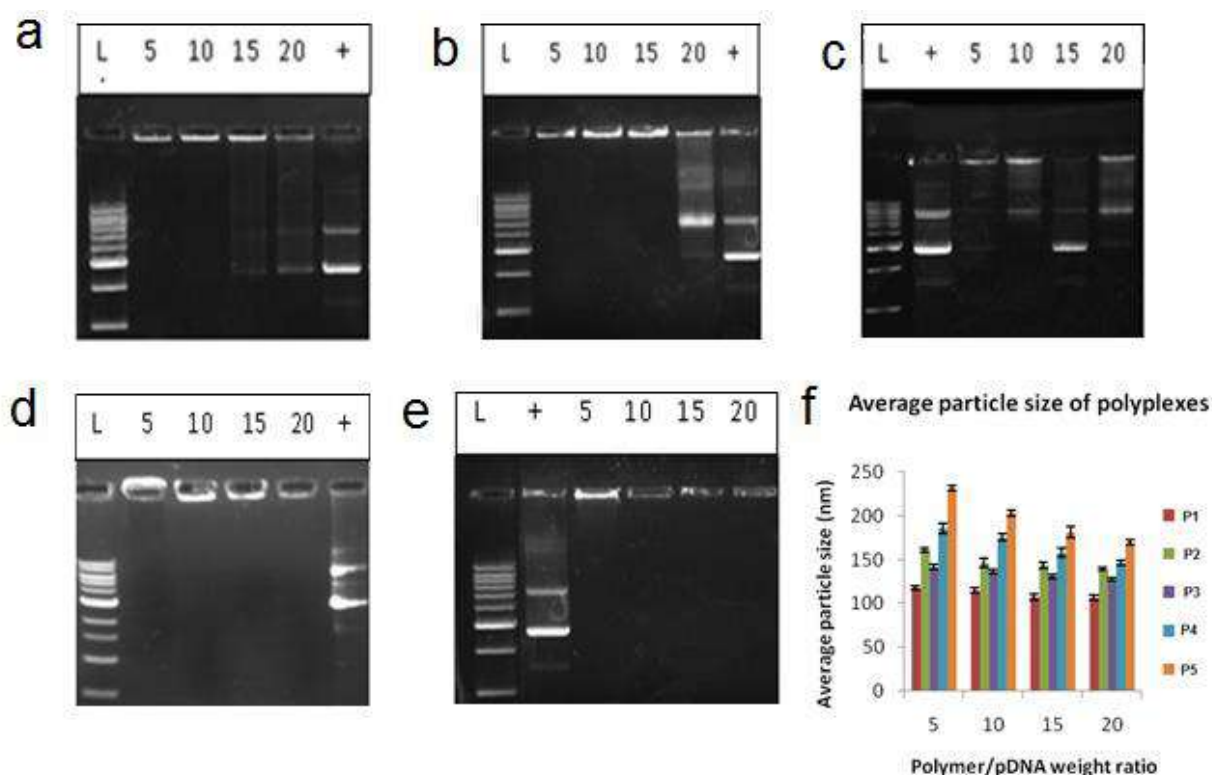
Figure 2.21. Agarose gel (1 %) electrophoresis showing bands of complexed pDNA in polyplexes of (a) **P1** (b) **P2** (c) **P3** (d) **P4** and (e) **P5**. 5, 10, 15 and 20 are the weight ratios of the polymer to pDNA. L represents ladder and + is pure pDNA (control) (f) Average particle sizes of polyplexes at different polymer/DNA weight ratios (Mean $\pm$ SD, n = 3).

Polyplexes of **P1** have shown maximum retardation at lower polymer to pDNA weight ratios (5 and 10), and comparatively increased DNA release at higher ratios viz.15 and 20. Quaternized piperazine grafted PSMA (**P2**) exhibited efficient gel retardation at weight ratios viz. 5, 10 and

15, whereas proper binding and condensation of pDNA was not observed at polymer/pDNA weight ratio of 20. The carboxylic acid groups of polymer side chains can ionize in gel loading buffers (pH 7.4) and induce electrostatic repulsive forces. This could be the reason for reduced gel retardation of pDNA at higher weight ratios. The electrostatic repulsive effect was more pronounced in case of **P3**, as shown in figure 5, where minimal retardation was observed at all weight ratios tested. Polyplexes of **P3** incorporated the pDNA predominantly through the cationic charges of glycidyl trimethyl ammonium chloride side chains. But in case of **P1**, additional binding forces viz. π-π stacking of aromatic side chains (isonicotinic acid) and hydrogen bonding of amide linkages could also take part in polyplex formation [25]. **P2** possesses more cationic charge densities due to the presence of two quaternary nitrogens per monomer unit, and remains positively charged at physiological pH. These could be the reasons for better gel retardation properties of **P1** and **P2**, in comparison to **P3**.

L-arginine conjugated PSMA (**P4**) and spermine grafted PSMA (**P5**) have shown efficient gel retardation of pDNA, at all weight ratios tested. This could be attributed to the ability of guanidino groups of L-arginine and multivalent cations of spermine to get protonated and retain positive charge, at physiological pH. The pattern of pDNA binding in the polyplexes of **P4** and **P5** seemed to be in reverse manner to that of the quaternized ones. As polymer/pDNA weight ratios were increased, more efficient binding and condensation of DNA was observed in **P4** and **P5**. This shows that, the primary and secondary amines present in **P4** and **P5** could effectively neutralize the electrostatic repulsive forces produced by the ionization of carboxylic acid groups.

Cell viability studies of polyplexes in MCF 7 and L929 cells indicated that, polyplexes of all the polymeric derivatives, except **P2**, were safer at different weight ratios tested (data not shown). But polyplexes of **P2** have shown increased % cell viability compared to the corresponding

concentrations of uncomplexed nanoparticles. This could be due to the neutralization of surface cationic charge by complexed pDNA molecules. Further, at polymer/ DNA weight ratio viz. 5, polyplexes of **P2** exhibited more than 90 % cell viability in both the cell lines. The polyplexes were also evaluated for their particle size and zeta potential, using DLS, by dispersing them in milliQ water. Particle size of various polyplexes exhibited slight to moderate increase with decrease in the polymer/pDNA weight ratio (Figure 2.21 f).

At higher weight ratios of polymer/pDNA, more cationic binding sites are available, which leads to better condensation of complexed pDNA. Hence, average particle size of polyplexes was found to increase with lowering the polymer/pDNA weight ratios. It has been observed that, less polydispersed nanoparticles viz. **P1** and **P3** have shown slight increase in particle size with decrease in weight ratio, whereas moderate increase in particle size was obtained for polyplexes of **P2**, **P4** and **P5**, whose PDI values were comparatively higher. Maximum particle sizes were obtained for the polyplexes of **P5**, whose average size increased from 169.6 ± 3.1 to 231.8 ± 2.1, with respective decrease in polymer/DNA weight ratios from 20 to 5. Zeta potentials of all polyplexes have shown slight decrease with the decrease in polymer/DNA weight ratio, due to the consequent reduction in cationic surface charge (data not shown). Maximum zeta potential was obtained for polyplexes of **P2** ($+ 47.5 \pm 2.54$), at the polymer/DNA weight ratio of 20. The zeta potential was reduced slightly to $+ 43.62 \pm 3.8$, with the corresponding decrease in weight ratio to 5. Other polyplexes also exhibited similar pattern of variation in zeta potential, w.r.t. polymer/DNA weight ratio.

2.3.6. DNase I protection assay

The efficiency of various polyplexes to protect complexed DNA was evaluated by treating with DNase I. Stable electrostatic interactions are required for efficient binding and condensation of

DNA in the nanoplexes. The results of DNase I degradation study of various polyplexes are shown in figure 2.22. Nanoplexes of spermine grafted PSMA (**P5**) have shown efficient condensation and protection of pDNA, at all weight ratios tested (Figure 2.22 a). At higher weight ratios viz. 20 and 15, the binding and condensation were strong enough to prevent the release of DNA, even after treatment with heparin. This could be due to the strong electrostatic interaction of the multivalent cations of spermine towards pDNA. At lower weight ratios of **P5** viz. 5 and 10, pDNA showed release from the polyplexes. L-arginine grafted PSMA (**P5**) nanoparticles were also effective in protecting pDNA from DNase degradation, as indicated by
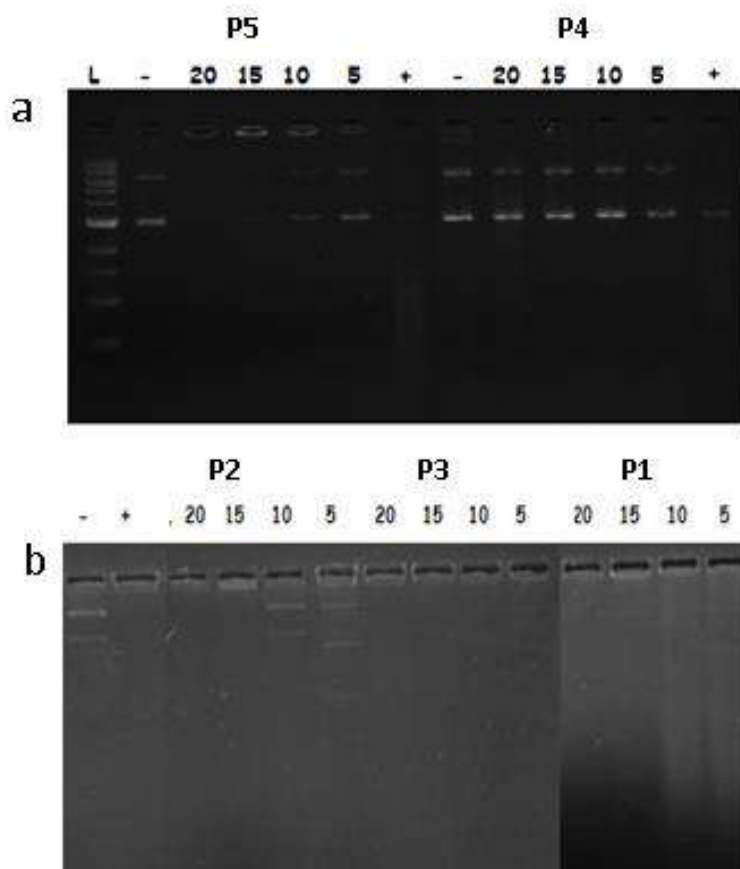
Figure 2.22. DNA release from the polyplexes of (a) **P4** and **P5** (b) **P2**, **P3** and **P1** at different weight ratios (20, 15, 10 and 5) after treatment with DNase and heparin. L represents ladder, - indicates untreated pDNA and + shows treated pDNA.

the release of DNA from their polyplexes. The ability of guanidino groups of L-arginine for binding and condensing pDNA, due to their cationic nature at physiological pH, is well established.

In case of quaternized polymeric grafts (**P1**, **P2** and **P3**), the surface cationic charge of nanoparticles had significant role in the protection of pDNA against DNase I (Figure 2.22 b). Polyplexes of **P1** exhibited complete degradation of DNA at higher weight ratio viz. 20. At lower weight ratios of **P1**, DNA bands were observed, but the conformation of released DNA seemed to be changed. This could be due to the partial digestion by DNase I. In case of **P2**, weight ratios of 5 and 10 have shown efficient protection of pDNA. The positive surface charge of the nanoparticles of **P2**, in physiological pH (Table 2.1), might have contributed to their stable binding and condensation of DNA. Polyplexes of **P3** exhibited complete digestion of pDNA, at all weight ratios tested. Nanoparticles of **P1** and **P3** were not able to condense DNA efficiently, probably due to their surface negative charge in physiological pH and electrostatic repulsive forces of carboxylic acid groups of PSMA. This indicates that, **P1** and **P3** need further chemical modification to enhance their efficiency for condensing and protecting DNA in physiological conditions.

2.3.7. *In vitro* transfection efficiency

Transfection efficiency of the polyplexes, at different weight ratios, was evaluated using MCF 7 cells as a model cell line. Polyplexes were suitably formulated and incubated with the cells in serum free media, up to 4 hours. This was to avoid the interference of proteins present in serum with the cellular uptake of polyplexes. Spermine grafted polyplexes exhibited comparable transfection efficiencies to that of PEI 25,000 Da, at weight ratios of 5 and 10, and even better

efficiency (1.45 fold higher) at weight ratio of 15. Transfection efficiency of spermine grafted polyplexes was slightly reduced at weight ratio of 20, indicating a possible triggering of cytotoxic effect. In case of L-arginine grafted polyplexes, tansfection efficiency enhanced with the increase in weight ratio and reached almost comparable to positive control, at weight ratios of
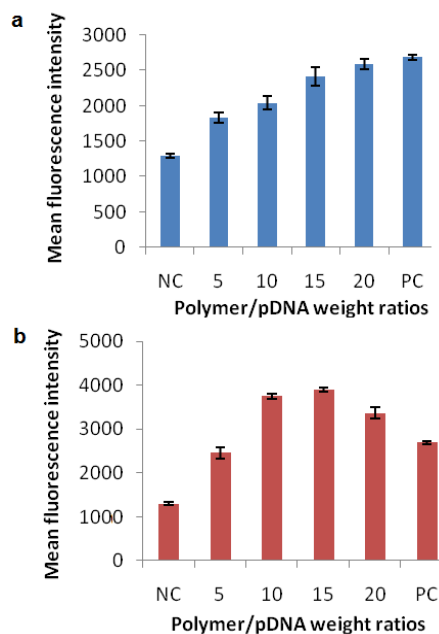
Figure 2.23. Transfection efficiency of the polyplexes of (a) **P4** and (b) **P5** at different weight ratios viz. 5,10,15 and 20 in MCF 7 cell line (Mean ± SD, n = 3). NC − untransfected cells (negative control); PC − PEI, 25000 Da − DNA complex at optimal N/P ratio of 10 (positive control).

15 and 20. The fluorescence quantification of cells treated with various polyplexes (**P4** and **P5**) is represented in figure 2.23 and images of the red fluorescent protein expression in cells treated with various polyplexes are provided in figure 2.24. The mean fluorescence observed with other polyplexes (**P1**, **P2** and **P3**) was negligible, in comparison to that of untreated cells, showing their poor transfection efficiency (data not shown). Based on the transfection efficiency of various polymeric derivatives, it can be hypothesized that combinations of PSMA with

primary/secondary amine containing cationic groups (such as spermine and arginine) have excellent capability to overcome various cellular barriers for successful intracellular gene delivery, in comparison to quaternary ammonium containing cationic structures. The transfection study also showed that polyplexes of L-arginine and spermine can be employed at significantly higher concentrations, without cytotoxic effects, for gene delivery applications. Most of the conventional transfection agents show cytotoxicity at concentrations suitable for *in vivo* applications. Hence developing a safe formulation for *in vivo* gene delivery is challenging. In this context, PSMA derivatives viz. **P4** and **P5** depicted their potential for therapeutic applications.
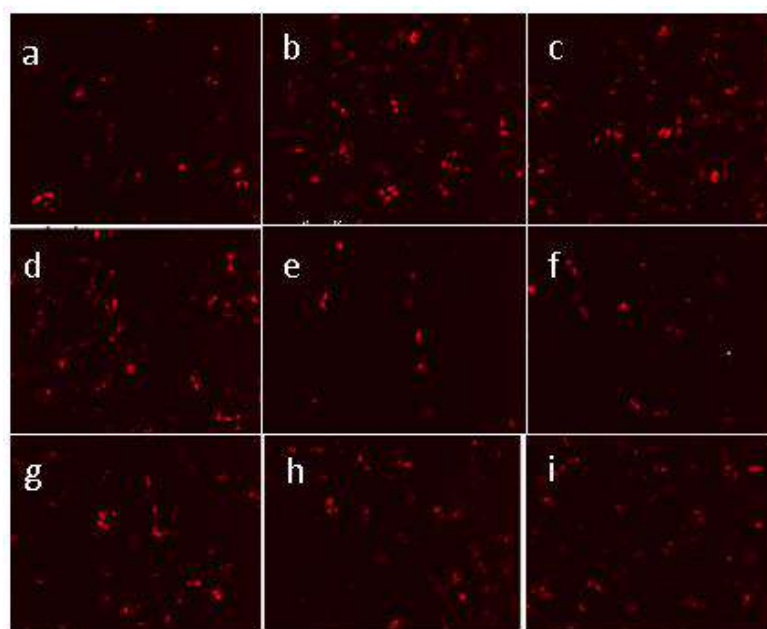
Figure 2.24. Fluorescence images (20 x) of MCF 7 cells transfected with polyplexes of **P5** in polymer/pDNA weight ratios (a) 5 (b) 10 (c)15 (d) 20, **P4** in polymer/pDNA weight ratios (e) 5 (f) 10 (g) 15 (h) 20 and (i) PEI (25,000 Da) at optimal N/P ratio = 10.

Among the various quaternized compounds evaluated, quaternized isonicotinic acid need special attention. Maximum endosomal rupturing property (% haemolysis at pH 5.5) was achieved by the hydrophobic isonicotinc acid units, compared to the other derivatizing agents. This indicates
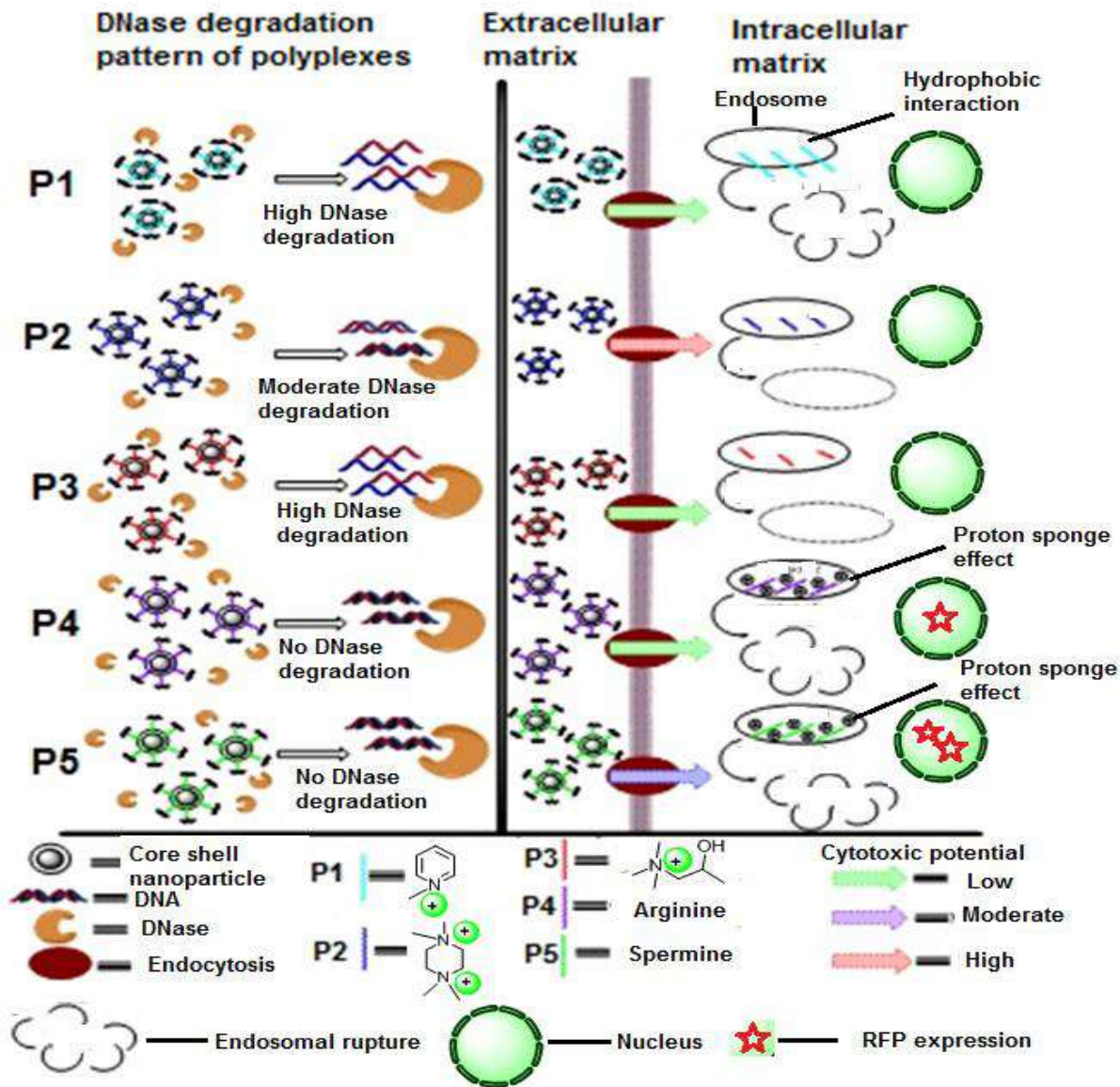
Figure 2.25. Graphical represention of intracellular gene delivery properties of various PSMA derivatives **P1-P5**

that PSMA embedded with hydrophobic cations can escape endolysosomes to achieve efficient transfection. Cytotoxic potential was also low for **P1**. The major drawback of **P1** was its low transfection efficiency due to probable electrostatic repulsive forces from their carboxylic acid counter parts. To overcome this, free carboxylic functional groups of PSMA side chains can be derivatized with various biocompatible moieties. This would minimize the electrostatic repulsive

forces of carboxylate ions and enhance the DNA condensation efficiency of embedded cations. Thus, grafting of PSMA with hydrophobic cations could be employed as an excellent strategy for gene delivery applications. **P2** and **P3** didn't exhibit significant haemolysis at pH 5.5, indicating their limited potential for endolysosomal uptake. Hence we can hypothesize that, grafting of hydrophilic quaternary compounds to PSMA will not be an effective method for achieving intracellular gene delivery. PSMA derivatized with primary/secondary amine containing compounds (**P4**, **P5**) depicted all round excellence as gene delivery vehicles. An overall summary of our research outputs is represented graphically in figure 2.25.

2.4. Conclusions

- Intracellular gene delivery application of low molecular weight PSMA was explored by grafting different types of cationic groups to the polymer backbone.

- All the polymeric derivatives could self assemble to form core shell type nanoparticles.

- Grafting of hydrophobic quaternary ammonium containing cationic groups to PSMA has shown to achieve excellent endosomal penetration property as observed with quaternized isonicotinic acid-PSMA conjugate (**P1**).

- The combinations of PSMA with quaternary ammonium containing cationic structures (**P1-P3**) could not achieve significant transfection efficiency.

- Grafting of primary/secondary amine containing cationic groups such as spermine and L-arginine depicted excellent transfection efficiency by overcoming the cellular barriers.

- Simplicity of nanoparticle preparation, feasibility of combinatorial delivery of genes and drugs due to the core shell structure, scalable nature etc. favour the application of PSMA based nanocarriers for therapeutic purpose.

References

1. Fessi, H.; Puisieux, F.; Devissaguet, J. P.; Ammoury, N.; Benita, S., Nanocapsule formation by interfacial polymer deposition following solvent displacement. *Int. J. Pharm.* **1989,** 55, (1), R1-R4.

2. Gulati, N.; Rastogi, R.; Dinda, A.K.; Saxena, R.; Koul, V., Characterization and cell material interactions of PEGylated PNIPAAM nanoparticles. *Colloids Surfaces B Biointerfaces* **2010,** 79, 164–173.

3. Lale, S.V.; Aswathy, R. G.; Aravind, A.; Kumar, D.S.; Koul, V., AS1411 Aptamer and Folic Acid Functionalized pH-Responsive ATRP Fabricated pPEGMA–PCL–pPEGMA Polymeric Nanoparticles for Targeted Drug Delivery in Cancer Therapy. *Biomacromolecules* **2014,** 15, 1737–1752.

4. Ilker, M.F.; Nüsslein, K.; Tew, G.N.; Coughlin, E.B., Tuning the Hemolytic and Antibacterial Activities of Amphiphilic Polynorbornene Derivatives. *J Am Chem Soc* **2004,** 126, 15870–15875.

5. Stals, P.J.M.; Gillissen, M.A.J.; Nicolay, R.; Palmans, A.R.A.; Meijer, E.W., The balance between intramolecular hydrogen bonding, polymer solubility and rigidity in single-chain polymeric nanoparticles. *Polym Chem* **2013,** 4, 2584–2597.

6. Isidro-Llobet, A.; Álvarez, M.; Albericio, F., Amino Acid-Protecting Groups. *Chem Rev* **2009,** 109, 2455–2504.

7. Kar,M.; Tiwari,N.; Tiwari, M.; Lahiri, M.; Gupta, S. S., Poly-L-Arginine Grafted Silica Mesoporous Nanoparticles for Enhanced Cellular Uptake and their Application in DNA Delivery and Controlled Drug Release. *Part Part Syst Charact* **2013,** 30, 166–179.

8. Plianwong, S.; Opanasopit, P.; Ngawhirunpat, T.; Rojanarata, T., Chitosan combined with

poly-l-arginine as efficient, safe, and serum-insensitive vehicle with RNase protection ability for siRNA delivery. *Biomed Res Int* **2013,** 2013, 1-9.

9.   Soda, K.; Kano, Y.; Nakamura, T.; Kasono, K.; Kawakami, M.; Konishi, F., Spermine, a Natural Polyamine, Suppresses LFA-1 Expression on Human Lymphocyte. *J Immunol.* **2005,** 175, 237–245.

10.   Weisell, J.; Hyvönen, M.T.; Häkkinen, M.R.; Grigorenko, N.A.; Pietilä, M.; Lampinen, A., et al. Synthesis and Biological Characterization of Novel Charge-Deficient Spermine Analogues. *J Med Chem.* **2010,** 53, 5738–5748.

11.   Kumar KS, Kumar VB, Paik P, Kumar KS, Kumar VB, Paik P. Recent Advancement in Functional Core-Shell Nanoparticles of Polymers: Synthesis, Physical Properties, and Applications in Medical Biotechnology. *J Nanoparticles* **2013,** 2013, 1–24.

12.   Hawe, A.; Hulse, W.L.; Jiskoot, W.; Forbes, R.T., Taylor Dispersion Analysis Compared to Dynamic Light Scattering for the Size Analysis of Therapeutic Peptides and Proteins and Their Aggregates. *Pharm Res* **2011**, 28, 2302–2310.

13.   Wang, Y.; Gao, S.; Ye, W-H.; Yoon, H.S.; Yang, Y-Y., Co-delivery of drugs and DNA from cationic core-shell nanoparticles self-assembled from a biodegradable copolymer. *Nat Mater* **2006,** 5, 791–796.

14.   Lee, J.H.; Nan, A., Combination drug delivery approaches in metastatic breast cancer. *J Drug Deliv* **2012**, 2012, 1–17.

15.   Al-Lazikani, B.; Banerji, U.; Workman, P., Combinatorial drug therapy for cancer in the post-genomic era. *Nat Biotech* **2012,** 30, 679–692.

16.   Uhrich, K.E.; Ibim, S.E.M.; Larrier, D.R.; Langer, R.; Laurencin, C.T., Chemical changes during in vivo degradation of poly(anhydride-imide) matrices. *Biomaterials* 1998, 19,

2045–2050.

17. Vaisman, B.; Ickowicz, D.E.; Abtew, E.; Haim-Zada, M.; Shikanov, A.; Domb, A.J., In Vivo Degradation and Elimination of Injectable Ricinoleic Acid-Based Poly(ester-anhydride). *Biomacromolecules* **2013,** 14, 1465–1473.

18. Zeng, S.; Wu, F.; Li, B.; Song, X.; Zheng, Y.; He, G., et al. Synthesis, characterization, and evaluation of a novel amphiphilic polymer RGD-PEG-Chol for target drug delivery system. *ScientificWorldJournal* **2014,** 2014, 546176-546185.

19. Su, G.; Zhou, H.; Mu, Q.; Zhang, Y.; Li, L.; Jiao, P., et al. Effective Surface Charge Density Determines the Electrostatic Attraction between Nanoparticles and Cells. *J Phys Chem C* **2012,** 116, 4993–4998.

20. Henry SM, El-Sayed MEH, Pirie CM, Hoffman AS, Stayton PS. pH-Responsive Poly(styrene-alt-maleic anhydride) Alkylamide Copolymers for Intracellular Drug Delivery. *Biomacromolecules* **2006,** 7, 2407–2414.

21. Chen, R.; Khormaee, S.; Eccleston, M.E.; Slater, N.K.H., The role of hydrophobic amino acid grafts in the enhancement of membrane-disruptive activity of pH-responsive pseudo-peptides. *Biomaterials* **2009,** 30, 1954–1961.

22. Cerda-Cristerna, B.I.; Flores, H.; Pozos-Guillén, A.; Pérez, E.; Sevrin, C.; Grandfils, C., Hemocompatibility assessment of poly(2-dimethylamino ethylmethacrylate) (PDMAEMA)-based polymers. *J Control Release* **2011,** 153, 269–77.

23. Benjaminsen, R.V.; Mattebjerg, M.A.; Henriksen, J.R.; Moghimi, S.M.; Andresen, T.L., The Possible "Proton Sponge " Effect of Polyethylenimine (PEI) Does Not Include Change in Lysosomal pH. *Mol Ther* **2013,** 21, 149–157.

24. Putnam, D., Polymers for gene delivery across length scales. *Nat Mater* **2006,** 5, 439–451.

25. Duan, X.; Xiao, J.; Yin, Q.; Zhang, Z.; Mao, S.; Li, Y., Amphiphilic Graft Copolymer Based on Poly(styrene-Co-Maleic Anhydride) with Low Molecular Weight Polyethylenimine for Efficient Gene Delivery. *International Journal of Nanomedicine*. **2012,** 7, 4961–4972.

CHAPTER III

Development of click modified amphiphilic graft co-polymeric micelles of PSMA for combinatorial delivery of doxorubicin and PLK-1 siRNA

CHAPTER III

Development of click modified amphiphilic graft co-polymeric micelles of PSMA for combinatorial delivery of doxorubicin and PLK-1 siRNA

3.1. Introduction

The chapter describes modification of the poly (styrene-alt-maleic anhydride) for combinatorial delivery of drug and nucleic acid. The amphiphilic graft co polymer was designed by incorporating various structural features which could overcome systemic and cellular barriers for efficient intracellular delivery of the active agents (Figure 3.1). Among the various cationic structures discussed in Chapter II, L-arginine and isonicotinic acid were selected for the modification of polymeric backbone due to their respective nucleic acid binding efficiency and endosomal penetration property. Eventhough spermine grafted polymer depicted excellent intracellular gene delivery efficacy its solubility in various solvents was too low to facilitate further chemical modification. L-arginine and isonicotinic acid were grafted to PSMA through short glycol chains. Efficient grafting of the amino acid side chain was achieved using click reaction. Acetyl lysine was also coupled to the amino acid side chain in order to improve nucleic acid binding efficiency and drug loading capacity. Nanocarriers of the synthesized polymer were formulated and evaluated for bio compatibility and serum stability. Safety of the polymeric nanocarriers was studied *in vivo* by performing seven day repeated dose toxicity study. Combinatorial delivery efficacy of the designed nanocarriers was evaluated by employing doxorubicin and PLK-1 siRNA as model drug and nucleic acid, respectively. *In vitro* evaluation of the formulations was performed using MCF 7 cells and *in vivo* anticancer efficacy was studied in Ehrlich ascites tumor (EAT) bearing Swiss albino mice.
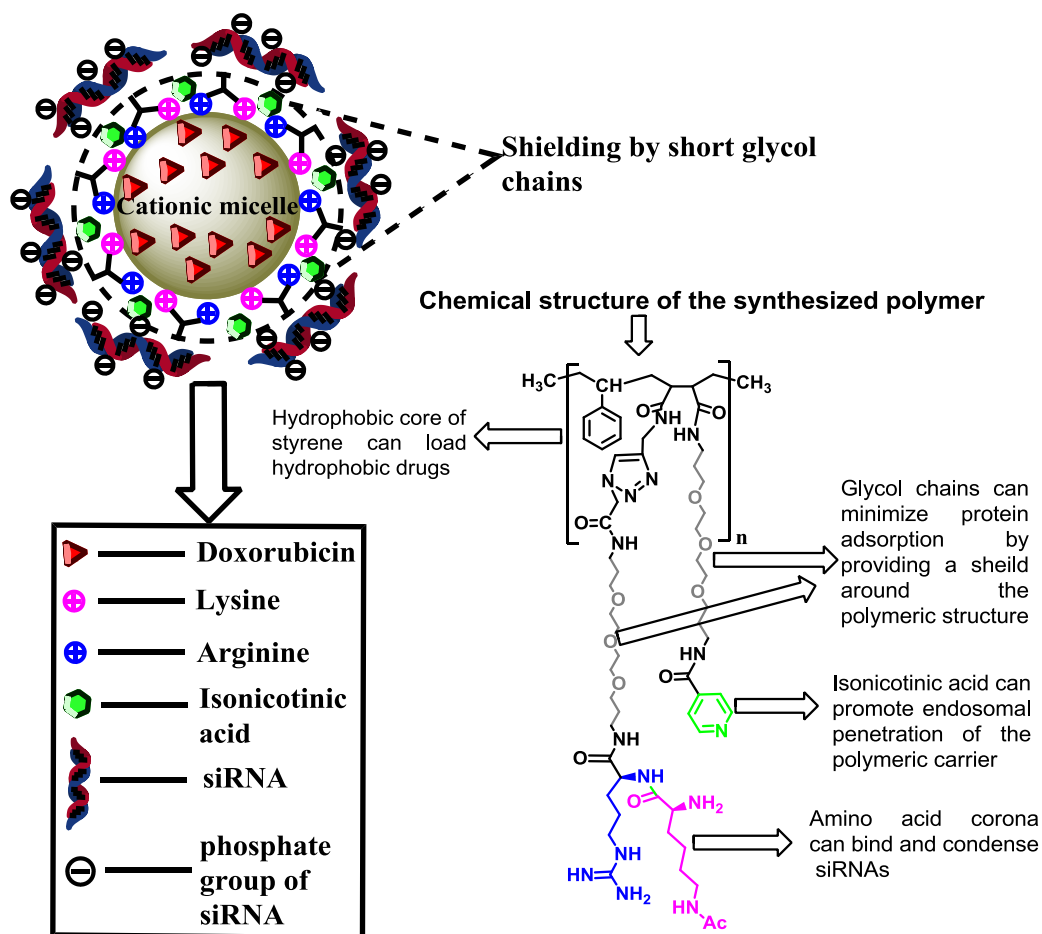
Figure 3.1. Schematic representation of the designed polymeric micelle and its structural features

3.2. Experimental

3.2.1. Materials

PSMA with a styrene to maleic anhydride molar ratio of 1:1 (M_w, 5500Da) was obtained from Sartomer Company Inc (Quarry bay, Hong Kong). Fmoc-Arg-pbf-OH, Fmoc-Lys-Boc-OH, 4,7,10-trioxa-1,13-tridecanediamine, Di-tert-butyl dicarbonate, N-hydroxy succinimide, propargyl alcohol, bovine serum albumin (molecular weight 66kDa), and ethidium bromide were purchased from Sigma-Aldrich (Bangalore, India). Trypsin-ethylenediamine tetra acetic acid, Dulbeccos modified eagles media (DMEM), penicillin/streptomycin antibiotic solution, fetal

bovine serum and agarose were purchased from Himedia (India). Validated silencer@select PLK-1 siRNA, scrambled siRNA (negative control siRNA) and FAM labeled negative control siRNA were obtained from Thermoscientific (USA). Comet assay kit was purchased from Trevigen Inc. Germany. Bradford reagent was purchased from Biorad (India) Triisopropylsilane, 1-ethyl-3-(3-dimethylaminopropyl) carbodiimide hydrochloride (EDC. HCl), isonicotinic acid, trifluoroacetic acid, and triethyl amine (NEt$_3$) were obtained from Merck millipore (India). Doxorubicin hydrochloride was obtained as a gift sample from Ranbaxy Laboratories ltd. New Delhi, India. Solvents and reagents of analytical grade were employed for the experiments. RNase free water (non DEPC treated, Ambion TM) was used for all studies involving siRNA.

3.2.2. Synthesis of amphiphilic graft co-polymer of poly (styrene-alt-maleic anhydride) (PSMA)

3.2.2.1. Grafting of PSMA with isonicotinic acid

Isonicotinic acid was conjugated to 4,7,10-trioxa-1,13-tridecanediamine by EDC/NHS coupling to obtain N-(3-(2-(2-(3-aminopropoxy) ethoxy) ethoxy) propyl) isonicotinamide. In the first step, mono N- Boc protected 4,7,10-trioxa-1,13-tridecanediamine was synthesized. Breifly, 4,7,10-trioxa-1,13-tridecanediamine (6 g, 29.7 mM) was dissolved in methanol (200 mL) along with triethyl amine (6 g, 60 mM). Di-tert-butyl dicarbonate (1.3 g, 6 mM)   in dichloromethane (1 mL) was added dropwise to the reaction mixture under continuous stirring (1200 rpm). The reaction was carried out at room temperature for 12 hours and the solvents were evaporated under vacuum using rotary flash evaporator (IKA 50, Germany). The residue was extracted between saturated sodium bicarbonate (50 mL)╱ dichloromethane (150 mL) mixture using separating flask. The organic layer was removed and the aqueous layer was once again extracted with dichloromethane (150 mL). The combined organic layers were dried using anhydrous

sodium sulphate and evaporated to obtain mono N-Boc protected 4,7,10-trioxa-1,13-tridecanediamine.

Conjugation of isonicotinic acid to mono N- Boc protected 4,7,10-trioxa-1,13-tridecanediamine was done as follows. Isonicotinic acid (1.5 g, 12.2 mM) was dissolved in dichloromethane (25 mL) followed by addition of N-hydroxy succinimide (1.65 g, 14.3 mM). After mixing the components for 15 minutes at room temperature, EDC.HCl (2.75 g, 14.3 mM) and triethylamine (2.15 g, 21.3mM) were added, and the reaction was continued for overnight. Dichloromethane was evaporated and the crude mixture was extracted three times between saturated sodium bicarbonate (50 mL) ∕ dichloromethane (150 mL). The combined organic layers were dried over anhydrous sodium sulphate and the solvent was evaporated to obtain tert-butyl (1-oxo-1-(pyridin-4-yl)-6,9,12-trioxa-2-azapentadecan-15-yl) carbamate (Step I, figure 3.2). The Boc groups were then cleaved by treating with dichloromethane: trifluoroacetic acid mixture at 1: 1 ratio for 3 hours. The purified conjugate was then grafted to PSMA backbone through alkaline hydrolysis. Briefly, 0.8 g PSMA (approx. 3.88 mM of monomer units) was added to dichloromethane (20 mL) containing N-(3-(2-(2-(3-aminopropoxy) ethoxy) ethoxy) propyl) isonicotinamide (2 g, 4.7 mM) and NEt$_3$ (0.4 g, 4 mM). The reaction was kept overnight at room temperature and solvent was evaporated using rotary flash evaporator. The polymeric derivative was purified by precipitating with ethyl acetate followed by washing with water.

3.2.2.2. Coupling of amino acids to the polymer

Free carboxylic acid groups in the N-(3-(2-(2-(3-aminopropoxy) ethoxy) ethoxy) propyl) isonicotinamide grafted PSMA were functionalized with propargylamine (Step I, figure 3.2). Briefly, 1 g of N-(3-(2-(2-(3-aminopropoxy) ethoxy) ethoxy) propyl) isonicotinamide grafted PSMA (approx. 3.533 mM of monomer units) was activated with N-hydroxysuccinimide (0.35 g,

3 mM) for 20 minutes in DMF (25 mL) followed by addition of EDC.HCl (0.58 g, 3 mM). After 30 minutes of reaction in ice bath, propargyl amine (0.21 g, 3.81 mM) and NEt$_3$ (0.385 g, 3.85 mM) were added to the reaction mixture. The reaction was allowed to continue for 24 hrs at room temperature. DMF was then evaporated using rotary flash evaporator and the propargyl amine functionalized polymer was purified by precipitating and dialyzing with water (4 L, dialysis membrane with a molecular weight cutoff 3500 Da). Water was changed every 6 hours and dialysis was continued for 2 days. The product was then lyophilized and recovered.

On the other hand, 4,7,10-trioxa-1,13-tridecanediamine was functionalized with azide and Fmoc-Arg-pbf-OH. Briefly, azidoacetic acid (1 g, 9.8 mM) was dissolved in dichloromethane (25 mL) and stirred for 15 minutes in an ice bath, under nitrogen. The carboxylic acid was activated with NHS (1.4 g, 12.2 mM) and EDC.HCl (2.26 g, 11.8 mM) for 15 minutes, successively. Mono N- Boc protected 4,7,10-trioxa-1,13-tridecanediamine (1 g, 3.1 mM) was added along with triethylamine (2.35 g, 23.5 mM) to the reaction mixture and the reaction was allowed to continue in ice bath for 4 h and then at room temperature for 24 h. The solvent was evaporated and residue was extracted between saturated sodium bicarbonate (150 mL) and dichloromethane (50 mL) for three times. Combined organic layers were dried using anhydrous sodium sulphate and dried to obtain azide functionalized mono N- Boc protected 4,7,10-trioxa-1,13-tridecanediamine (Step II, figure 3.2).

Coupling of Fmoc-Arg-pbf-OH to the azide functionalized glycol amine was done using EDC∕ NHS (Step II, figure 3.2). Breifly, Fmoc-Arg-pbf-OH (1 g, 1.54 mM) was activated with NHS (0.4 g, 3.5 mM) and EDC.HCl (0.65 g, 3.4 mM) , successively for 15 minutes, in dichloromethane (50 mL). Azide functionalized mono N- Boc protected 4,7,10-trioxa-1,13-tridecanediamine (1.75 g, 4.16 mM) was deprotected from Boc by reacting with mixture of DCM
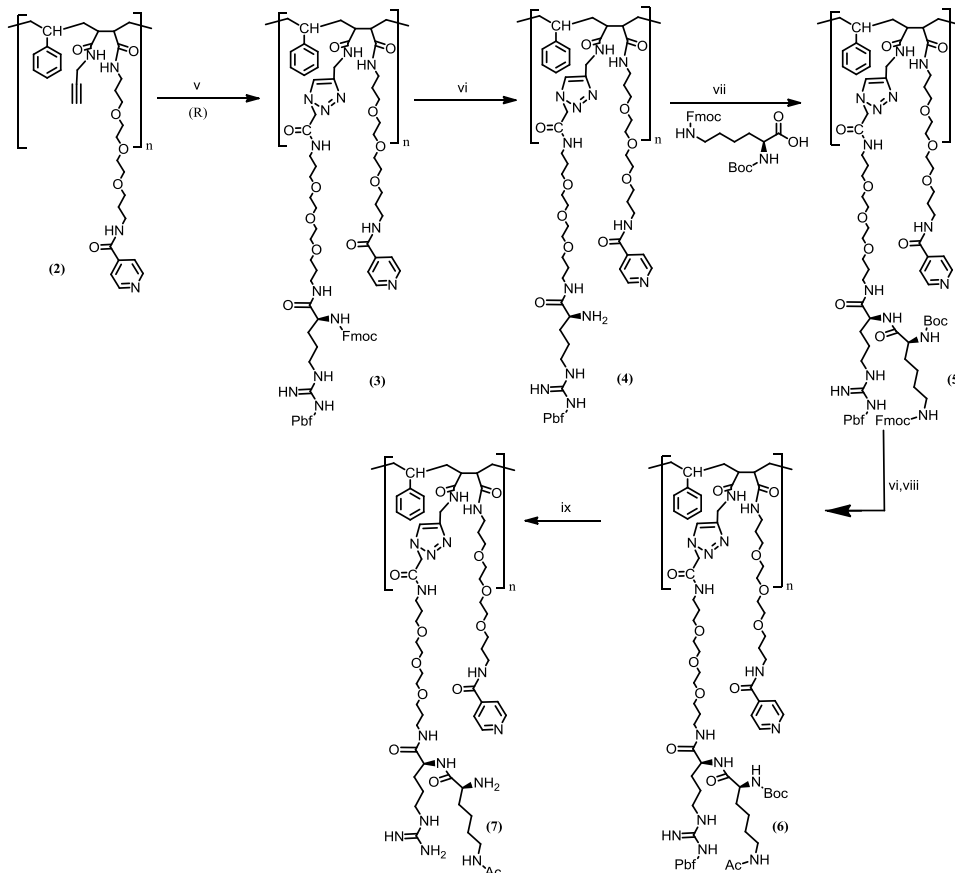
Figure 3.2. Synthetic scheme of cationic polymer. (i) NEt$_3$, RT, 12 h (CH$_3$OH) (ii) EDC/NHS, NEt$_3$, 0 ℃ - RT, 24 h (iii) TFA- CH$_2$Cl$_2$, RT, 3 h (iv) NEt$_3$, RT, 12 h (dry CH$_2$Cl$_2$) (v) DIPEA, CuI, RT, N$_2$, 24 h (vi) DMF: Piperidine (1:1 v/v), RT, 3 h (vii) HBTU, DIPEA, 0 ℃ - RT, 12 h (viii) (CH$_3$CO)$_2$O, NEt$_3$, RT, 12 h (dry DMF) (ix) TFA: triisopropylsilane: water (95 :2.5 : 2.5 v/v/v), RT, 3 h

and TFA (1:1) for 3 h and the obtained product along with triethylamine (2 g, 20 mM) were added to the activated Fmoc-Arg-pbf-OH, under stirring. After 24 h, the solvent was evaporated and the residue was extracted between water (150 mL) and DCM (50 mL). The extractions were carried out thrice and the organic layers were dried using anhydrous sodium sulphate. DCM was evaporated to obtain Fmoc-Arg-pbf-OH and azide functionalized 4,7,10-trioxa-1,13-tridecanediamine.

The obtained product was grafted to polymer backbone by Husigen 1,3- dipolar cycloaddition (Step III, figure 3.2). Briefly, propargylamine grafted polymeric derivative (0.7 g, 1.26 mM) was dissolved in dry DMF (50 mL) followed by addition of DIPEA (0.25 g, 1.9 mM) and azide functionalized 4,7,10-trioxa-1,13-tridecanediamine conjugate (1.6 g, 1.65 mM) under nitrogen atmosphere. To the reaction mixture, copper iodide (0.12 g, 0.63 mM) was added as catalyst and the reaction was continued for 24 hours at room temperature under nitrogen. DMF was evaporated using rotary flash evaporator and the residue was dispersed in dichloromethane. Copper was removed from the reaction mixture by extracting with aqueous phase composed of saturated ammonium chloride: ammonium hydroxide (9:1 volume ratio). After repeated extractions, organic layers were concentrated and the product was precipitated with ethylacetate repeatedly to obtain the purified polymer grafted with L-arginine.

Conjugation of lysine to arginine was done via coupling reaction (Step III, figure 3.2). Fmoc-Arg-pbf-OH grafted polymer was dissolved in DMF: piperidine mixture (50:50 volume ratio) and reacted for 3 hours to remove Fmoc. The polymer was purified by washing with ethylacetate and coupled with Fmoc-Lys-Boc-OH using HBTU. Briefly, Fmoc-Lys-Boc-OH (0.5 g, 1 mM) was dissolved in dry DMF (50 mL) and reacted with HBTU (0.485 g, 1.2 mM) in ice bath for 15 minutes. Arg-pbf-OH grafted polymer (0.6 g, 0.4 mM) and DIPEA (0.275 g, 2.1 mM) were

added to the reaction mixture and reaction was allowed to continue for overnight at room temperature. DMF was evaporated and the residue was precipitated with ethylacetate and acetonitrile successively, to obtain purified polymer. The Fmoc-Lys-Boc-OH grafted polymeric derivative (5) was dissolved in DMF: piperidine mixture (1:1 v/v) and reacted for 3 hours to remove Fmoc. The polymer was then purified by precipitating with ethylacetate. Dried polymer (0.5 g) was dissolved in dry DMF in the presence of triethylamine (0.2 g, 2 mM) followed by slow addition of acetic anhydride (0.35 g, 3.4 mM). The reaction was continued for overnight at room temperature. The solvent was then evaporated and residue was repeatedly washed with ethylacetate. The obtained product was treated with 15 mL of TFA: triisopropylsilane: phenol mixture in the volume ratio 95:2.5:2.5, for 3 hours, to remove pbf and Boc. The polymer was then purified by precipitating with ethylacetate.

Various chemical conjugates and polymeric derivatives were characterized using ^{1}H NMR and the final product was characterized with ATR-FTIR. Average molecular weight of the polymer was determined by gel permeation chromatography (Waters, USA, Styragel HR column) using Waters 2414 RI detector equipped with DMF column. Average molecular weight of the polymer (M_w) was determined from standard calibration curve obtained by polyethylene glycols of known molecular weights.

3.2.3. Formulation and evaluation of polymeric micelles

Blank polymeric micelles were prepared by nanoprecipitation method [1]. Polymer (50 mg) was dissolved in 10 mL of DMSO followed by addition of 10 mL of water (milliQ) under continuous stirring (1200 rpm) for 30 minutes. The dispersion was dialyzed against water (4 L) overnight, using dialysis membrane having molecular weight cut off 3500 Da, to remove DMSO. Water was changed only once during the course of dialysis. The polymeric dispersions were filtered

using 0.45 μm syringe filter and their particle size and zeta potential were measured using dynamic light scattering (DLS). Aqueous dispersion of the obtained micelles was then pre freezed overnight at – 20 ˚C and lyophilized (Labconco, 4.5 L, Cascade bench top freeze dry system). Morphological characterizations of nanoparticles were performed by TEM, FESEM and AFM. Critical micellar concentration (CMC) of the polymeric micelles was determined using standard pyrene method. Briefly, aliquots of pyrene stock solution (0.1 mg/mL) in chloroform were added to clean glass vials. Chloroform was then allowed to evaporate in dark. Polymeric micelles in HEPES buffer, pH 7.4 were incubated with the dried pyrene for overnight, at 37 ℃ in a shaking incubator. Final concentrations of polymeric micelles examined were in the range of 1-50 μg/mL and the concentration of pyrene was 6.5×10^{-7} M in all the vials. Pyrene was excited at 334 nm and emission spectra of the dispersions were recorded from 339 -400 nm, using a F-2000 fluorescence spectrometer (Hitachi, Japan).

Stability of the polymeric nanoparticles in cell culture media supplemented with 10% fetal bovine serum (FBS) was evaluated by checking the particle size up to 72 hours. Nanoparticles were dispersed in complete cell culture media (RPMI 1640 media supplemented with 10 % FBS) at a final polymer concentration of 0.3 mg/mL, and particle size of the dispersion was measured up to 72 hours by storing at 37 º C.

The primary amine content of polymeric micelles was determined using TNBS assay according to previously reported method, with slight modification. Briefly, lyophilized nanoparticles were dispersed in double distilled water (400 μL) and mixed with 400 μL of 4 % sodium bicarbonate solution. 400 μL of aqueous TNBS solution (0.1 %) was added to the mixture and the reaction was carried out at 37 ° C for 2 h, at 1200 rpm. Final concentration of nanoparticles was kept at 100 μg/mL. Gamma amino butyric acid was used as standard. Known concentrations of the

amino acid were treated with TNBS in the same manner as that of the nanoparticles and absorbances were recorded at 349 nm using micro plate spectrophotometer (PowerWave XS2, Bio Tek Instruments, USA). Experiments were carried out in triplicate.

Interaction of the   polymer with plasma proteins was evaluated by Bradford assay. Human plasma was obtained from blood bank, All India Institute of Medical Sciences (AIIMS), New Delhi, India. Polymeric particles (10 mg) were uniformly dispersed in 1 mL of phosphate buffer saline (PBS), pH 7.4 by probe sonication (100 W, 15 seconds). The dispersions were diluted with 4 mL of human plasma and incubated for 1 h at 37 º C. Following incubation, the dispersions were centrifuged at 20000 g for 1 h. Residues were washed thrice with PBS, dried by lyophilization and treated with urea-thiourea buffer (2 M thiourea, 7 M urea and 4 % CHAPS detergent) to elute adsorbed proteins. Protein content was quantified using Bradford reagent (Biorad). BSA was used as standard and calibration curve was prepared as per the manufacturers' protocol.

Haemolytic behavior of the polymeric micelles at various pH values (7.4 and 5.5) was evaluated as per previously reported procedures, with slight modification. Heparinized human blood was obtained from blood bank, All India Institute of Medical Sciences (AIIMS), New Delhi, India. Whole blood (1 mL) was centrifuged at 1500 rpm for 10 minutes. The settled red blood cells (RBC s) were washed thrice with phosphate buffer saline (PBS), pH 7.4. RBC stock solution was prepared by diluting 50 µL of RBCs to 10 mL with PBS. Polymeric nanoparticles in PBS (100 µL) were incubated with equal volumes of RBC stock solution at 37 °C for 1 h. Final concentrations of nanoparticles were in the range of 125 – 2500 µg∕ mL. After incubation, the mixtures were centrifuged at 1500 rpm for 10 minutes and haemoglobin released was quantified by recording the absorbance of supernatants at 540 nm using micro plate spectrophotometer (PowerWave XS2, Bio Tek Instruments, USA). PBS and 1 % Triton X-100 were used as

negative and positive controls respectively. % haemolysis at pH 5.5 was determined, in the same way as that at pH 7.4, using PBS pH 5.5 as the incubation media for nanoparticles and RBCs. % haemolysis was calculated using the following equation -

$$\% \text{ haemolysis} = \frac{\left\{ \begin{array}{c} \text{Absorbance of} \\ \text{sample} \end{array} - \begin{array}{c} \text{Absorbance of} \\ \text{negative control} \end{array} \right\} \times 100}{\left\{ \begin{array}{c} \text{Absorbance of} \\ \text{positive control} \end{array} - \begin{array}{c} \text{Absorbance of} \\ \text{negative control} \end{array} \right\}}$$

Genotoxic evaluation of the micelles was performed using comet assay. Briefly, cells (MCF 7) were seeded in T-25 culture flask and experiments were performed once 80 % confluency was achieved. Polymeric nanoparticles were incubated with the cells at a concentration of 1 mg/ml for 48 h. Following incubation, alkaline comet assay was performed with Trevigen comet assay kit, according to the manufacturers' protocol. Reactive oxygen species (ROS) generation was studied using DCFH-DA dye [2]. Briefly, cells were seeded in 96 well plate at a density of 5000cells/well and incubated for 24 hours at 37 °C and 5 % CO_2. Polymeric nanoparticles were added to the wells at final concentrations ranging from 50 to 1000 µg/mL and incubated for 48 hours at 37 °C and 5 % CO_2. After incubation, wells were supplemented with fresh media followed by addition of 20 µL of DCFH-DA dye at a concentration of 10 mM. Fluorescence in each well was measured, after 30 minutes incubation, at 480 nm excitation using a microplate reader. Untreated cells were kept as control.

3.2.4. Formulation and evaluation of drug loaded micelles

Doxorubicin loaded polymeric nanoparticles were prepared in the same way as that of blank nanoparticles except the addition of doxorubicin HCl (at various feed ratios ranging from 5-20 mg) and triethylamine (equal molar amount of Doxorubicin HCl) in succession to the DMSO

phase. Drug loading of Doxorubicin in the nanoparticles was analyzed by UV-Visible spectrophotometry. Briefly, the dialyzed Dox loaded polymeric nanoparticles were lyophilized and dissolved (5 mg of Dox loaded nanoparticles) in DMSO by probe sonication. The drug loading of nanoparticles was determined by recording absorbance at 481 nm and calculating the respective concentration using standard calibration curve of doxorubicin in DMSO. *In vitro* drug release was examined at different pH values (5.5 and 7.4). Briefly, 25mg of doxorubicin loaded polymeric micelles were dialyzed against corresponding phosphate buffer salines (100 mL) using dialysis bag with molecular weight cutoff 3500 Da. The release media was collected at different time points and replaced with equal volumes of fresh media. Absorbance of the samples collected at different time points was determined at 481 nm, using UV-Visible spectrophotometer, and the concentrations were calculated from the standard calibration curves of doxorubicin in the respective phosphate buffer salines.

3.2.5. Formulation and evaluation of polyplexes

Polyplexes of PLK-1 siRNA with polymeric nanoparticles were formed by mixing aqueous solutions of PLK-1 siRNA with equal volumes of aqueous dispersions of nanoparticles. Both drug loaded and blank polymeric nanoparticles were complexed with siRNA in the same manner. After mixing by gentle vortexing, the polyplexes were allowed to stabilize by keeping at room temperature for 30 minutes. Prior to all in vitro studies, the polyplexes were freshly prepared. Polyplex stability was assessed using agarose gel electrophoresis. The polyplexes were loaded in to the wells of 1.2 % agarose gel. Ethidium bromide (0.5 µg/mL of gel) in Tris –acetate-ethylenediamine tetra acetic acid was incorporated in the gel for staining of the nucleotide sequence. Electrophoresis was performed for 20 minutes at 70 V using horizontal gel

electrophoresis unit. The bands of siRNA were visualized with UV illuminator, and images were captured using molecular imager (Gel Doc XR, BIO RAD).

The efficiency of polyplexes in knocking down PLK-1 mRNA was examined using real time PCR. Briefly, MCF 7 cells were seeded into 6 well plates and transfected with polyplexes, once ~ 80 % confluency was attained, for 48 hours. The cells were then lysed using Trizol reagent for isolation of total RNA, according to manufacturers' protocol. Total RNA from the harvested cells were isolated using Trizol regent. Briefly, 5×10^5 cells were incubated with 500 µL of trizol reagent for 5 minutes. 100 µL of chloroform was added to the mixture and shaken vigorously for 30 sec. The dispersions were centrifuged at 12500 rpm for 15 minutes. Aqueous layers were separated and mixed with 250 µL of isopropanol. After incubating at – 20 º C for 15-20 minutes, the separated aqueous layers were again centrifuged at 12500 rpm for 15 minutes. Supernatants were then discarded and the pellets were washed with 75 % ethanol. The washed pellets were dried and dissolved in RNase free water and incubated at 65 º C for 15 minutes. Isolated RNAs were purified from any genomic DNA by treating them with DNase (1 U). cDNA was prepared from the RNA contents using cDNA kit (Biorad). Briefly, RNA solutions were mixed with appropriate amounts of 10 x cDNA reaction buffer and reverse transcriptase enzyme according to the manufacturers' protocol. Final volume was reconstituted with nuclease free water to make the cDNA reaction buffer concentration 1x. PCR cycles employed were 65 ºC for 5 minutes, 42 ºC for 30 minutes and 70 ºC for 15 minutes. The obtained cDNA samples were stored at 4 ºC till they were used for real time PCR analysis. For real time PCR and cDNA, primers (forward and reverse) were mixed with q PCR master mix (QuantiNova SYBR Green PCR Kit) at final primer concentrations of 10 µM. PLK- 1 expression was normalized with that of GAPDH. Delta delta

Ct (2 ΔΔ Ct) method was used to determine the fold change in gene expression. Primer sequences of PLK-1 and GAPDH primers used are as follows.

PLK-1 forward: 5' - CCCATCTTCTGGGTCAGCAAG

PLK-1 reverse: 5' - AAGAGCACCCCCACGCTGTT

GAPDH forward: 5' - TGCACCACCAACTGCTTAGC

GAPDH reverse: 5' - GGCATGGACTGTGGTCATGAG

3.2.6. Cellular uptake studies

MCF 7 cells in complete media (supplemented with 10% fetal bovine serum) were added to confocal plates and incubated for 24 hours, at 37 °C and 5 % CO_2, to attain 70-80 % confluency. Doxorubicin and FAM-labeled siRNA loaded polymeric nanoparticles were incubated with the cells for 3 hours. Final concentrations of doxorubicin and FAM-labeled siRNA were 5 µg/mL and 100 nM respectively. After incubation, cells were washed thrice with PBS and treated with Nuc Blue for 10 minutes. Fluorescence of doxorubicin, FAM-labeled siRNA and Nuc Blue were visualized, using confocal laser scanning microscope (CLSM, Olympus IX 81 under DU897 mode), at respective emission wavelengths of 561 nm, 488 nm and 405 nm.

For evaluating the nuclear localization of doxorubicin loaded nanoparticles, MCF 7 cells in complete media were seeded in to 24 well plates containing spherical glass slides. After obtaining ~70-80 % confluency, cells were treated with doxorubicin (10 µg/mL) and PLK-1 siRNA (100 nM) loaded polymeric micelles. Post incubation, cells were washed thrice with PBS and stained with lysotracker green (invitrogen), at a concentration of 100 nM, for 25 minutes. Nuclear staining was performed in the end using DAPI dihydrochloride (2 µg/mL) for 5 minutes. Repeated washing of the cells with phosphate buffer saline (pH 7.4) was performed after each

staining.   The cells were fixed with 4 % paraformaldehyde solution and visualized using confocal laser scanning microscope (Olympus, Fluoview FV1000).

3.2.7. Cell proliferation assay and live/dead staining of treated cells

Cells were seeded in to 96 well plate at a density of 10^4 cells/well and incubated for 24 hours at 37 °C under 5 % CO_2. Polymeric micelles loaded with doxorubicin and scrambled siRNA (100 nM) at various concentrations were added to one set of wells. Another set of wells were treated with polyplexes containing 100 nM PLK-1 siRNA along with different concentrations of doxorubicin. The cells were incubated with the samples up to 48 hours. The wells were then replaced with fresh media (200 µL) and incubated with 10 µL of MTT solution (5 mg/ml) for 3 hours. The crystals formed were then dissolved in 200 µL of DMSO and absorbance was recorded at 540 nm using microplate spectrophotometer (PowerWave XS2, Bio Tek Instruments, USA). For determining the live/dead ratio of cells treated with formulations, cells were seeded in to confocal plates and incubated at 37 ºC under 5 % CO_2**,** till ~ 80 % confluency was attained. The plates were then treated with either polymeric micelles bearing doxorubicin∕ scrambled siRNA or doxorubicin∕ PLK-1 siRNA at siRNA concentration of 100 nM. After 48 hours of incubation with the samples, cells were stained with calcein/PI (according to manufacturers' protocol) and images were recorded using CLSM at 4x magnification.

3.2.8. Animal studies

7-8 week old female Swiss albino mice (24 ± 5 g) were obtained from Central Animal Facility, AIIMS, New Delhi, India. The experiments were conducted as per the guidelines of Animal Ethical Committee (796∕IAEC∕14) of AIIMS. Animals were housed at 25º C with adequate humidity in polycarbonate cages, with chow food and sterile water ad libitum, throughout the experiment. Consistent and uninterrupted 12 h light∕ dark cycle was maintained. Animal

experiments included toxicological evaluation of the synthesized polymer and *in vivo* anti tumor efficacy of various formulations.

3.2.8.1. Toxicological evaluation of the cationic micelles

Female Swiss albino mice were randomly grouped in to two groups (n = 4) for performing repeated dose toxicity study. Dispersions of polymeric micelles in PBS, pH 7.4 (0.3 mL) were administered in one group (on days 1, 4 and 7) at a dose of 100 mg∕kg, intraperitoneally. The second group was similarly injected with blank PBS. On day 8, blood samples were collected from the mice by retro orbital venous puncture for evaluation of serum biochemistry and hematology analysis. The animals were then sacrificed by cervical dislocation and vital organs were collected in 4 % formalin for histopathological analysis.

3.2.8.2. *In vivo* anti cancer efficacy

Various polymeric formulations were evaluated for their anti cancer efficacy using Ehrlich ascites tumor (EAT) model. EAT cell line was obtained as a gift from INMAS, New Delhi, India. 150 µL of EAT cell suspension (containing $\sim 2 \times 10^7$ cells) was injected subcutaneously on the dorsal side of female Swiss albino mice. Tumor volumes were estimated twice in a week, by measuring the length and breadth of tumors using Vernier caliper, following the inoculation. Volumes were calculated using the formula $\pi ∕ 6$ (length) (width) (height), where length was measured as the longest diameter across the tumor. Mice bearing solid tumors with an average volume of 300 mm^3 were divided in to five groups (4 animals each). Group I was treated with doxorubicin and PLK-1 siRNA carrying polyplexes. Group II, III, IV and V were treated respectively with doxorubicin and scrambled siRNA loaded polymeric micelles, free Doxorubicin, PLK-1 siRNA complexed polymeric micelles and blank PBS (designated as control). All the formulations were administered intratumorally. For intratumoral injection, 50

µL of various formulations (in PBS) were injected in the longitudinal direction from the edge to centre of the tumors. Each injection was administered slowly over 1 minute. Following each injection, the needle was kept at the injection site for further 5 minutes in order to prevent any leakage of the sample. Four injections were given over a period of 2 weeks. Doxorubicin and siRNA were respectively administered at 1.5 mg∕kg and 0.5 mg∕kg dose. At the end point of study, animals were sacrificed by cervical dislocation followed by collecting tumors, vital organs and blood. Tumors and vital organs were evaluated using histopathological analysis. Serum biochemical parameters of blood samples were also studied.

3.3. Results and Discussion

3.3.1. Synthesis and characterization of isonicotinic acid grafted polymer

Isonicotinic acid was conjugated to PSMA using 4,7,10-trioxa-1,13-tridecanediamine as the linker molecule. Mono N-Boc protected 4,7,10-trioxa-1,13-tridecanediamine and its conjugate with isonicotinic acid were synthesized and characterized using ^{1}H NMR (Figure 3.3). N-(3-(2-(2-(3-aminopropoxy) ethoxy) ethoxy) propyl) isonicotinamide was then grafted to PSMA, after deprotecting the amino group, to obtain product (1) as shown in step I (Figure 3.2). ^{1}H NMR of the polymeric graft (I) exhibited characteristic peaks at δ 7.8 and 8.74 ppm attributed to aromatic hydrogens present in isonicotinic acid. The methylene groups of N-(3-(2-(2-(3-aminopropoxy) ethoxy) ethoxy) propyl) isonicotinamide showed sharp peak at δ 3.48 ppm (Figure 3.4). The ability of pyridine containing structures to permeate through lysosomal membrane has been experimentally reported [3]. Lysosomal permeability of substrates varies in accordance with their total hydrogen bonding capacity. Lower hydrogen bonding capacities as observed in pyridines are favorable for the lysosomal permeability. Pyridines can remain significantly unprotonated even at pH 5.0 and possess the ability to disrupt lysosomal membrane due to their hydrophobic

interaction [3, 4]. We have observed significantly higher haemolytic property of isonicotinic acid grafted PSMA at pH 5.5, indicative of their ability to permeate endolysosomal compartment, in our previous experiments. Based on these experimentally proven facts, isonicotinic acid was introduced in to the polymeric structure to promote permeation through lysosomes.
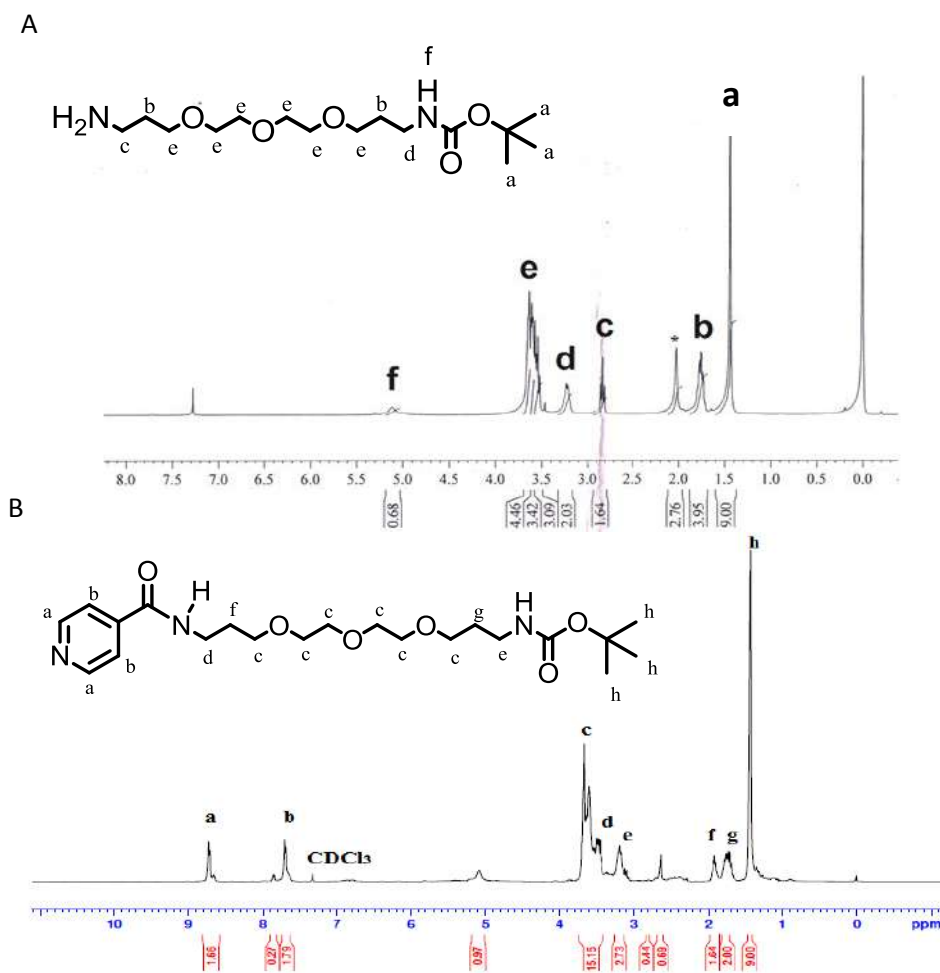
Figure 3.3. ^{1}H NMR spectra (300 MHz, CDCl$_3$) of (A) Mono Boc protected 4,7,10 – trioxa-1,13- tridecanediamine; δ 1.43 (s, 9H, Boc C$\underline{H}_3$), 1.75 (m, 4H, NH-CH$_2$-C$\underline{H}_2$), 2.83 (t, J = 6.6 Hz, 2H, -O-C$\underline{H}_2$), 3.22 (m, 2H, HN- C$\underline{H}_2$), 3.5-3.8 (m, 12H, -O-C$\underline{H}_2$), 5.15 (brs, 1H, N$\underline{H}$) and (B) isonicotinic acid conjugate of Boc protected 4,7,10 – trioxa-1,13- tridecanediamine; δ 1.445 (s, 9H, Boc C$\underline{H}_3$), 1.725 (m, 2H, NH-CH$_2$-C$\underline{H}_2$), 1.879 (m, 2H, NH-CH$_2$-C$\underline{H}_2$), 3.2 (m, 2H, HN-C$\underline{H}_2$), 3.45 (m, 2H, HN- C$\underline{H}_2$), 3.54-3.78 (m, 12H, -O-C$\underline{H}_2$), 8.4 (d, J = 7.2 Hz, 2H,Ar C$\underline{H}$), 9 (d, J = 7.2 Hz, 2H, Ar C$\underline{H}$)
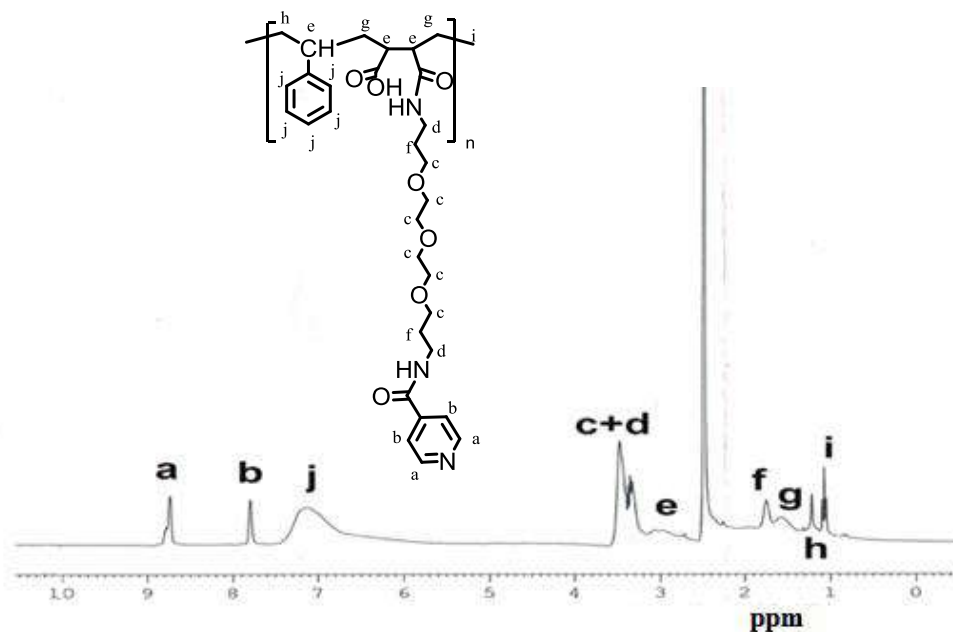
Figure 3.4. ^{1}H NMR spectrum (300 MHz, DMSO-d_6) of isonicotinic acid grafted polymer (1)

3.3.2. Coupling of amino acids to the polymer backbone

Alkyl functionality was incorporated in to the polymer backbone, by reacting the free carboxylic acid groups in the polymer (1) with propargyl amine, using EDC/NHS coupling and characterized with ^{1}H NMR. The alkyl functionalized polymer (2) depicted an additional peak, in
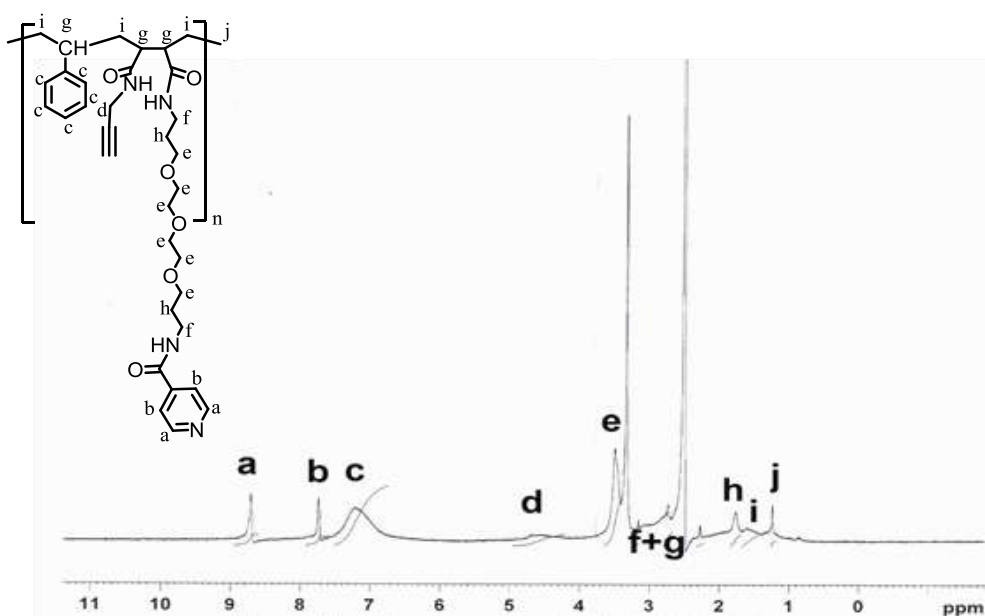
Figure 3.5. ^{1}H NMR spectrum (300 MHz, DMSO-d_6) of alkyne functionalized polymer (2)
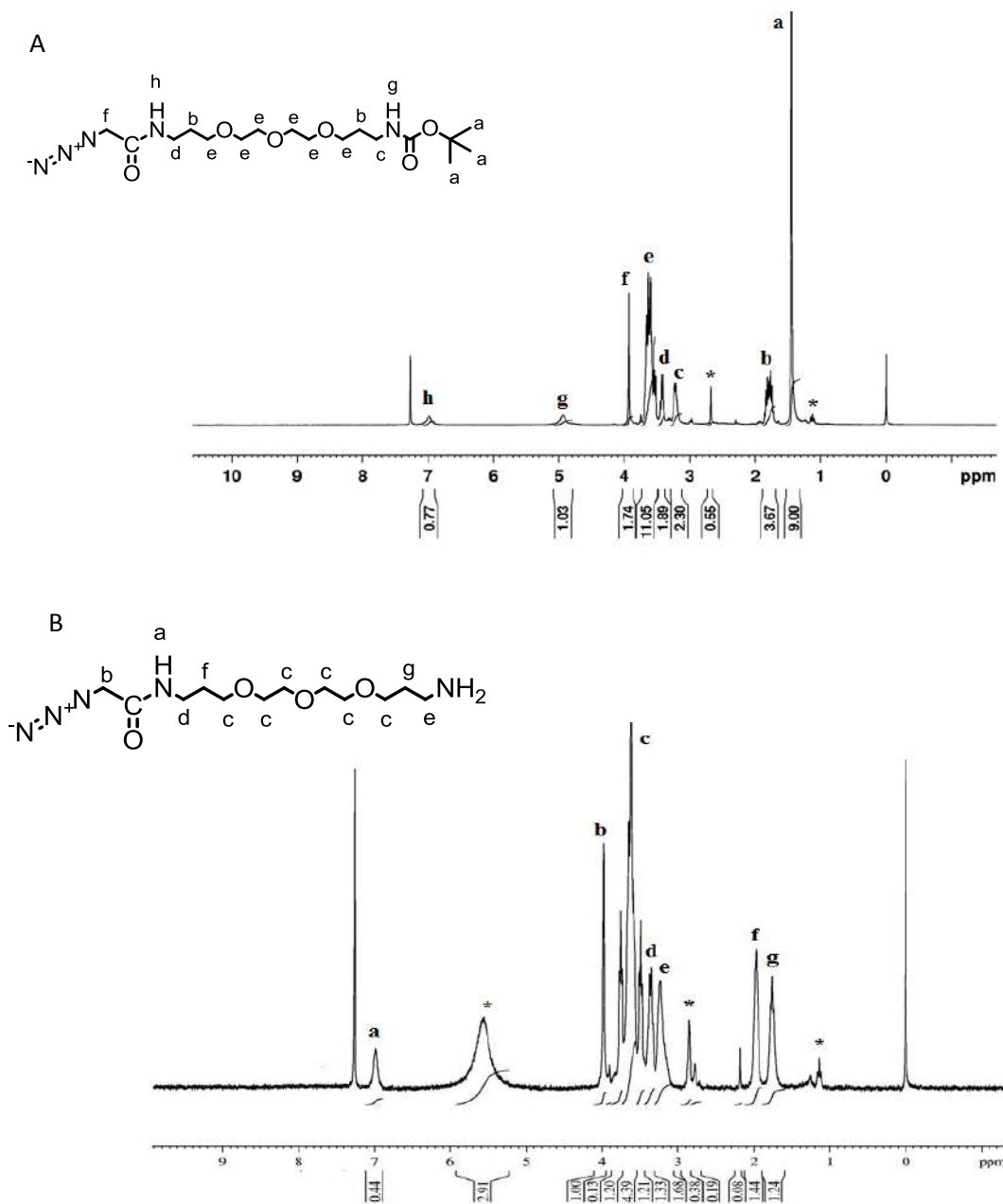
Figure 3.6. ^{1}H NMR spectra (300 MHz, CDCl$_3$) of (A) azide functionalized mono N- Boc protected 4,7,10-trioxa-1,13-tridecanediamine; δ 1.44 (s, 9H, Boc C$\underline{H}_3$), 1.8 (m, 4H, NH-CH$_2$-C$\underline{H}_2$), 3.2 (m, 2H, HN- C$\underline{H}_2$), 3.4 (m, 2H, HN- C$\underline{H}_2$), 3.51-3.75 (m, 12H, -O-C$\underline{H}_2$), 3.93 (s, 2H, N- C$\underline{H}_2$), 4.93 (brs, 1H, N$\underline{H}$), 6.98 (brs, 1H, N$\underline{H}$) and (B) azide functionalized 4,7,10-trioxa-1,13-tridecanediamine; δ 1.78 (m, 2H, NH-CH$_2$-C$\underline{H}_2$), 1.97(m, 2H, NH-CH$_2$-C$\underline{H}_2$), 3.35 (m, 2H, HN-C$\underline{H}_2$), 3.47 (m, 2H, HN- C$\underline{H}_2$), 3.5-3.77 (m, 12H, -O-C$\underline{H}_2$), 3.98 (s, 2H, N- C$\underline{H}_2$), 6.99 (brs, 1H, N$\underline{H}$)

124

comparison to those observed in isonicotinic acid grafted polymer (1), at δ 4.6 ppm corresponding to the methylene group of propargylamine (Figure 3.5). On the other hand, mono N-Boc protected 4, 7, 10-trioxa-1,13-tridecanediamine was derivatized with azido acetic acid and the resulting conjugate (R') was deprotected and coupled with Fmoc-Arg-Pbf-OH to obtain 'R' as shown in step II (Figure 3.2). Both the conjugates were characterized using ^{1}H NMR (Figure 3.6-3.7).
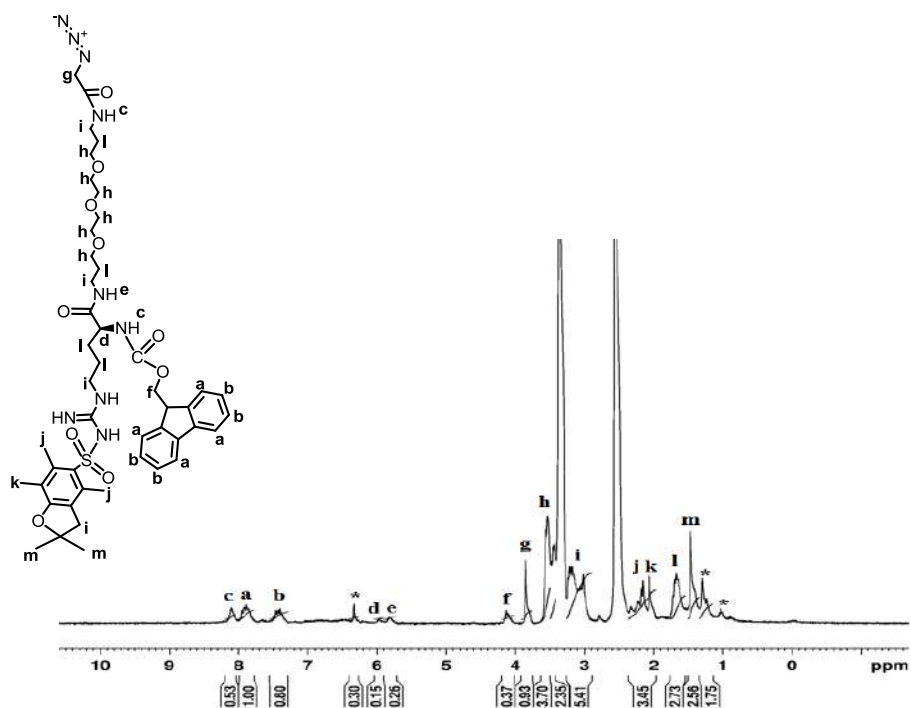
Figure 3.7. ^{1}H NMR spectrum (300 MHz, DMSO-d_6) of azide functionalized 4,7,10-trioxa-1,13-tridecanediamine; 1.46 (s, C-C$\underline{H}_3$), 1.71(m, NH-CH$_2$-C$\underline{H}_2$), 2. 064 (s, Ar- C$\underline{H}_3$), 2.154 (s, Ar-C$\underline{H}_3$), 3.2-3.558 (m, -O-C$\underline{H}_2$), 3.85 (s, 2H, N- C$\underline{H}_2$), 5.8 (brs, N$\underline{H}$), 5.98 (brs, NH-C$\underline{H}$), 7.4 (m, Ar- C$\underline{H}$), 7.8 (m, Ar C$\underline{H}$), 8.1 (brs, N$\underline{H}$)

The azide functionalized conjugate (R) was reacted with polymer (2) through copper catalyzed azide - alkyne cycloaddition to obtain L-arginine grafted polymer (3). ^{1}H NMR of the polymer (3) depicted characteristic aromatic peaks of Fmoc at δ 7.65 and 7.32 ppm. Presence of pbf group was confirmed by the peaks corresponding to methyl group at δ 1.3, 2.16 and 2.33 ppm (Figure

125

3.8). Click reaction was selected for coupling due to its selective reactivity and ability to overcome steric hindrance. Another advantageous feature of click based polymers is their ease
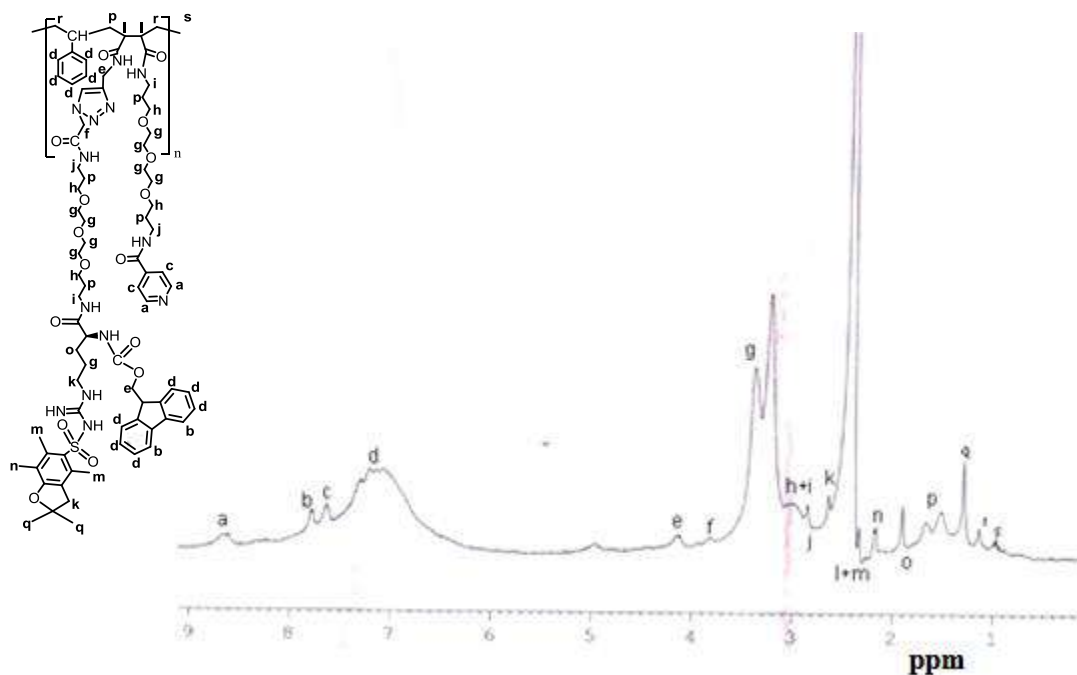
Figure 3.8. ^{1}H NMR spectrum (300 MHz, DMSO-*d*6) of click modified Fmoc-Arg-pbf-OH grafted polymer

of synthesis [5]. The unique 1,2,3 triazole moiety, which was formed during the reaction, could act as H-bond acceptors thereby promoting hydrophobic interactions of the polymer with siRNA. Triazole ring can render proteolytic stability to the polymer and can also facilitate endosomal penetration [6, 7, 8]. All these features could enhance the stability of the polyplexes during its transit through various systemic and cellular barriers. 4,7,10-trioxa-1,13-tridecanediamine, which is a short polyethylene glycol (PEG) like molecule, was employed as linker for making the copolymeric graft. Incorporation of this linker molecule into the polymer structure was expected to promote its aqueous solubility and assist in the formation of stable nanocarriers. The presence of primary amine groups in this linker molecule was particularly useful in tailoring the final

polymeric graft, due to their coupling efficiency. Further, these short glycol chains could significantly shield the charged areas of the polymeric nanocarriers thereby minimizing their clearance from the circulation by reticulo endothelial system [9, 10]. L-arginine was deprotected from Fmoc and the resulting free amine was coupled with Fmoc-Lys-Boc-OH.
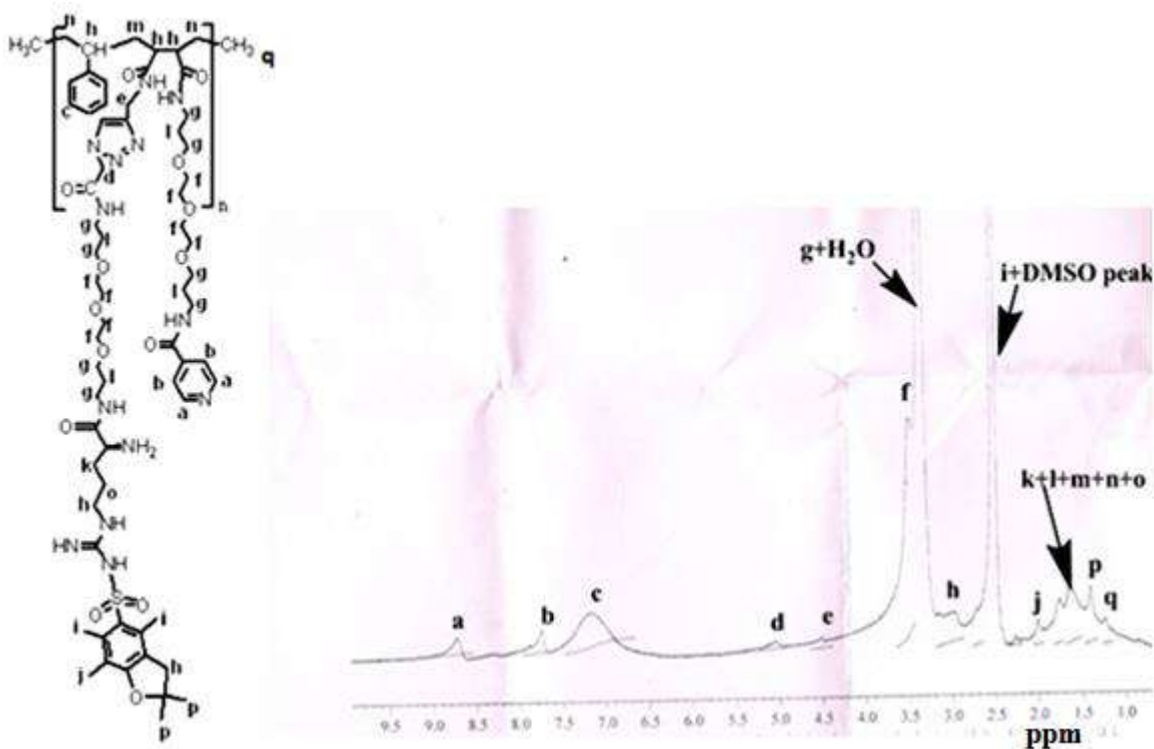
Figure 3.9. ^{1}H NMR spectrum (300 MHz, DMSO-d_6) of click modified arginine grafted polymer after removal of Fmoc

Cleavage of Fmoc from the polymeric derivative (4) was confirmed by the absence of aromatic peaks of Fmoc in ^{1}H NMR (Figure 3.9). After the deprotection, peak due to aromatic protons of styrene at δ 7.2 ppm became broad and smooth. Conjugation of Fmoc-Lys-Boc-OH was confirmed by characteristic aromatic peaks of Fmoc at δ 7.3 and 7.4 ppm and sharp peak of Boc at δ 1.363 ppm (Figure 3.10 A). Removal of Fmoc from lysine was confirmed by the absence of aromatic Fmoc peaks in ^{1}H NMR (Figure 3.10 B).
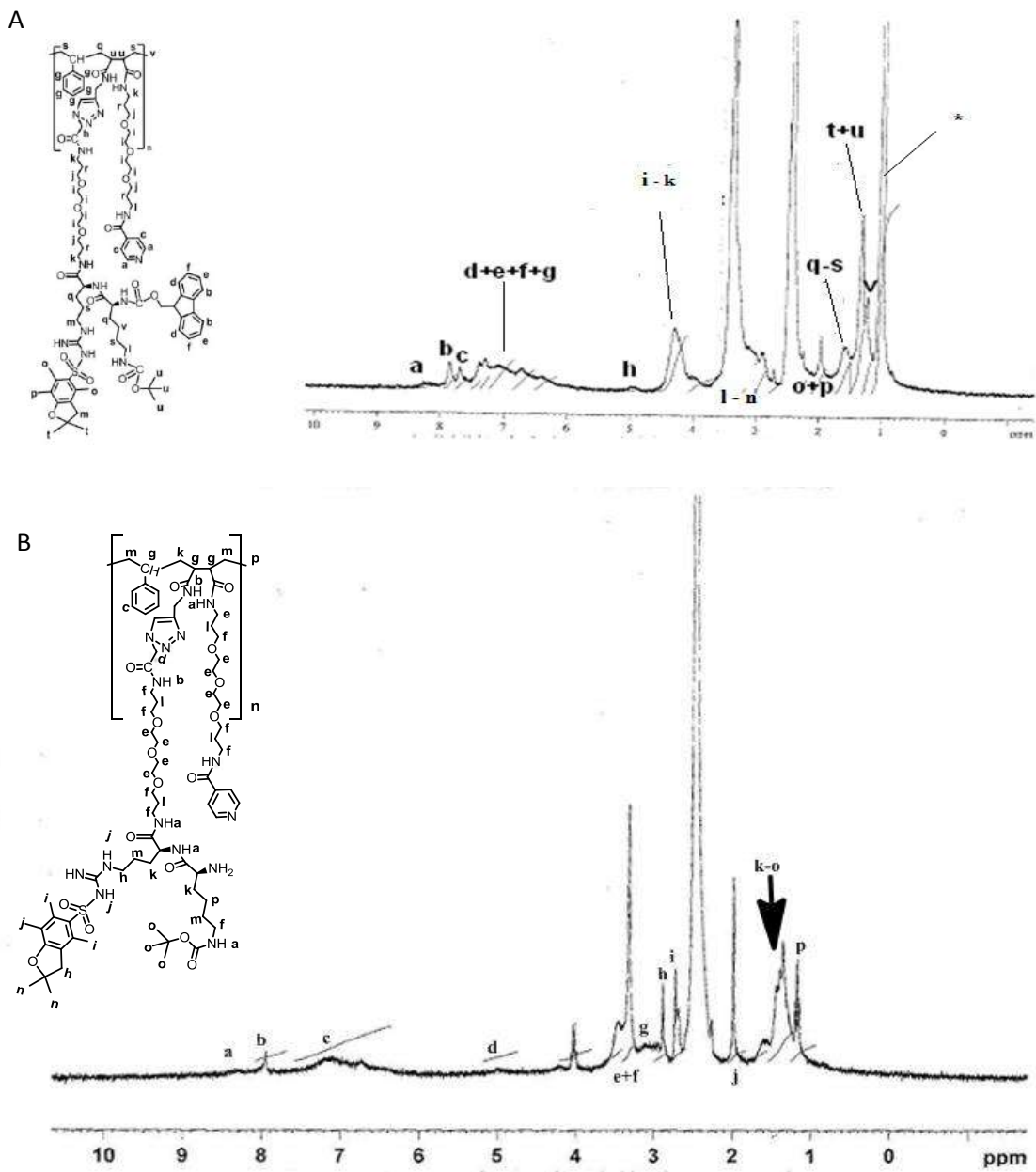
Figure 3.10. ^{1}H NMR spectra (300 MHz, DMSO-d_6) of (A) click modified polymer after grafting of Fmoc-Lys-Boc-OH and (B) Fmoc deprotected lysine grafted polymer

Final polymeric derivative, after its deprotection from Boc and pbf, was characterized by the absence of characteristic peaks of the corresponding protecting groups (Figure 3.11). ATR–FTIR spectrum of the final polymer (Figure 3.12) exhibited characteristic bands at 1454, 1548 and 1658 cm^{-1}, respectively indicating CN stretching, NH bending and carbonyl stretching

128

of amide bonds. Asymmetric stretch due to aliphatic C-O-C ether linkages occured at 1131 cm^{-1}.

In addition, bands starting at 1750 cm^{-1} (vibration of triazole ring), 920 cm^{-1} (CN stretch) showed that cycloaddition has been achieved. Average molecular weight of the polymer (M_w) was determined using GPC from standard calibration curve obtained by polyethylene glycols of known molecular weights and calculated to be ~ 22.5 kDa (Figure 3.13).
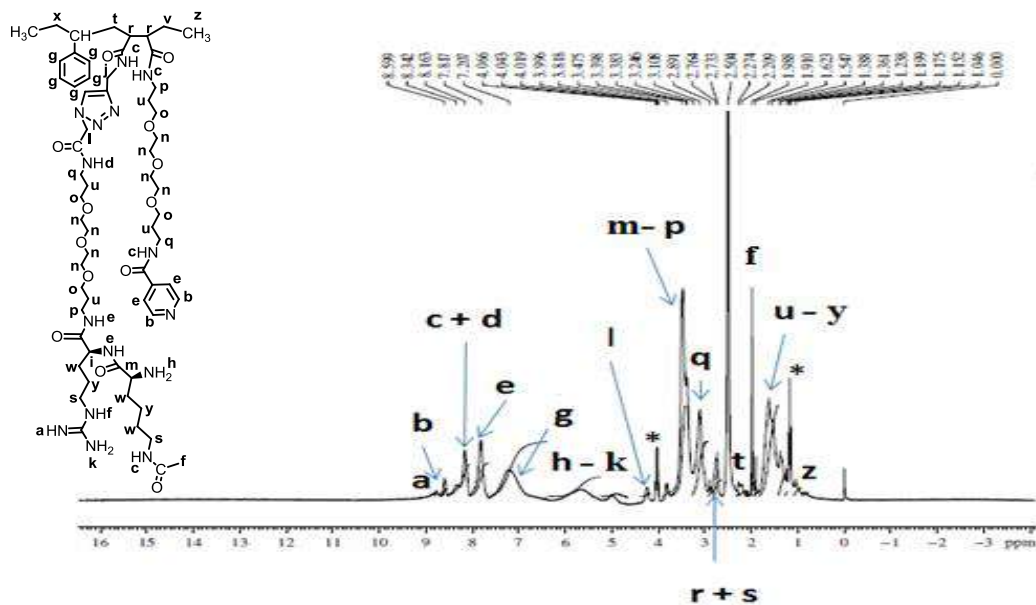
Figure 3.11. ^{1}H NMR spectrum (400 MHz, DMSO-d_6) of arginine and acetyl lysine grafted polymer after removal of protecting groups
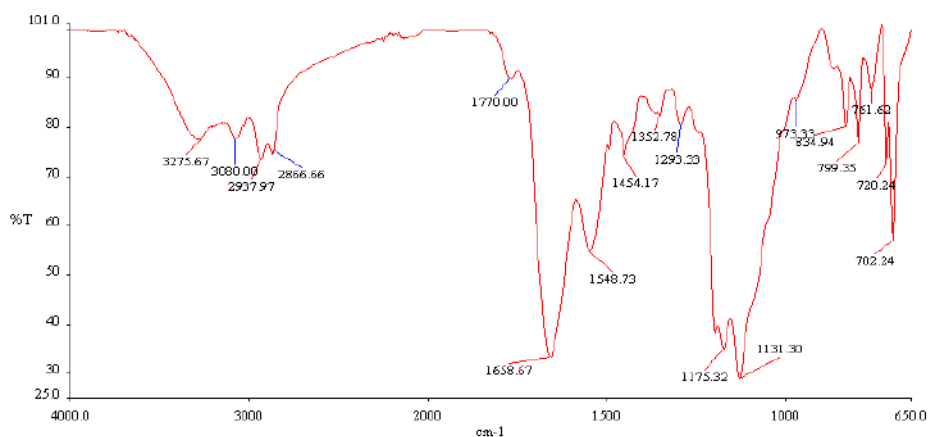
Figure 3.12. ATR-FTIR spectrum of arginine and acetyl lysine grafted polymer
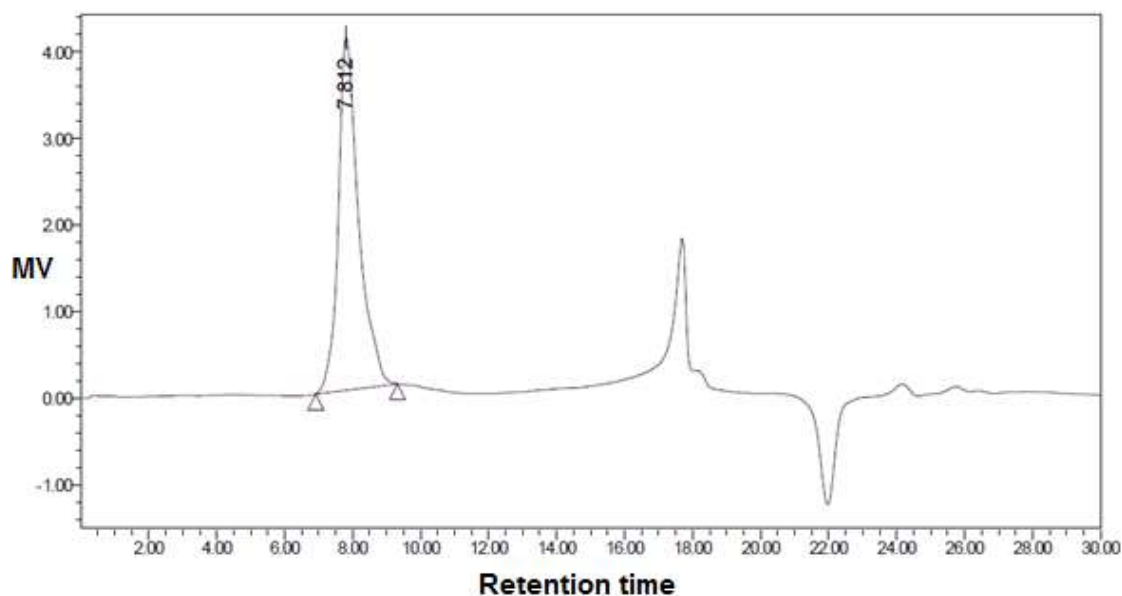
Figure 3.13. GPC spectrum of polymeric derivative (5) shown in step II, figure 3.2

3.3.3. Formulation and evaluation of the polymeric micelles

The amphiphilic polymer was easily self assembled to form stable micelles with an average particle size of 98.74 ± 1.1 nm (measured by DLS). Morphological characterization of the polymeric micelles using TEM (Figure 3.14) exhibited even lower particle size distribution (for individual micelles) ranging from ~14-30 nm. AFM image of the polymeric micelles depicted average height of the micelles, which was found to be ~12 nm. The obtained micellar structures were smooth and spherical in shape as shown by FESEM. The larger particle size of polymeric micelles shown in DLS measurement could be explained on the basis of formation of secondary micelles during the dialysis procedure. The dispersion obtained after prolonged dialysis could be secondary aggregates of individual micelles [11]. DLS measures the hydrodynamic radius of the polymeric particles, which could also contribute to the larger particle size [12]. Micelles exhibited excellent stability in deionized water and PBS, pH 7.4 with respective zeta potentials of 44.5 ± 4.12 mV and 21.62 ± 2.85 mV. This reduction in zeta potential could be attributed to the interaction of the surface cationic charge of micelles with salts present in the buffer saline.
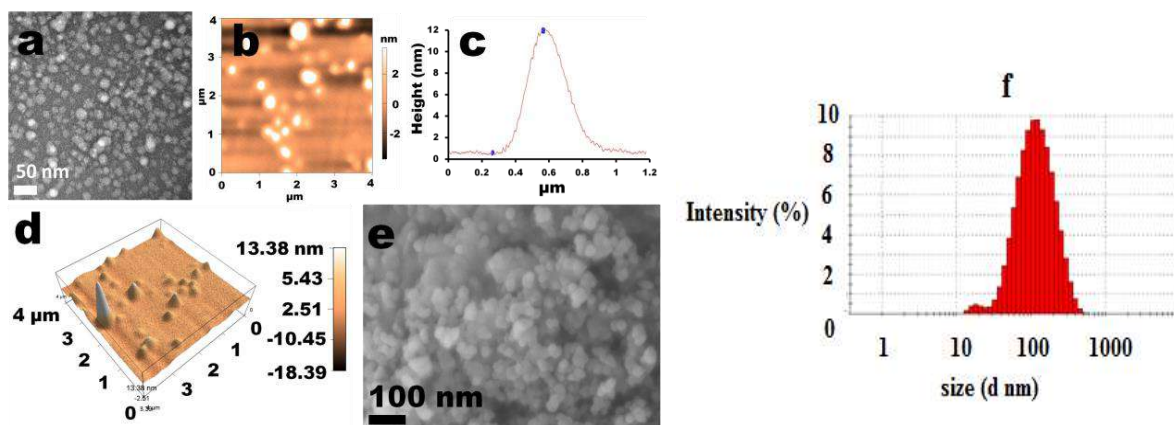
Figure 3.14. Morphological characterizations of polymeric micelles by TEM (a) AFM (b shows 2D image, c is the algorithm depicting average height of the micelles and d represents 3D image), FESEM (e) and DLS (f)

Critical micellar concentration (CMC) of the polymeric micelles was determined using fluorometry. Pyrene was employed as the fluorescent probe due to its preferential migration to hydrophobic core of micelles in aqueous environment. The enhancement in emission intensity of pyrene versus polymer concentration can indicate the conversion of unimer to micellar structures [13]. The ratio of emission intensities of the fifth and first highest energy bands of pyrene (I 394/I 373) was plotted against the corresponding micelle concentrations to determine CMC (Figure 3.15). Crossover point at low concentrations of micelles was taken as CMC. CMC of the polymeric micelles was found to be 3 µg∕mL. CMC is a good indicator of the kinetic stability of polymeric micelles employed for systemic delivery of active agents. When administered intravenously, the micelles will undergo dilution in a large volume of blood. If this diluted concentration is below the CMC, micelles will dissociate rendering them less effective as a therapeutic vehicle [15, 16]. Hence the dose of polymer should be kept above the CMC for better kinetic stability in blood. Amine content of the polymer was found to be 76.33 ± 6.97 µM ∕ 200 µg nanoparticles, using TNBS assay.
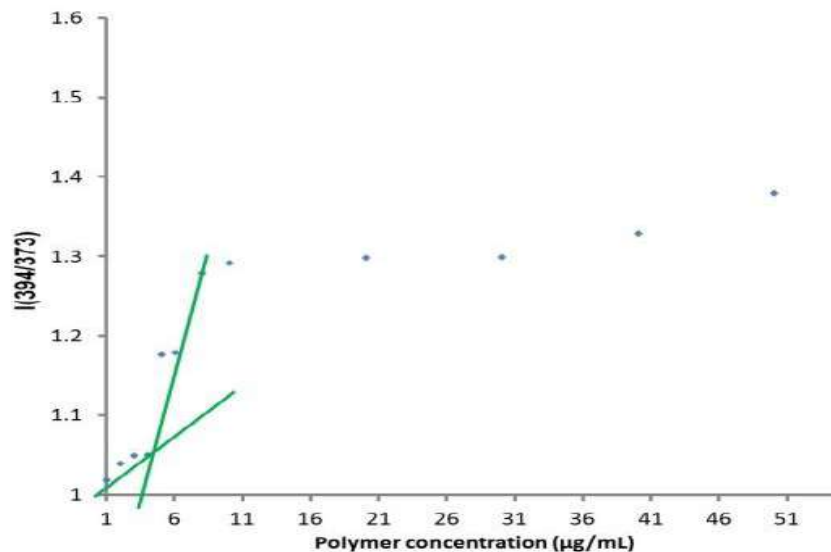
Figure 3.15. CMC determination of polymeric micelles

3.3.3.1. Protein adsorption of polymeric micelles

Non specific adsoprtion of plasma proteins to the polymer surface has been considered as one of the major factors in reducing the circulation half life of nanocarriers. Imparting a stealth effect to the particles through approaches like pegylation can minimize this non specific protein adsorption [14, 15]. % plasma protein adsorption to the polymeric surface was determined and compared with L - arginine grafted PSMA. Synthesis and characterization of L - arginine grafted PSMA has been reported in chapter II. Total protein concentration of plasma was found out to be 65.88 ± 2 mg/mL. Dried polymer - protein pellet of glycol grafted cationic polymer exhibited significantly lower protein adsorption (31.55 ± 2.35 µg/mg of polymer) compared to that of L-arginine grafted PSMA (81.26 ± 7.14 µg/mg of polymer). Non pegylated polyplexes generally shows higher protein adsorption. The presence of glycol chains of 4,7,10-trioxa-1,13-tridecanediamine could provide shielding to the micellar structures which in turn might have reduced the protein adsorption . High molecular weight polyethylene glycols, which are non biodegradable polyethers, can get accumulated in the body after prolonged administration and
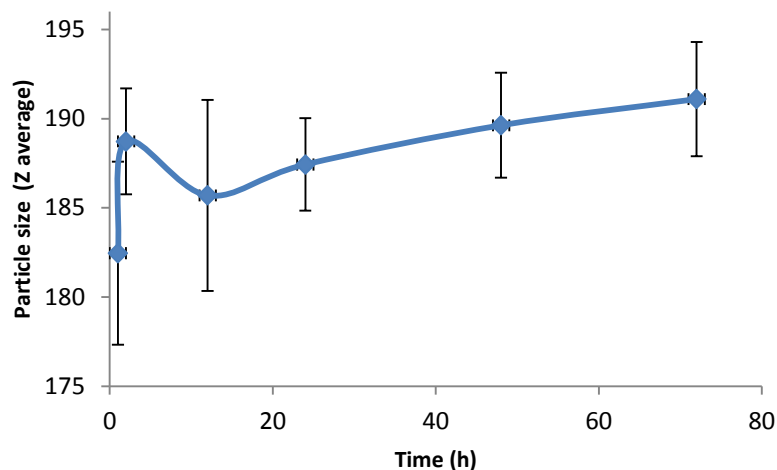
Figure 3.16. Stability of the polymeric micelles in RPMI 1640 media supplemented with 10 % FBS

are often reported to evoke immune response [16]. 4,7,10-trioxa-1,13-tridecanediamine is a short glycol chain (Mol.wt 202 Da), with high solubility in aqueous media, which can be easily eliminated from the systemic circulation. Hence this molecule could be employed as a safe alternative in designing stealth nanocarriers for therapeutic applications. Stability of the polymeric micelles in presence of 10 % FBS is shown in figure 3.16. Nanoparticles were dispersed in complete cell culture media at a final polymer concentration of 0.3 mg/mL, and stored at 37 ºC for performing DLS measurements at different time intervals. The polymeric micelles exhibited an average particle size of 168.6 ± 3.8 nm immediately after dispersion, which was slightly increased to 182.46 ± 5.13 nm on storage (after 1 h). But on prolonged storage, there was negligible increase in the size and the dispersion remained transparent. Zeta potential of the particles shifted to negative range (- 6.21 ± 0.92 mV). Slight increase in particle size within the first one hour of storage could have occurred due to adsorption of albumin to the surface of nanoparticles [17, 18]. Presence of abundant negatively charged albumin in the cell culture media could be the reason for negative zeta potential. Various reports are suggesting increase in

several hundreds of nanometers of size for nanoparticles after prolonged exposure to proteins [19, 20]. Hence it can be assumed that the minimal increase in size could be due to the stealth property induced by glycol chains and the resultant reduction in protein adsorption.

3.3.3.2. Haemolysis study

Haemocomatability of nanoparticles is widely evaluated based on their *in vitro* haemolytic potential. According to the standards set by Austian, up to 5 % haemolysis is generally considered as safe for biomaterials. But several other studies have reported that % haemolysis ranging from 5 – 25 % can be considered as ʽno concernʼ for nanoparticles. This is based on the correlation of *in vitro* and *in vivo* haemolytic effect of nanosystems. Nanoparticles exhibit much lesser haemolysis *in vivo* compared to that at *in vitro* conditions, due to the interactions from components of systemic circulation [21]. Our results have demonstrated that haemolytic activity of the cationic polymeric micelles was concentration and pH dependent (Figure 3.17). At both pH values (7.4 and 5.5), concentration dependent increase in % haemolysis was observed. Significantly higher haemolytic effect was seen at pH 5.5 compared to that at 7.4. This could be due to the enhanced protonation of the amine functionalities at lower pH. Aromatic pyridine rings of the grafted isonicotinic acid can interact with RBC membranes, thereby promoting their destabilization, at acidic pH. % haemolysis by the cationic micelles at pH 7.4 was below 25%, even at the highest concentration tested (2.5 mg∕mL), suggesting their haemocompatibility. Further, higher haemolytic effect at acidic pH indicate their ability to destabilize endolysosomal membranes, which is an advantageous feature for nanocarriers post cellular uptake [22].
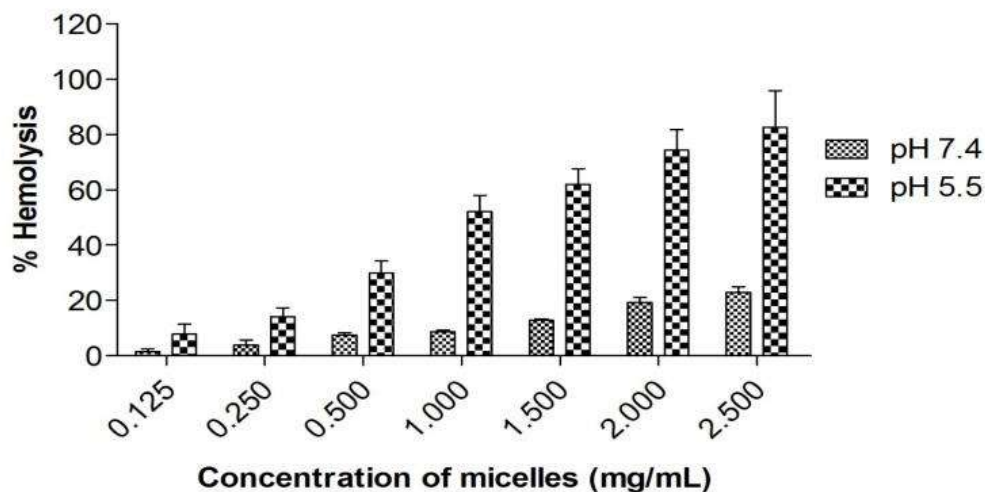
Figure 3.17. Haemolysis of nanoparticles at various concentrations (mg∕mL)

3.3.3.3. Evaluation of the polymer for genotoxicity and ROS generation

There was no significant ROS generation in MCF 7 cells treated with polymeric micelles (50 - 1000 µg/mL). The absorbance values in the wells treated with polymeric particles were similar to that of control (data not shown). Hence it can be concluded that the polymeric carrier don't possess any potential to increase the ROS load in mitochondria. Genotoxic potential of the polymer was studied using comet assay, which is a single cell gel electrophoresis method to measure the DNA strand breaks in cells. In this method, cells were encapsulated in agarose gel suspension followed by their lysis in alkaline conditions. The lysed cells were then subjected to electrophoresis and observed for any change in the intensity of comet tail. The increase in intensity of comet tail is directly proportional to the extent of DNA strand breaks [23, 24]. MCF 7 cells treated with 1 mg/mL of polymer did not show any difference compared to untreated cells, indicating negligible genotoxic potential of the carrier (Figure 3.18).
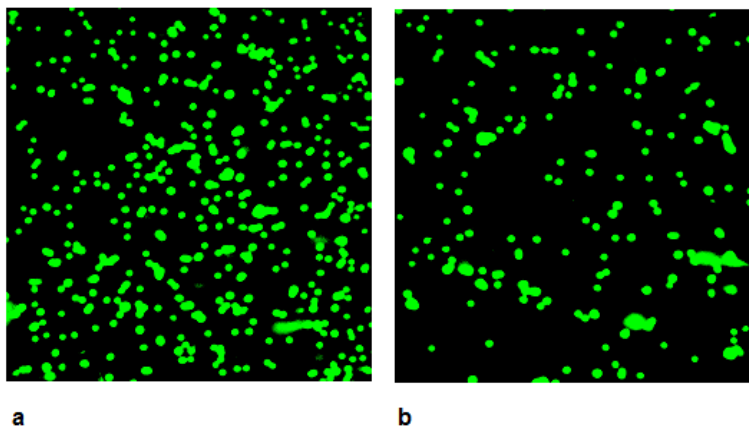
Figure 3.18. Images of MCF 7 cells treated with 1 mg/mL polymer (b) and control (a) using CLSM after performing comet assay (lysed cells after electrophoresis were stained with SYBR$^{@}$ green)

3.3.4. Formulation and evaluation of polyplexes

Polyplex formation was studied using agarose gel electrophoresis. Polymeric micelles were complexed with siRNA at various polymer∕siRNA weight ratios. Complete retardation of siRNA occurred above the polymer∕siRNA weight ratio of 10 (Figure 3.19 a). Complexation of siRNA to the polymeric micelles in RNase free water did not result in any significant change in average size or zetapotential, in comparison to the bare micelles. DLS size for the polyplexes formed at polymer∕siRNA weight ratio of 50 was 89 ± 4.2 nm. Silencing of PLK-1 gene in MCF 7 cells by the polymeric micelles bearing PLK-1 siRNA was evaluated at mRNA level by real time polymerase chain reaction (RTPCR) assay. Cells treated with polyplexes bearing scrambled (Scr) siRNAs exhibited almost same gene expression as that of untreated cells. Cells treated with polyplexes of PLK-1 siRNA resulted in significantly low levels of corresponding mRNA, in comparison to the control. Efficient mRNA knock down of ~ 63 % was obtained with the polyplexes at 100 nM concentration of PLK-1 siRNA (Figure 3.19 b). Further increase in siRNA concentration did not achieve significant increase in the down regulation of PLK-1 mRNA.
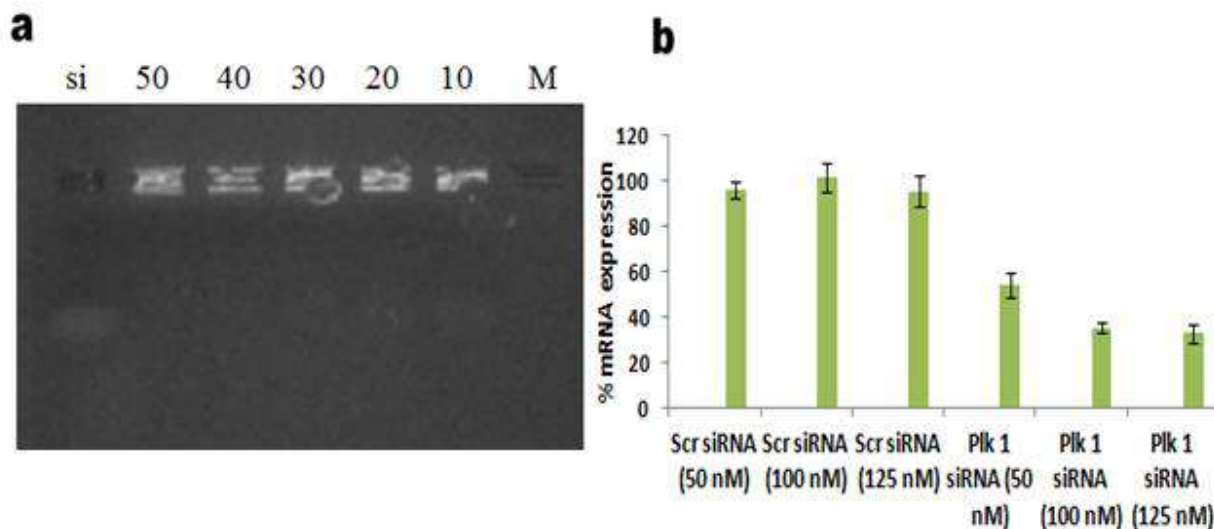
Figure 3.19. (a) Agarose gel (1.2 %) electrophoresis of polyplexes. 100 bp ladder, pure siRNA (negative control) and blank micelles are labelled by L, si and M respectively, above the wells. Polymer∕siRNA weight ratios are shown with numbers (10 - 50); (b) % mRNA expression in MCF 7 cells transfected with polyplexes bearing PLK-1 siRNA and scrambled siRNA (polymer∕ siRNA weight ratio 50). % mRNA are represented with respect to control (untreated cells)

3.3.5. Formulation and evaluation of drug loaded polyplexes

Doxorubicin loaded polymeric micelles were optimized based on the drug loading content. Different feed ratios of drug and polymer were employed to optimize the formulation (table 3.1). Drug loading content (% w/w of polymer) was found to be increasing with higher drug/polymer weight ratio. Optimum drug loading of 9.05 ± 0.6 % w/w was obtained with drug/polymer weight ratio of 1: 2.5. Further increase in drug/polymer weight ratio exhibited higher particle size distribution without any significant improvement in drug loading. Doxorubicin loading resulted in slight increase in particle size distribution of polymeric micelles and the extent of increase was directly proportional to drug/polymer weight ratio. DLS data of optimized drug loaded micelles

Table 3.1. Physicochemical properties of drug loaded micelles in PBS, pH 7.4

Drug ∕ Polymer feed ratio	*Drug loading (% w ∕ w)*	*Average particle size (nm)*	*Polydispersity index (PDI)*	*Zetapotential (mV)*
1: 5	5.37 ± 0.94	118.8 ± 3.3	0.285 ± 0.013	19.15 ± 1.65
1:1.67	7.5 ± 1.16	136. 13 ± 6.64	0.225 ± 0.08	20.86 ± 1.96
1:2.5	9. 05 ± 0.6	144.8 ± 6.3	0.248 ± 0.027	18.68 ± 2.12
1:2	9.17± 0.74	167 ± 8.43	0.263 ± 0.06	17.25 ± 1.82

Mean ± SD, n = 3

exhibited an average particle size of 144.8 ± 6.3 nm. Particle size, PDI and zeta potential of various formulations are summarized in table 1. *In vitro* release of drug from the polymeric micelles was found to be enhanced at pH 5.0 compared to that at pH 7.4 (Figure 3.20). After 24 hours, 26.55 ± 2.15 % release was observed at pH 7.4 compared to 55.1 ± 7.2 % at pH 5.0. At lower pH, the amino acid groups will be almost completely protonated resulting in their enhanced hydrophilicity and electrostatic repulsions [25, 26]. To counter this, the polymer could swell and lead to pronounced release of drug. This release pattern is beneficial for their disposal of the incorporated active ingredients at the acidic pH of tumor microenvironment.
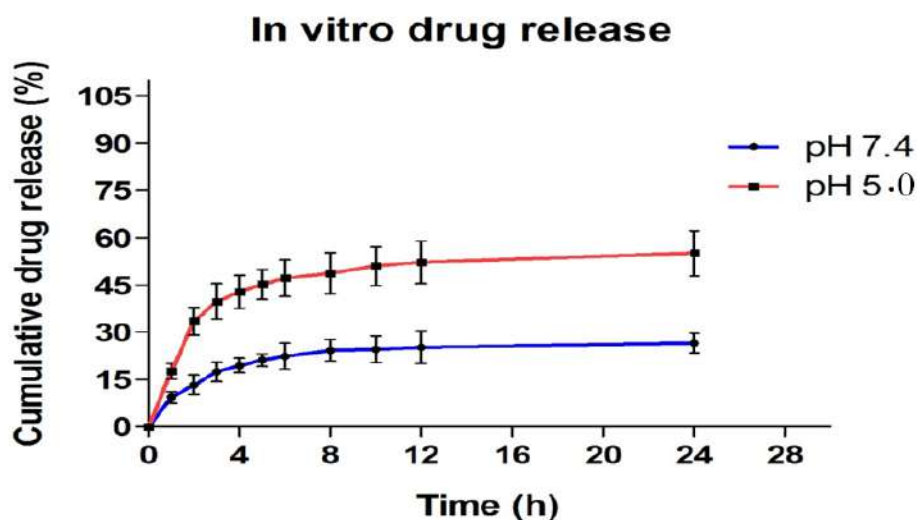
Figure 3.20. *In vitro* drug release from the optimized micelles at pH 7.4 and 5

Polymer⁄siRNA weight ratios required for efficient complexation was similar for both drug loaded micelles and blank polymeric micelles (Figure 3.21). Doxorubicin release from the polyplexes was also evaluated at different pH values (7.4 and 5). Drug release from polyplexes
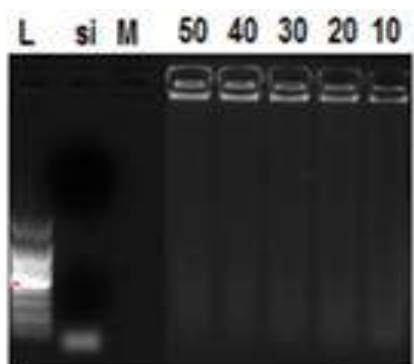
Figure 3.21. Agarose gel (1.2 %) electrophoresis of drug loaded polyplexes. siRNA (negative control) and blank micelles are labelled by si and M, respectively. Polymer⁄siRNA weight ratios are shown with numbers (10 – 50)

was observed to be retarded compared to that from bare micelles (Figure 3.22). Maximum % cumulative release of 16.71 ± 1.4 and 38.63 ± 3.5 was obtained after 24 hours, at pH 7.4 and 5 respectively. This reduction in drug release could be due to the utilization of amino groups of the micelles by the complexing siRNA molecules, thereby inhibiting their swelling in release media, and an additional barrier for drug diffusion created by the complexed siRNA molecules.
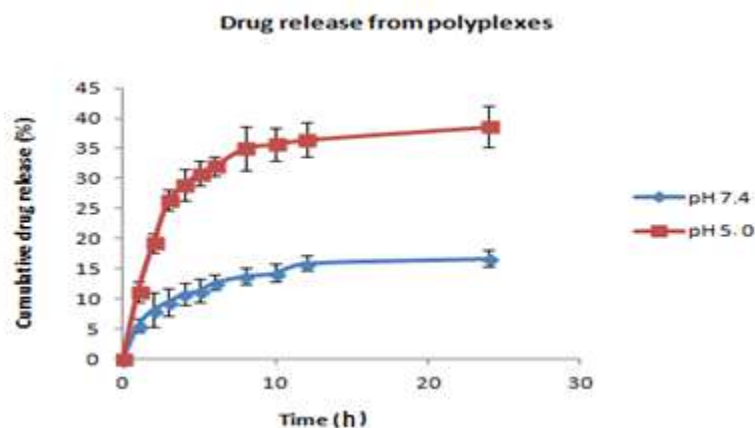
Figure 3.22. *In vitro* drug release from the optimized polyplexes at pH 7.4 and 5

3.3.6. Evaluation of the polymeric micelles for co-delivery of drug and siRNA

Co-delivery of Dox and FAM labeled siRNA was evaluated using CLSM (Figure 3.23 A). Dox and FAM labeled siRNA incorporated in to the micelles have shown excellent co-localization within the cytoplasm. Yellow color shows the overlapping of the fluorescence from Dox and FAM labelled siRNA. Majority of the cells depicted co-localization. This indicates ability of the polyplexes to co-deliver both the active ingredients to the cells. Further, nuclear localization of released doxorubicin from the polymeric micelles was evaluated. Most of the drug molecules reached nucleus of MCF 7 cells, after 12 h incubation, with a smaller proportion still remaining within the cytoplasm (Figure 3.23 B). Efficient cellular uptake of the polymeric nanocarriers
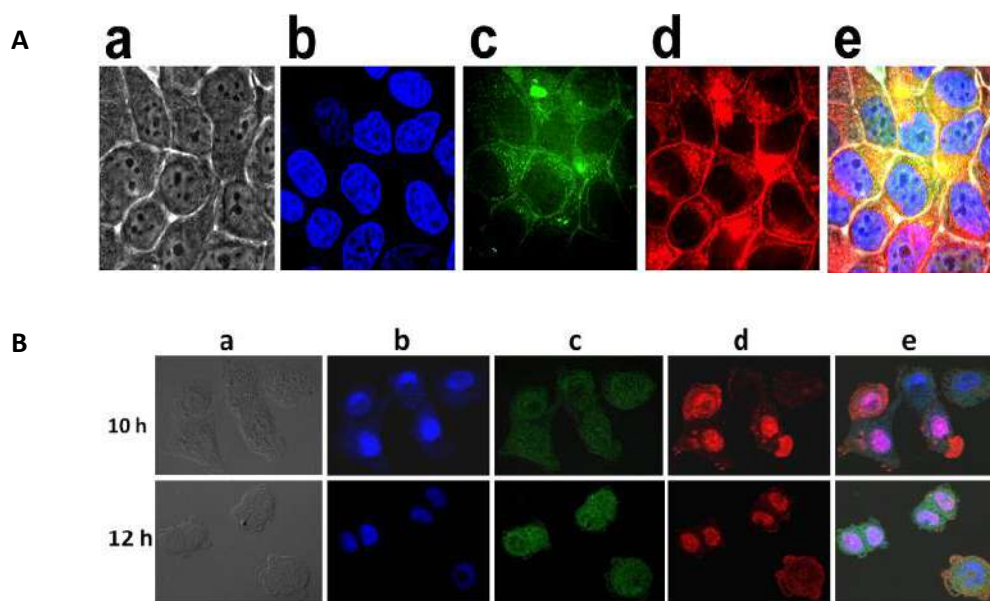
Figure 3.23. (A) CLSM image depicting the co-delivery of Dox and FAM labeled negative control siRNA. Images of bright field, Nuc Blue stained nucleus, FAM fluorescence and Dox fluorescence are indicated by a, b, c and d respectively. 'e' represents merged image. (B) Nuclear localization of doxorubicin delivered using polymeric micelles in MCF 7 cells at different time points (10 h and 12 h). Fluorescent images of DAPI, lysotracker green, doxorubicin and merged image are represented by a, b, c, d and e respectively.

could have been facilitated by their smaller particle size and cationic charge interaction with the cellular membrane. The synergistic effect of Dox and PLK-1 siRNA in inhibiting cell proliferation was evaluated by MTT assay (Figure 3.24 A). MCF 7 cells were treated with polymeric micelles bearing different concentrations of Dox in combination with 100 nM PLK-1 siRNA. As shown in figure 3.24 A, formulations with PLK-1 siRNA induced more toxicity in
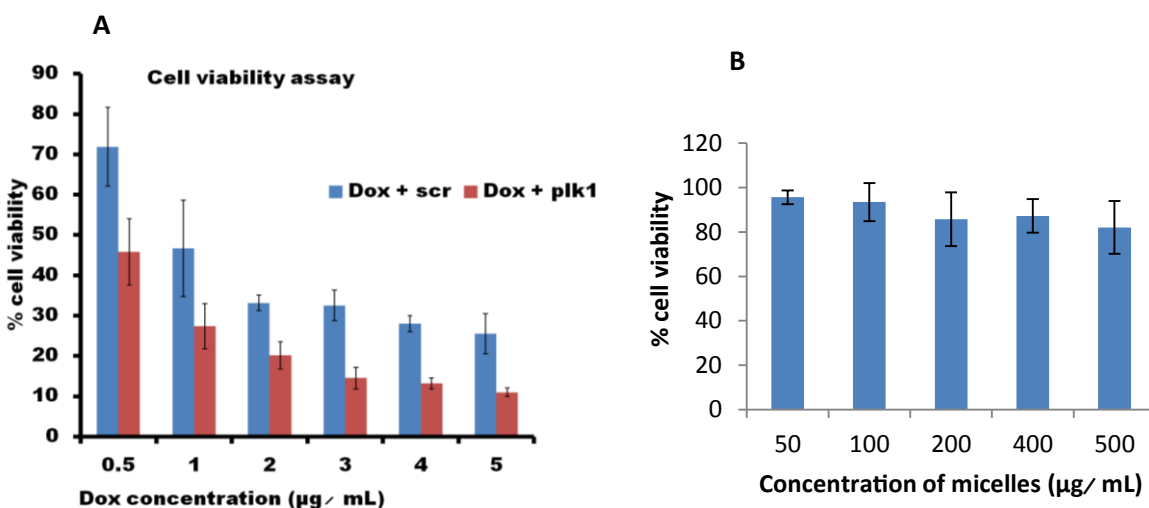
Figure 3.24. Cell proliferation assay of polyplexes (A) and blank micelles (B)

comparison to that with scrambled siRNA. The increase in cytotoxicity was evident at all the concentrations of doxorubicin tested. Cytotoxicity of blank polymeric micelles evaluated at different concentrations (50 - 500 µg∕mL) did not show any significant toxicity (Figure 3.24 B), which indicated that the polymeric carrier could be safely employed for biological applications.

Polo like kinases are important regulators of the mitotic pathway in tumor cells. They help in the formation and changes of spindle and also regulates cell cycle progression through G2 and M phase. Mitotic activity of the rapidly proliferating tumor cells is predominantly dependent on polo like kinases. Knock down of polo like kinase proteins can lead to mitotic arrest and reduced proliferation of cancer cells. Further, inhibitory effect of PLK-1 siRNAs on the cell proliferation

of normal cells is weak compared to that of tumor cells [27, 28]. This makes PLK-1 siRNA an attractive candidate for cancer therapy. In short, combination therapy of PLK-1 siRNA with anti cancer drugs can be employed to achieve better pharmacological activity with lower drug dose, thereby reducing the unwanted side effects of chemotherapeutics. The synergistic effect of drug loaded polyplexes in inhibiting cell proliferation was further evaluated by live∕dead staining of the treated cells. MCF 7 cells were treated with polyplexes with Dox and scrambled siRNA or with Dox and PLK-1 siRNA for 48 hours followed by staining the cells with calcein and propidium iodide (Figure 3.25). Co-delivery of PLK-1 siRNA resulted in less proliferation of the
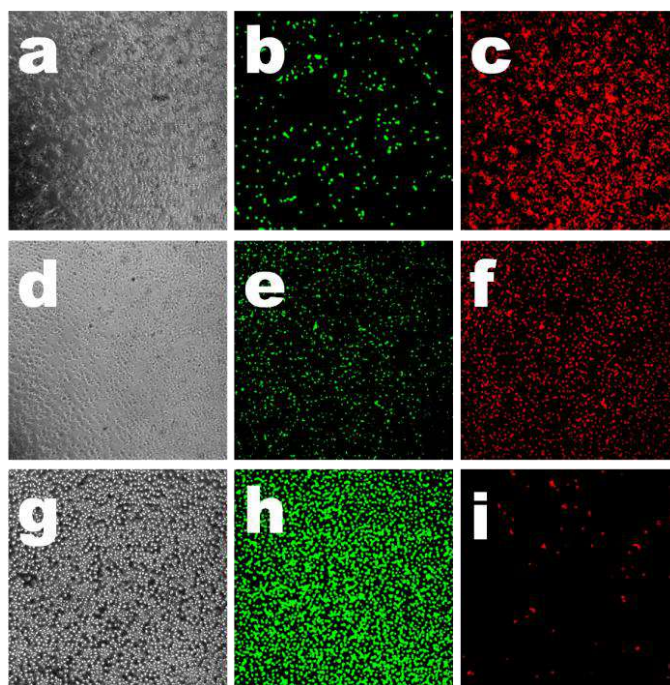
Figure 3.25. Calcein (green) ∕ PI (red) staining of MCF 7 cells after treatment with polyplexes bearing Dox (2.5µg∕mL) and 100 nm PLK-1 siRNA (a – c); Dox and 100 nm scrambled (Scr) siRNA (d – f). Untreated cells are shown in the bottom lane (g – i). Complete view of the confocal plates was captured at 4x magnification. a, d and g shows bright field images, b,e and h represents calcein staining and c,f and i exhibits PI staining.

cancer cells as shown in the figure 3.25. More dead cells (proidium iodide stained) were

visualized in the cell population treated with both drug and PLK-1 siRNA, in comparison to that with drug and scrambled siRNA. This could have been facilitated by the mitotic arrest of MCF 7 cells after down regulation of PLK-1 gene. Anti apoptotic defense of the tumor cells is predominantly dependent upon the proteins like PLK-1, survivin, BCl-2 etc. which can promote cell proliferation or induce drug resistance. Down regulation of these proteins by utilizing RNAi interference is well established [29, 30]. Further, simultaneous delivery of the chemotherapeutic drugs along with siRNAs has been experimentally reported to achieve improved pharmacological effects [31, 32]. The major obstacle in this therapeutic arena is the need of a well designed delivery system which can efficiently overcome various cellular and systemic barriers for the delivery of these therapeutic cargos to target site. Our results clearly show that, the designed click modified stealth nanocarrier has remarkable potential for the co-delivery of hydrophobic anticancer drugs and siRNAs, utilizing enhanced permeation and retention (EPR) effect.

3.3.7. Toxicological evaluation of the polymeric micelles *in vivo*

To assess the safety of the synthesized cationic micelles for biological application, seven day repeated dose toxicity study was conducted in male Swiss albino mice. Dose of the cationic micelles (100 mg∕ kg) used for toxicological evaluation was selected based on previously reported literature [33]. The group of mice treated with cationic micelles did not show any significant change in body weights compared to the control group (data not shown). Hematology and serum biochemistry parameters were having negligible difference between control and treated groups (Table 3.2). Histopathological evaluation of the vital organs (Figure 3.26) did not indicate any toxicity caused by accumulation of the nanoparticles. These observations suggested that the designed nanocarriers were safe for delivery applications *in vivo.*

Table 3.2. Hematology and serum biochemistry analysis from repeated dose toxicity study of cationic micelles in male Swiss albino mice

Hematology and serum biochemistry parameters with units	Control group (PBS)	Cationic micelles (100 mg∕kg)
WBC $(10^3∕$ mm $^3)$	6.725 ± 2.866	$5.325 \pm 0 .79$
Lymphocytes (%)	55.45 ± 4.8	60.87 ± 7
Monocytes (%)	31.2 ± 8	27.2 ± 1.5
Granulocytes (%)	13.78 ± 4.39	11.5 ± 5.8
RBC $(10^6∕$ mm $^3)$	$8.535 \pm .59$	$9.23 \pm .4$
HGB	$14.45 \pm .65$	14.5 ± 1.82
HCT	$42.4 \pm .94$	44.2 ± 1.32
MCV	50.25 ± 1.91	48.75 ± 1.6
MCH	16.77 ± 1.11	$15.46 \pm .9$
MCHC	$33.51 \pm .665$	32.44 ± 1
RDW	$14.52 \pm .63$	$15.71 \pm .83$
PLT	916.75 ± 83.44	818.5 ± 85
MPV	$5.17 \pm .5$	$6.2 \pm .7$
PCT	$0.524 \pm .1$	$0.549 \pm .12$
PDW	$5.5 \pm .53$	4 ± 1.44
SGOT (IU ∕ L)	101.86 ± 12.47	112.6 ± 12.76
SGPT (IU ∕ L)	42.5 ± 5.83	38.36 ± 2.76
Creatinine (mg∕dL)	$0.34 \pm 0. 06$	$0.4 \pm 0. 04$
Urea (mg∕dL)	37.22 ± 3	42.9 ± 3.8

Mean $\pm$ SD, n = 4
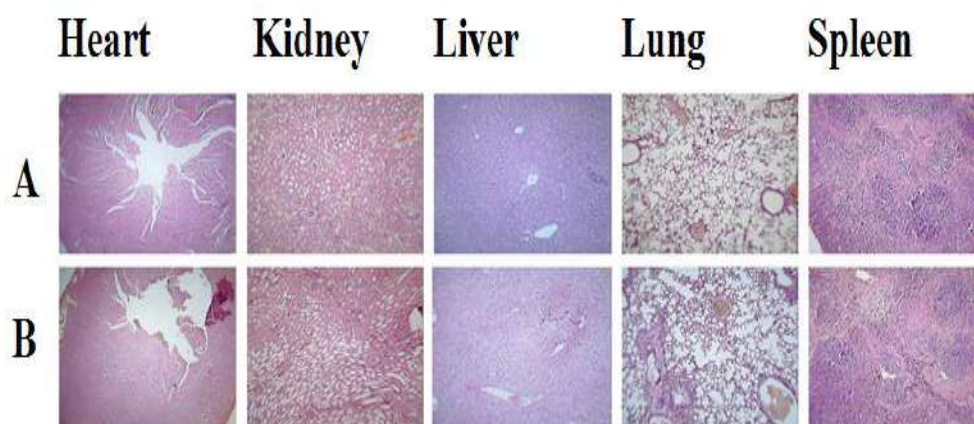
Figure 3.26. Histopathological evaluation of vital organs of mice in repeated dose toxicity study. ˈAˈ shows organs of control mice and ˈBˈ represents that of nanoparticle treated mice

3.3.8. Anti tumor efficacy in EAT tumor model

Synergistic effect of the dual motif loaded cationic micelles on cell proliferation inhibition *in vitro* was further assessed *in vivo,* using EAT tumor model. As shown in figure 3.27, all the treatment groups exhibited tumor growth retardation compared to control. Administration of siRNA alone (group iv) caused 1.86 fold reduction in % relative tumor volume, in comparison to control. Both Dox + scrambled siRNA loaded micelles and free Dox treated groups shown almost comparable inhibition in tumor growth (5.9 and 5.4 fold decrease in % relative tumor volume, respectively). Co-delivery of Dox and PLK-1 siRNA via the synthesized cationic micelles (group i) achieved the most significant reduction, of 13.16 fold, in % relative tumor volume. Histopathological evaluation of the organs and tumors of various groups was performed (Figure 3.28). Maximum necrosis was observed in siRNA and Dox treated group, confirming the enhanced antitumor efficacy. Major serum biochemical parameters of various groups of tumor regression study are shown in table 3.3.

Table 3.3. Serum biochemistry analysis of EAT tumor bearing mice treated with various formulations

Serum biochemistry parameters with units	Group i	Group ii	Group iii	Group iv	Group v
SGPT (IU ∕ L)	47.41 ± 6.29	45.3 ± 1.41	49.47 ± 9	46.52 ± 3.24	41.43 ± 6.4
SGOT (IU ∕ L)	127 ± 4.1	128.66 ± 12.7	134 ± 8.8	119 ± 3.22	115± 13.9
Creatinine (mg∕dL)	0.46 ± 0. 06	0.455 ± 0. 05	0.49 ± 0. 09	0.42 ± 0. 04	0.4 ± .01
Urea (mg∕dL)	43.22 ± 8.1	42.46 ± 7.3	51.67±13.17	38.68 ± 1.37	37.96 ± 2.65
CK - MB (IU∕ L)	2.4 ± 0.6	3.1 ± 0.45	3.8 ± .75	2.6 ± .48	2.2 ± .62

Mean ± SD, n = 4
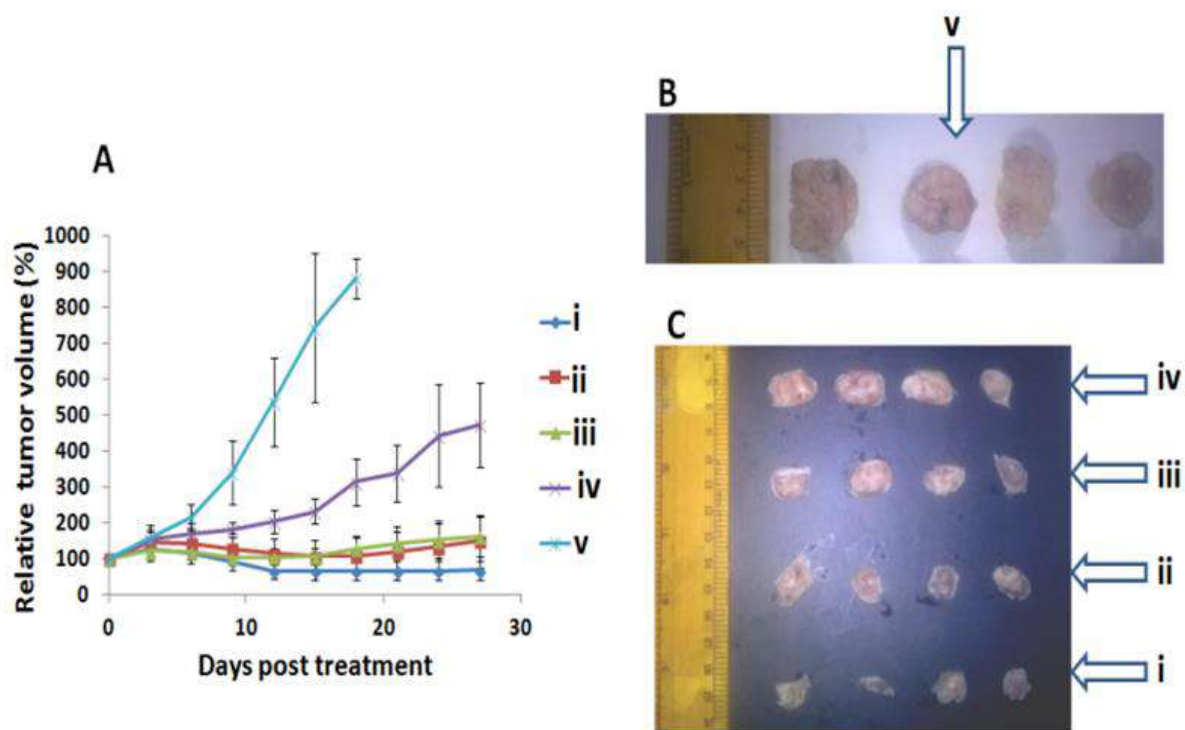
Figure 3.27. (A) Relative % increase in tumor volumes of various groups. Dox and PLK-1 siRNA loaded micelles (i), Dox and scrambled siRNA loaded micelles (ii), free Dox (iii), PLK-1 siRNA carrying micelles (iv) and PBS, pH 7.4 (v) were administered intratumorally. Treatment was started on day 14 post subcutaneous implantation of tumor cells, and first day of injection is designated as day 0. Four injections were given on days 0, 3, 6 and 9. Cumulative dose of Dox administered in each mice was 6 mg⁄kg and that of siRNA was 2 mg⁄kg. Tumor images of control (PBS, pH 7.4 treated) group (B) and other treatment groups (C) at the end point of study is also shown.

There was only slight difference in the parameters of treated groups with respect to control. Even in free doxorubicin treated group, there was no significant alteration in the serum biochemical values. This could be due to the fact that route of administration chosen for the study was intratumoral and also due to low cumulative dose of doxorubicin (6 mg⁄kg) administered, compared to that for intravenous administration. Survival rate of the various treatment groups was analyzed using Kaplan Meier survival curve (Figure 3.29).

146
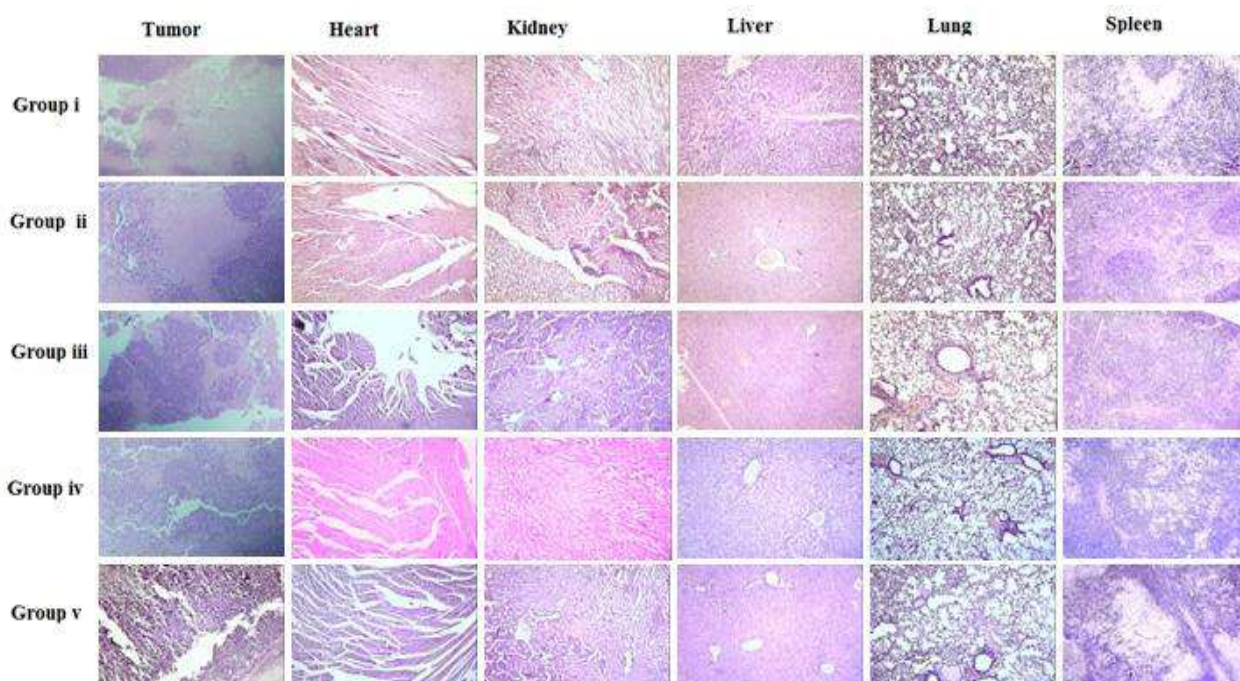
Figure 3.28. Histopathological evaluation of vital organs and tumors of mice in tumor regression study.
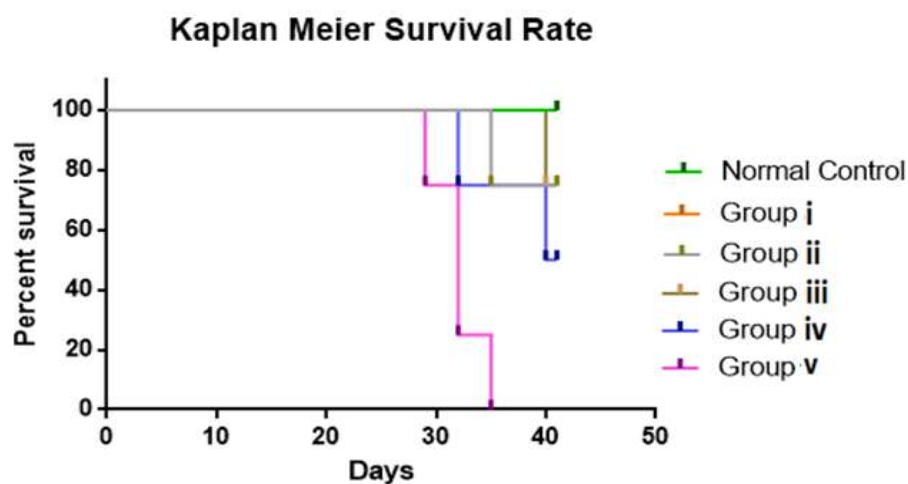
Figure 3.29. Survival curve of the different groups of mice used in tumor regression study

Combination of chemotherapy with siRNA based therapy is emerging as a promising strategy for efficient cancer treatment, with reduced side effects. Developing an ideal carrier system which can improve efficiency of the active agents and has the feasibility to be manufactured in large

scale is the biggest challenge. In this context, the designed poly (styrene-alt-maleic anhydride) based cationic micelles possess enormous potential to be employed for *in vivo* applications. Lyophilized polymeric micelles were able to be dispersed in phosphate buffer saline (pH 7.4) by bath sonication, even at very high concentration of 5 mg∕mL. No salt induced aggregation was observed after storing them for few days at room temperature. There is no need of tedious formulation procedures for preparing the micelles as they readily self assemble in aqueous environment. All these features guarantee their utility as an efficient delivery system in pharmaceutical applications.

3.4. Conclusions

- A promising nanosystem was successfully designed for the co- delivery of anti cancer drugs and siRNAs.

- In aqueous media, the amphiphilic polymer self assembles in to micellar structures which incorporates the hydrophobic anti cancer drug in to its core and effectively condense the siRNA to its charged hydrophilic layer.

- Short glycol chains used for grafting the polymer has rendered good stability for the obtained polymeric micelles in physiological media, and depicts its potential to be used as an alternative to long chain PEGs for imparting stealth nature.

- The nanocarriers were able to down regulate PLK-1 gene expression in cancer cells and synergistically arrest the tumor growth after co- delivery of drug and siRNA, *in vitro* and *in vivo*.

- The results reveal great potential of the designed polymeric system as an effective carrier for achieving combinatorial chemotherapeutic and siRNA delivery in tumor therapy.

References

1. Fessi, H.; Puisieux, F.; Devissaguet, J. P.; Ammoury, N.; Benita, S., Nanocapsule formation by interfacial polymer deposition following solvent displacement. *Int. J. Pharm.* **1989,** 55, (1), R1-R4.

2. Mohamed, M.S.; Veeranarayanan, S.; Minegishi, H.; Sakamoto, Y.; Shimane, Y.; Nagaoka, Y., et al., Cytological and Subcellular Response of Cells Exposed to the Type-1 RIP Curcin and its Hemocompatibility Analysis. *Sci Rep* **2014,** 4, 1-13.

3. Andrew, C.L.; Klemm, A.R.; Lloyd, J.B., Lysosome membrane permeability to amines. *Biochim Biophys Acta - Biomembr* **1997,** 1330, 71–82.

4. Pijper, D.; Bulten, E.; Šmisterová, J.; Wagenaar, A.; Hoekstra, D.; Engberts, J.B.F.N., et al., Novel Biodegradable Pyridinium Amphiphiles for Gene Delivery. *European J Org Chem* **2003,** 2003, 4406–4412.

5. Castro, V.; Rodríguez, H.; Albericio, F., CuAAC: An Efficient Click Chemistry Reaction on Solid Phase. *ACS Comb Sci* **2016,** 18, 1–14.

6. Li, H.; Aneja, R.; Chaiken, I., Click chemistry in peptide-based drug design. *Molecules* **2013,** 18, 9797–9817.

7. Gao, Y.; Chen, L.; Zhang, Z.; Gu, W.; Li, Y., Linear cationic click polymer for gene delivery: Synthesis, biocompatibility, and in Vitro Transfection. *Biomacromolecules* **2010,** 11, 3102–3111.

8. Le Droumaguet, B.; Velonia, K., Click chemistry: A powerful tool to create polymer-based macromolecular chimeras. *Macromol Rapid Commun* **2008,** 29, 1073–1089.

9. Crownover, E.; Duvall, C.L.; Convertine, A.; Hoffman, A.S.; Stayton, P.S., RAFT-synthesized graft copolymers that enhance pH dependent membrane destabilization and

protein circulation times. *J. Control. Release* **2012,** 155, 167–174.

10. Tang, C.; Edelstein, J.N.; Mikitsh, J.L.; Xiao, E.; Hemphill, A.H.; Pagels, R.F., et al., Biodistribution and fate of core-labeled ^{125} I-polymeric nanocarriers prepared by Flash NanoPrecipitation (FNP). *J Mater Chem B* **2016,** 4, 2428–2434.

11. Li, S-D.; Huang, L., Nanoparticles Evading The Reticuloendothelial System: Role of The Supported Bilayer. *Biochim Biophys Acta* **2009,** 1788, 2259–66.

12. Wu, H.; Zhu, L.; Torchilin, V.P., pH-sensitive poly (histidine)-PEG/DSPE-PEG co-polymer micelles for cytosolic drug delivery. *Biomaterials* **2013,** 34, 1213-1222.

13. Lale, S.V.; Kumar, A.; Prasad, S.; Bharti, A.C.; Koul, V., Folic acid and trastuzumab functionalized redox responsive polymersomes for intracellular doxorubicin delivery in breast cancer. *Biomacromolecules* **2015,** 16, 1736–1752.

14. Poon, Z.; Engler, A.C.; Daniel, K.; Hammond, P.T.; Stability, E.; Link, C., Enhanced stability of polymeric micelles based on post - functionalized poly (ethylene glycol)-b- poly (γ-propargyl ʟ- glutamate): the substituent effect *Biomacromolecules* **2013,** 13, 1315–1322.

15. Sezgin, Z.; Yüksel, N.; Baykara, T., Preparation and characterization of polymeric micelles for solubilization of poorly soluble anticancer drugs. *Eur J Pharm Biopharm* **2006,** 64, 261–268.

16. Lee, S.C.; Huh, K.M.; Lee, J.; Cho, Y.W.; Galinsky, R.E.; Park, K., Hydrotropic polymeric micelles for enhanced paclitaxel solubility : in vitro and in vivo characterization. *Biomacromolecules* **2008,** 8, 202–208.

17. Nogueira, E.; Loureiro, A.; Nogueira, P.; Freitas, J.; Almeida, C.R.; Harmark, J., et al., Liposome and protein based stealth nanoparticles. *Faraday Discuss* **2013,** 166, 417–429.

18. Li, S-D.; Huang, L., Stealth nanoparticles: High Density but Sheddable PEGeg is a Key for Tumor Targeting. *Journalf Con* **2011,** 145, 178–181.

19. Schöttler, S.; Becker, G.; Winzen, S.; Steinbach, T.; Mohr, K.; Landfester, K., et al., Protein adsorption is required for stealth effect of poly(ethylene glycol)- and poly(phosphoester)-coated nanocarriers. *Nat Nanotechnol* **2016,** 11, 202–208.

20. Dobrovolskaia, M.A.; Clogston, J.D.; Neun, B.W.; Hall, J.B.; Anil, K.; Mcneil, S.E., Method for analaysis of nanoparticle hemolytic properties in vitro. *Nano Lett.* **2009,** 8, 2180–2187.

21. Scott, M. H.; El-Sayed, M.E.H.; Pirie, C.M.; Hoffman, A.S.; Stayton P.S., pH-Responsive Poly(styrene-alt-maleic anhydride) Alkylamide Copolymers for Intracellular Drug Delivery. *Biomacromolecules* **2006,** 7, 2407–2414.

22. Khatri, M.; Bello, D.; Pal, A.K.; Cohen, J.M.; Woskie, S.; Gassert, T., et al., Evaluation of cytotoxic , genotoxic and inflammatory responses of nanoparticles from photocopiers in three human cell lines. *Part Fibre Toxicol* **2013,** 10, 1-22.

23. Hamzeh, M.; Sunahara, G.I., In vitro cytotoxicity and genotoxicity studies of titanium dioxide (TiO2) nanoparticles in Chinese hamster lung fibroblast cells. *Toxicol Vitr* **2013,** 27, 864–873.

24. Karajanagi, S.S.; Vertegel, A.; Kane, R.S.; Dordick, J.S., Structure and Function of Enzymes Adsorbed\rSingle-Walled Carbon Nanotubes. *Langmuir* **2004,** 20, 11594–11599.

25. Casalas, E.; Pfaller, T.; Duschl, A.; Oostingh, G.J.; Puntus, V., Time Evolution of the Nanoparticle Protein Corona. *ACS Nano* **2010,** 4, 3623–3632.

26. Koshkina, O.; Lang, T.; Thiermann, R.; Docter, D.; Stauber, R.H.; Secker, C., et al., Temperature-Triggered Protein Adsorption on Polymer-Coated Nanoparticles in Serum. *Langmuir* **2015,** 31, 8873–8881.

27. Aguilar-Castillo, B.A.; Santos, J.L.; Luo, H.; Aguirre-Chagala, Y.E.; Palacios-Hernández, T.; Herrera-Alonso, M., Nanoparticle stability in biologically relevant media: influence of polymer architecture. *Soft Matter* **2015,** 11, 7296–7307.

28. Burke, S.E.; Barrett, C.J., pH-responsive properties of multilayered poly(L-lysine)/hyaluronic acid surfaces. *Biomacromolecules* **2003,** 4, 1773–1783.

29. Gatzeva-topalova, P.Z.; Warner, L.R.; Pardi, A.; Carlos, M., Structure and flexibility of the complete periplasmic domain of BamA: the protein insertion machine of the outer membrane. *Structure* **2011,** 18, 1492–1501.

30. Dou, S.; Yang, X.Z.; Xiong, M.H.; Sun, C.Y.; Yao, Y.D.; Zhu, Y.H., et al., ScFv-decorated PEG-PLA-based nanoparticles for enhanced siRNA delivery to Her2+ breast cancer. *Adv Healthc Mater* **2014,** 3, 1792–1803.

31. Spänkuch-Schmitt, B.; Bereiter-Hahn, J.; Kaufmann, M.; Strebhardt, K., Effect of RNA silencing of polo-like kinase-1 (PLK1) on apoptosis and spindle formation in human cancer cells. *J Natl Cancer Inst* **2002,** 94, 1863–1877.

32. Mccarroll, J.A.; Dwarte, T.; Baigude, H.; Dang, J.; Yang, L.; Erlich, R.B., et al., Therapeutic targeting of polo-like kinase 1 using RNA-interfering nanoparticles (iNOPs) for the treatment of non-small cell lung cancer. *Oncotarget* **2015,** 6, 12020–12034.

33. Knudsen, K.B.; Northeved, H.; Ek, P.K.; Permin, A.; Gjetting, T.; Andresen, T.L., et al., In vivo toxicity of cationic micelles and liposomes. *Nanomedicine: NBM* **2015,** 11, 467–477.

CHAPTER IV

Development of stimuli sensitive polymeric micelles based on poly (styrene-alt-maleic anhydride) for combinatorial delivery of doxorubicin and PLK-1 siRNA

CHAPTER IV

Development of stimuli sensitive polymeric micelles based on poly (styrene-alt-maleic anhydride) for combinatorial delivery of doxorubicin and PLK-1 siRNA

4.1. Introduction

The chapter describes development of dual stimuli responsive graft co-polymer of poly (styrene-alt-maleic anhydride) for combinatorial delivery of drug and siRNA. The co-polymer was designed by grafting methoxy polyethyleneglycol (methoxy PEG) to PSMA backbone and derivatizing the free carboxylic acid groups with amino acids via disulfide linkages. Arginine and histidine were selected as cationic structures due to their nucleic acid binding efficiency and endosomal penetration property. Nanocarriers of the graft co-polymer were formulated and assessed for their bio compatibility, *in vitro* and *in vivo*. Stability of the nanocarriers in salt containing media was improved by mixing them with bovine serum albumin (BSA). This nanosystem represent an improvement over the one described in chapter III, in terms of its ability to release the loaded active ingredient more specifically to the tumor microenvironment. The dual responsive nanosystem can facilitate release of the loaded active agents in response to higher glutathione concentration and acidic pH. Stable drug loaded nanoplexes, for clinical administration, could be easily formulated by gently dispersing them in physiological saline containing appropriate amount of albumin. Efficiency of the nanocarriers in co-delivering drug and nucleic acid was evaluated by employing doxorubicin and PLK-1 siRNA as model drug and nucleic acid, respectively. *In vitro* evaluation of the formulations was performed using MCF 7 and L929 cells and *in vivo* anticancer efficacy of the polyplexes was studied in Ehrlich ascites tumor (EAT) bearing Swiss albino mice.

4.2. Experimental

4.2.1. Materials

Poly (styrene-alt-maleic anhydride) (M_w, 5500 Da) was purchased from Sartomer Company Inc (Quarry bay, Hong Kong). Methoxy PEG (M_n, 350), cystamine dihydrochloride salt, Fmoc-Arg-pbf-OH, Fmoc-His (Trt)-OH, Di-tert-butyl dicarbonate, bovine serum albumin (molecular weight 66 kDa), HBTU and diisopropylethylamine (DIPEA) were purchased from Sigma-Aldrich (Bangalore, India). Trifluoroacetic acid, triisopropylsilane, piperidine and triethyl amine (NEt_3) were purchased from Merck millipore (India). Doxorubicin hydrochloride was obtained as a gift sample from Ranbaxy laboratories ltd. India. Primer sequences of PLK-1 and GAPDH genes were purchased from Sigma-Aldrich (Bangalore, India). Anti- PLK-1 (phospho S137) primary antibody and DyLight 488 Goat anti-Rabbit IgG secondary antibody were purchased from abcam. Dulbeccos modified eagles media (DMEM), penicillin/streptomycin solution, Trypsin-EDTA, fetal bovine serum (FBS) and agarose powder were purchased from Himedia (India). silencer@select PLK-1 siRNA (validated), negative control siRNA and fluorescent (FAM) labeled negative control siRNA were obtained from Thermoscientific (USA). Comet assay kit was purchased from Trevigen. All other solvents and reagents employed for the experiments were of analytical grade. RNase free water was used for all the studies involving siRNA.

4.2.2. Synthesis of amphiphilic graft copolymer of PSMA

4.2.2.1. Grafting of PSMA with methoxy PEG

Methoxy PEG was conjugated to PSMA backbone through alkaline hydrolysis. Briefly, methoxy PEG (2.5 g, 7.14 mM) and NEt_3 (1.33 g, 13.3 mM) were dissolved in dichloromethane (35 mL). The reaction mixture was kept under continuous stirring, at room temperature, followed by slow

addition of PSMA (1 g, ~ 4.85 mM of monomer units). The reaction was allowed to continue overnight and solvent was evaporated using rotary flash evaporator. Purified polymer was then obtained by repeatedly precipitating the concentrated reaction mixture in diethyl ether.

4.2.2.2. Coupling of amino acids using cystamine as linker

Mono-N-Boc protected cystamine was synthesized as described in the following section. Cystamine dihydrochloride (6 g, 26.63 mM) was dissolved in methanol (225 mL), under continuous stirring (1200 rpm), followed by addition of triethyl amine (6.75 g, 67.5 mM). Di-tert-butyl dicarbonate (1.15 g, 5.26 mM) was dissolved in dichloromethane (25 mL) and the mixture was added drop wise to the reaction vessel, under continuous stirring (1200 rpm). The reaction was allowed to proceed overnight, at room temperature. The reaction mixture was then concentrated by evaporating the solvents, using rotary flash evaporator (IKA 50, Germany). The residue was dispersed in saturated sodium bicarbonate solution (50 mL) and extracted thrice with dichloromethane (150 mL). The combined organic layers were dried over anhydrous sodium sulphate, filtered and concentrated under vacuum, using rotary flash evaporator, to obtain mono N- Boc protected cystamine.

Mono-N-Boc protected cystamine was then coupled to the free carboxylic acid groups of methoxy PEG grafted PSMA. Briefly, polymeric graft (1 g, ~ 1.8 mM of monomer units) was dissolved in 25 mL dimethylformamide (DMF) followed by addition of HBTU (1.35 g, 3.57 mM). The mixture was stirred for 25 minutes, in ice bath, followed by successive addition of mono-N-Boc protected cystamine (1 g, 3.9 mM) and DIPEA (1 g, 7.75 mM). Reaction was continued for overnight, at room temperature. DMF was evaporated using rotary flash evaporator and the concentrated reaction mixture was repeatedly precipitated in diethylether to obtain the cystamine grafted polymer. The obtained polymer was treated with DCM: trifluoroacetic acid

mixture (1:1 v/v), for 3 hours, to remove Boc groups. The reaction mixture was then concentrated, by evaporating the solvents, and repeatedly precipitated using diethyl ether to obtain pure polymeric derivative.

Conjugation of arginine and histidine to the polymer was achieved by successive HBTU coupling reactions. Briefly, Fmoc-Arg-pbf-OH (1.8 g, 2.78 mM) and HBTU (1.6 g, 4.2 mM) were dissolved in dry DMF. The mixture was stirred under ice bath for 25 minutes, followed by addition of cystamine grafted polymer (1 g, ~ 1.4 mM of monomer units) and DIPEA (1 g, 7.75 mM), in succession. The reaction was continued for overnight. Reaction mixture was then concentrated by evaporating the solvent and precipitated using ethylacetate, repeatedly, to obtain purified polymer. Fmoc groups of the grafted arginine were removed by treating the polymeric derivative with DMF: piperidine mixture (1:1 v/v) for 3 hours, at room temperature. Polymer was then precipitated repeatedly using ethylacetate and dried.

Fmoc-His (Trt)-OH was conjugated to the free amino groups of arginine grafted polymer by HBTU coupling. Briefly, Fmoc-His(Trt)-OH (0.85 g, 1.37 mM) was treated with HBTU (0.8 g, 2.1 mM) in dry DMF, under ice bath, for 20 minutes. Arginine grafted polymer (0.75 g, ~ 0.66 mM of monomer units) and DIPEA (0.55 g, 4.25 mM) were added in succession to the reaction mixture and the reaction was allowed to continue for overnight, at room temperature. The reaction mixture was then concentrated and repeatedly precipitated with eythylacetate to obtain the pure polymer. The obtained polymer was then treated with DMF: piperidine mixture (1:1 v/v) for 3 hours, at room temperature, to remove Fmoc groups. The polymeric derivative was then purified by successive precipitation using ethylacetate. Removal of Trt and pbf protecting groups was done by treating the polymeric system with TFA: triisopropylsilane: water (95:2.5:2.5 v/v/v), for 3 hours. The reaction mixture was then concentrated using rotary flash

evaporator and precipitated in ethyl acetate, successively, to obtain the purified polymer.

Reaction Scheme
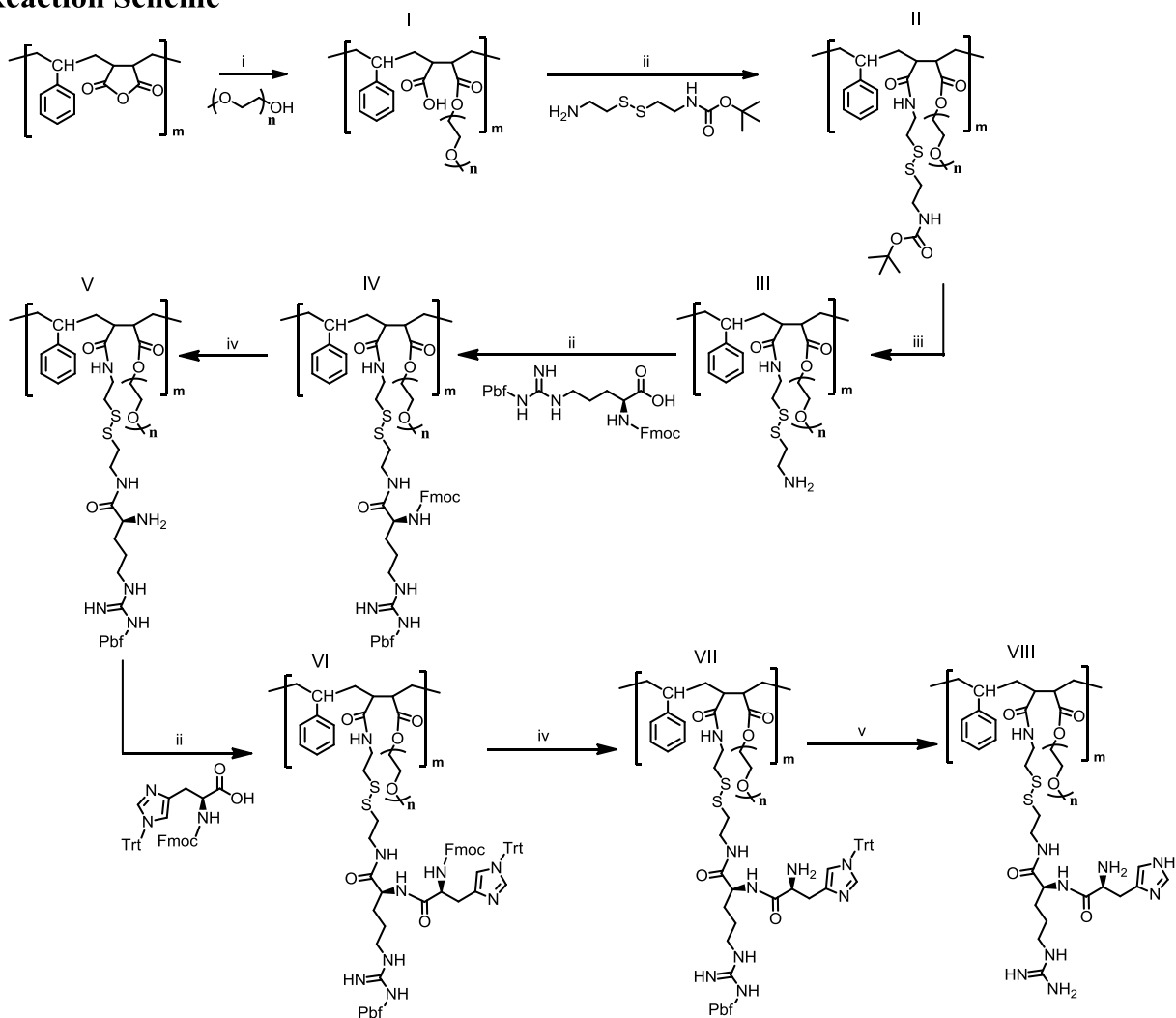
Figure 4.1. Synthesis scheme for the cationic polymer. (i) NEt$_3$, RT, 12 h (dry CH$_2$Cl$_2$) (ii) HBTU, DIPEA, 0 ºC - RT, 12 h (dry DMF) (iii) TFA: CH$_2$Cl$_2$ (1:1 v/v), RT, 3 h (iv) DMF: Piperidine (1:1 v/v), RT, 3 h (v) TFA: triisopropylsilane: water (95:2.5: 2.5 v/v/v), RT, 3 h

All the compounds and polymeric derivatives prepared during the synthesis process were characterized using ^{1}H NMR. Average molecular weight of the polymeric derivative was determined using gel permeation chromatography. Fmoc-Arg-pbf-OH grafted polymer

(Compound IV, Figure 4.1) was dissolved in dimethylformamide (HPLC grade) at a concentration of 5 mg∕mL, filtered using 0.4 μ syringe filter and used for molecular weight determination. Final polymeric derivative (Compound VIII, Figure 4.1), grafted with short polyethylene glycols and cystamine-arginine-histidine conjugate, was characterized using ATR-FTIR.

4.2.3. Formulation and evaluation of polymeric micelles

Nanoprecipitation method was used to prepare the polymeric micelles [1]. Solution of the polymer in DMSO was mixed with water (milliQ), under continuous stirring (800 rpm), for 15 minutes. DMSO: water ratio and polymer concentration were kept at 1:10 v/v and 250 μg/mL, respectively. The dispersion was then subjected to probe sonication, at 100 W, for 30 seconds. The obtained nanoparticulate dispersion was filtered using Amicon ultra centrifugal filter units (10 kDa molecular weight cut-off), and the residue was redispersed in milliQ water. The dispersion was filtered through 0.2 μ syringe filter, and particle size and zeta potential were determined using dynamic light scattering (DLS). The micelles were characterized morphologically using transmission electron microscopy (TEM), field emission scanning electron microscopy (FESEM) and atomic force microscopy (AFM).

Critical micellar concentration (CMC) of the polymeric micelles was determined using fluorometry, employing pyrene as the fluorescent probe [2]. Aliquots of pyrene stock solution in ethanol (50 μL) were mixed with aqueous dispersions of polymeric micelles (2.95 mL).Concentration of pyrene in all the dispersions were kept constant at 6.5×10^{-7} M. Concentrations of polymeric micelles in the dispersions ranged from 0.5-150 μg/mL. Pyrene was excited at 334 nm and emission spectra of the dispersions were recorded from 339-400 nm, using a F-2000 fluorescence spectrophotometer (Hitachi, Japan). CMC of the micelles was determined

by plotting intensity ratios of the third and first highest energy bands in the emission spectra against corresponding concentrations of micelles.

The primary amine content of Arginine-histidine grafted polymer was determined using TNBS assay. Briefly, polymeric micelles were dispersed in demonized water (400 µL) and mixed with 400 µL of sodium hydrogen carbonate solution (4 %). 400 µL of aqueous TNBS solution (0.1 %) was introduced to the mixture and incubated at 37 °C and 1200 rpm, for 2 h. Final concentration of micelles in the dispersions (in triplicate) was 100 µg/mL. Gamma amino butyric acid was used for making standard calibration curve. Known concentrations of the amino acid were treated with TNBS in the same manner as that of the micelles and absorbances of resulting mixtures were measured at 349 nm using micro plate spectrophotometer (Power Wave XS2, Bio Tek Instruments, USA). Experiments were performed in triplicate.

4.2.3.1. Evaluation of the biocompatibility of polymeric micelles *in vitro*

Polymeric micelles were evaluated for their cytocompatability, in MCF 7 and L929 cells, using MTT assay. Briefly, cells were dispersed in Dulbeccos Modified Eagles Media (DMEM) supplemented with 10 % fetal bovine serum (FBS), and seeded in 96 well plates at a density of 5×10^3 cells∕well. After incubation at 37 ºC and 5 % CO_2, for 24 h, cell culture media were replaced with fresh media containing polymeric micelles. Concentrations of micelles used ranged from 50-1000 µg∕mL. Cells were treated with micelles for 48 h, at 37 ºC and 5 % CO_2, and the media were replaced with fresh media (200 µL). 10 µL of MTT solution (5 mg∕mL) was added to each well and incubated for 3 h, at 37 ºC. Formazan crystals formed were dissolved in DMSO (200 µL) and the absorbances of wells were recorded at 540 nm, using microplate spectrophotometer (PowerWave XS2, Bio Tek Instruments, USA).

Genotoxicity of the micelles was evaluated, in MCF 7 and L929 cells, using comet assay reagent kit (Trevigen). The cells were dispersed in DMEM supplemented with 10 % FBS, and seeded in T-25 culture flasks. The culture flasks were incubated with micelles (1 mg/ml), at 37 °C and 5 % CO_2, once ~ 70-80 % cell confluency was reached. After 48 h incubation, alkaline comet assay was performed according to manufacturer's protocol.

Ability of the micelles to induce reactive oxygen species (ROS) generation was assessed with DCFH-DA dye [3]. Briefly, MCF 7 and L929 cells, dispersed in DMEM supplemented with 10% FBS, were seeded in 96 well plate at a density of 5×10^3 cells ∕well and incubated for 24 h, at 37 °C and 5 % CO_2. Polymeric micelles (concentrations ranging from 50 to 1000 µg/mL) were added to the wells and incubated for 48 h, at 37 °C and 5 % CO_2. Wells with untreated cells were used as control. The culture media were then replaced with fresh media (100 µL) containing DCFH-DA dye, at a concentration of 10 mM, and incubated for 30 minutes. Fluorescence of the wells was recorded at 480 nm excitation using a microplate reader.

Stability of polymeric micelles in the presence of serum proteins was evaluated by dispersing them in DMEM media supplemented with 10 % FBS, at a final polymer concentration of 0.3 mg/mL, and determining the particle size. Particle size measurements were done at different time intervals, up to 24 hours, by storing the dispersion at 37 ° C.

4.2.4. Formulation and evaluation of drug loaded micelles

Doxorubicin loaded polymeric micelles were formulated by dissolving polymer, doxorubicin HCl and triethylamine (equal molar amount of Doxorubicin HCl) in DMSO and mixing it with the water phase (800 rpm for 15 minutes). The dispersion was then sonicated for 30 seconds, at 100 W, using probe sonicator. Optimized drug loaded formulation was selected using central circumscribed design (CCD). Polymer: drug weight ratios (w/w) and solvent (DMSO): non

solvent (water) ratios (v/v) were taken as the independent variables. Dependent variables chosen were average particle size of the drug loaded micelles, polydispersity index (PDI) and percentage

Table 4.1. Central circumscribed design (CCD) matrix

Experiment	Formulation code	Polymer:Drug ratio (coded)	Solvent: Non-solvent ratio (coded)	Polymer:Drug ratio (w∕w)	Solvent: Non-solvent ratio (v∕v)
1	F1	1	1	4.5	0.18
2	F2	-1	-1	2.5	0. 05
3	F3	-1.414	0	2. 09	0.11
4	F4	-1	1	2.5	0.18
5	F5	0	0	3.5	0.11
6	F6	0	0	3.5	0.11
7	F7	0	0	3.5	0.11
8	F8	0	-1.414	3.5	0. 03
9	F9	1	-1	4.5	0. 05
10	F10	1.414	0	4.91	0.11
11	F11	0	0	3.5	0.11
12	F12	0	0	3.5	0.11
13	F13	0	1.414	3.5	0.21

entrapment efficiency (% EE). CCD design matrix is provided in table 4.1. Sonication time (30 seconds) was kept constant for all the formulations. Entrapment efficiency of the formulations was determined using UV- Visible spectrophotometry (Perkin Elmer, Lambda 25, US). Briefly, the dispersions of drug loaded micelles were filtered using Amicon ultra centrifugal filter units with 10 kDa molecular weight cut-off. Absorbances of the filtrates were recorded at 481 nm, and

161

the respective concentrations were determined form standard calibration curve of free doxorubicin in the same dispersion media. Entrapment efficiency was calculated using the formula -

$$\% \, EE = \frac{(\text{Total amount of drug used for formulation} - \text{Amount of drug in the filtrate})}{(\text{Total amount of drug used for formulation})} * 100$$

Optimized drug loaded formulation (50 mg) was dialyzed against milliQ water (2.5 L), overnight, to remove free doxorubicin, DMSO and triethylamine. Water was changed once during the dialysis course. The nanoparticulate dispersion was then lyophilized (Labconco freezone plus, 2.5 L), and drug loading content was determined. Lyophilized drug loaded nanoparticles (5 mg) were dissolved in DMSO (2 mL) and absorbance was determined at 481 nm, using UV visible spectrophotometer. Standard calibration curve of doxorubicin in DMSO was prepared to determine the unknown concentration of drug.

4.2.5. Formulation and evaluation of siRNA-micelle complexes

Complexation of siRNA with the cationic micelles was achieved by electrostatic interaction. Equal volumes (100 µL) of micellar suspensions and siRNA solutions, in RNase free water, were mixed using gentle vortexing. The mixtures were kept at room temperature, for 30 minutes, to stabilize the complexes. Polyplexes of both drug loaded and blank micelles were formulated in the same manner. All the polyplexes were freshly prepared for *in vitro* and *in vivo* evaluations. Optimum weight ratios of polymeric micelles : siRNA, for stable complexation, were determined using horizontal gel electrophoresis. 1.2 % agarose gel was employed for the electrophoretic analysis. Polyplex suspensions were mixed with siRNA gel loading buffer at 1:5 v∕v ratio, respectively, and loaded in to the agarose gel wells. Electrophoresis was carried out at 70 V, for 20 minutes, using horizontal gel electrophoresis apparatus (BIO RAD). Visualization of siRNA

bands was performed by incubating the gel in SYBR green solution, for 1 h, and imaging using molecular imager (Gel Doc XR, BIO RAD). Optimized polyplex suspensions were stabilized with albumin by mixing them with varying concentrations of albumin solutions in aqueous media. Stability of complexed siRNA in the albumin coated formulations was assessed using horizontal gel electrophoresis, as explained before. Characterization of albumin coated polyplexes was performed using UV-Visible spectroscopy, DLS and horizontal gel electrophoresis.

The drug loaded polyplex formulations were evaluated for their *in vitro* release behavior at different pH values (5.5 and 7.4). Briefly, 100 mg of drug loaded polyplexes were sealed in dialysis bag (molecular weight cut off 12 kDa) and dialyzed against respective release media (100 mL). Phosphate buffer salines (pH 5.5 and 7.4) were used as release media, to evaluate release behavior at particular pH. To evaluate redox sensitivity of micelles, release behavior of drug loaded micelles in the presence of 10 mM glutathione reductase (GSH) was also studied. Cumulative amount of drug released at different time points was determined by recording absorbances of the release media, at 481 nm, using UV-Visible spectrophotometer. Volumes of release media withdrawn for measurements were replaced with equal volumes of fresh media. Unknown concentrations were calculated using standard calibration curves of doxorubicin in the respective release media.

The efficiency of polyplexes in knocking down PLK-1 mRNA was examined using real time PCR. MCF 7 and L929 cells were dispersed in DMEM supplemented with 10 % FBS, seeded in 6 well plates and incubated at 37 °C, under 5 % CO_2, till ~ 70-80 % cell confluency was attained. Control wells were left untreated and the test wells were treated with polyplexes bearing PLK-1 siRNA∕scrambled siRNA, at different siRNA concentrations (50, 100 and 125 nM). After 48 h

incubation, at 37 °C and 5 % CO_2, cells were harvested to isolate total RNA. RNA isolation was done using Trizol regent. Briefly, ~ 5 × 10^5 cells were dispersed in 500 µL of Trizol reagent for 5 minutes. 100 µL of chloroform was added to the dispersion and the resulting mixture was vortexed for 30 sec. Aqueous layers in the dispersions were separated, by centrifuging at 12500 rpm for 15 minutes, and mixed with 250 µL of isopropanol. The mixtures were incubated at – 20 ° C for 15-20 minutes, and centrifuged at 12500 rpm for 15 minutes. Supernatants were discarded and the settled pellets were given wash with 75 % ethanol. The washed pellets were allowed to dry and dissolved using RNase free water followed by incubating them at 65 ° C, for 15 minutes. The isolated RNAs were then treated with DNase (1 U) to remove any genomic DNA. Preparation of cDNA was performed using cDNA kit (Biorad). Briefly, isolated RNA solutions were mixed with appropriate ratios of 10x cDNA reaction buffer and reverse transcriptase enzyme as per the manufacturer's protocol. Final volumes of the mixtures were reconstituted with nuclease free water to adjust the cDNA reaction buffer concentration to 1x. Three PCR cycles were employed (65 ºC for 5 minutes, 42 ºC for 30 minutes and 70 ºC for 15 minutes) using PCR analyzer (Biorad). The prepared cDNA samples were stored at 4 ºC. cDNA samples were mixed with primers (forward and reverse) and qPCR master mix (QuantiNova SYBR Green PCR Kit). PLK-1 gene expression was normalized with that of housekeeping gene, GAPDH. Fold change in gene expression was determined using delta delta Ct (2 ΔΔ Ct) method. The primer sequences of PLK-1 and GAPDH used for the study were as follows.

PLK-1 forward: 5' – CCCATCTTCTGGGTCAGCAAG

PLK-1 reverse: 5' – AAGAGCACCCCCACGCTGTT

GAPDH forward: 5' – TGCACCACCAACTGCTTAGC

GAPDH reverse: 5' – GGCATGGACTGTGGTCATGAG

The knock down efficiency of polyplexes was studied at protein level using immunofluorescence analysis. Briefly, MCF 7 and L929 cells, dispersed in DMEM supplemented with 10 % FBS, were seeded on confocal dishes (Nunc^{TM} glass bottom dish) and incubated at 37 °C, under 5 % CO_2, till ~70-80 % cell confluency was observed. Cells were treated with polyplexes bearing PLK-1 siRNA or scrambled siRNA, at siRNA concentration of 125 nM, for 48 h. After incubation, cells were washed twice with cold PBS, pH 7.4. Cells were then fixed with 4 % (v∕v) formaldehyde solution (in PBS, pH 7.4) for 20 minutes, in dark, at room temperature. Fixed cells were then washed twice with PBS, pH 7.4 and treated with PBS, pH 7.4 containing 1% BSA ∕10 % normal goat serum∕0.3 M glycine∕0.1 % Tween (v∕v), for 1 h, to permeabilise the cells and block non specific protein-protein interactions. The cells were then washed with PBS, pH 7.4, two times, and treated with anti PLK-1 (phospho S137) antibody (5 µg∕mL), overnight, at 4 ºC. Cells were again washed twice with PBS, pH 7.4 and treated with DyLight 488 Goat anti-Rabbit IgG (green fluorescent secondary antibody) for 1 h (at 1∕200 dilution). Actin filaments and nucleus were stained using Alexa Flour 594-phalloidin and DAPI, respectively. Images were recorded using confocal laser scanning microscope (Olympus Fluoview FV1000). Untreated cells incubated with DyLight 488 Goat anti-Rabbit IgG alone (at 1∕200 dilution) was visualized to optimize the settings of confocal laser scanning microscope, so that any green fluorescence caused by interaction of the secondary antibody with cells could be nullified. The optimized settings for imaging were kept constant throughout the analysis. Fluorescence of the images of immunostained cells was quantified using ImageJ software.

4.2.6. **Cellular uptake studies**

Cellular uptake of doxorubicin and siRNA loaded micelles was evaluated using confocal laser scanning microscopy (CLSM). Briefly, MCF 7 and L929 cells were seeded on confocal dishes

(Nunc^{TM} glass bottom dish) and incubated at 37°C, under 5 % CO_2. DMEM supplemented with 10 % fetal bovine serum was used as the culture media. When the cells attained ~ 70-80 % confluency, they were treated with polymeric micelles loaded with doxorubicin (5 µg/mL) and FAM-labeled siRNA (100 nM). Following incubation for 3 h, cells were washed thrice with PBS. Fluorescence of the drug and FAM-labeled siRNA were visualized, at respective wavelengths of 561 nm and 488 nm, using confocal laser scanning microscope (Olympus IX 81 under DU897 mode).

4.2.7. Cell proliferation assay and apoptosis

Cytotoxicity was evaluated by MTT assay as described in 4.2.3.1. Concentration of siRNAs (either PLK-1 or scrambled) in the nanoplexes were kept constant at 125 nM. Doxorubicin concentrations were varied from 0.25-10 µg/mL. Apoptotic effect of the formulations was assessed using Annexin V-FITC-propidium iodide staining. Briefly, MCF 7 and L929 cells dispersed in DMEM supplemented with 10 % FBS, were seeded in 6 well plates and incubated at 37 °C, under 5 % CO_2, till ~70-80 % cell confluency was attained. Cells were then treated with drug (2.5 µg/mL) loaded nanoplexes bearing PLK-1 or scrambled siRNA (125 nM), for 24 h, and stained with AnnexinV-FITC and propidium iodide (invitrogen) as per the manufacturers' protocol. Stained cells were analyzed using flow cytometry (BD Accuri). 10000 events were measured for each sample.

4.2.8. *In vivo* studies

In vivo studies were conducted at Central Animal Facility, AIIMS, New Delhi, India. All the experiments were performed according to the Animal Ethical Committee (796∕ IAEC ∕ 14) guidelines of AIIMS. 8 week old female Swiss albino mice (23 ± 4.5 g) were employed for the studies. The Animals were housed in polycarbonate cages, at 25 º C, throughout the experiment.

12 h light⁄dark cycle was maintained uninterrupted and consistently. Animals were supplied with chow food and sterile water *ad libitum*. *In vivo* toxicological evaluation of the polymeric micelles was performed as follows. Mice were randomly grouped in to two groups (n = 4). Control group was administered with PBS, pH 7.4 (0.3 mL) and test group was treated with micelle : albumin mixture (respective weight ratio of 1:6), on days 1, 4 and 7, at a micelle dose of 100 mg⁄kg. The formulations were administered intraperitoneally. Blood samples of the animals were collected from their retro orbital vein and evaluated for serum biochemical and hematological parameters, 24 h post last dose. Animals were sacrificed by cervical dislocation and their vital organs were collected in 4 % formalin. Histopathological analysis of the organs was performed using Haematoxylin-Eosin (H & E) staining.

Anti cancer efficacy was evaluated using Ehrlich ascites tumor (EAT) model. EAT cells were obtained from INMAS, New Delhi, India. Female Swiss albino mice (23 ± 4.5g average body weight) were employed for the study. 150 µL of EAT cell suspension (containing ~ 2×10^7 cells) was administered to the mice, subcutaneously, on the dorsal side. Tumor volumes were measured twice in a week, using Vernier caliper, and calculated using the formula $\pi⁄6$ (length) (width) (height). Longest diameter across the tumor was considered as the length. Treatment was initiated once the average tumor volume reached ~250 mm^3. Animals bearing solid tumors were then divided in to five groups (5 animals each). Group I, II, III, IV and V were respectively treated with doxorubicin and PLK-1 siRNA carrying nanoplexes, doxorubicin and scrambled siRNA loaded nanoplexes, free Doxorubicin, PLK-1 siRNA complexed nanoplexes and control vehicle (PBS, pH 7.4). All the formulations were dispersed in PBS, pH 7.4 and administered intratumorally. Briefly, 50 µL of the suspensions (in PBS) were injected slowly, over 1 minute, in the longitudinal direction (from the edge to centre) of solid tumors. Post injection, the needle

was kept intact at the injection site for further 5 minutes to avoid any sample leakage. Five intratumoral injections were given to the animals, twice weekly. Dose of Doxorubicin and siRNA in the formulations were 1.2 mg∕kg and 0.5 mg∕kg, respectively. Animals were sacrificed by cervical dislocation, at the end point of study, and their blood, tumors and vital organs were collected. Histopathology of the tumors and vital organs was evaluated. Serum biochemical analysis of the collected blood samples was also performed.

4.3. Results and Discussion

4.3.1. Synthesis and characterization of cationic graft co-polymer

Anhydride units of PSMA were ring opened using methoxy PEG to obtain product I (Figure 4.1). Grafting of mPEG units to PSMA was confirmed by ^{1}H NMR of the polymeric graft (I) depicting characteristic aromatic peaks of styrene units ranging from δ 7- 7.3 ppm, methylene
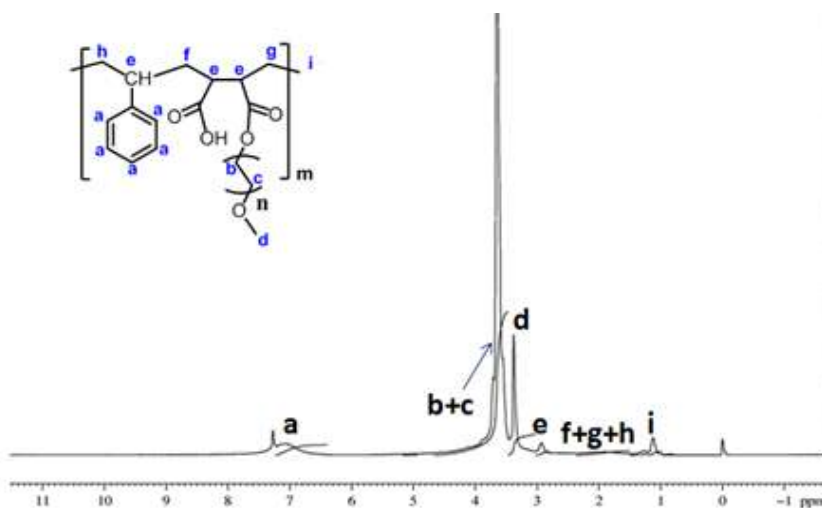
Figure 4.2. ^{1}H NMR spectrum (300 MHz, CDCl$_3$) of methoxypolyethyleneglycol grafted PSMA: δ 1.128 (brm, -C$\underline{H}_3$), 1.258-2.19 (br, aliphatic C$\underline{H}_2$), 2.8 (brm, aliphatic C$\underline{H}$), 3.378 (brm, -O-C$\underline{H}_3$), 3.55-4 (brm, aliphatic C$\underline{H}_2$), 7.274 (brm, Ar C$\underline{H}$)

groups of mPEG from δ 3.55-3.9 ppm and terminal methyl group of mPEG at δ 3.378 ppm (Figure 4.2). Conjugation of mPEG units to PSMA backbone can provide stealth nature to the

polymer, which can render long circulation time for the polymeric carrier *in vivo*. We have

employed short PEG (~ Mn 350) for grafting based on the facts that, short PEG chains are easily
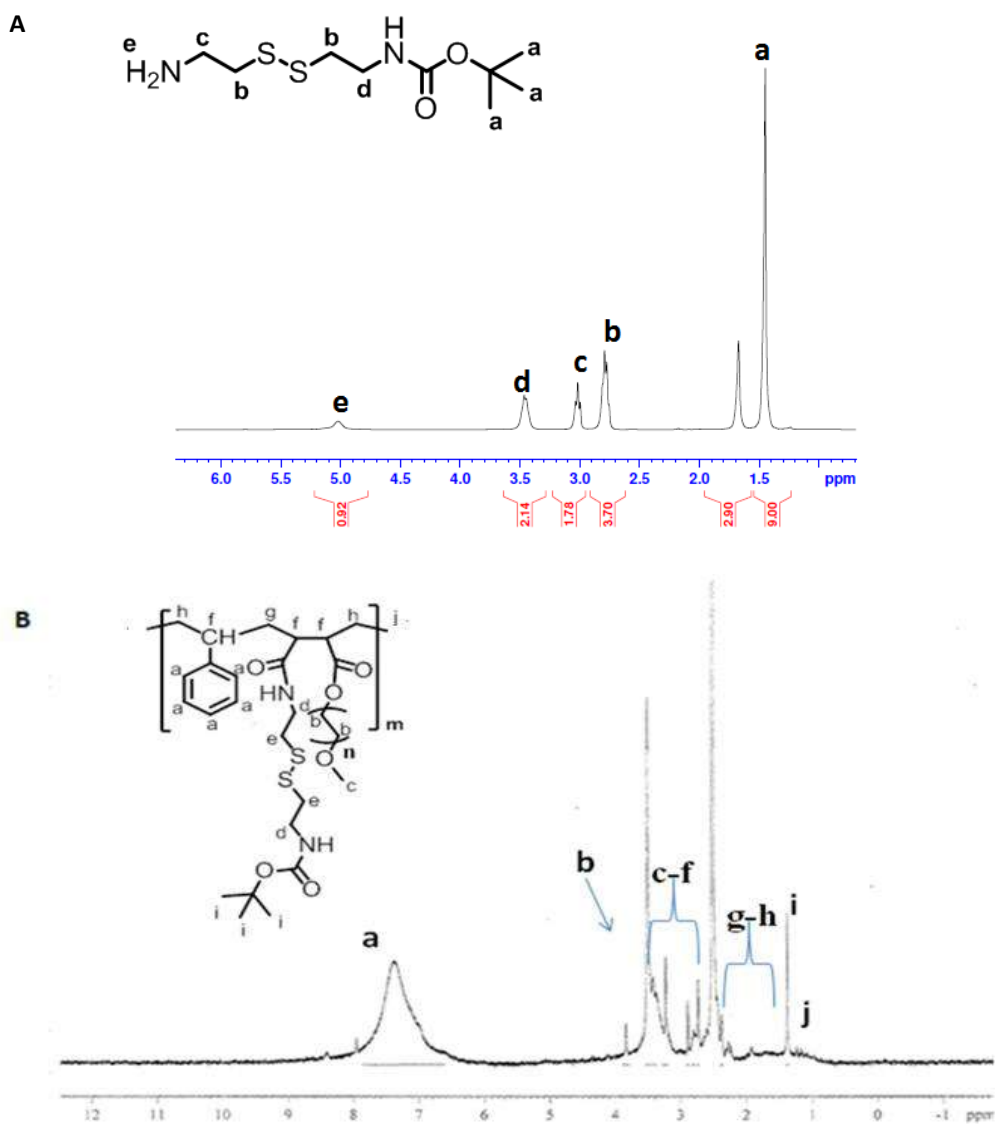
Figure 4.3. (A) ^{1}H NMR spectrum (300 MHz, CDCl$_3$) of mono-Boc cystamine : δ 1.448 (s, 9H, Boc C$\underline{H}_3$), 2.755-2.792 (m, 4H, S-C$\underline{H}_2$), 3 (m, 2H, NH-C$\underline{H}_2$), 3.44 (m, 2H, NH$_2$- C$\underline{H}_2$), 5 (brs, 1H, CON$\underline{H}$), (B) ^{1}H NMR spectrum (300 MHz, DMSO-d_6) of Boc-cystamine grafted polymer: δ 1.178 (br s, cumene C$\underline{H}_3$) 1.38 (br s, Boc C$\underline{H}_3$), 1.7-2.45 (br m, CH-C$\underline{H}_2$), 2.6-2.81 (br m, S-C$\underline{H}_2$-C$\underline{H}_2$), 2.86-3 (br m, C$\underline{H}$), 3.236 (br s, O-C$\underline{H}_3$), 3.43-3.72 (br m, O-C$\underline{H}_2$-C$\underline{H}_2$), 3.839-4 (br m, C$\underline{H}_2$), 6.8-7.65 (br m, Ar C$\underline{H}$)

excreted from the body and are less likely to evoke any immune response. The free carboxylic acid functionalities of mPEG grafted PSMA were derivatized with disulfide containing cystamine units. Mono-N-Boc protected cystamine grafted polymer (II) was characterized by sharp peak corresponding to the methyl groups of Boc at δ 1.380 ppm and methylene peaks of cystamine at δ 2.73 and 3.15 ppm (Figure 4.3.B). Deprotection of primary amine groups of grafted cystamine was confirmed by the absence of Boc peak in the ^{1}H NMR of the polymeric derivative (III) (Figure 4.4). Repeating disulfide linkages of the polymer can constitute hydrophobic core of the polymeric graft which in turn shall facilitate redox responsive release of the entrapped drug molecules.
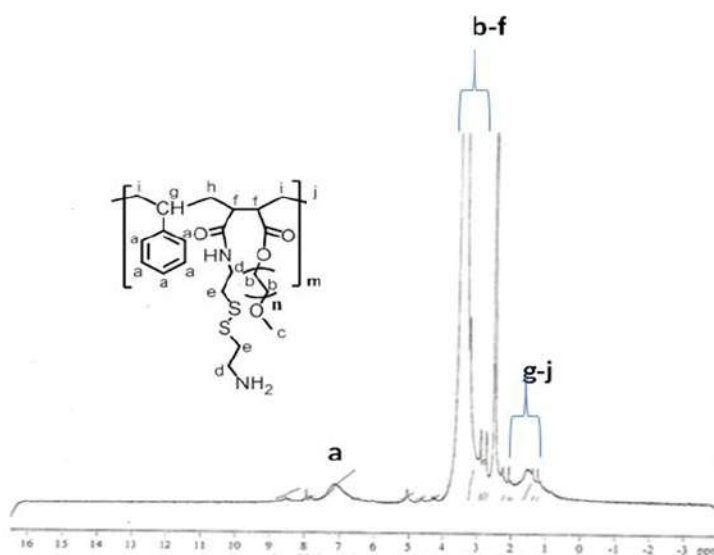
Figure 4.4. ^{1}H NMR spectrum (300 MHz, DMSO-d_6) of cystamine grafted polymer: δ 1.235 (br s, cumene C$\underline{H}_3$), 1.41-2.07 (br m, CH-C$\underline{H}_2$), 2.7-2.89 (br m, S-C$\underline{H}_2$-CH_2 + C$\underline{H}$), 3.235 (br s, O-C$\underline{H}_3$), 3.43-3.8 (br m, O-C$\underline{H}_2$-CH_2), 4-4.2 (br m, C$\underline{H}_2$), 6.8-7.4 (br m, Ar C$\underline{H}$)

Final steps of polymer synthesis included successive coupling of amino acid units for efficient siRNA complexation. Free amino groups of cystamine grafted polymer (III) were conjugated to carboxylic groups of Fmoc-Arg-pbf-OH. Conjugation of Fmoc-Arg-pbf-OH was confirmed by the presence of characteristic peaks of Fmoc ranging from δ 7.3 - 7.884 ppm (Figure 4.5).

Presence of pbf groups in the polymeric derivative (IV) was indicated by characteristic methyl group signals at δ 1.38, 1.988 and 2.424 ppm. After deprotection of Fmoc groups, ^{1}H NMR spectra of the polymeric derivative (V) exhibited disappearance of the aromatic Fmoc peaks (Figure 4.6).
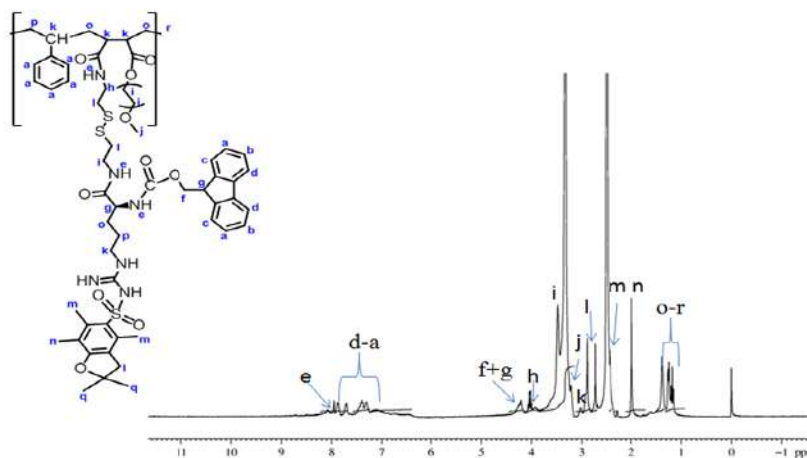
Figure 4.5. ^{1}H NMR spectrum (300 MHz, DMSO-d_6) of Fmoc-Arginine-pbf-OH grafted polymer: δ 1.152-1.6 (br m, aliphatic C$\underline{H}_3$ + CH-C$\underline{H}_2$), 1.988 – 2.424 (br m, Ar C$\underline{H}_3$), 2.69-3 (br m, S-C$\underline{H}_2$-C$\underline{H}_2$ + C$\underline{H}$), 3.214 (br s, O-C$\underline{H}_3$), 3.48-3.8 (br m, O-C$\underline{H}_2$-C$\underline{H}_2$), 4.14 - 4.259 (br m, C$\underline{H}_2$), 6.96-7.9 (br m, Ar C$\underline{H}$)
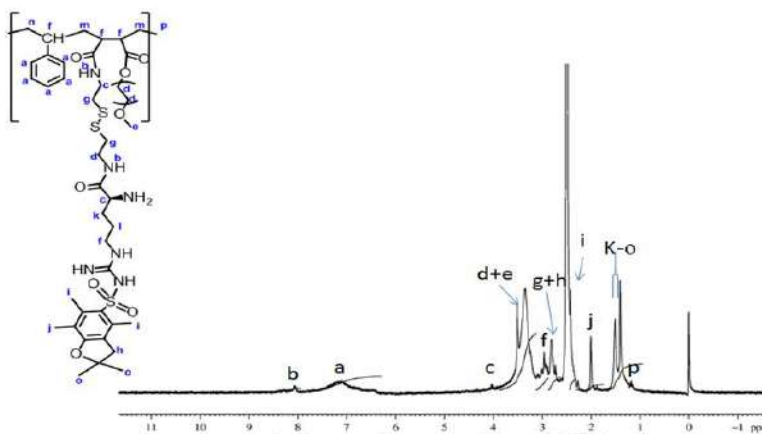
Figure 4.6. ^{1}H NMR spectrum (300 MHz, DMSO-d_6) of Arginine-pbf-OH grafted polymer (Fmoc deprotected) : δ 1.175 -1.5 (br m, aliphatic C$\underline{H}_3$ + CH-C$\underline{H}_2$), 2 – 2.426 (br m, Ar C$\underline{H}_3$), 2.73-3 (br m, S-C$\underline{H}_2$-C$\underline{H}_2$ + C$\underline{H}$), 3.241- 3.789 (br m, O-C$\underline{H}_3$ + O-C$\underline{H}_2$-C$\underline{H}_2$), 4 (br m, C$\underline{H}_2$), 7-7.33 (br m, Ar C$\underline{H}$)

171

Coupling of Fmoc-His(Trt)-OH to the free amino groups of arginine was characterized by the multiple aromatic signals attributed to benzene rings of styrene and Trt group, ranging from δ 6.78 - 7.31 ppm. Fmoc groups of the histidine grafted polymeric graft (VI) were confirmed by aromatic proton signals ranging from δ 7.31-7.862 ppm (Figure 4.7).
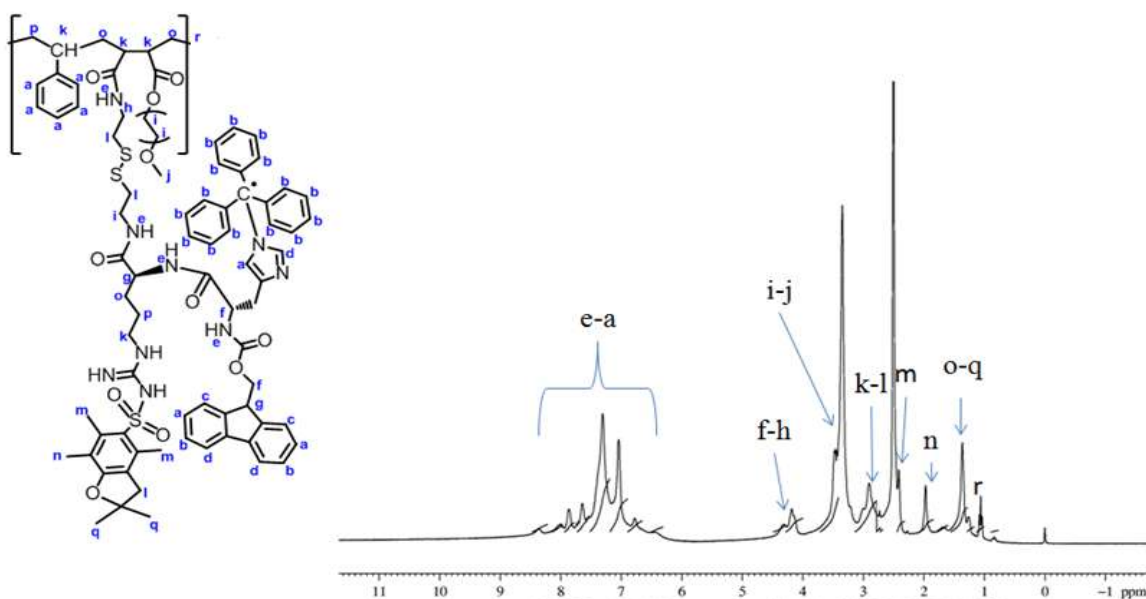
Figure 4.7. ^{1}H NMR spectrum (300 MHz, DMSO-d_6) of the polymeric derivative after conjugating Fmoc-Histidine-Trt-OH : δ 1-1.674 (br m, aliphatic C$\underline{H}_3$ + CH-C$\underline{H}_2$), 1.971 – 2.413 (br m, Ar C$\underline{H}_3$), 2.733-2.91 (br m, S-C$\underline{H}_2$-C$\underline{H}_2$ + C$\underline{H}$), 3.2- 3.6 (br m, O-C$\underline{H}_3$ + O-C$\underline{H}_2$-C$\underline{H}_2$), 4.181 (br m, C$\underline{H}_2$), 6.781-8 (br m, Ar C$\underline{H}$)

Successive cleavage of Fmoc and pbf groups of the polymer was confirmed by the absence of characteristic peaks of protecting groups in the respective ^{1}H NMR spectra (Figures 4.8-4.9). Arginine–histidine combination was employed as cationic groups due to their efficiency in complexing and condensing genetic materials, and ability to overcome endolysosomal uptake through proton sponge effect. ATR-FTIR spectrum of the final polymer (Figure 4.10) exhibited characteristic bands ranging from 1450 to 1680 cm^{-1} indicating CN stretching, NH bending and carbonyl stretching of amide bonds. Asymmetric stretch due to aliphatic C-O-C ether linkages is

indicated by characteristic band at 1100 cm^{-1}. Average molecular wieght (M$_w$) of the polymeric derivative (VII, figure 4.1) was calculated to be ~18.4 kDa by GPC spectra (Figure 4.11).
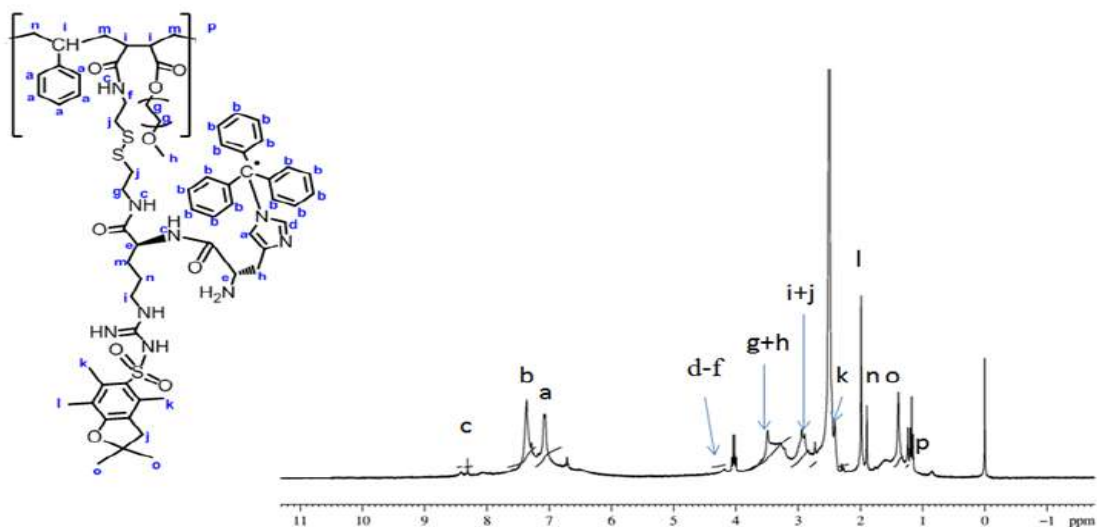
Figure 4.8. ^{1}H NMR spectrum (300 MHz, DMSO-d_6) of the polymeric derivative after deprotection of Fmoc groups of histidine. δ 1.151-1.897 (br m, aliphatic CH_3 + CH-CH_2), 1.99 – 2.41 (br m, Ar CH_3), 2.65-2.94 (br m, S-CH_2-CH_2 + CH), 3.3- 3.5 (br m, O-CH_3 + O-CH_2-CH_2), 4.1 (br m, CH_2), 7-7.365 (br m, Ar CH)
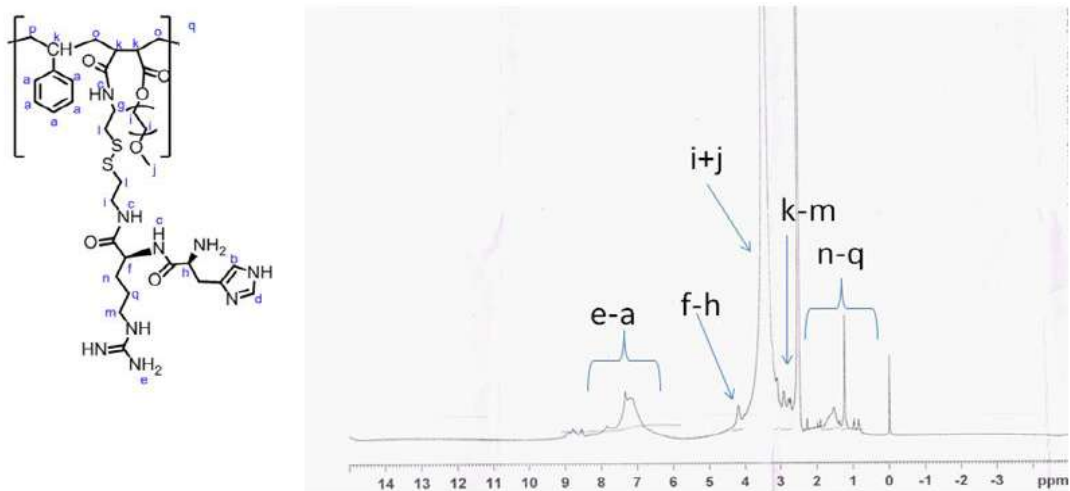
Figure 4.9. ^{1}H NMR spectrum (300 MHz, DMSO-d_6) of the polymeric derivative grafted with arginine and histidine, after deprotection of protecting groups : δ 0.96-1.52 (br m CH-CH_2), 2.72-2.9 (br m, S-CH_2-CH_2 + CH), 3.1- 3.7 (br m, O-CH_3 + O-CH_2-CH_2), 4.18 (br m, CH_2), 6.9-7.32 (br m, Ar CH)

173
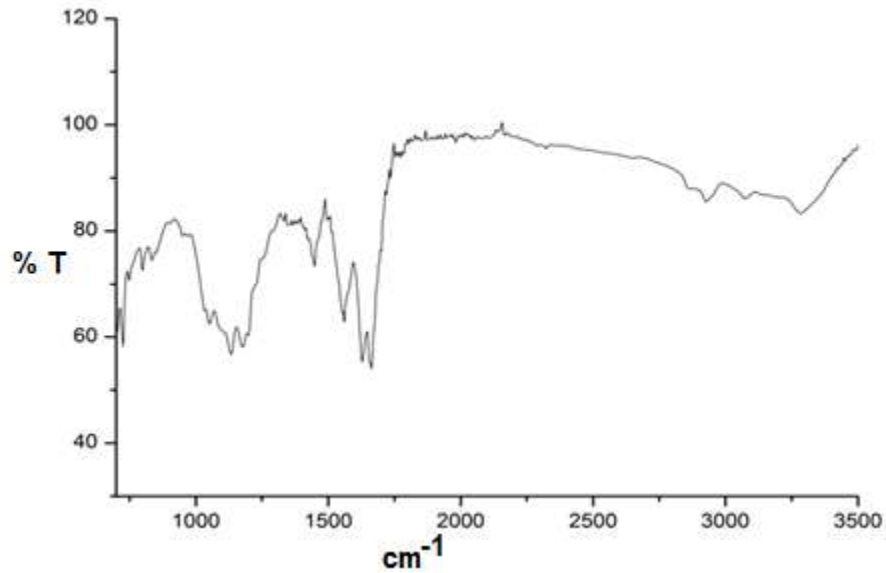
Figure 4.10. ATR-FTIR spectrum of the arginine and histidine grafted polymer (VIII, Figure 4.1)
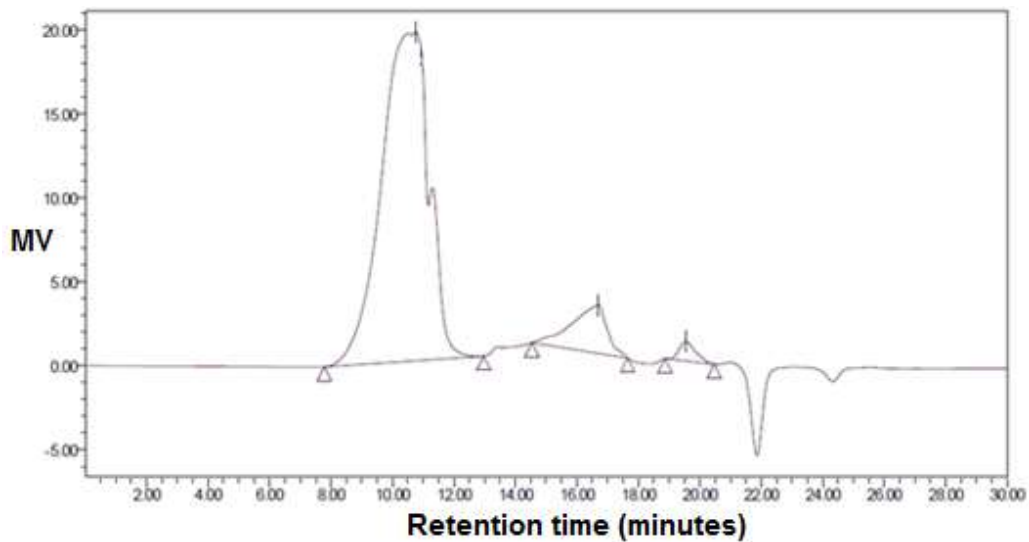
Figure 4.11. GPC spectrum of the polymeric derivative (VII, figure 4.1)

4.3.2. Formulation and evaluation of polymeric micelles

The cationic polymer readily self assembled in to micelles, in aqueous media, with an average particle size of 82.2 ± 4.3 nm (DLS size). The obtained nanostructures were spherical in nature
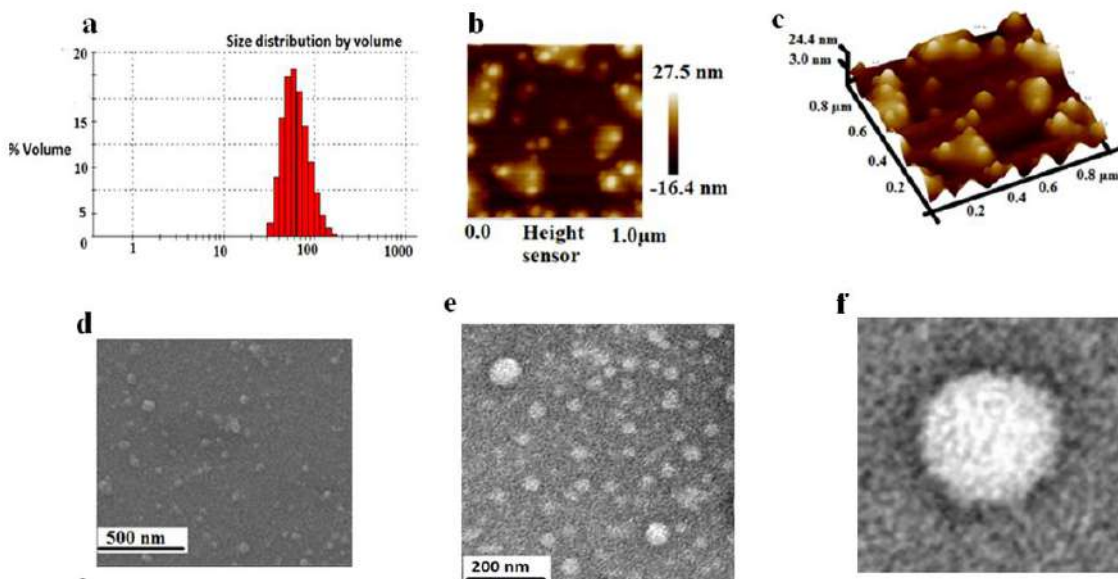
Figure 4.12. Morphological characterizations of the cationic polymeric micelles using DLS (a) AFM ('b' depicts 2D image and 'c' shows 3D view of the micelles), FESEM (d) and TEM (e-f). 'f' shows the enlarged view of a single micelle.

as depicted by AFM, FESEM and TEM (Figure 4.12), and exhibited lower particle size than that shown by DLS measurement. DLS measures hydrodynamic radii of the nanoparticles, due to which it shows slightly increased average particle size for the micelles [4, 5]. Zeta potential of the polymeric micelles in deionized water was measured to be 26.1 ± 1.3 mV. Critical micellar concentration (CMC) of the polymeric micelles was evaluated using fluorescence spectroscopy, employing pyrene as fluorescent probe. Hydrophobicity of pyrene facilitates its preferential partition in to hydrophobic domains of micelles. Emission spectra of pyrene depict vibronic peaks. Ratio of the intensities of third and first vibronic peaks (I_3/I_1) of pyrene emission is widely used for determining any conformational changes of polymers, dispersed in aqueous media [6]. I_3/I_1 is close to 0.59 for free pyrene, dispersed in water. The ratio increases rapidly in the presence of hydrophobic domains. In the present study, I_3/I_1 ratios of pyrene were plotted against corresponding concentrations of micelles (Figure 4.13). Crossover point of micellar

concentration, at which I_3/I_1 values essentially reached a plateau level, was calculated as CMC (~7 µg/mL).
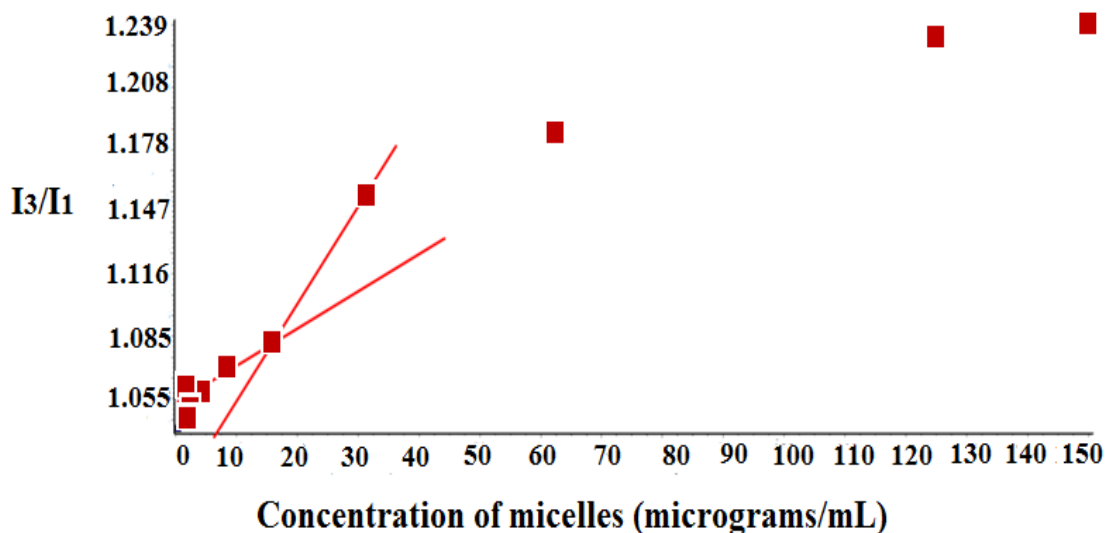
Figure 4.13. CMC determination of polymeric micelles

CMC can dictate kinetic stability of the polymeric micelles in systemic circulation. *In vivo*, micelles will be subjected to dilution in a large volume of physiological fluid. This diluted concentration of micelles should be above CMC for facilitating their prolonged circulation and achieving therapeutic efficacy [7, 8]. Hence CMC is a critical parameter to consider, while designing the dose of micelles, for therapeutic applications. Serum stability of polymeric micelles was evaluated by incubating them in complete cell culture media (DMEM supplemented with 10 % FBS). Micelles exhibited stable and uniform particle size distribution, up to 24 h (Figure 4.14). Slight increase in average particle size was observed after 1 h of incubation, possibly due to the coating of serum proteins over the cationic micelles. No significant increase was observed during further incubation. Primary amine content of the polymeric micelles was calculated as 46.5 ± 5.37 µM/100 µg nanoparticles, using TNBS assay.
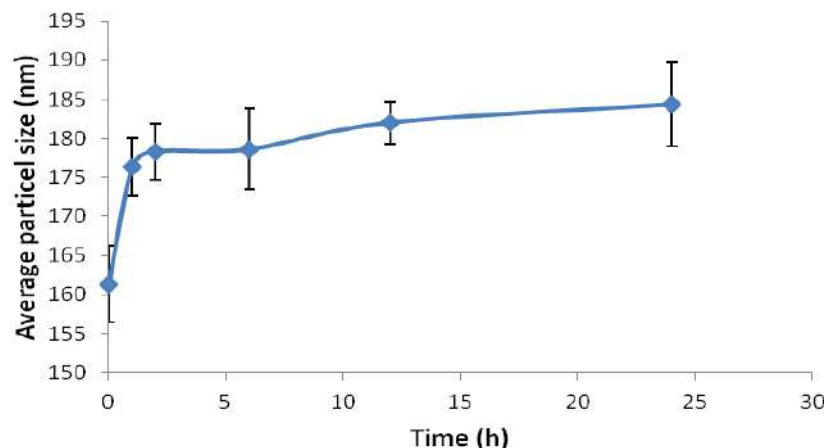
Figure 4.14. Stability of the polymeric micelles in DMEM media supplemented with 10 % FBS

Biocompatibility of the polymeric micelles was evaluated in MCF 7 and L929 cell lines, using MTT assay. There was no indication of toxicity due to micelles over the tested concentration range (50-1000 µg/mL), in both the cell lines (Figure 4.15). MCF 7 and L929 cells treated with various concentrations of polymeric micelles (50-1000 µg/mL) did not exhibit any significant ROS generation (data not shown).
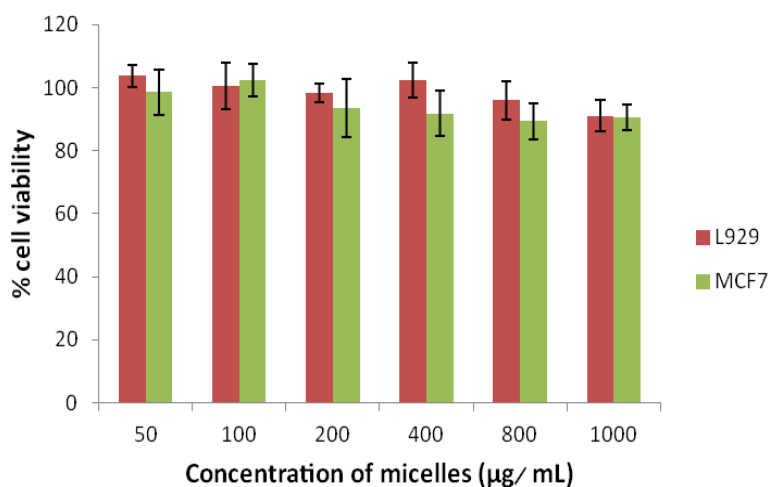
Figure 4.15. MTT assay of blank polymeric micelles in MCF 7 and L929 cells

Genotoxic potential of the micelles was evaluated using comet assay. The cells were lysed post treatment with the micelles (1 mg/mL), subjected to electrophoresis and observed for any alteration in the intensity of comet tail. If any DNA strand breakage had occurred within the treated cells, a proportional increase in the intensity of comet tail would have been observed [9, 10]. The treatment of cell lines (MCF 7 and L929) with micelles did not show any significant change in comet tail intensity (Figure 4.16). The obtained results suggested safety of the polymeric micelles for biological applications.
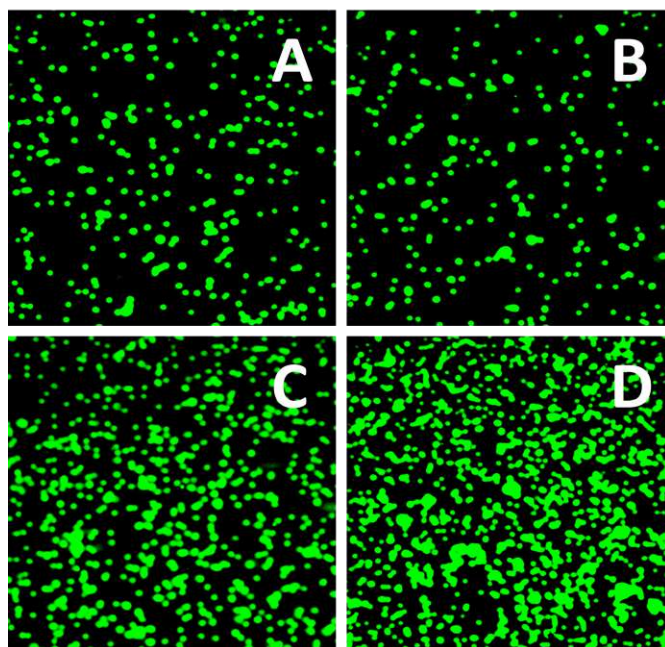
Figure 4.16. CLSM images of lysed cells stained with SYBR$^{@}$ green after performing comet assay (A: Untreated MCF 7 cells, B: MCF 7 cells treated with micelles, C: Untreated L929 cells, D: L929 cells treated with micelles)

4.3.3. Optimization of drug loaded micelles by CCD

Design of experiments (DOE) is a systematic and formal approach to investigate a system or process. It includes designing planned changes to the independent variables of a system or process, by conducting a series of structured tests. The effects of these changes on a pre-defined

Table 4.2. Optimization of nanoparticles using CCD

Formulation code	Independent Factors		Responses		
	Polymer: Drug ratio (w/w)	Solvent: Non-solvent ratio (v/v)	Entrapment efficiency (%)	Particle size (nm)	Polydispersity index (PDI)
F1	4.50	0.18	53.45	98.54	0.203
F2	2.50	0.05	39.99	82.00	0.261
F3	2.09	0.11	38.29	76.76	0.224
F4	2.50	0.18	41.37	73.87	0.180
F5	3.50	0.11	44.10	87.18	0.240
F6	3.50	0.11	45.57	91.84	0.227
F7	3.50	0.11	45.23	89.87	0.214
F8	3.50	0.03	41.87	110.20	0.287
F9	4.50	0.05	47.99	121.50	0.306
F10	4.91	0.11	52.97	115.80	0.292
F11	3.50	0.11	43.11	87.54	0.228
F12	3.50	0.11	46.41	89.83	0.246
F13	3.50	0.21	47.45	81.84	0.205

output can be evaluated. Fascinating aspect of DOE is the feasibility to gain maximum information about a system or process while minimizing resources needed for the same. It also offers significant advantage over 'one change at a time' experimental methods, because it can judge the influence of independent variables acting alone or in combination with other variables to the output [11]. Response surface designs are normally employed for evaluating the differences between formulations [12]. Central circumscribed design (CCD) and Box- Behnken designs are the two commonly used response surface designs. We have selected CCD, for comparing and optimizing doxorubicin loaded formulations, due to its suitability for optimization of nanoparticulate formulations [13]. Combinations of the independent variables and their respective outputs are provided in table 4.2. Statistical evaluation of the experimental

design was performed using Design-Expert 10 software. Each response was interpreted based on corresponding quadratic model suggested by the software.

Table 4.3. Levels of independent factors used in experiments

Factor Code	Independent Factor	Levels				
		-1.414	-1	0	+1	+1.414
A	Polymer: Drug ratio	2. 09	2.5	3.5	4.5	4.91
B	Solvent:Non solvent ratio	0.03	0. 05	0.11	0.18	0.21

Response: Entrapment efficiency

A quadratic model was suggested by the Design-Expert® 10 software (Statease, Minneapolis, USA) for entrapment efficiency. The model proposed the following polynomial equation for percentage entrapment efficiency -

$Y_1 = 35.97 - 0.27A - 20.22B + 15.54AB + 0.52A^2 - 23.75B^2$

ANOVA for Response Surface Quadratic Model

Table 4.4. Analysis of variance table [Partial sum of squares - Type III]

Source	Sum of squares	DF	Mean square	F value	Prob > F	-
Model	241.47	5	48.29	44.25	0.0001	Significant
Polymer: Drug Ratio (A)	8.831E-003	1	8.831E-003	8. 090E-003	0.9308	-
Solvent: Non-Solvent Ratio (B)	0.33	1	0.33	0.3	0.6011	-
AB	4.09	1	4.09	3.75	0. 0941	-
A^2	1.86	1	1.86	1.7	0.2332	-
B^2	0. 065	1	0. 065	0. 060	0.8143	-
Residual	7.64	7	1.09	-	-	-
Lack of fit	0.96	3	0.32	0.19	0.8971	Not significant
Pure error	6.68	4	1.67	-	-	-
Cor total	249.11	12	-	-	-	-

Where Y_1 is the percentage entrapment efficiency, A is the Polymer: Drug Ratio and B is the Solvent: Non-Solvent Ratio. The Model F-value of 44.25 implied the model was significant. There was only a 0.01% chance that a "Model F-Value" this large could occur due to noise. The

Figure 4.17. 3D (response surface plot) and 2D (contour plot) plots of % entrapment efficiency

'Lack of Fit F-value' of 0.19 implied that the Lack of Fit was not significant. There was a 89.71% chance that a "Lack of Fit F-value" this large could occur due to noise. The "Pred R-Squared" of 0.9326 was in reasonable agreement with the "Adj R-Squared" of 0.9474. "Adeq Precision" measures the signal to noise ratio. A ratio greater than 4 is desirable. Our ratio of 20.73 indicated an adequate signal. This model can thus be used to navigate the design space.

Response: Particle Size

A quadratic model was suggested by the Design-Expert® 10 software (Statease, Minneapolis , USA) for particle size. The model proposed the following equation for particle size -

$$Y_2 = 77.60 + 0.70A - 138.08B - 55.58AB + 2.93A^2 + 828.47B^2$$

ANOVA for Response Surface Quadratic Model

Table 4.5. Analysis of variance table [Partial sum of squares - Type III]

Source	Sum of squares	DF	Mean square	F value	Prob > F	-
Model	2562.86	5	512.57	64.65	0.0001	Significant
Polymer: Drug Ratio (A)	0.062	1	0.062	7.795E-003	0.9321	-
Solvent: Non-Solvent Ratio (B)	15.26	1	15.26	1.92	0.2079	-
AB	52.36	1	52.36	6.60	0. 0370	-
A^2	59.26	1	59.26	7.48	0. 0292	-
B^2	79.04	1	79.04	9.97	0. 0160	-
Residual	55.50	7	7.93	-	-	-
Lack of fit	40.86	3	13.62	3.72	0.1183	Not significant
Pure error	14.64	4	3.66	-	-	-
Cor total	2618.35	12	-	-	-	-

Where Y_2 is the particle size, Polymer: Drug Ratio and B is the Solvent: Non-Solvent Ratio. In this model AB, A^2 and B^2 were significant model terms. Interaction between the independent factors was found to be significant as AB was found to be significant in the model. The Model F-value of 64.65 implied the model was significant. There was only a 0.01% chance that a "Model F-Value" this large could occur due to noise. Values of "Prob > F" less than 0.0500 indicated model terms were significant. In this case AB, A^2 and B^2 were significant model terms. Values greater than 0.1000 indicate the model terms are not significant. The 'Lack of Fit F-value' of 3.72 implied that the Lack of Fit was not significant. There was a 11.83% chance that a "Lack of Fit F-value" this large could occur due to noise. The "Pred R-Squared" of 0.8878 was in reasonable agreement with the "Adj R-Squared" of 0.9637. "Adeq Precision" measures the signal to noise ratio. A ratio greater than 4 is desirable. Our ratio of 25.51 indicated an adequate signal. This model can thus be used to navigate the design space.

Response surface plot

Contour plot
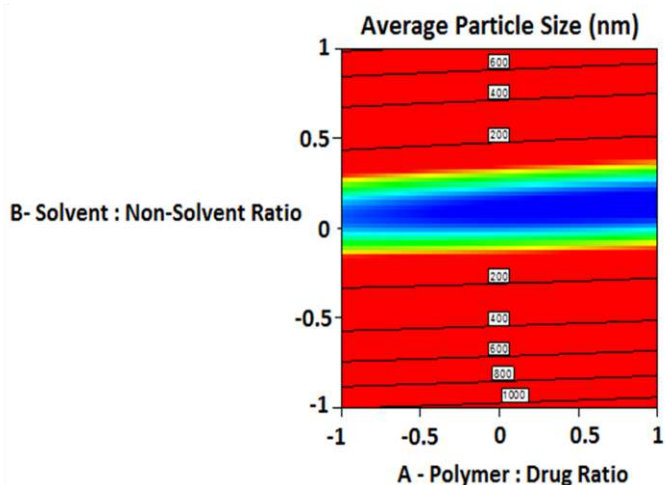
Figure 4.18. 3D (response surface plot) and 2D (contour plot) plots of average particle size

Response: Polydispersity index

A quadratic model was suggested by the Design-Expert® 10 software (Statease, Minneapolis , USA) for polydispersity index. The model proposed the following equation for polydispersity index -

$$Y_3 = 0.33 - 0.039A - 0.70B - 0.089AB + 9.894E{-}003A^2 + 1.8B^2$$

Where Y_3 is the polydispersity index, A is the Polymer: Drug Ratio and B is the Solvent: Non-Solvent Ratio The Model F-value of 13.59 implied the model was significant. There was only a 0.17% chance that a "Model F-Value" this lar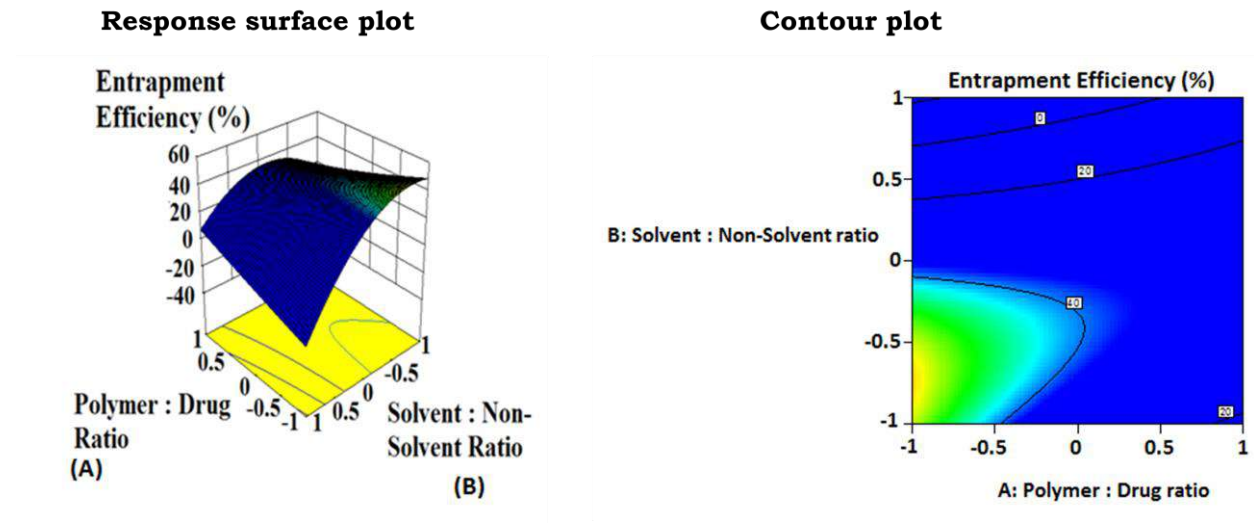ge could occur due to noise. The 'Lack of Fit F-value' of 2.12 implied that the Lack of Fit was not significant. There was a 24.09% chance that a "Lack of Fit F-value" this large could occur due to noise. "Adeq Precision" measures the signal to noise ratio. A ratio greater than 4 is desirable. Our ratio of 11.894 indicated an adequate signal. This model can thus be used to navigate the design space.
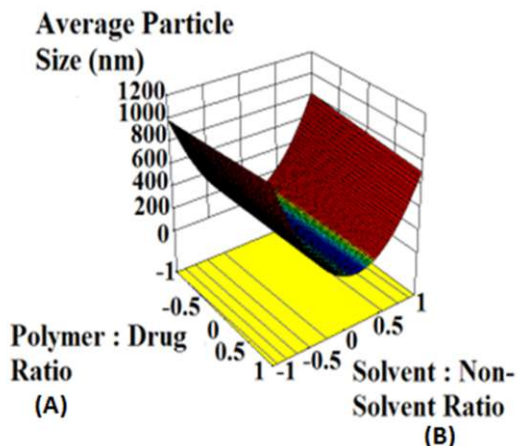
ANOVA for Response Surface Quadratic Model

Table 4.6. Analysis of variance table [Partial sum of squares - Type III]

Source	Sum of squares	DF	Mean square	F value	Prob > F	-
Model	0.016	5	53.115E-003	13.59	0.0017	Significant
Polymer: Drug Ratio (A)	1.886E-004	1	11.886E-004	0.82	0.3945	-
Solvent: Non-Solvent Ratio (B)	3.894E-004	1	13.894E-004	1.7	0.2336	-
AB	1.329E-004	1	11.329E-004	0.58	0.4712	-
A^2	6.766E-004	1	16.766E-004	2.95	0.1294	-
B^2	3.727E-004	1	13.727E-004	1.63	0.2429	-
Residual	1.604E-003	7	72.292E-004	-	-	-
Lack of fit	9.842E-004	3	33.28E-004	2.12	0.2409	Not significant
Pure error	6.2E-004	4	41.55E-004	-	-	-
Cor total	0. 017	12	-	-	-	-

Among the responses evaluated, PDI was varying within a narrow range of 0.18-0.3. PDI below 0.3 is recommended by Malvern (zetasizer nano zs), for considering uniform distribution of nanoparticles. Accordingly, all the formulations tested have shown PDI within the acceptable range. Particle size of the formulations ranged from 73.87 nm-121.5 nm. For selecting an optimum formulation from the design matrix, we have preferred those with higher entrapment efficiency and particle size close to 100nm. Even though F1 and F10 were showing almost similar % EE, based on the lower average particle size, F1 was selected as the optimized formulation for further studies.
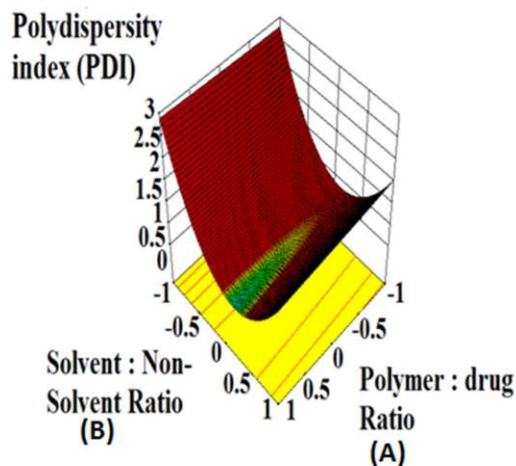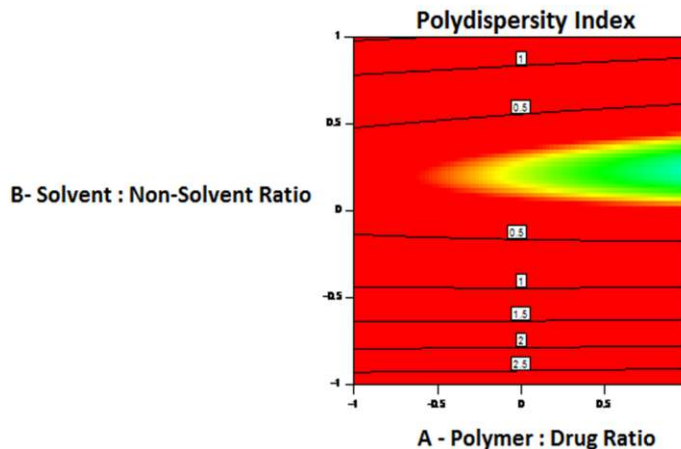
Figure 4.19. 3D (response surface plot) and 2D (contour plot) plots of polydispersity index

4.3.4. Formulation and evaluation of polyplexes

Blank polymeric micelles were formulated by combining the independent factors of optimized drug loaded formulation (F1). The resulting formulation was dialyzed against RNase free water, to remove DMSO. The obtained polymeric particles were mixed with siRNA, at different weight ratios, to evaluate their electrostatic complexation. Effective binding and condensation of siRNA to the polymeric micelles was observed above polymer∕ siRNA weight ratio of 40 (Figure 4.20.A). The polyplexes were able to suspend in RNase free water, for prolonged time, without any signs of aggregation. But when they were dispersed in buffer saline with high ionic strength (1 M PBS, pH 7.4) the suspensions tend to become turbid. After prolonged storage in buffer saline, visible aggregation of the polyplexes was observed.

This phenomenon could be explained by the DLVO theory. According to DLVO theory, colloidal stability of nanosuspensions is governed by the net balance of electrostatic repulsion which prevents particle agglomeration and van der Waals attraction which facilitates mutual binding of the dispersed particles [14]. When charged nanoparticles are dispersed in electrolyte

solutions, counter ion clouds will be formed over the particle surface in order to charge-compensate the surface charge of dispersed particles. In dilute electrolyte solutions, these counter ion clouds stay far from the particle surface causing a long range double layer interaction. Due to the relatively weak Van der Waals attractive forces, at long range, electrostatic repulsive forces between the particles dominate resulting in stable particle dispersions. However, electrolyte solutions with high ionic strength (eg: cell culture media) compresses the electrical double layer and reduce the magnitude of inter particle repulsive barrier. As a result, van der Waals attraction dominates and the net interactive force turns purely attractive causing agglomeration of particles.

For pharmaceutical applications, stability of the formulation during storage is a prerequisite. We have stabilized the polyplexes using bovine serum albumin (BSA). Motivations for selecting albumin as a stabilizing agent were our own experimentally observed facts and available literature support. The designed redox sensitive nanoparticles depicted excellent serum stability in cell culture media supplemented with 10 % FBS (Figure 4.14). This clearly indicated the role of proteins present in the media in stabilizing the nanocarriers. Random mixing of the agglomerated particles, in electrolyte solutions having high ionic strength, with albumin (at arbitrary weight ratios) resulted in clear and stable dispersions (data not shown). Existing literature also support this approach [15]. Agglomeration of TiO_2 nanoparticles in various cell culture media were prevented by the addition of BSA [16]. Nab technology is the clinically successful example of albumin bound delivery systems. Abraxane is an injectable, solvent and Cremophor-free formulation of albumin bound paclitaxel, which is approved for breast cancer treatment by FDA [17, 18].
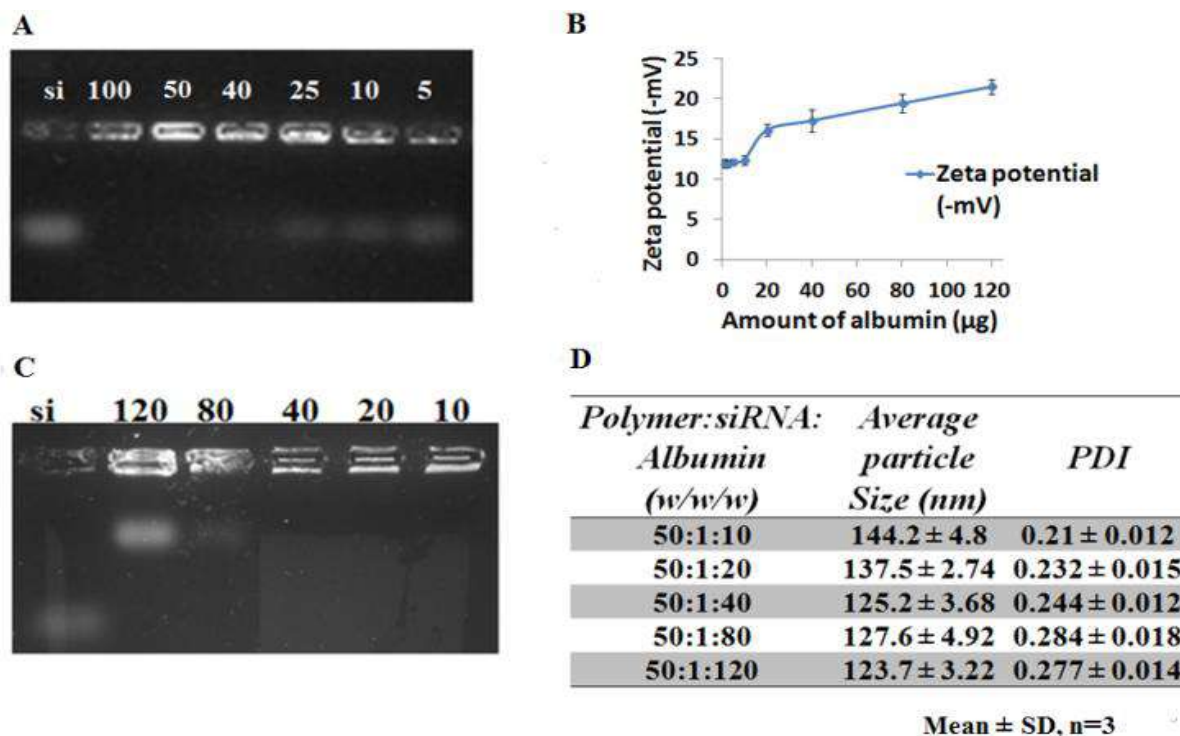
Figure 4.20. (A) Agarose gel electrophoresis of polyplexes ('si' shows bare siRNA, 5-100 represents polymer: siRNA weight ratios); **(B)** Zeta potential of polyplex formulations (at constant polymer/siRNA weight ratio of 50:1) in the presence of varying amounts of albumin; **(C)** Agarose gel electrophoresis of polyplex formulations (at constant polymer/siRNA weight ratio of 50:1) in the presence of varying amounts of albumin (10-120 μg); **(D)** Average particle size and PDI of polymer/siRNA/albumin complexes in PBS, pH 7.4.

We have investigated the pattern of interaction of polyplexes with albumin using DLS, UV-visible spectroscopy and horizontal gel electrophoresis (Figure 4.20). Polyplexes with polymer / siRNA weight ratio of 50 was selected for the interaction studies based on the complete gel retardation of siRNA observed at this combination (Figure 4.20.A). To properly investigate the effect of albumin on zeta potential of polyplexes, selected polyplex formulation was mixed with varying amounts of albumin in RNase free water. Water was selected as dispersion medium in order to nullify any interaction from salts on zeta potential measurements. After complexation with siRNA, average zeta potential of the polymeric micelles reduced from + 25.4 ± 1.52 mV to

+4.1 ± 0.21 mV. This could be attributed to the utilization of cationic charges on the surface of micelles by anionic phosphate groups of siRNAs. Polymer: siRNA complex (50:1 weight ratio)
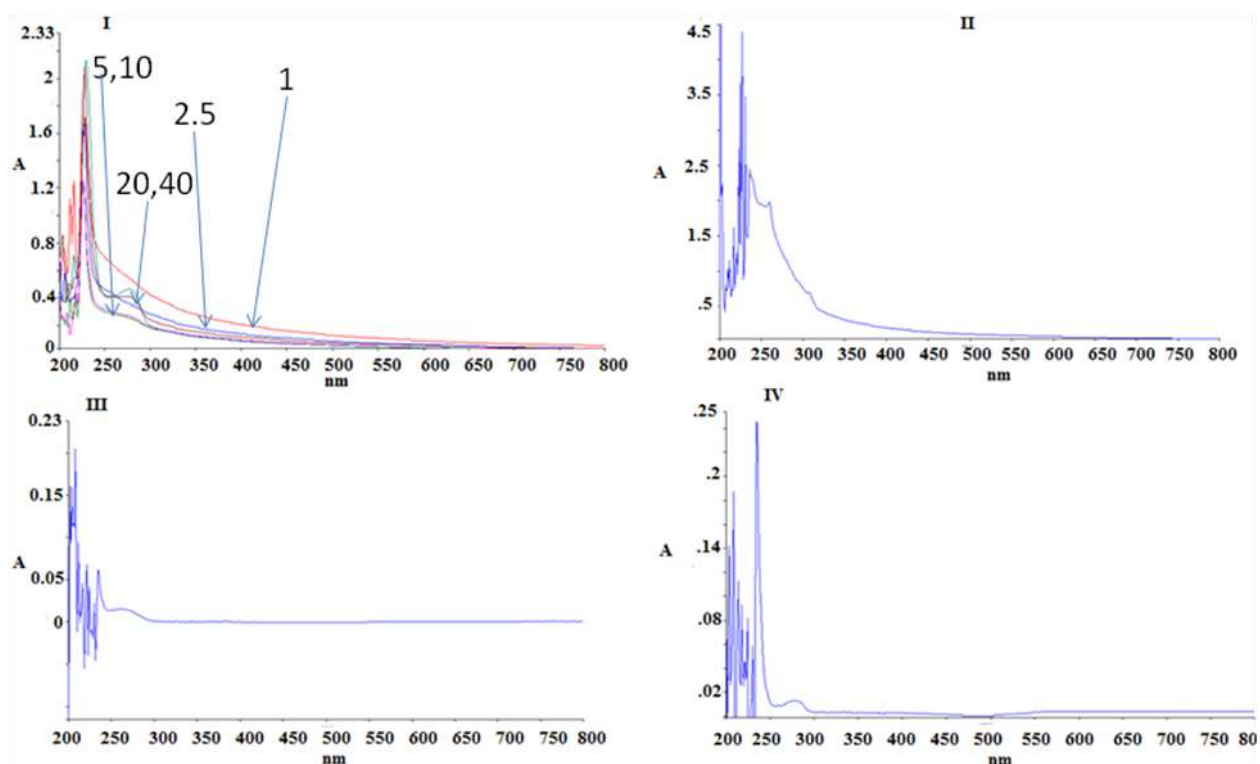
Figure 4.21. UV-Visible spectroscopic analysis of polyplex-protein complexes (I). Polymer: siRNA weight ratio was kept constant in all mixtures at 50:1. Weight ratio of albumin was varied from 1-40 as indicated by the numbers in figure I. Individual spectra of polymer, siRNA and albumin are represented by figures II, III and IV, respectively.

was then mixed with varying ratios of albumin, in RNase free water, and the respective zeta potentials were recorded (Figure 4.20.B). Zeta potentials of the dispersions shifted to negative range with the addition of albumin, and the increase towards negative side was proportional to the amount of protein added. When albumin content was increased above 20 μg (polymer and siRNA contents were kept constant at 50 μg and 1 μg, respectively), zeta potential in the negative range shifted from ~12 mV to ~17 mV. This significant shift in zeta potential could be due to the saturation of polyplexes with bound albumin and the subsequent release of free

albumin. UV-Visible spectroscopic evaluation of the mixtures (Figure 4.21) confirmed the observations based on zeta potential measurements. Scanned spectra of blank polymeric micelles, siRNA, albumin and the mixtures were recorded in the range of 200-800 nm, and interpreted. Albumin exhibited two absorption peaks at 220 nm and 280 nm. Strong peak of albumin at 220 nm is due to the chromophores in its backbone and weak peak at 280 nm arises due to the aromatic amino acid residues [19]. Absorption spectra of polymer/siRNA/albumin mixtures depicted mutual quenching of the absorption peaks between polymer and albumin, with change in their ratio. siRNA peaks were not significant in the spectra of mixtures, probably due to its complete condensation by the polymeric micelles and lower concentration (1 µg/mL) used. At lowest albumin content tested (1 µg/mL), absorption due to the polymer was significant. As albumin content was increased to 2.5 µg/mL, quenching of the UV absorption by polymer was observed. This quenching became more significant with further increase in albumin concentration. Above 20 µg/mL, weak peak of albumin attributed to its aromatic amino acids became prominent. This could be due to the presence of unbound albumin at higher concentrations. Interestingly, shift in the pattern of protein binding was observed at same concentration range (20 µg/mL and above) with both DLS (sudden shift in zeta potential) and UV-Visible analysis.

However, the stability of siRNA in the polymer/siRNA/albumin was yet to be confirmed. This was assessed using horizontal gel electrophoresis of the mixtures (Figure 4.20.C). Even though concentration range of albumin needed to saturate the polyplex formulation was determined to be 20 µg/mL and above, using DLS and spectroscopy, much higher concentration was needed to stably bind and pack them under electrophoretic conditions. siRNA was safely and stably bound to the polymeric micelles at all the albumin concentrations tested. At higher concentrations of

albumin (80 and 120 μg/mL), some portion of the polyplexes packed in the albumin was moving towards the anode. This could be due to the acquisition of net negative charge by the polyplexes after getting packed in to negatively charged albumin. Another important pharmaceutical parameter required for an efficient polymeric nanosystem is optimum particle size (10-200 nm). Particle sizes were evaluated by dispersing the mixtures in PBS, pH 7.4 (Figure 4.20.D). The average particle sizes of polymer/siRNA/albumin mixtures were found to decrease with increase in albumin content and became constant after a particular concentration. All the formulations depicted excellent particle size (ranged from 123-144 nm), with prolonged stability.
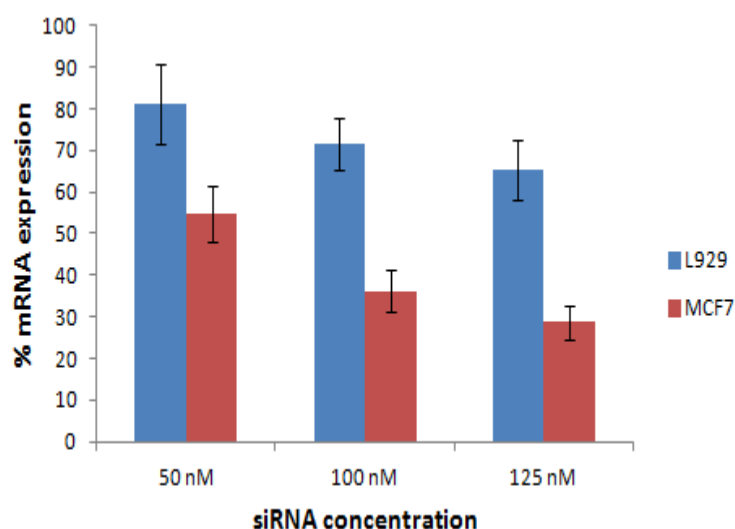
Figure 4.22. RTPCR evaluation of the PLK-1 siRNA loaded polyplexes (B), in MCF 7 and L929 cells, after 48 h treatment.

mRNA knock down efficiency of the polyplex formulation was evaluated in MCF 7 and L929 cells, using real time polymerase chain reaction (RTPCR) assay (Figure 4.22). In MCF 7 cells, efficient knockdown of mRNA expression was observed (~ 72 % reduction in mRNA expression) when siRNA was administered at a concentration of 125 nM. Knock down efficiency in L929 cells was significantly lower (~ 34 % reduction in mRNA expression) in comparison to that in MCF 7 cells. This could be probably
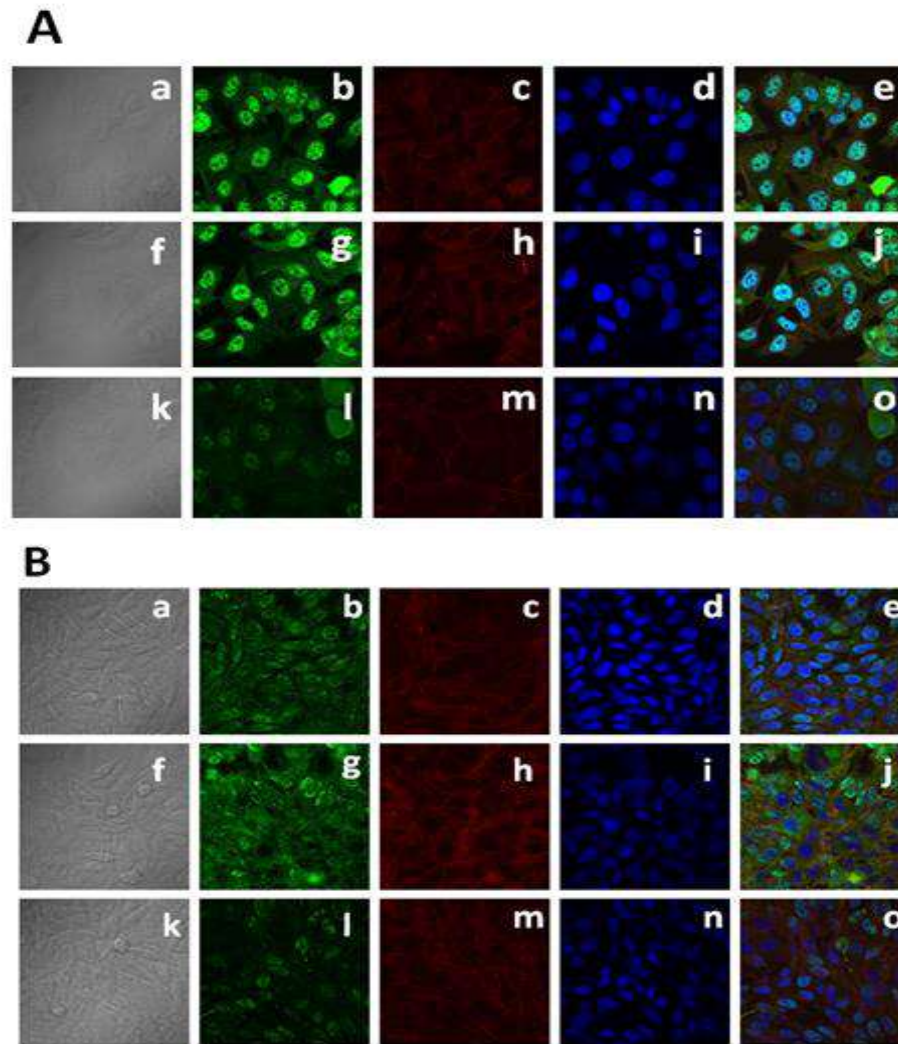
Figure 4.23. Evaluation of PLK-1 protein expression, in MCF 7 (A) and L929 (B) cells, using immunofluorescence analysis. 'a-e', 'f-j' and 'k-o' represents respective bright field, immunostained target protein (PLK-1), immunostained β-actin, DAPI stained nucleus and merged images of untreated cells, cells treated with polyplexes bearing scrambled siRNA and cells treated with polyplexes bearing PLK-1 siRNA. siRNA concentration used was 125 nM and incubation time was 48 h.

due to the redox responsive nature of polymeric micelles [20]. Cationic groups of the micelles binding siRNAs were grafted to the polymer via disulfide linkages. Glutathione rich environment

of cancer cells could have facilitated more efficient release of siRNAs within cancer cells (MCF 7), in comparison to L929 cells, resulting in enhanced knockdown of the target gene.

Efficiency of the polyplexes in knocking down polo-like kinase 1 (PLK-1) protein, in MCF 7 and L929 cells, was evaluated using immunofluorescence (Figure 4.23). PLK-1 has significant role in multiple aspects of mitosis such as maturation of centrosomes, spindle assembly, sister chromatin separation, cytokinesis etc. Cellular level of PLK-1 remains maximum during the G_2-M phase of mitosis. During this phase, phosphorylation of PLK-1 occurs and its kinase function gets stimulated. Nuclear localization and nucleocytoplasmic translocation of the protein is facilitated by the presence of nuclear localization sequence (NLS) in its domain [21]. For immunofluorescence analysis, active PLK-1 (phosphorylated) in the cells were stained using corresponding primary and secondary antibodies. Green fluorescence of the stained target protein was quantified using ImageJ software. As shown in Figure 8, MCF 7 cells (untreated) depicted higher mean fluorescence intensity than untreated (~ 3 fold) L929 cells (untreated). This could be probably due to the fact that, actively dividing tumor cells are highly dependent upon PLK-1 protein for their proliferation, in comparison to normal cells [22].

After treating the cells with polyplexes bearing PLK-1 siRNA (125 nM), reduction in protein fluorescence was observed. MCF7 cells depicted ~ 5 fold and L929 cells have shown ~ 2.6 fold decrease in mean fluorescent intensity of the expressed PLK-1 protein. This observation was in line with that of RTPCR results and confirms the redox responsive behavior of polymeric micelles. Treatment with polyplexes bearing scrambled siRNA (125 nM) did not induce any significant change in fluorescent intensity of immunostained PLK-1 protein, in both the cell lines.

4.3.5. Co-delivery efficacy of the drug loaded polyplexes *in vitro*

Drug loading content (% w/w) of the optimized drug loaded polymeric micelles was calculated to be 8.6 ± 0.58 %. The pattern of siRNA complexation with optimized drug loaded polymeric micelles (F1) was similar to that with blank micelles (Figure 4.24). Particle size distribution of the optimized drug loaded micelle/siRNA/albumin mixture was also closer to blank micelle/siRNA/albumin mixture (data not shown).
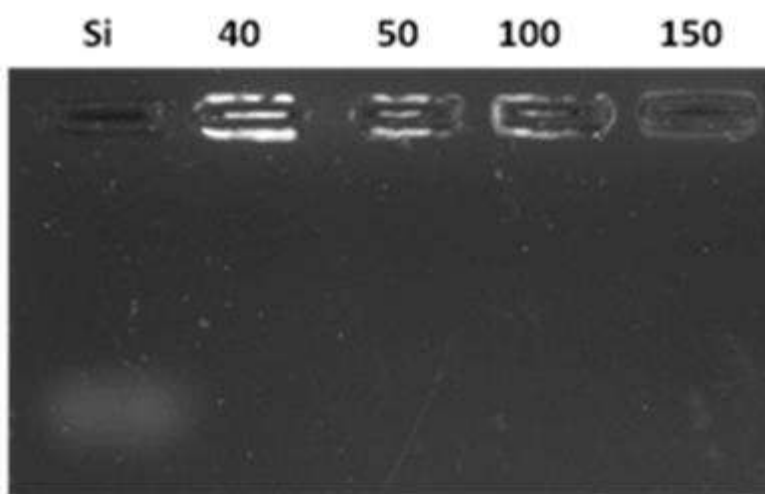
Figure 4.24. Gel retardation of siRNA by drug loaded polyplexes. Si indicates bare siRNA and numbers 40-150 indicate polymer:siRNA weight ratios.

In vitro drug release pattern of the optimized drug loaded polyplex formulation has shown redox responsive behavior of the micelles. Drug release from nanocarriers is primarily a diffusion based phenomenon. Dispersion media shall travel through the matrix of nanocarriers and solubilize the loaded drug, facilitating their release. Release rate from the optimized drug loaded polymeric micelle/siRNA/albumin mixture (Figure 4.25) was very slow at pH 7.4, resulting in a cumulative drug release of 11.52 ± 2.2% (after 24 h). The siRNA bound interlayer and protein rich outer layer rendered a compact barrier to the nanocomplex, which effectively restricted the diffusion of drug, at pH7.4. Addition of glutathione (GSH) at a concentration of 5 µM

(concentration of GSH in systemic circulation) had negligible effect on the release rate, whereas higher concentration of GSH (10 mM) promoted the drug release up to 23.82 ± 3.15%. Substantial increase in % drug release was observed at pH 5, in the presence (~51 %) and absence (~37 %) of 10 mM GSH. Enhanced released observed at pH 5, in the absence of 10 mM GSH, could be due to protonation of the amino acid residues of the polymer. Extensive protonation could have imposed predominant hydrophilic nature to the micelles, promoted their swelling and facilitated enhanced diffusion of the release media throughout the matrix [23]. Destabilization of the micelles by GSH (10 mM) induced disulfide bond cleavage could have resulted in further increase in drug release.
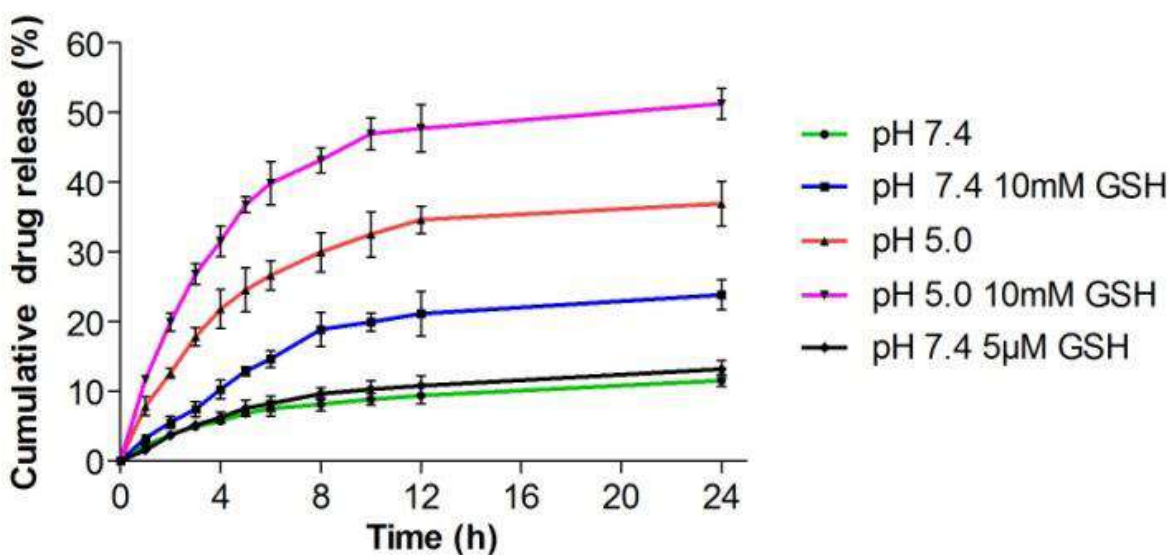
Figure 4.25. *In vitro* release profile of doxorubicin from nanoplex (Polymer/siRNA/albumin weight ratio of 50:1:120) in phosphate buffered saline (PBS) under various conditions (GSH concentrations were 5 µM or 10 mM,if added; temperature was maintained at 37 °C; data points represent mean ± standard deviation of three parallel samples).

The observed drug release pattern of polymeric micelles showed both pH and redox responsive nature of the nanosystem. This dual stimuli responsive behavior of designed formulation can accomplish maximum drug release at endosomal pH and glutathione rich microenvironment of

cancer cells, with minimal release during their systemic circulation. Cytosolic co-localization of the loaded drug and siRNA indicates their successful combinatorial delivery to cells. For evaluating the co-localization, cells (MCF 7 and L929) were treated with micelles bearing doxorubicin and FAM labeled siRNA. As shown in Figure 4.26, red fluorescence of doxorubicin and green fluorescence emitted by FAM labeled siRNA were merging in the cellular cytoplasm (yellow color in the merged image). This clearly depicts that the micelles were able to load both the active agents stably, and achieve their simultaneous intracellular delivery.
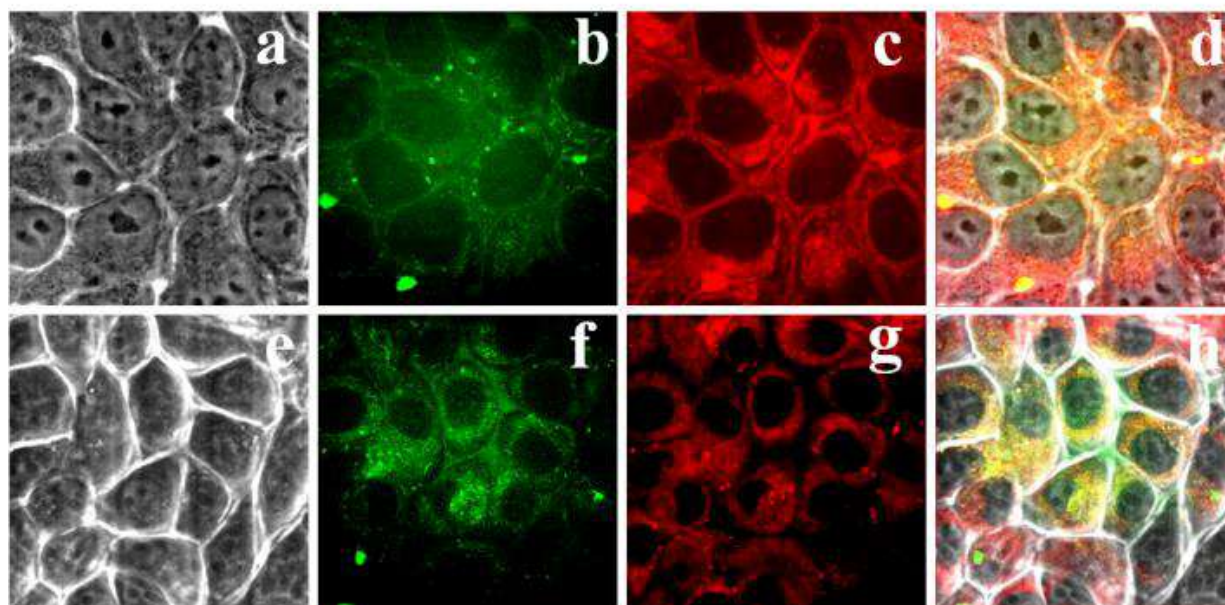
Figure 4.26. Evaluation of the cellular uptake of doxorubicin and FAM labeled negative control siRNA loaded nanoplexes using CLSM. 'a-d' represents respective bright field, FAM fluorescence, Dox fluorescence and merged images of treated MCF 7 cells. 'e-h' indicates respective bright field, FAM fluorescence, Dox fluorescence and merged images of treated L929 cells.

Effect of the combinatorial delivery of doxorubicin and PLK-1 siRNA on cell proliferation was evaluated using MTT assay (Figure 4.27). Proliferation of MCF 7 cells was significantly inhibited, when PLK-1 siRNA was co-delivered with doxorubicin. L929 cells did not depict

significant difference in cell viability between groups treated with drug- PLK-1 siRNA and drug-scrambled siRNA combinations. This could be explained based on the fact that cancer cells are highly dependent on polo-like kinases for their mitosis, in comparison to normal cells [24]. Hence it can be concluded that, polo-like kinase is a promising therapeutic target for sensitizing cancer cells for chemotherapeutic drug mediated death. This strategy may cause minimal side effects to normal healthy cells either by enabling reduction in chemotherapeutic dose or by minimizing any off target effects of siRNA. Redox responsive nature of the micelles was also evident from the pronounced cytotoxic effect of micelles bearing drug-scrambled siRNA combination on MCF 7 cells, in comparison to that on L929 cells.
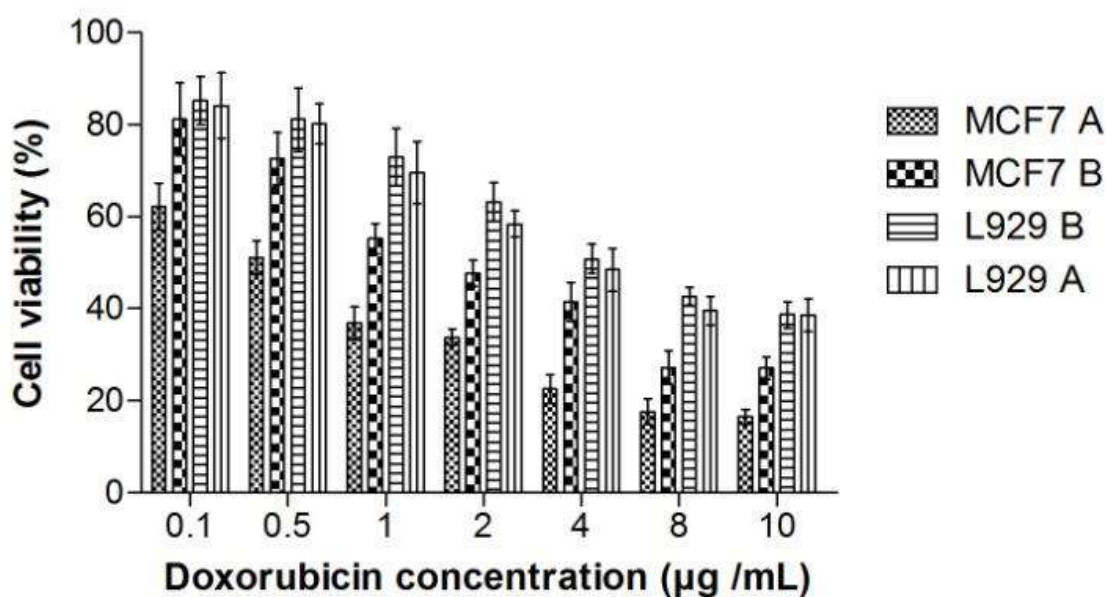
Figure 4.27. Effect of nanoplexes on proliferation of MCF 7 and L929 cells. A and B represents presence of PLK-1 siRNA and scrambled siRNA, respectively, in the nanoplexes. siRNA concentration was kept at 125 nM in all the wells. Data points are mean $\pm$ SD, n=4.

The synergistic effect of co-delivered drug and siRNA molecules in promoting cell death was further confirmed by apoptosis assay (Figure 4.28). Knockdown of PLK-1 in MCF 7 cells has shown induction of apoptosis. For determination of apoptosis, cells (MCF 7 and L929) were

treated with nanoplexes bearing drug (2.5 µg/mL) and 125 nM siRNA (PLK-1 or scrambled) and stained with Annexin-V-FITC and propidium iodide. Nanoplexes bearing drug and PLK-1 siRNA was able to induce ~52 % of cell apoptosis (including early apoptotic and late apoptotic cells), in MCF 7 cells, compared to ~35 % apoptosis induced by drug and scrambled siRNA loaded nanoplexes. No significant difference in % apoptosis was observed in L929 cells, after treatment with the same formulations.
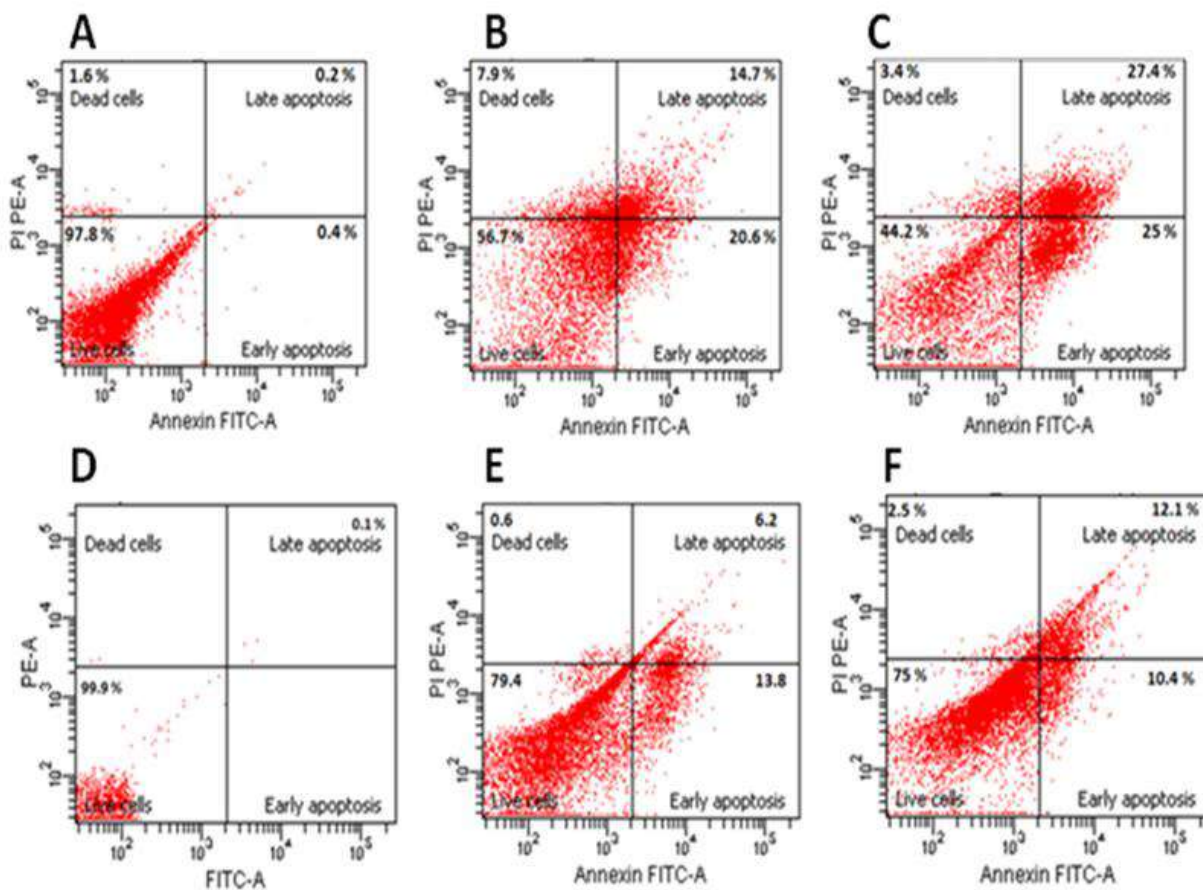
Figure 4.28. Apoptosis evaluation of MCF 7 cells (A-C) and L929 cells (D-F) 24 h post polyplex treatment. Untreated MCF 7 and L929 cells are depicted by A and D, respectively. B and C shows MCF 7 cells treated respectively with drug + scrambled siRNA loaded nanoplexes and drug + PLK-1 siRNA loaded nanoplexes. E and F shows L929 cells treated respectively with drug + scrambled siRNA loaded nanoplexes and drug + PLK-1 siRNA loaded nanoplexes.

4.3.6. *In vivo* toxicological evaluation of the polymeric micelles

Seven day repeated dose toxicity study was conducted in male Swiss albino mice for evaluating the safety of polymeric micelles, *in vivo*. Dose of the micelles (100 mg⁄kg) for toxicological study was determined according to previously reported literature [25]. Histopathological evaluation of the vital organs of treated mice did not depict any evidence of toxicity (Figure 4.29). Serum biochemical and haematological parameters of the treatment group were comparable to that of saline treated control group (data not shown). These observations indicate that the designed polymeric micelles can be used as a safe therapeutic vehicle for *in vivo* applications.
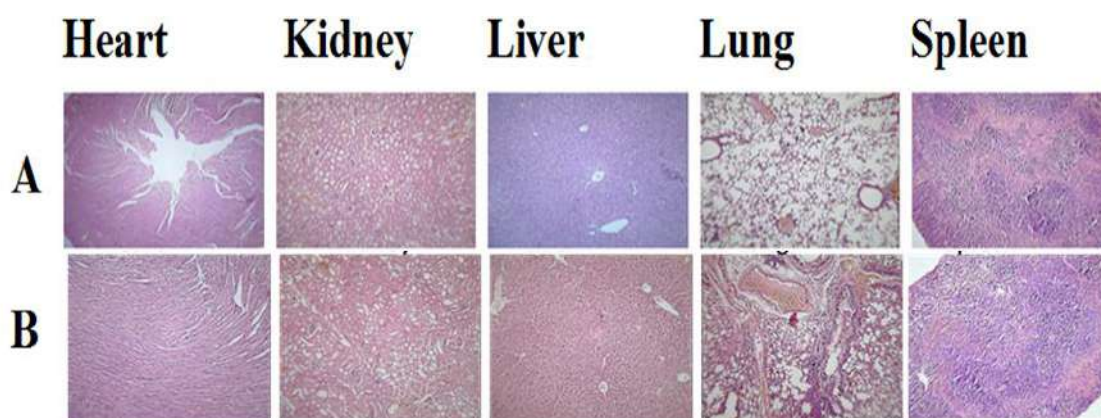
Figure 4.29. Histopathological evaluation of vital organs of mice treated with blank nanocarriers (B) and with phosphate buffer saline, pH 7.4

4.3.7. *In vivo* anticancer efficacy

For evaluating combinatorial delivery efficacy of the designed nanosystem, *in vivo*, EAT tumor model was employed. Control group, administered with phosphate buffer saline (PBS), pH 7.4, has shown rapid growth in tumor volumes than the treatment groups (Figure 4.30 A). Administration of nanoplexes carrying PLK-1 siRNA has achieved ~2 fold decrease in % relative tumor volume, compared to control. Free doxorubicin (dissolved in PBS) and

doxorubicin loaded nanoplexes (complexed with scrambled siRNA) depicted ~ 5 fold and ~ 7.1 fold reduction in % relative tumor volume, respectively, in comparison to control group. Maximum reduction in the % relative tumor volume was observed in group treated with doxorubicin and PLK-1 siRNA bearing nanoplexes (~ 15 fold). These results indicate efficacy of the nanoplexes in accomplishing synergistic cytotoxic effect of the loaded active agents in tumor
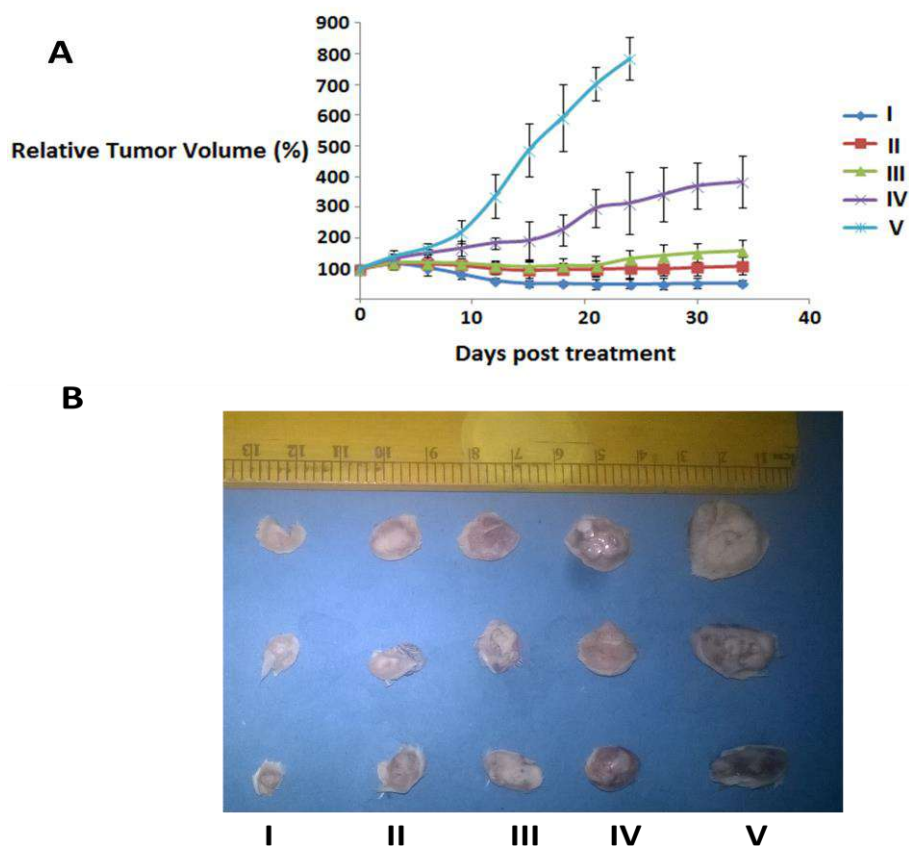
Figure 4.30. (A) Relative % increase in tumor volumes of various treatment groups, compared to the tumor volume at first day of treatment (day 0). Doxorubicin and PLK-1 siRNA bearing nanoplexes (I), Doxorubicin and scrambled siRNA loaded polymeric formulation (II), free Doxorubicin (III), PLK-1 siRNA loaded nanoplexes (IV) and phosphate buffer saline, pH 7.4 (V) were administered to EAT tumor bearing mice, intratumorally. Treatment was initiated on day 12 post subcutaneous implantation of EAT tumor cells, and five injections were given on days 0, 3, 6, 9 and 12. Cumulative dose of doxorubicin and siRNA administered to each mice were 6 mg/kg and 2.5 mg/kg, respectively. (B) Tumor images of various treatment groups.

cells. Tumor was not visible in two out of the five animals treated with doxorubicin and PLK-1 siRNA loaded nanoplexes. Images of the tumors excised at the end point of study are shown in figure 4.30 B.
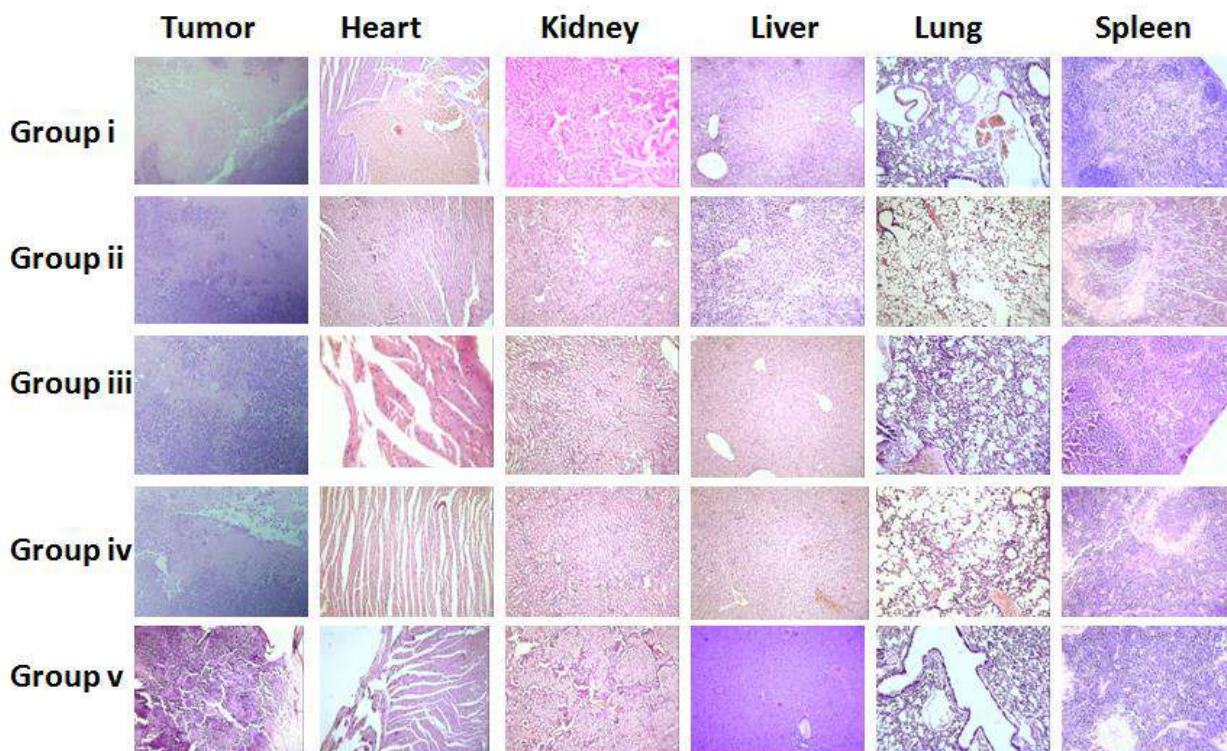
Figure 4.31. Histopathological evaluation of vital organs and tumors of mice employed in tumor regression study. Group i - Doxorubicin and PLK-1 siRNA loaded micelles, Group ii - Doxorubicin and scrambled siRNA loaded micelles, Group iii - Free Doxorubicin, Group iv - PLK-1 siRNA loaded micelles, Group v - Control (saline treated).

Stimuli (redox and pH) responsive nature and the tumor targeting property of albumin (through SPARC receptors) could have helped in improving the antitumor efficacy of nanoplexes. PLK-1 siRNA, which was used as a model nucleic acid for the study, clearly depicts its potential to be used as a powerful tool in knocking down the anti apoptotic defence of tumor cells. Tumor necrosis was evaluated by performing histopathological evaluation of the tumors, after

sacrificing the animals. Maximum necrosis was observed in the group treated with doxorubicin and PLK-1 siRNA loaded nanoplexes, and the necrosis pattern was in line with the results obtained in tumor regression study (Figure 4.31). Serum biochemical analysis of animals used for the study did not depict any significant difference among various groups (data not shown).

4.4. Conclusions

- A dual stimuli sensitive polymeric nanosystem was successfully designed, which could simultaneously incorporate any hydrophobic anticancer drug (such as doxorubicin, paclitaxel etc.) and any nucleic acid (such as pDNA, siRNA, shRNA, miRNA etc) for their combinatorial delivery.

- Nanoplexes formulated from the stimuli sensitive polymer were able to effectively down regulate PLK-1 gene expression in cancer cells, and induced less pronounced knock down effect in normal cells.

- Stabilization of the nanoplexes in salt containing media was achieved by coating them with albumin, enabling the nanocarriers to be dispersed stably in salines, which are commonly used dispersion media for the administration of therapeutic agents to patients.

- A stable and clinically translatable pharmaceutical formulation can be developed using our proposed formulation protocol.

- Synergistic effect of the drug and siRNA in inhibiting tumor cell proliferation was evident, *in vitro* and *in vivo*, after their combinatorial delivery via the designed nanocarriers.

- The results depict great potential of the designed nanosystem as an effective delivery vehicle for a wide variety of drug-nucleic acid combinations.

References

1.   Fessi, H.; Puisieux, F.; Devissaguet, J. P.; Ammoury, N.; Benita, S., Nanocapsule formation by interfacial polymer deposition following solvent displacement. *Int. J. Pharm.* **1989,** 55, (1), R1-R4.

2.   Domínguez, A.; Fernández, A.; González, N.; Iglesias, E.; Montenegro, L. Determination of Critical Micelle Concentration of Some Surfactants by Three Techniques. *J. Chem. Educ.* **1997**, *74* (10), 1227–1231.

3.   Mohamed, M. S.; Veeranarayanan, S.; Minegishi, H.; Sakamoto, Y.; Shimane, Y.; Nagaoka, Y.; Aki, A.; Poulose, A. C.; Echigo, A.; Yoshida, Y.; Maekawa, T.; Kumar, D. S. Cytological and Subcellular Response of Cells Exposed to the Type-1 RIP Curcin and Its Hemocompatibility Analysis. *Sci. Rep.* **2014**, *4*, 5747.

4.   Wang, H.; Zhao, Y.; Wu, Y.; Hu, Y. lin; Nan, K.; Nie, G.; Chen, H. Enhanced Anti-Tumor Efficacy by Co-Delivery of Doxorubicin and Paclitaxel with Amphiphilic Methoxy PEG-PLGA Copolymer Nanoparticles. *Biomaterials* **2011**, *32* (32), 8281–8290.

5.   Remaut, K.; Lucas, B.; Braeckmans, K.; Demeester, J.; De Smedt, S. C. Pegylation of Liposomes Favours the Endosomal Degradation of the Delivered Phosphodiester Oligonucleotides. *J. Control. Release* **2007**, *117* (2), 256–266.

6.   Zhao, M. W. C.; Wang, Y.; Xu, R.; Winnik, M. A.; Croucher, M. D. Poly(styrene-Ethylene Oxide) Block Copolymer Micelle Formation in Water: A Fluorescence Probe Study'. *Macromolecules* **1991**, 24, 1033–1040.

7.   Chen, C.; Yu, C. H.; Cheng, Y. C.; Yu, P. H. F.; Cheung, M. K. Biodegradable Nanoparticles of Amphiphilic Triblock Copolymers Based on poly(3-Hydroxybutyrate) and Poly(ethylene Glycol) as Drug Carriers. *Biomaterials* **2006**, *27* (27), 4804–4814.

8. Sezgin, Z.; Yüksel, N.; Baykara, T. Preparation and Characterization of Polymeric Micelles for Solubilization of Poorly Soluble Anticancer Drugs. *Eur. J. Pharm. Biopharm.* **2006**, *64* (3), 261–268.

9. Hamzeh, M.; Sunahara, G. I. In Vitro Cytotoxicity and Genotoxicity Studies of Titanium Dioxide (TiO2) Nanoparticles in Chinese Hamster Lung Fibroblast Cells. *Toxicol. Vitr.* **2013**, *27* (2), 864–873.

10. Barnard, J., Screening and surveillance recommendations for pediatric gastrointestinal polyposis syndromes. *J Pediatr Gastroenterol Nutr* **2010**, *48* (Suppl 2), 1–6.

11. Ranga, S.; Jaimini, M.; Sharma, S. K.; Chauhan, B. S.; Kumar, A. Review Article A Review on Design OF Experiments (DOE). *Int. J. Pharm. Chem. Sci.* **2014**, *3* (1), 216–224.

12. González, A. G. Optimization of Pharmaceutical Formulations Based on Response-Surface Experimental Designs. *Int. J. Pharm.* **1993**, *97* (1), 149–159.

13. Chawla, R.; Jaiswal, S.; Mishra, B. Development and Optimization of Polymeric Nanoparticles of Antitubercular Drugs Using Central Composite Factorial Design*. *Expert Opin. Drug Deliv.* **2014**, *11* (1), 31–43.

14. Moore, T. L.; Rodriguez-lorenzo, L.; Hirsch, V.; Balog, S.; Urban, D.; Jud, C.; Rothen-rutishauser, B.; Petri-fink, A. Chem Soc Rev Media and Impact on Cellular Interactions †. *Chem. Soc. Rev.* **2015**, *44*, 6287–6305.

15. Bhirde, A. A.; Hassan, S. A.; Harr, E.; Chen, X. Role of Albumin in the Formation and Stabilization of Nanoparticle Aggregates in Serum Studied by Continuous Photon Correlation Spectroscopy and Multiscale Computer Simulations. *J Phys Chem C Nanomater Interfaces* **2014**, 118, 16199-16208.

16. Allouni, Z. E.; Cimpan, M. R.; Høl, P. J.; Skodvin, T.; Gjerdet, N. R. Agglomeration and Sedimentation of TiO2 Nanoparticles in Cell Culture Medium. *Colloids Surfaces B Biointerfaces* **2009**, *68* (1), 83–87.

17. Scripture, C. D.; Figg, W. D.; Sparreboom, A. Peripheral Neuropathy Induced by Paclitaxel: Recent Insights and Future Perspectives. *Curr. Neuropharmacol.* **2006**, *4* (2), 165–172.

18. Lammers, T.; Kiessling, F.; Hennink, W. E.; Storm, G. Drug Targeting to Tumors: Principles, Pitfalls and (Pre-) Clinical Progress. *J. Control. Release* **2012**, *161* (2), 175–187.

19. He, Y.; Wang, Y.; Tang, L.; Liu, H. Binding of Puerarin to Human Serum Albumin : A Spectroscopic Analysis and Molecular Docking. J Fluoresc **2008**, 433–442.

20. Kumar, A.; Lale, S. V.; Aji Alex, M. R.; Choudhary, V.; Koul, V. Folic Acid and Trastuzumab Conjugated Redox Responsive Random Multiblock Copolymeric Nanocarriers for Breast Cancer Therapy: In-Vitro and in-Vivo Studies. *Colloids Surfaces B Biointerfaces* **2017**, *149*, 369–378.

21. Taniguchi, E.; Toyoshima-morimoto, F.; Nishida, E., Nuclear Translocation of PLK-1 Mediated by Its Bipartite Nuclear Localization Signal. *J Biol Chem* **2002,** 277, 48884–48888.

22. Spänkuch-Schmitt, B.; Bereiter-Hahn, J.; Kaufmann, M.; Strebhardt, K. Effect of RNA Silencing of Polo-like Kinase-1 (PLK1) on Apoptosis and Spindle Formation in Human Cancer Cells. *J. Natl. Cancer Inst.* **2002**, *94* (24), 1863–1877.

23. Wu, H.; Zhu, L.; Torchilin, V. P., pH-sensitive poly (histidine)-PEG ∕ DSPE-PEG co-polymer micelles for cytosolic drug delivery. *Biomaterials* **2014**, *34* (4), 1213–1222.

24.   Spänkuch, B.; Steinhauser, I.; Wartlick, H.; Kurunci-Csacsko, E.; Strebhardt, K. I.; Langer, K. Downregulation of Plk1 Expression by Receptor-Mediated Uptake of Antisense Oligonucleotide-Loaded Nanoparticles. *Neoplasia* **2008**, *10* (3), 223–234.

25.   Titlow, W.B.; Lee, C.; Ryou, C., Characterization of toxicological properties of L–lysine polymers in CD–1 mice. *J.Microbiol. Biotechnol.* **2013,** 23, 1015–1022.

CHAPTER V

Summary, Conclusions and Future Perspectives

CHAPTER V

Summary, Conclusions and Future Perspectives

5.1. Summary

The thesis presents synthesis, characterization and evaluation of graft co-polymers of poly (styrene-alt-maleic anhydride) for gene delivery and drug-gene co-delivery applications. Poly (styrene-alt-maleic anhydride) was derivatized with different cationic structures to obtain a series of graft co-polymers. Cationic moieties with different structural properties were selected for synthesizing the graft co-polymers. The graft co-polymers could easily self assemble in water to form core-shell type nanocarriers. The polymeric nanosystems were characterized and further evaluated for their biocompatibility using hemolysis and cell viability assay. Endosomolytic ability of the polymeric nanocarriers was assessed by their hemolytic behavior at pH 5.0. Efficiency of the polymeric nanocarriers to achieve intracellular gene delivery was evaluated using red fluorescent protein encoding pDNA as a model nucleic acid. Comparison of the properties of various cationic moieties is shown in table 5.1.

Table 5.1. Comparison of the cationic moieties with respect to various parameters

Cationic moiety	DNA binding efficiency	Endosomolytic potential	Transfection Efficiency
Isonicotinic acid	Moderate	Good	Low
Piperazine	Good	Poor	Low
Glycidyl trimethylammonium chloride	Poor	Poor	Low
L-arginine	Good	Good	Good
Spermine	Good	Good	Good

Core-shell type morphology of the nanocarriers indicated that the cationic amphiphilic graft co-polymers of PSMA could load hydrophobic drugs and nucleic acids, simultaneously. Based on this observation, different graft co-polymers of PSMA were synthesized and evaluated for their efficacy to co-deliver drug and nucleic acid, *in vitro* and *in vivo*. Among the various cationic structures tested, L-arginine and spermine were able to achieve efficient transfection. Conjugation of spermine to PSMA resulted in poor solubility of the polymeric derivative rendering it difficult to modify further. Hence L-arginine was selected as the nucleic acid binding moiety for designing graft co-polymers for co-delivery of drug and nucleic acid. Two successful polymeric nanosystems were developed for co-delivery of drug and nucleic acid.

The first polymeric nanosystem was developed by grafting isonicotinic acid and arginine-acetyllysine conjugate to the PSMA backbone through short glycol chains. Isonicotinic acid was employed to impart endosomolytic property to the polymeric carrier and arginine-acetyllysine conjugate could facilitate the nucleic acid binding. Click reaction was used to improve the grafting efficiency of amino acid residues. Second nanosystem was developed by imparting stimuli sensitive nature to the graft co-polymer. Arginine-histidine conjugates were grafted to PSMA backbone through disulfide linkages. Multiple disulfide linkages in the polymer can facilitate release of the loaded active agents in response to the glutathione rich environment of cancer cells. pH sensitive behavior of histidine molecules renders dual stimuli responsive nature to the polymeric graft.

Both the nanosystems could self assemble in water to form micelles and depicted excellent biocompatibility and stability in serum containing media. Arginine-histidine grafted PSMA nanocarriers needed to be stabilized in salt containing meida to prevent their agglomeration. Safe and biocompatible albumin was used for stabilizing the nanocarriers. Simple mixing with

albumin could yield stable nanoplexes with size ranging between 120-130 nm. Doxorubicin, a widely used anticancer drug for epithelial cancers, and PLK-1 siRNA, a potential tumor growth suppressor, were respectively employed as model drug and nucleic acid for evaluating the co-delivery efficacy of nanocarriers. Optimum doxorubicin loading of ~ 9% and ~ 8.6% was achieved with the click modified nanosystem and redox sensitive nanosystem, respectively.

Table 5.2. Comparison of the PSMA based nanosystems developed for drug-siRNA co-delivery

Parameters	Isonicotinic acid-Arginine-Acetyllysine grafted PSMA	Cystamine-Arginine-Histidine grafted PSMA
Sensitivity	pH sensitivity	pH sensitivity & Redox sensitivity
Size of nanoparticles	~89nm	~98nm
Dox content	~9%	~8.6%
Drug release after 24 h	~26%	~11.5%
Minimum polymer / siRNA weight ratio required for efficient siRNA complexation	10	40
Fold increase in antitumor efficacy with respect to control	~13 fold	~15 fold

Efficient complexation of siRNA to the drug loaded micelles could be achieved enabling co-delivery of both the active agents. Co-delivery of drug and siRNA using the designed nanosystems depicted synergistic effect in inhibiting cancer cell proliferation, *in vitro and in vivo.* The experimental observations depict great potential of employing poly (styrene-alt-maleic anhydride) based nanocarriers for drug-gene co-delivery applications. Ease of chemical modification and self assembling property make the poly (styrene-alt-maleic anhydride) based nanocarriers suitable for large scale production. A comparison of the two nanosystems developed for co-delivery of drug and siRNA is provided in table 5.2.

5.2. Conclusions

Our study demonstrated improved antitumor efficacy of developed polymeric nanosystems carrying doxorubicin and PLK-1 siRNA as compared to conventional doxorubicin therapy. The salient features of the developed polymeric nanosystems include-

- Amphiphilic graft co-polymeric nanosystems of PSMA depicted excellent self assembling property in aqueous media.

- Grafting of cationic groups like L-arginine and spermine to the PSMA backbone helped in achieving efficiecnt intracellular gene delivery.

- The nanosystems based on PSMA could be further tailored to incorporate both drug and nucleic acid simultaneously for their co-delivery to cancer cells.

- Two graft co-polymeric nanosystems were successfully developed for co-delivery of doxorubicin and PLK-1 siRNA which have shown biocompatibility and self assembling behavior in aqueous media.

- Redox and pH sensitive nanosystem based on PSMA depicted enhanced release of the loaded drug molecules in response to higher glutathione concentration and low pH.

- Both the graft co-polymeric nanosystems depicted synergistic effect in inhibiting cancer cell proliferation, *in vitro* and *in vivo*, and depicted improved antitumor efficacy in comparison to conventional chemotherapy.

- In summary, graft co-polymers of PSMA offers ease of chemical synthesis, self assembling property, biocompatibility, scalability and clinical translation potential of their nanocarriers for drug-gene co-delivery applications.

5.3. Future directions

- Scale up studies for polymer synthesis and formulation of nanocarriers can be carried out to assess their feasibility for bulk production.

- The *in vivo* anticancer efficacy of the nanosystems can be further studied using nude mice model to authenticate the results obtained from EAT model.

- Polymeric nanosystems can be taken further for clinical trials.

- Nanocarriers can be modified with active targeting ligands like folic acid, monoclonal antibodies etc. to achieve more specific delivery of the active agents to cancer cells.

International Research Publications on PhD Research Topic

- **Aji Alex, M. R**.; Nagpal, N.; Kulshreshtha, R.; Koul, V. Synthesis and Evaluation of Cationically Modified Poly(styrene-alt-Maleic Anhydride) Nanocarriers for Intracellular Gene Delivery. *RSC Adv.* **2015**, *5* (28), 21931–21944.

- **Aji Alex, M. R**.; Veeranarayanan, S.; Poulose, A. C.; Nehate, C.; Kumar, D. S.; Koul, V. Click Modified Amphiphilic Graft Copolymeric Micelles of Poly(styrene-Alt-Maleic Anhydride) for Combinatorial Delivery of Doxorubicin and PLK-1 siRNA in Cancer Therapy. *J. Mater. Chem. B* **2016**, *4* (45), 7303–7313.

- **Aji Alex, M.R**.; Nehate Chetan.; Veeranarayanan, S.; Kumar, D.S.; Kulshreshtha, R.; Koul, V. Self Assembled Dual Responsive Micelles Stabilized with Protein for Co-delivery of Drug and siRNA in Cancer Therapy. *Biomaterials* **2017**, 133, 94–106.

Patent on PhD Research Topic

- Stimuli sensitive polymeric nanosystem for co-delivery of drugs and nucleic acids.

  Indian patent application number: 201711008171

  Inventors: Veena Koul and **Aji Alex M.R.**

Conference Presentations

- <u>Poster presentation</u> titled 'Design and development of smart polymeric nanoparticles for overcoming challenges of chemotherapy in cancer' in **10th Annual Open House** held at Indian Institute of Technology Delhi, India on 14th April 2014.

- <u>Poster presentation</u> titled 'Synthesis and evaluation of poly (styrene-alt-maleic anhydride) based nanocarriers for gene delivery application' in **International Conference on**

Polymeric Biomaterials, Bioengineering & Biodiagnostics held at New Delhi, India from 27th-30th October 2014.

- Oral presentation titled 'Designing of safe and effective polymeric nanocarriers for delivery of drugs and genes in cancer therapy' at the **ACS on Campus event** held at Indian Institute of Technology Delhi, India on 1st October 2015.

- Poster presentation titled 'Development of poly (styrene-alt-maleic anhydride) based nanocarriers for intracellular gene delivery' in **The 13th International Symposium on Bioscience and Nanotechnology** held at Bio-Nano Electronics Research centre, Toyo University, Japan from 26th-28th November 2015.

- Poster presentation titled 'Click modified amphiphilic graft copolymeric micelles of poly(styrene-alt-maleic anhydride) for combinatorial delivery of doxorubicin and plk-1 siRNA in cancer therapy' in **1st Annual Conference of Indian Society of Nanomedicine** held at All India Institute of Medical Science, New Delhi, India from 24th-26th November 2016 (**Received best poster award**).

Curriculum Vitae

Name: Aji Alex M.R.

Date of Birth: 8th May 1985

Languages Known: English (Fluent), Malayalam (Mother-tongue), Hindi (Fluent),

ACADEMIC CREDENTIALS

Master of Pharmacy (M.Pharm.)   Department of Pharmaceutics

College of Pharmaceutical Sciences,

Mahatma Gandhi University,

Kerala, India

2007-2009

Bachelor of Pharmacy (B.Pharm.)   College of Pharmacy, Trivandrum Medical College,

Kerala, India

2002-2007

Examination	University	Year of passing	Percentage/CGPA
M.Pharm.	Mahatma Gandhi University, Kerala, India.	2009	75.5% (Distinction)
GATE[*]	IIT Kanpur	2007	97.34 Percentile
B.Pharm.	Kerala University	2007	66.39% (First Class)
Senior Secondary	Kerala Board	2002	83.11% (Distinction)
High School	Kerala Board	2000	89.83% (Distinction)

[*]GATE: Graduate Aptitude Test in Engineering (in Pharmaceutical Sciences)

SCIENTIFIC EXPERTISE

- Polymer synthesis, Bioconjugation techniques

- Formulation development

- Well versed with the use of-

  - Analytical instruments and techniques like HPLC, GPC, FTIR, NMR, DSC, UV-visible spectroscopy, fluorescence spectroscopy, optical and polarized light microscopy, hot and cold stage microscopy, circular dichroism, Malvern zeta sizer, homogenizer, probe sonicator, bench top lyophilizer, gel electrophoresis.

  - Processing equipments like high pressure homogenizer, single station and multi station tablet punching machine, spray dryer, air jet mill and fluid bed dryer.

  - Cell culture techniques like confocal microscopy, flow cytometry, fluorescence microscopy, real time PCT (RT-PCR) and immunostaining.

- Good knowledge and understanding of preformulation studies-

  - Solubility and dissolution studies

  - Hygroscopicity studies

  - Stability studies as per ICH guidelines

- Solid state characterization (molecular, particle and bulk level properties)

  - Concepts of crystallinity, polymorphism, hydrates, solvates, desolvates and amorphous state

  - Solid state stability

- Appreciable understanding of the data interpretation of FTIR, ^{1}H-NMR, ^{13}C-NMR, GPC, SEM, TEM, AFM, EDX, XPS, FACS, circular dichroism, CHN, DSC, TGA etc.

- Appreciable understanding of the concepts related to Intellectual Property Rights (IPRs) and drug regulatory affairs.

- Well versed with softwares like Chemdraw, ACD ChemSketch, Origin, CasaXPS, SigmaStat, Flowing Software, Endnote and Microsoft office.

- Well versed with search engines like SciFinder, Scopus, Sciencedirect, Pubmed and Google Scholar.

- Experience in handling small animals (rats, wistar mice and nude mice) with various routes of administration such as oral, intravenous, intraperitoneal and subcutaneous.

RESEARCH PUBLICATIONS

- **M. R. Aji Alex**, C. Nehate, S. Veeranarayanan, D. S. Kumar, R.Kulshreshtha and V. Koul. Self assembled dual responsive micelles stabilized with protein for co delivery of drug and siRNA in cancer therapy, Biomaterials, **2017**, 133, 94–106 **[Imapct factor- 8.4]**

- Nehate C, **M. R. Aji Alex**, Kumar A, Koul V. Combinatorial delivery of superparamagnetic iron oxide nanoparticles and doxorubicin using folate conjugated redox sensitive multiblock polymeric nanocarriers for enhancing the chemotherapeutic efficacy in cancer cells. Materials Science and Engineering: C 2017; 75: 1128-1143 **[Imapct factor- 3.42]**

- Kumar A, Lale S V., **M. R. Aji Alex**, Choudhary V, Koul V. Folic acid and trastuzumab conjugated redox responsive random multiblock copolymeric nanocarriers for breast cancer therapy: In-vitro and in-vivo studies. Colloids Surfaces B Biointerfaces 2017;149:369–78. **[Imapct factor- 3.9]**

- **M. R. Aji Alex**, S. Veeranarayanan, A. C. Poulose, C. Nehate, D. S. Kumar and V. Koul. Click modified amphiphilic graft copolymeric micelles of poly (styrene -alt-maleic anhydride) for combinatorial delivery of doxorubicin and plk-1 siRNA in cancer therapy, *J. Mater. Chem. B*, 2016, 4, 7303–7313 **[Imapct factor- 4.872]**

- Kannissery Pramod, **M.R. Aji Alex,** Manisha Singh, Shweta Singh, Shahid.H.Ansari, Javed Ali. Eugenol nanocapsule for enhanced therapeutic activity against periodontal infections. J Drug target. 2015 **[Imapct factor- 2.741]**

- **M.R. Aji Alex,** Neha Nagpal, Ritu Kulshreshtha, Veena Koul. Synthesis and evaluation of cationically modified poly (styrene-*alt*-maleic anhydride) nanocarriers for intracellular gene delivery, RSC Adv. 2015; 5: 21931-21944. **[Imapct factor- 3.71]**

- **M.R. Aji Alex**, A.J. Chacko, S. Jose, E.B.Souto. Lopinavir loaded solid lipid nanoparticles for intestinal lymphatic targeting, Eur.J.Pharm.Sci. 2011;42 (1-2): 11-18 **[Imapct factor- 3.2]**

- Kumar N, **Aji Alex MR**, Mittal G, Soni S, Nishad DK, Singh T, Ahmad FJ, Bhatnagar A. Development and *in vitro* evaluation of an oral floating matrix tablet formulation of calcium di-sodium EDTA using gamma scintigraphy. Radiopharmacy. Indian J Nucl Med 2010; 25:81.

- Raisuddin A , Bajaj M , Singla YP , **Aji Alex MR** , Dutta M , Singh Thakuri, Ahmad FJ , Khar RK , Bhatnagar A. Scintigraphic evaluation of floating, gastroretentive formulation of clarithramycin in healthy human volunteers. Radiopharmacy. Indian J Nucl Med 2010; 25:82.

PATENTS

- Stimuli sensitive polymeric nanosystem for co-delivery of drugs and nucleic acids.

  Indian patent application number: 201711008171

  Inventors: Veena Koul and **Aji Alex M.R.**

AWARDS & ACHIEVEMENTS

- Dogra Educational Endowment Award from CBME, IIT, Delhi, for best research publication in 2017.

- Selected amongst 50 PhD students to represent 'Centre for Biomedical Engineering' for presenting research work on Research Scholars' Day 2014, held at IIT Delhi on 10th April 2014.

- Qualified **Graduate Aptitude Test in Engineering (GATE)**, 2007 with **97.34 percentile**.

INDUSTRIAL & RESEARCH EXPERIENCE

- Worked at **Bionano Electronics Research Centre (BNERC), Toyo University, Japan** from November 2015- February 2016 (**3 months**) during PhD and got experience in **handling small animals (including nude mice).**

- Worked as **project assistant** at **Institute of Nuclear medicine and Allied Sciences, DRDO,** New Delhi from March 2010-December 2010 (**9 months**) and got expertise in **radio labelling of pharmaceuticals and pharmacoscintigraphic analysis.**

- Worked as **Trainee** at Biosurface Technology lab, **Sree Chithra Thirunal Institute of Medical Sciences and Technology (SCTIMST), Kerala** from April 2009-November 2009 (**8 months**) and got expertise in **formulation and evaluation of lipid based nanosystems.**

- **One month** certificate course in **High Performance Liquid Chromatography (HPLC)** at **Madras Industrial Co-operative Analytical Laboratories**, Guindy, Chennai.

- Manufacturing of parenteral preparations like Ampoules, Vials, Large volume and Small volume Parenterals; Quality control and analysis of Parenterals - Kokad Pharmaceuticals, Kottayam, and Kerala, India. (**1 month**; 2006).

- Manufacturing of Tablets, Capsules, Oral suspensions, Liquids; Extraction processes – Maceration and Percolation (tinctures); Repacking and refilling; Quality control and analysis according to Indian Pharmacopoeia - Pharmaceutical Company of Travancore, Thiruvananthapuram, Kerala, India. (**1 month**; 2006).

EXTRACURRICULAR ACTIVITIES

- Active member in various cultural activities in college and hostel.
- Served as a coordinator for Centre for Biomedical Engineering in 10th Open House event at IIT Delhi (April 2014).
- Elected as student representative of Nalanda Hostel, Indian Institute of Technology, Delhi (2014-2015).
- Active in sports events like badminton, cricket and football.